Discovery and investigation of an ATG4B- IMPDH2 axis in breast cancer cells

by

Cally Ho

B.Sc. (Hons., Biochemistry), University of Victoria, 2016

Thesis Submitted in Partial Fulfillment of the
Requirements for the Degree of
Doctor of Philosophy

in the
Department of Molecular Biology and Biochemistry
Faculty of Science

SIMON FRASER UNIVERSITY
Fall 2023

Declaration of Committee

Name: **Cally Ho**

Degree: **Doctor of Philosophy (Molecular Biology and Biochemistry)**

Title: **Discovery and investigation of an ATG4B-IMPDH2 axis in breast cancer cells**

Committee:

Chair: **Edgar Young**
Associate Professor, Molecular Biology and Biochemistry

Sharon Gorski
Supervisor
Professor, Molecular Biology and Biochemistry

Kevin Bennewith
Committee Member
Associate professor, Pathology and Laboratory Medicine
University of British Columbia

Esther Verheyen
Committee Member
Professor, Molecular Biology and Biochemistry

Mani Larijani
Examiner
Professor, Molecular Biology and Biochemistry

Ryan Russell
External Examiner
Associate Professor, Cellular and Molecular Medicine
University of Ottawa

Abstract

Autophagy is an intracellular catabolic process that plays both pro- and anti-tumorigenic roles depending on cancer stage and context. ATG4B is a core cysteine protease in autophagy and has been associated with modulating the responses of breast cancer cells to nutrient deprivation and targeted treatment. To date, the molecular mechanisms underlying ATG4B in nutrient stress and treatment response in breast cancers remain poorly defined. To this end, I identified a new protein-protein interaction between ATG4B and IMPDH2, a metabolic enzyme involved in *de novo* GTP biosynthesis. A key amide donor in the de novo biosynthesis of purines, like GTP, is glutamine, a critical amino acid for cancer cell growth. I discovered that ATG4B is important for assembly of IMPDH2 into ring-and-rod structures under glutamine deprivation, suggesting that ATG4B may be important in regulating cellular GTP. I discovered that genetic loss of ATG4B is associated with an enrichment in purine nucleotides and metabolites involved in the purine salvage pathway, an alternate pathway for GTP production, suggesting an increased utilization of the purine salvage pathway. To investigate potential cellular consequences of this metabolic shift, I examined growth of parental and ATG4B knockout (KO) breast cancer cells and found that ATG4B KO significantly impaired growth under glutamine deprivation. Inhibition of IMPDH had a modest effect on growth of glutamine-deprived ATG4B KO cells, suggesting a reliance on IMPDH-independent pathways for growth. Depletion of exogenous purines resulted in a significant impairment in ability of ATG4B KO cells to grow in glutamine-depleted media, supporting a reliance on the purine salvage pathway for growth. I then investigated the potential therapeutic applications of the ATG4B-IMPDH2 axis in breast cancer cells and found that pharmacological inhibition of ATG4 and IMPDH results in a modest but synergistic reduction in growth. Collectively*, my research has identified a new protein-protein interaction between ATG4B and IMPDH2, and a novel metabolic reprogram wherein cells may increase utilization of the purine salvage pathway for growth in glutamine-deprived conditions in breast cancer cells.*

Keywords: ATG4B; IMPDH2; autophagy-related protein; purine metabolism; breast cancer

To the kind folks I’ve met along the way.

Acknowledgements

I'd like to firstly thank my senior supervisor, Dr. Sharon Gorski, for her mentorship and unwavering support during my graduate school journey. Thank you for believing in me and helping me see the potential in myself over the years. I'd like to also thank my committee members, Dr. Esther Verheyen and Dr. Kevin Bennewith, for their continued guidance and the wonderful scientific conversations we've had over the past years. Thank you for helping me grow as a better scientist and learning to take pauses (especially when communicating my science!). I want to also thank my very first "boss", Dr. Thomas Fyles, who gave me my first preview and experience working in a scientific research lab. Thank you for taking a chance in me all those years ago and all the important lessons you've imparted in resilience and patience. I want to also thank Drs. Lindsay DeVorkin and Julian Lum for introducing me to the wonderful world of autophagy, and for their kindness and support in helping me cultivate good work ethics and scientific thinking when I was very green.

Thank you to past and present members of the Gorski lab, especially Dr. Morgana J. Xu, who has been and continues to be a great mentor and, most importantly, amazing friend from the very beginning. I'd like to also thank Nancy E. Go for her support and help navigating experiments, especially during the last stretches of my project, and Dr. Suganthi Chittaranjan for sharing her scientific insights over the years and helping me develop important critical thinking skills. Thank you as well to Drs. Gregg Morin and Gian Negri for proteomics collaborations and Dr. Seth Parker and Jessica Koe for metabolomics collaborations. I want to thank to Dr. Vincent Chen for his kindness and patience in teaching me all about proteomics. Dr. Chen was a phenomenal mentor, and I am grateful for the opportunity to learn about proteomics data analysis from him. Thank you also to Maiya Moore for her daily positivity and support with lab operations over the years.

Finally, I want to thank Dr. Justin Jia, my partner, scientific collaborator, and best friend. Thank you for supporting me through the ups and downs (especially the downs).

Table of Contents

List of Tables

List of Figures

List of Acronyms

3-MA	3-Methyladenine
5’NT	5′-Nucleotidase
ABL	Abelson Tyrosine-Protein Kinase 1
AKT	AKT Serine/Threonine Kinase
AMBRA1	Autophagy And Beclin 1 Regulator 1
AMP	Adenosine monophosphate
AMPK	5' adenosine monophosphate-activated protein kinase
Apg	Autophagy
ARL2	ADP-Ribosylation Factor-Like Protein 2
ASCL1	Achaete-scute homolog-1
ATG	Autophagy-related
ATP	Adenosine triphosphate
ATPase	Adenosine triphosphate-hydrolyzing enzyme
Aut	Autophagocytosis
BAX	BCL2 Associated X
BCKDH	Branched Chain Keto Acid Dehydrogenase E1 Subunit
BCL2	B-Cell CLL/Lymphoma 2
BCR	BCR Activator Of RhoGEF And GTPase
BECN1	Beclin 1
C12orf44	Chromosome 12 Open Reading Frame 44
CAD	Carbamoyl-Phosphate Synthetase 2, Aspartate Transcarbamylase, And Dihydroorotase
Cas9	CRISPR associated protein 9
cDNA	Complementary DNA
CRISPR	Clustered regularly interspaced short palindromic repeats
CTP	Cytidine triphosphate
CTPS1	CTP Synthase 1
DHFR	Dihydrofolate reductase
DHODH	Dihydroorotate Dehydrogenase
DMEM	Dulbecco's Modified Eagle Medium

DNA	Deoxyribonucleic acid
DON	6-Diazo-5-oxo-L-norleucine
DRD3	Dopamine Receptor D3
E1	Ubiquitin-activating enzyme
E2	Ubiquitin-conjugating enzyme
E2F1	E2F Transcription Factor 1
E3	Ubiquitin ligase
Egr-1	Early Growth Response 1
EMT	Epithelial mesenchymal transition
FDA	Food and Drug Administration
FGAM	5′-Phosphoribosylformylglycinamidine
FGAR	Phosphoribosyl-N-formylglycineamide
FIP200	FAK Family Kinase-Interacting Protein Of 200 KDa
FOXO1	Forkhead Box O1
FOXO3	Forkhead Box O3
G1 phase	Growth 1 phase; gap 1 phase
GABARAP	Gamma-aminobutyric acid receptor-associated protein
GAP	GTPase activating protein
GATE-16	Golgi-Associated ATPase Enhancer Of 16 KDa
GDP	Guanosine diphosphate
GLS	Glutaminase
GMP	Guanosine monophosphate
GMPS	Guanine Monophosphate Synthase
GST	Glutathione S-transferase
GTP	Guanosine triphosphate
GTPase	Guanine nucleotide-binding proteins
HER2	Human Epidermal growth factor Receptor 2
HPRT	Hypoxanthine Phosphoribosyltransferase
HR	Hormone receptor
IMP	Inosine monophosphate
IMPDH	Inosine monophosphate dehydrogenase

KEAP1	Kelch Like ECH Associated Protein 1
Ki67	Marker Of Proliferation Ki-67
KRAS	Kirsten Rat Sarcoma Viral Oncogene Homolog
LC3	Microtubule Associated Protein 1 Light Chain 3 (MAP1LC3)
LKB1	Liver Kinase B1
MAP1LC3	Microtubule Associated Protein 1 Light Chain 3 (LC3)
MAPK	Mitogen-activated protein kinase
MEM	Minimum essential medium
MK2	MAPK Activated Protein Kinase 2
MPA	Mycophenolic acid
mRNA	Messenger ribonucleic acid
MSOX	Methionine sulfoximine
MST4	Mammalian Ste20-Like Protein Kinase 4
MTHFD2	Methylenetetrahydrofolate Dehydrogenase (NADP+ Dependent) 2
mTOR	Mechanistic Target Of Rapamycin Kinase
MYBL2	MYB Proto-Oncogene Like 2
NAD	Nicotinamide adenine dinucleotide
NADH	Reduced nicotinamide adenine dinucleotide
NADP	Nicotinamide adenine dinucleotide phosphate
NAM	Nicotinamide
NMDA	N-Methyl-D-aspartic acid
NRBF2	Nuclear Receptor Binding Factor 2
NRF2	Nuclear Factor Erythroid 2-Related Factor 2
P300	E1A-Binding Protein, 300kD; Histone Acetyltransferase P300
p62	Ubiquitin-Binding Protein P62
PAM50	Prediction Analysis of Microarray 50
PCNA	Proliferating cell nuclear antigen
PDB	Protein data bank
Pep4	Saccharopepsin; Vacuolar aspartyl protease; proteinase A
PFKP	Phosphofructokinase, Platelet

pH	Potential of hydrogen
PI3K	Phosphoinositide 3-kinase
PI3P	Phosphatidylinositol 3-phosphate
PI5P	Phosphatidylinositol 5-phosphate
PIK3C3	Phosphatidylinositol 3-Kinase Catalytic Subunit Type 3
PIK3R4	Phosphoinositide-3-Kinase Regulatory Subunit 4
PIKfyve	Phosphoinositide Kinase, FYVE-Type Zinc Finger Containing
Pnp	Purine Nucleoside Phosphorylase
PP2A	Protein Phosphatase 2 Phosphatase Activator
PPAT	Phosphoribosyl Pyrophosphate Amidotransferase
PRA	Phosphoribosylamine
Prb1	Cerevisin; vacuolar proteinase B
PRPP	Phosphoribosyl pyrophosphate
PtdIns3k	Phosphatidylinositol 3-kinases
PUMA	P53-Upregulated Modulator Of Apoptosis
PyMT	Polyoma middle tumor-antigen
RAPTOR	Regulatory Associated Protein Of MTOR Complex 1
RAS	Rat sarcoma virus
RavZ	Region allowing vacuole colocalization protein Z
RB	Retinoblastoma-Associated Protein
RB1CC1	RB1-Inducible Coiled-Coil Protein 1
RHEB	Ras homolog enriched in brain
RNA	Ribonucleic acid
RNF5	Ring Finger Protein 5
Rny1	Ribonuclease T2-like
rRNA	Ribosomal RNA
RUBCN	Rubicon Autophagy Regulator
S phase	Synthesis phase
SHMT	Serine hydroxymethyltransferase
shRNA	Small hairpin RNA

siRNA	Small interfering RNA
SIRT	Sirtuin
SLC1A5	Solute Carrier Family 1 Member 5
SLC7A11	Solute Carrier Family 7 Member 11
SNARE	SNAP (Soluble N-ethylmaleimide-Sensitive Factor Attachment Proteins) receptor
SOD1	Superoxide Dismutase 1
TCA	Tricarboxylic acid cycle
TFEB	Transcription factor EB
THF	Tetrahydrofolate
TNBC	Triple-Negative Breast Cancer
tRNA	Transfer RNA
TSC2	Tuberous Sclerosis 2
ULK	Unc-51 Like Autophagy Activating Kinase
UMP	Uridine monophosphate
Urh	Uridine nucleosidase
UTP	Uridine triphosphate
V-type	Vacuolar type
VDAC1	Voltage Dependent Anion Channel 1
VPS	Vacuolar Protein Sorting
XMP	Xanthosine monophosphate
YB-1	Y-Box Binding Protein 1

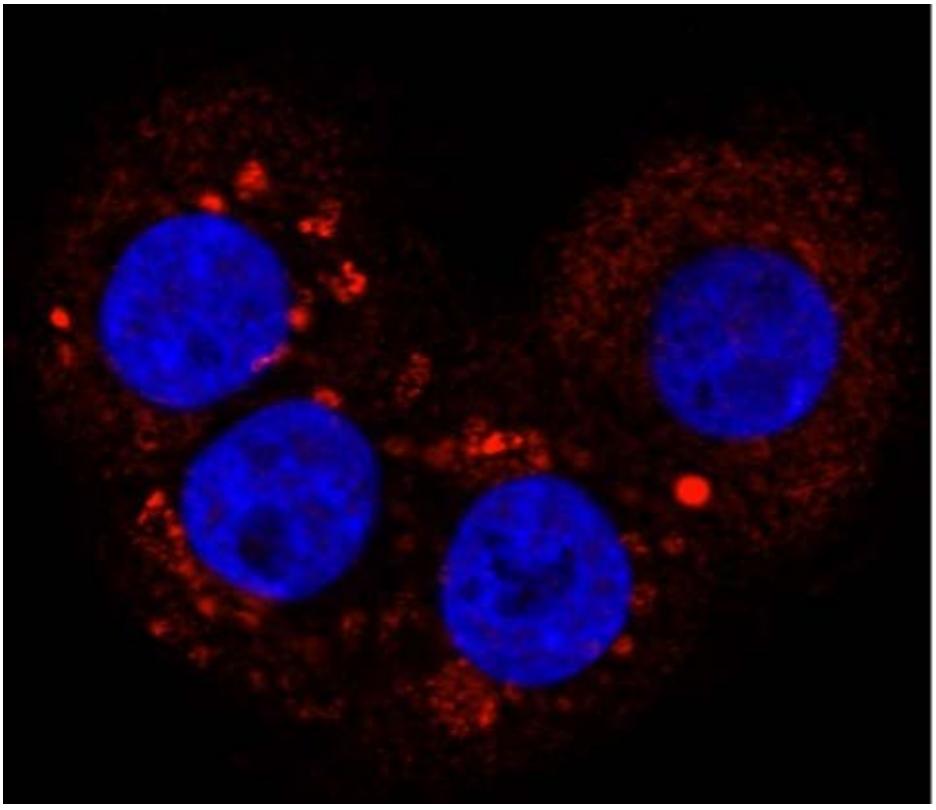

Chapter 1. Introduction

Parts of chapter 1 were previously published in the review article: Ho, C. J. & Gorski, S. M. Molecular Mechanisms Underlying Autophagy-Mediated Treatment Resistance in Cancer. *Cancers* **11**, 1775 (2019). I performed the literature research and wrote the manuscript, under the mentorship of my senior supervisor, Dr. Sharon Gorski.

1.1. Autophagy

1.1.1. Overview of autophagy

Autophagy is a major intracellular quality control mechanism that mediates the degradation and recycling of cytosolic components through lysosomes [1]. "Autophagy" was first coined by Christiane De Duve at the 1963 Ciba Foundation Symposium on Lysosomes and stems from the Greek words "auto-", meaning "oneself", and "-phagy", meaning "to eat" [2]. Seminal work in yeast led by Yoshinori Ohsumi and colleagues led to the discovery and characterization of genes fundamental for the autophagic process, termed autophagy-related (Atg) genes, during the 1990s[3]. This body of work was recognized in 2016 where Yoshinori Ohsumi was awarded the Nobel Prize in Physiology and Medicine for his important discoveries relating to autophagy[4]. Significant progress has been made since, with the identification of more than 40 Atg proteins in yeast, many of which are evolutionarily conserved in mammalian systems[5].

1.1.2. Types of mammalian autophagy

Three morphologically distinct forms of autophagy have been described in mammalian systems. Microautophagy involves the uptake of small cytosolic contents through lysosomal protrusions or invaginations, or endosomal invaginations, and is followed by the subsequent degradation of cargo in endolysosomal lumens[6]. Chaperone-mediated autophagy is a highly specific form of autophagy that recognizes cargo bearing KFERQ peptide motifs and unfolds them through the coordinated action of chaperone proteins. This is followed by the direct translocation of the unfolded cargo from the cytosol to the lysosomal lumen for degradation[7]. In macroautophagy, cytosolic components are sequestered into double-membrane structures, known as

autophagosomes, that form *de novo* and fuse with lysosomes. The resulting structures, termed autolysosomes, facilitate the degradation of engulfed cargo, which are subsequently released back to the cytosol as building blocks for other cellular processes. Macroautophagy is characterized by a concerted morphological progression from phagophore nucleation to membrane elongation, autophagosome-lysosome fusion, and, finally, cargo degradation and release[7] (Figure 1.1). Of the three, macroautophagy is currently the most studied form of autophagy[7].

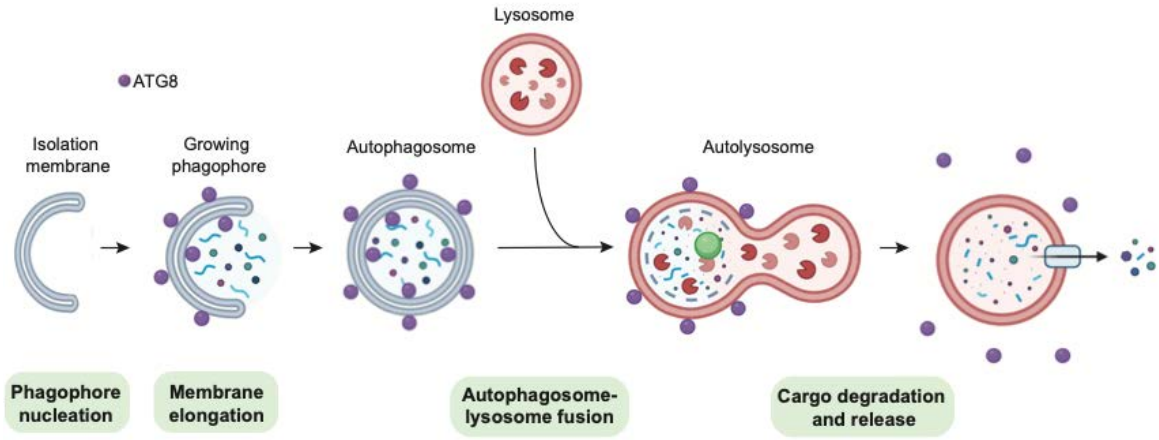

Figure 1.1 Overview of macroautophagy
Macroautophagy begins with the initial formation of an isolation membrane. Membrane elongation facilitates growth of the phagophore and is coupled with the encapsulation of cytosolic cargo. During this process, mammalian Atg8 proteins, hereafter ATG8 proteins, are processed and conjugated to phosphatidylethanolamine on the surface of the growing phagophore as part of autophagosome formation. Autophagosomes fuse with lysosomes, and encapsulated cargo are then degraded and released back to the cytosol for recycling. Image created using BioRender. Derived from data and information provided in Paryzch and Klionsky, 2014[7] and Yang, et al. 2018[8].

It is important to note that non-canonical forms of autophagy, characterized by the Conjugation of mammalian Atg8-like proteins (hereafter ATG8) to Single Membranes (CASM), have also been described in mammalian systems [9,10]. Non-canonical autophagy can be classified as secretory or recycling/degradative depending on the fate of their encapsulated cargoes[10]. Microtubule associated protein 1 light chain 3 (LC3)-dependent extracellular vesicle loading and secretion (LDELS) is an example of secretory non-canonical autophagy and involves the encapsulation of cytosolic components via LC3-decorated multivesicular bodies and their subsequent release as

extracellular cargoes[11]. In contrast, degradative forms of non-canonical autophagy, like LC3-associated phagocytosis (LAP)[12] and LC3-associated endocytosis (LANDO)[13], involve the fusion of phagosomes and endosomes with lysosomes and the subsequent degradation of their encapsulated cargoes. Although ULK1, FIP200 and ATG14, core components of the initiation and nucleation complexes of canonical macroautophagy, are dispensable for certain non-canonical autophagic processes, like LAP and LANDO[13–15], it has been proposed that most non-canonical autophagy is dependent on the same core ATG8 conjugation machinery as canonical macroautophagy[10].

1.1.3. Molecular machinery of macroautophagy

The main molecular machinery of macroautophagy (hereafter autophagy) is comprised of functional units of ATG proteins that work in concert. In mammals, the induction of autophagy leads to the assembly of an initiation complex consisting of Unc-51-like autophagy-activating kinase (ULK) 1/2, ATG13, FAK family kinase-interacting protein of 200kDa (FIP200) and ATG101, at ATG9-containing sites. ULK1 phosphorylates ATG9 and this initiates the elongation of pre-autophagosomal (PAS) membranes, and the recruitment of the class III PtdIns3k nucleation complex, consisting of vacuolar protein sorting 34 homolog (VPS34), VPS15, ATG14, autophagy and beclin 1 regulator 1 (AMBRA1), nuclear receptor binding factor 2 (NRBF2) and beclin 1 (BECN1)[16]. VPS34 facilitates the production of phosphatidylinositol-3-phosphate (PI3P) phospholipids that are incorporated into autophagosomal membranes during phagophore expansion. Further expansion of the nascent phagophore is mediated by two ubiquitin-like conjugation systems, namely the ATG12 conjugation system and the ATG8 conjugation system[7] . The ATG12 conjugation system involves the ATP-dependent activation of ATG12 by the E1-like enzyme ATG7, and the formation of a thioester intermediate with consisting of ATG12, ATG7 and the E2-like enzyme ATG10. ATG12 is then conjugated to ATG5, and forms a complex with ATG16L[17]. The ATG8 conjugation system involves the cleavage of pro-ATG8 proteins by the ATG4 cysteine proteases to form processed ATG8 (ATG8-I). ATG8-I is then activated by the E1-like enzyme ATG7 and transferred to the E2-like enzyme ATG3 before conjugation to phosphatidylethanolamine (PE) on growing phagophores, forming ATG8-II. The ATG12-ATG5 conjugate functions as an E3-like enzyme that promotes ATG8-PE conjugation

through interactions between ATG12 and ATG3, whereas ATG16L dictates ATG8 lipidation sites[17] (Figure 1.2).

Autophagosomes are formed following cargo encapsulation and phagophore closure. Autophagosome-lysosome fusion is mediated by various SNARE proteins, small GTPases, tethering factors, adaptors and motor proteins[18], and leads to the formation of autolysosomes. Autophagic cargo within autolysosomes are then degraded as the inner autophagosomal membrane is disassembled by ATG3[19], a core E2-like enzyme in the ATG12 and ATG8 the conjugation systems, and the autolysosomal lumen is acidified by V-type ATPases[16] . Degraded cargo are released back to the cytosol through lysosomal and vacuolar membrane transporters and recycled as biomolecules[20] (Figure 1.2).

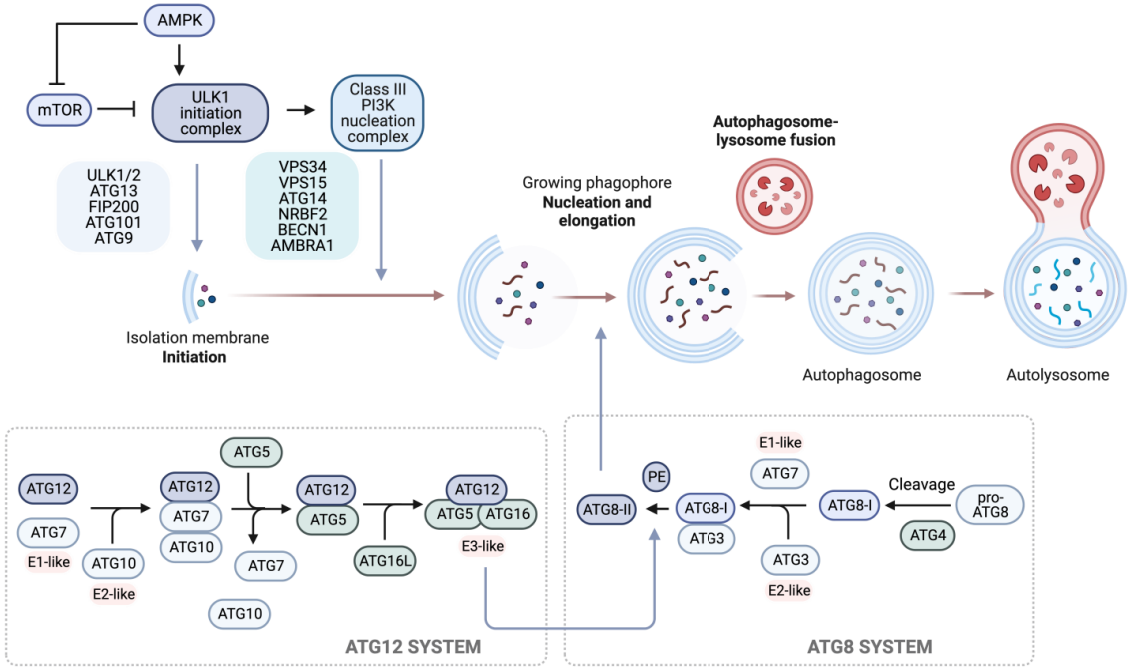

Figure 1.2 The molecular machinery of autophagy
Core ATG proteins involved in the autophagy machinery are shown. The autophagy machinery is induced in response to different stresses in the cell. A classic example is the induction of autophagy in response to nutrient stress, which is frequently regulated by the metabolic sensors AMPK and mTOR, as described in chapter 1.5.3 of this thesis. Generally, mTOR suppresses

autophagy in the absence of nutrient stress, whereas AMPK activates autophagy in response to low nutrient availability. Induction of autophagy leads to the activation of the ULK1 initiation complex which facilitates PAS elongation. This is followed by the activation of the class III PI3K nucleation complex, which facilitates phagophore nucleation and expansion. Two ubiquitin-like conjugation systems, the ATG12 and the ATG8 systems, also mediate the continued expansion of the nascent phagophore and autophagosome formation. Fully formed autophagosomes fuse with lysosomes to form autolysosomes, and encapsulated cargo are degraded and released back to the cytosol. Image generated using BioRender. Derived from data and information derived from Galluzzi et al. 2017[16] and Mizushima and Levine, 2020[21].

1.2. Autophagy and treatment resistance in cancer

1.2.1. The autophagy paradox

Autophagy plays dual roles in tumor suppression and progression (Figure 1.3). In general, autophagy suppresses tumor onset in normal cells through several mechanisms including cellular quality control, cell death activation, and maintenance of genetic and genome integrity. In established tumors, autophagy may promote cancer progression through the provision of energy and nutrients, therapy resistance, and evasion of cell death[22,23]. The pro-tumorigenic roles of autophagy prime it as an attractive therapeutic target for cancer treatment.

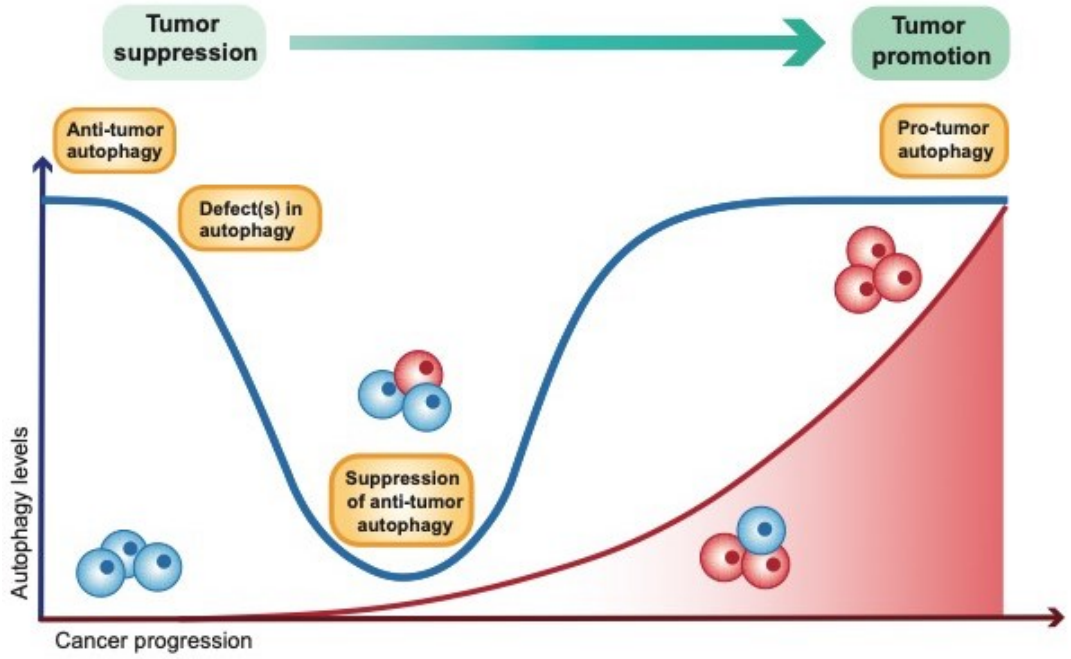

Figure 1.3 Dual roles of autophagy in cancer progression
Proficient autophagy mitigates the onset of cancer in normal cells. Defects that lead to the impairment or suppression of the autophagy machinery in normal cells facilitate oncogenic

transformation and cancer onset. The restoration of autophagy to mediate tumor progression is proposed in established tumors. To date, the mechanisms underlying the restoration of pro-tumorigenic autophagy remain poorly understood. Derived from Galluzzi et al. 2015[22] and Bustos, S., et al. 2020[24]. Both licensed under CC BY.

1.2.2. Autophagy promotes treatment resistance

Tumor initiation is largely stochastic by nature and involves a coordinated destabilization of major cellular processes. The dynamic and evolutionary manner by which this occurs creates molecularly heterogenous tumors[25,26]. The ability of cancers to adapt to and survive the effects of cancer therapies remains one of the greatest impediments in medical and clinical oncology. Treatment resistance directly translates to the ineffectiveness and eventual failures of cancer therapies[27–32]. Innate treatment resistance predates therapeutic intervention, whereas acquired treatment resistance is a refractory outcome of cancer therapy that occurs when subpopulations of cancer cells within tumors acquire mutations and adaptations that desensitize them to ongoing treatment[33–37]. To date, treatment resistance remains a major challenge to successful cancer treatment and control, but the mechanisms involved remain poorly understood[38,39]. A number of pre-clinical studies have demonstrated that the inhibition of autophagy and ATG proteins are potential therapeutic avenues for improving the efficacies of and overcoming resistance to cancer therapies[40]. The crosstalk between autophagy and the p62-KEAP1-NRF2[41] and FOXO3A-PUMA[42] pathways have been described to promote chemoresistance in certain cancer types[40]. *To date, the molecular mechanisms underlying autophagy in resistance to targeted therapies remain poorly defined.*

1.3. Autophagy and breast cancer

1.3.1. Breast cancer

Breast cancer remains the top commonly diagnosed form of cancer and the 2nd leading cause of cancer-related deaths amongst Canadian women as of 2022[43]. Currently, breast cancer tumors may fall under one of four clinical subtypes based on expression of the hormone receptors, the estrogen receptor (ER) and progesterone

receptor (PR), and overexpression of the human epidermal growth factor receptor 2 (HER2): i) luminal A: ER+, PR+ HER2-, ii) luminal B: ER+, PR+, HER2+/-, iii) HER2-positive: ER-, PR-, HER2+, and iv) triple-negative: ER-, PR- HER2-[44]. Clinical subtyping is based primarily on fluorescence in situ hybridization and immunohistochemical assessment of these receptors. It is important to note that these methods are limited by a number of factors, including reproducibility, scoring cut-off variations and subjectivity, and tumor heterogeneity[44]. In the clinic, treatment regimens for breast cancer patients are routinely determined by evaluating histological and pathological traits of the tumor and assessing the receptor statuses of ER, PR and HER2. Luminal A and B breast cancers are typically treated with a combination of hormone therapy and chemotherapy because of their expression of ER and PR, and patients typically have better prognosis compared to other subtypes[45–47]. Currently, treatment options for patients with triple-negative breast cancer are limited to chemotherapy due to poor responses to targeted therapies, *and chemoresistance remains an outstanding challenges*[48,49]*.* Breast cancer patients with HER2-positive breast tumors are usually treated with HER2-targeted therapies, like trastuzumab, but *treatment resistance often occurs in advanced and metastatic cases and, similarly, remains an outstanding challenge*[50,51].

Breast tumors may also be subtyped by their gene expression signatures through technologies like DNA microarrays and RNA sequencing[44]. The PAM50 molecular classifier is an example of an assay used often for the molecular classification of breast tumor and is based on the evaluation of a 50-gene signature in breast tumor samples. The 5 molecular subtypes based on the PAM50 classifier are: i) basal-like, ii) HER2-enriched, iii) luminal A, iv) luminal B, and v) normal-like[52]. Methods for the molecular classification of breast cancers are limited by reproducibility, detection accuracy, and tumor heterogeneity. The stratification of breast cancer patients based on gene expression profiles is currently not part of standard clinical practices[44].

1.3.2. Dual roles of autophagy in breast cancer

Breast cancer

The role of autophagy in breast cancer initiation and progression is largely context dependent. Numerous studies have surfaced revealing how genetic modulation

of core ATGs or pharmacological modulation of the autophagic process can have differing effects on breast cancer cells and tumors depending on the model.

Autophagy in tumor suppression

The tumor-suppressive roles of autophagy in breast cancer have been studied in the context of the core autophagy gene, BECN1. Early studies by Beth Levine and colleagues showed that increased basal and starvation-induced autophagy through induced expression of BECN1 in the luminal A breast cancer cell line, MCF-7, reduced cell growth and clonogenicity *in vitro*, and impaired tumor formation in murine models[53]. In HER2-positive breast cancer cell lines, genetic knock-in of a BECN1 mutant with reduced Bcl2-binding affinity bypassed HER2-mediated suppression of autophagy and impaired tumor formation. Further, expression of the autophagy-inducing peptide, Tat-Beclin1, led to an induction of autophagic flux and mitigated the growth of HER2-positive breast tumor xenografts in mice [54].

Other ATG genes have also been implicated as tumor suppressors in cell line and murine models of breast cancer. Studies in mice revealed that genetic ablation of core ATG genes, like ATG12 and ATG5, in PyMT tumor cells impaired autophagy and increased the formation of metastatic lesions *in vivo*. Genetic induction of autophagy through stable depletion of RUBCN, a negative regulator of autophagy, in PyMT cells inhibited tumor metastases and subsequent deletion of ATG7 restored metastatic outgrowth in mice. Of note, inhibition of stromal autophagy through systemic deletion of ATG12 or chloroquine treatment did not impact metastatic outgrowth of tumors, supporting a role for tumor cell autophagy in mitigating the metastatic potential of breast tumors[55]. ATG7 overexpression in cell line models of TNBC was also previously shown to mitigate tumor progression by promoting apoptosis, and impair cell proliferation, aerobic glycolysis, and cell migration[56].

Autophagy in tumor promotion

Autophagy is primed as an attractive therapeutic target for the treatment of cancers, like breast, given its tumor-promoting potential. Several pre-clinical studies have explored the therapeutic benefits of autophagy inhibition in overcoming treatment resistance and potentiating treatment responses in breast cancer models[40]. Epirubicin-resistant TNBC cells were found to exhibit elevated basal autophagy levels, and

pharmacological inhibition of autophagy, through hydroxychloroquine or chloroquine treatment, increased the sensitivity of resistant cells to epirubicin and led to a significant reduction in *in vitro* cell viability and *in vivo* tumor growth [57]. Interestingly, genetic loss of BECN1 in the triple-negative breast cancer cell line, MDA-MB-231, led to an impairment in cell proliferation, colony formation, and cell migration[58], suggesting differential roles of BECN1 in breast tumorigenesis that may be dependent on the breast cancer subtype. Genetic inhibition of autophagy through knockdown of the ubiquitin-like autophagy protein, LC3, increased the sensitivity of trastuzumab resistant HER2-positive breast cancer cells to trastuzumab, highlighting a role for LC3-mediated autophagy in trastuzumab resistance[59]. Genetic knockdown of ATG12 [60] or ATG4B [61] was also shown to increase the sensitivity of resistant HER2-positive breast cancer cells to trastuzumab treatment. Gefitinib treatment was found to induce autophagic flux in breast cancer cells and treatment with the autophagy inhibitors, hydroxychloroquine or bafilomycin A1, potentiates the efficacy of gefitinib, leading to greater reductions in cell viability and induction of apoptosis[62]. Similarly, pharmacological inhibition of autophagy through 3-MA or bafilomycin A1 augmented the effects of gefitinib treatment, leading to greater reductions in TNBC cell viability and colony formation *in vitro*, and significant reductions in tumor growth in TNBC cell line-derived xenografts[63] .

Autophagy has also been found to promote metastases in breast cancer cells[64]. Pharmacological inhibition of autophagy with hydroxychloroquine significantly reduced the viability of dormant breast cancer cells and impaired their ability to switch from a dormant-to-proliferative state. Additionally, genetic knockdown of ATG7 or HCQ treatment in breast cancer cells also led to a significant reduction in lung metastases in mice[65]. In RAS-transformed MCF10A cells, genetic knockdown of ATG7 or ATG12 inhibited the secretion of interleukin-6, a pro-migratory factor, and significantly impaired cell migration and pulmonary metastases[66].

Autophagy plays an important role in cellular survival under conditions of nutrient stress[67]. Studies also observed that bafilomycin A1-treated MDA-MB-231 cells presented with a significant decrease in cell viability and increase in apoptosis between 12 to 24 hours of amino acid starvation. Of note, a transient increase in total amino acid levels was observed following 6 hours of amino acid starvation and dropped significantly at 12 hours. This transient surge in total amino acids was abolished following bafilomycin treatment of starved MDA-MB-231 cells, supporting a role for autophagy in the provision

of amino acids during early stages of nutrient stress in breast cancer cells to sustain viability and mitigate apoptosis[68]. In line with total amino acid levels, the maintenance of cellular ATP in MDA-MB-231 cells during early time points of amino acid starvation was also diminished following bafilomycin treatment[68]. In addition to its role in trastuzumab resistance, the core autophagy cysteine protease, ATG4B, has also been found to promote survival under conditions of nutrient starvation in HER2-positive breast cancer cell lines [61].

1.3.3. Autophagy inhibition as a therapeutic avenue in breast cancer

Currently available tools for autophagy inhibition

Genetic tools, like small interfering RNAs (siRNAs) and small hairpin RNAs (shRNAs) that target select ATGs, have been employed in pre-clinical studies to inhibit autophagy in cancer cells. Similarly, a number of pharmacological inhibitors that target specific stages of the autophagy process have also been developed and used successfully to impair autophagy in pre-clinical cancer models[40,69,70]. Although these genetic and pharmacological approaches have yielded promising results in cancer cells and murine tumor models, including breast, their therapeutic potential in the clinic remains to be determined.

Autophagy inhibitors in breast cancer clinical trials

The therapeutic utility of the lysosomotropic agents, chloroquine and hydroxychloroquine has been evaluated in a number of breast cancer clinical trials. Hydroxychloroquine and chloroquine inhibit autophagy by interfering with the acidification of lysosomes, thereby impairing autophagosome-lysosome fusion[40]. A phase 2 clinical trial found that chloroquine treatment alone in breast cancer patients was not associated with any substantial clinical benefit. No significant changes in Ki67, a cell proliferative marker, were observed and approximately 15% of patients withdrew from grade 1 adverse effects[71]. Interestingly, another clinical trial involving the surgical removal of breast ductal carcinoma in situ (DCIS) lesions from breast cancer patients treated with chloroquine found that these DCIS lesions presented with reduced proliferating cell nuclear antigen (PCNA) indices and mammosphere formation ability and were unable to generate tumors in mice[72]. The efficacy and safety of chloroquine in combination with taxanes was also previously evaluated in a clinical trial involving breast

cancer patients presenting with advanced or metastatic anthracycline-resistant breast cancers. Results from this phase 2 clinical trial were promising, with patients demonstrating an objective response rate of 45.16%, with only 13.15% of patients experiencing severe adverse effects[73]. Several clinical trials evaluating the use of hydroxychloroquine in combination with chemotherapy or targeted therapies in breast cancer patients are also currently underway (http://clinicaltrials.gov/).

Currently, the only FDA-approved autophagy inhibitors evaluated as part of clinical trials are chloroquine and hydroxychloroquine. Given their properties as lysosomotropic agents, the effects of chloroquine and hydroxychloroquine are not just limited to perturbing lysosome-mediated degradation of autophagic cargo. The acidity of vesicles derived from endocytic and secretory pathways can also be perturbed by the effects of chloroquine and hydroxychloroquine, and lead to off-target effects outside of the autophagy pathway[74]. Although early phase clinical trials in breast cancers that have concluded so far are promising, there is certainly a need to expand our available repertoire of tools for autophagy inhibition in the clinic. In addition, the lack of reliable biomarkers for the identification of breast cancer patients, and cancer patients in general, that may benefit from autophagy inhibition remains a pending issue[75,76].

1.4. The ATG4 family of proteins

Autophagy-related genes are evolutionarily conserved across most eukaryotic systems. The yeast Apg4/Aut2 protein, now termed the Atg4 protein, was first identified as a novel cysteine protease that interacts with and processes newly synthesized yeast Atg8 proteins to facilitate autophagy[77,78]. There are currently 4 reported human homologs of the Atg4 cysteine protease, namely ATG4A, ATG4B, ATG4C, and ATG4D[79,80]. The ATG4 proteins are core cysteine proteases that mediate the processing and subsequent deconjugation of ATG8 proteins during the autophagy process[80]. Unlike in yeast which only possesses a single Atg8, a number of human ATG8 homologs have been identified and can be classified into two subfamilies, namely the MAP1LC3 family (LC3A, LC3B, LC3B2, LC3C) and the GABARAP family (GABARAP, GABARAPL1, GABARAPL2)[81,82]. Both the LC3 and GABARAP proteins are important for the autophagic machinery, but differ in their exact roles during autophagosome biogenesis, where LC3 proteins are important for membrane elongation[83] while GABARAP proteins play crucial roles in autophagosome-lysosome fusion event[84].

1.4.1. Structure of ATG4 proteins

Of the four ATG4 paralogs in humans, crystal structures for ATG4A (PDB: 2P82) and ATG4B (PDB: 2C7Y) have been reported. Although structures for ATG4C and ATG4D have not yet been resolved, studies have successfully generated homology models of these paralogs using ATG4B as a template[85]. A core structural characteristic of all four ATG4 family members is the presence of a C54 peptidase domain comprising of a catalytic triad of aspartate, cysteine, and histidine residues[85–88] (Figure 1.4).

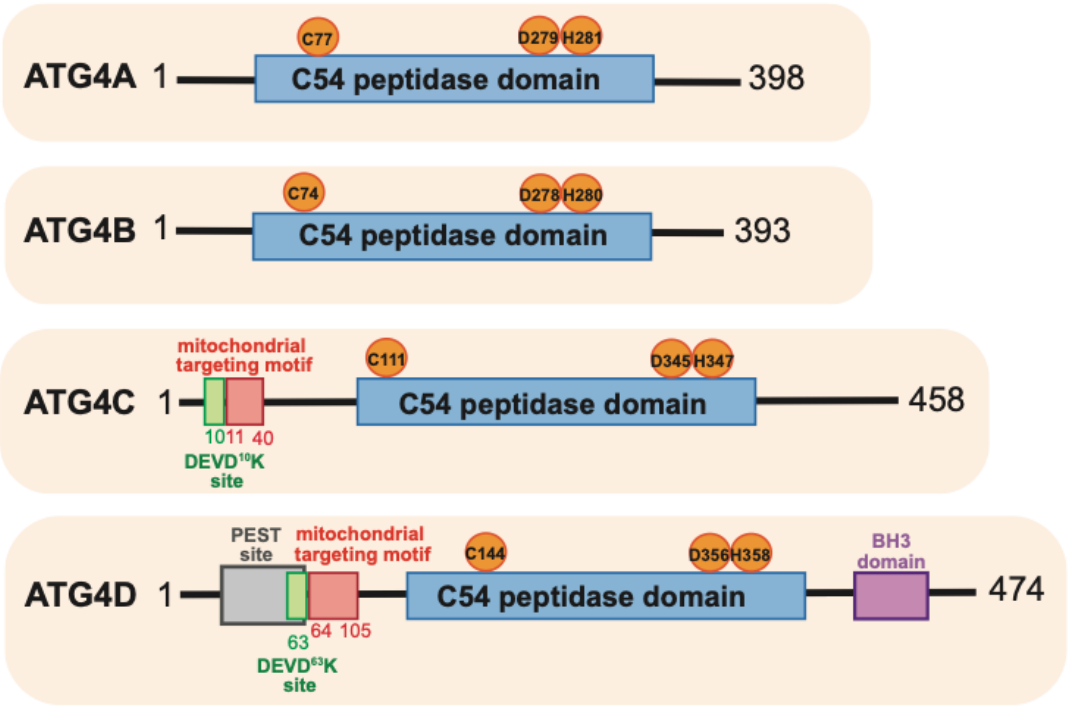

Figure 1.4 Overview of the structures of the four human ATG4 proteins
ATG4 proteins are cysteine proteases that possess a C54 peptidase domain consisting of 3 core residues: cysteine, aspartate, and histidine. ATG4C and ATG4D possess mitochondrial targeting motifs and DEVD sites at their N-terminal end. DEVD sites are cleaved by caspases to induce activation of the priming activities of ATG4C and ATG4D. Additionally, ATG4D possesses a putative N-terminal PEST site, suggesting regulation by the proteasome, and a putative C-terminal BH3 domain, suggesting regulation of apoptosis. Derived from data and information provided in Kauffman et al. 2018[88] and Sathiyaseelan, 2022[89].

Of note, it has been reported that ATG4B takes on a papain-like fold and possesses a catalytic triad consisting of the residues cysteine 74, histidine 280 and aspartate 278 [90,91]. Unbound ATG4B exists in an auto-inhibited state, with both the N-

terminal tail of the cysteine protease and an inhibitory loop masking the catalytic site. Structural studies revealed that LC3 binding induces a large conformational change in ATG4B, which relinquishes the sequestration of the entrance and exit of the catalytic triad by the inhibitory loop and N-terminal tail respectively[92]. This allows for substrate entry into the active site for catalysis, and concurrent binding of a second non-substrate LC3 by the N-terminal tail to stabilize its open conformation[92].

The structure of ATG4B is also comprised of sequence motifs that interact with LC3 and GABARAP proteins, termed LC3-interacting regions (LIRs). Studies have identified a C-terminal LIR motif on ATG4B that interacts with both LC3 and GABARAP proteins and is important for efficient substrate cleavage[93]. This FEIL C-terminal LIR motif on ATG4B is completely conserved at the functional level in ATG4A, but only partially conserved in ATG4C and ATG4D (FVLL and FVFL)[93].

1.4.2. Function of ATG4 proteins

In mammalian systems, the ATG4 proteins facilitate the initial priming of ATG8 proteins, by cleaving pro-ATG8 proteins at their c-terminal end to reveal a glycine residue (Figure 1.5). Through the concerted actions of ATG7 (E1), ATG3 (E2) and the ATG12-ATG5-ATG5 complex (E3-like), cleaved ATG8 (ATG8-I) is conjugated to phosphatidylethanolamine on the surface of growing phagophores (ATG8-II) to facilitate proper and efficient autophagosome formation[80,88]. Indeed, genetic inhibition of ATG4B activity via a C74S mutation that sequesters LC3 has been associated with defects in autophagosome membrane closure, leading to the formation of open cup-shaped phagophores[94]. ATG4 proteins also mediate the delipidation of ATG8-II transient membrane reservoirs to supply primed ATG8s to pre-autophagosome (PAS) sites, and from maturing autophagosomes to facilitate autophagosome turnover (Figure 1.5).

Studies in yeast have found that Atg4-deficient deconjugation-defective cells present with a reduction in Atg8 at pre-autophagosome (PAS) sites, an accumulation of Atg8 proteins at non-PAS sites, like the vacuoles, and a reduction in autophagic flux[95]. Expression of primed Atg8 proteins only partially restored autophagy levels, suggesting that the maintenance of an Atg8 supply in the cell is not the only function of the Atg4 deconjugation. Expression of vacuole-specific Atg4 in yeast restored Atg8 at PAS sites but was associated with an increase in Atg8 puncta and lower autophagic flux compared

to deconjugation-proficient cells. These studies suggest the deconjugation of Atg8 is important for late stages of the autophagy machinery that mediate autophagosome turnover[95]. The delipidation of Atg8-II from maturing autophagosome is a delayed and rate-limiting step that restricts Atg8-II release to the final stages of autophagosome maturation[88]. In line with this, studies in HEK293 cells showed that an irreversible increase in the deconjugation of LC3 and GABARAP proteins from autophagosomes using the Legionella bacterial enzyme, RavZ, impaired LC3 puncta formation and is associated with autophagy blockade[96], highlighting the importance of a delayed delipidation event in mammalian systems as well.

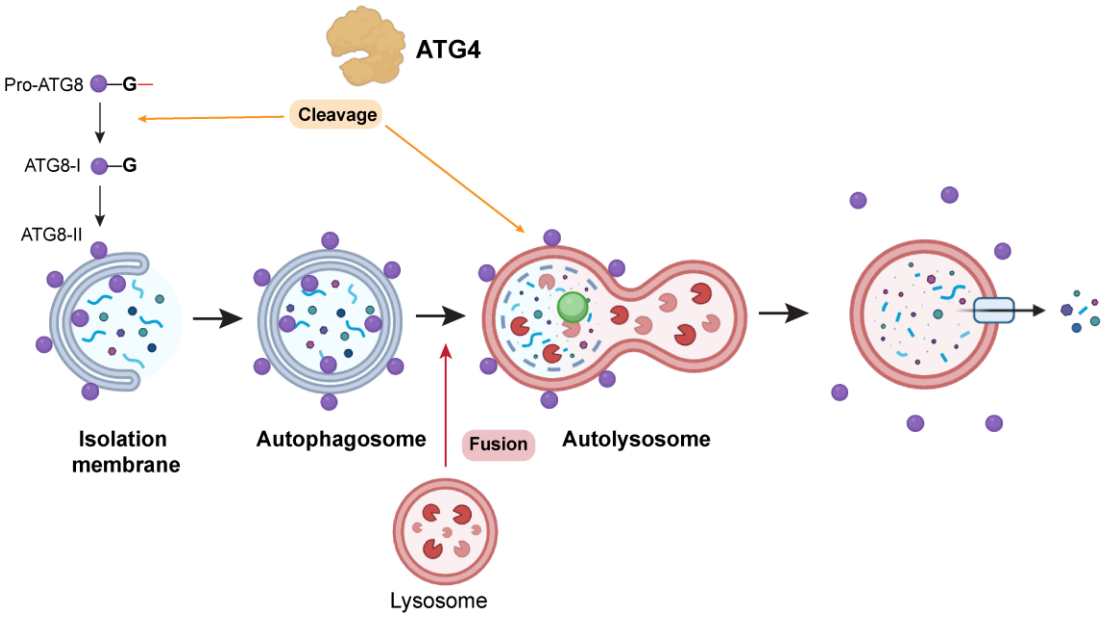

Figure 1.5 ATG4 facilitates the priming and deconjugation of ATG8 proteins
ATG4 cleaves the pro-form of ATG8 proteins to facilitate their conjugation onto the surface of autophagosomes during the autophagic process. ATG4 also mediates the delipidation of ATG8-II from the surface of maturing autophagosomes to ensure proper autophagosome turnover. Image created using BioRender. Derived from Yang, et al. 2018[8].

1.4.3. Kinetics and substrate specificity of ATG4 proteins

Of the 4 human ATG4 paralogs, ATG4B is considered the dominant cysteine protease in autophagy based on substrate processing kinetics and substrate specificity[80]. Kinetic studies involving GST-tagged LC3B, GATE-16/GABARAPL2, GABARAP and Atg8L (also known as GABARAPL1) revealed that human ATG4B possessed the highest catalytic efficiency against all 4 tested substrates. This is followed

by ATG4A, which exhibited slower catalytic activity against GATE-16/GABARAPL2, GABARAP and GABARAPL1, and very modest cleavage of LC3B. ATG4C and ATG4D possessed the lowest catalytic activities, with very modest cleavage activity against LC3B and GATE-16 and no cleavage of GABARAP or GABARAPL1[97].

In line with these observations, subsequent studies also found that ATG4B presented with high cleavage activity against soluble GABARAPL1, GABARAPL2 and LC3B. Cleavage of lipid-conjugated GABARAPL1, GABARAPL2 and LC3B by ATG4B was notably slower than the processing of the soluble forms of these proteins, supporting previous notions that the delipidation of ATG8 proteins is an intrinsically slower process compared to priming[88]. ATG4A only presented with catalytic activity against GABARAPL1 and GABARAPL2 and processed their soluble forms much slower than ATG4B. Of note, ATG4A presented with higher catalytic activity against lipidated GABARAPL1 and GABARAPL2 compared to ATG4B, suggesting that ATG4A may function more so in the delipidation step rather than the initial priming step[88]. ATG4C and ATG4D presented with little to no activity against soluble or lipidated substrates, with the exception of lipidated GABARAPL2 by ATG4C. Interestingly, truncations at the DEVD sites of ATG4C and ATG4D induced their catalytic activity against lipidated LC3B, GABARAPL1 and GABARAPL2, underscoring their role as delipidation-specific cysteine proteases[88].

1.4.4. Regulation of ATG4 proteins

The regulation of ATG4 proteins has been extensively studied at the post-translational level. Several post-translational modifications (PTMs) have been reported for human ATG4s in the literature, with a focus on ATG4B [98].

Phosphorylation

The protein kinase, MST4, phosphorylates ATG4B at serine 383, and this is associated with an increase in ATG4B activity, autophagy, and tumorigenic potential in glioblastoma cells[99]. Studies have also shown that the protein kinase, AKT1, can phosphorylate ATG4B at a serine 34 residue in hepatocellular carcinoma cells. Although this phosphorylation did not lead to any substantial effect on autophagic flux, it was associated with ATG4B mitochondrial translocation, and increased lactate production and glycolysis and reduced oxygen consumption, indicative of the Warburg effect[100].

AKT2 has also been identified as an ATG4B kinase for multiple phosphorylation sites, including serine 34, 121 and 262, and overexpression of AKT2 was associated with an increase in LC3 processing, suggesting that AKT2 may phospho-activate ATG4B[101]. The metabolic enzyme, PFKP, was also previously identified as a positive regulator of ATG4B activity and autophagy, through its phosphorylation of the ATG4B serine 34 residue under conditions of amino acid starvation[102]. ATG4B can also be regulated through phosphorylation events at serine 316 by the ULK1 kinase and PP2A phosphatase. The phosphorylation of serine 316 by ULK1 leads to an impairment in ATG4B activity and LC3B processing. Inhibition of PP2A was associated with an increase in phosphorylation at the serine 316 of ATG4B, suggesting that it may be involved in removing inhibitory phosphorylation modifications deposited at this site by ULK1[103].

O-GlcNAcylation

ATG4B can be regulated by O-GlcNAcylation modifications through glycosylation events mediated by the enzymes O-GlcNAc transferase (OGT) and O-GlcNAcase (OGA). O-GlcNAcylation modifications are deposited by OGT and removed by OGA, and the O-GlcNAcylation of ATG4B is associated with an increase in ATG4B activity. Of note, O-GlcNAcylation of ATG4B is increased under conditions of glucose depletion, suggesting that this mode of ATG4B regulation may act to enhance ATG4B activity under conditions of nutrient stress[104].

Redox

ATG4B is redox regulated through reversible oxidative modifications at two key sites, cysteine 292 and cysteine 361. The oxidation of ATG4B is associated with an impairment in ATG4B cleavage activity, whereas mutations that prevent the oxidation of cysteine 292 and 361 are associated with elevated ATG4B cleavage activity and increased autophagic flux[105].

Ubiquitination

The E3 ligase, RNF5, regulates the stability of ATG4B by ubiquitination modifications that promote the proteasome-mediated degradation of ATG4B. Indeed, genetic knockdown of RNF5 was associated with an increase in LC3 cleavage, and genetic knockout of RNF5 led to an increase in LC3-II under conditions of starvation.

LC3 puncta also increased upon RNF knockout under basal conditions, supporting a model whereby the ubiquitination and subsequent inhibition of ATG4B activity by RNF5 negatively regulates autophagy[106].

Acetylation

The acetyltransferase p300 and deacetylase SIRT2 were previously identified as regulators of ATG4B acetylation at lysine 39. P300 protein levels are markedly reduced under starvation and are associated with a significant reduction in ATG4B acetylation. In line with this, it was also observed that inhibition of SIRT2 in starved cells leads to an increase in acetylated ATG4B and p62 accumulation, and a reduction in LC3-II, suggesting that starvation induces SIRT2-mediated deacetylation to promote ATG4B activity and autophagy[107].

Proteolytic cleavage

The ATG4 homologs can be proteolytically cleaved by a number of cell death proteases. The cleavage of ATG4D by caspase-3 at a DEVA[63]K motif was found to promote the ability of ATG4D to prime and delipidate of GABARAPL1[86]. It was also previously shown that ATG4A, ATG4B, and ATG4C can be cleaved by caspase-3 and calpain-1 at varying levels in the presence of calcium ions[108], *but the functional significance of these cleavage events, especially in the case of ATG4A and ATG4V, remains poorly understood.*

1.5. ATG4B in cancer

1.5.1. ATG4B in cancer progression and survival

The role of ATG4B in cancer growth and survival has been a subject of great interest, given its role as the main cysteine protease in autophagy. In addition, studies have also examined the therapeutic benefits of ATG4B inhibition in combination with currently existing treatments to augment therapeutic efficacies.

Breast cancer

Previous studies by Bortnik and colleagues revealed that genetic knockdown of ATG4B in HER2-positive (HER2+) breast cancer cells was associated with a significant

reduction in cell viability under conditions of amino acid and growth factor starvation[61]. The observed sensitization to nutrient starvation following genetic knockdown of ATG4B was not observed in HER2-negative (HER2-) breast cancer cells, highlighting a differential role for ATG4B in modulating nutrient stress responses in HER2+ versus HER2- breast cancer cells[61]. Of note, genetic knockdown of ATG4B also suppressed autophagic flux and increased the sensitivity of both sensitive and resistant HER2+ breast cancer cells to the anti-HER2-targeted agent, trastuzumab[61]. These findings suggest that ATG4B may be important in modulating the responses of HER2+ breast cancer cells to nutrient stress and anti-HER2 targeted therapy.

Conversely, treatment of the TNBC cell line, MDA-MB-231, with the ATG4B agonist, flubendazole, induced autophagy and was associated with increased reactive oxidative species production and a significant reduction in cell proliferation [109]. Previous studies also found that expression of a dominant-negative ATG4B suppressed autophagic flux and was associated with an increase in cell migration in MDA-MB-231 cells under normoxia and hypoxia [110]. These findings suggest that that ATG4B may play a tumor suppressing role in TNBC cells by mitigating proliferation and metastases.

Other cancer types

Colorectal cancer

Genetic inhibition of ATG4B was associated with a suppression of tumor cell growth *in vitro* and *in vivo* in colorectal cancer cells. Interestingly, ATG4B knockdown led to an increase in autophagic flux, an impairment in G1/S transition, and a reduction in mTOR phosphorylation and cyclin D1 levels. Further, genetic or pharmacological inhibition of autophagy in ATG4B-knockdown colorectal cancer cells did not rescue the impairment in G1/S transition nor reduction in cyclin D1 levels. This suggests that the suppression of colorectal cancer cell growth from ATG4B inhibition is unlikely a result of autophagy modulation, but from an impairment in cell cycle progression[111].

Chronic myeloid leukemia (CML)

ATG4B inhibition was previously shown to be a potential therapeutic strategy for improving the responses of CML cells to the BCR-ABL tyrosine kinase inhibitor, imatinib. Imatinib treatment was associated with an increase in ATG4B mRNA and protein levels, and an induction in autophagic flux. It was shown that the genetic knockdown of ATG4B

and consequent reduction in autophagic flux was associated with a decrease in cell viability and increased sensitivity to imatinib in resistant CML cells. These findings suggest that ATG4B may promote imatinib resistance in CML cells through upregulation of autophagy[112].

Hepatocellular carcinoma (HCC)

Previous studies have found that inhibition of autophagy in HCC cells with the autophagy inhibitor, 3-MA, or expression of a catalytically inactive form of ATG4B, $ATG4B^{C74A}$, was associated with a reduction in HCC proliferation under conditions of hypoxia [113]. Interestingly, these autophagy-inhibited cells presented with a significant reduction in cellular ATP levels, and an increase mitochondrial membrane permeability. These changes were also coupled with a reduction in several key enzymes involved in β-oxidation. These findings suggest that ATG4B may promote the proliferation of HCC cells under hypoxic conditions, through autophagy-mediated clearance of damaged mitochondria to allow for proper mitochondrial β-oxidation to proceed and maintain cellular ATP levels [113].

Subsequent studies also revealed that autophagy also plays a role in promoting radioresistance in HCC cells, through the transcription factor Egr-1. Egr-1 was found to promote HCC survival and migration following radiation treatment, by upregulating autophagy through transcription of ATG4B. The pharmacological inhibition of autophagy, or ATG4B knockdown was associated with an increase in caspase-3 cleavage and the pro-apoptotic marker, Bax, and a reduction in the anti-apoptotic marker, Bcl-2, in HCC cells, and was reversed upon Egr-1 overexpression. Further, impairment in colony formation from autophagy inhibition was also rescued upon Egr-1 overexpression. These findings suggest that Egr-1 may also promote ATG4B-mediated autophagy to confer resistance to radiation in HCC cells[114].

1.5.2. Current tools for ATG4B inhibition

Genetic

ATG4B inhibition has been achieved in cell line models through genetic knockdown approaches, like siRNA or shRNA[40,61,111,112], or genetic knock-out by gene editing technologies, like CRISPR/Cas9[115]. Studies have also found that mutations at the

cysteine 74 site of the ATG4B catalytic triad impairs the ability of ATG4B to process ATG8 substrates, like LC3B, in cells [94,113,116]. In addition, a viable ATG4B knock-out (KO) mouse model deficient in autophagy was also previously generated, suggesting that ATG4B is dispensable for embryonic and adult development[117]. Given that evidence for residual atg4-like processing of the atg8 proteins were observed in certain tissues of atg4b-/- mice[117], it is possible that some compensation by other atg4 isoforms may have enabled survivability of these atg4b-/- mice. Reportedly, abnormalities in these mice include balancing and inner ear defects[117], lesions in the central nervous system (CNS)[118], and increased susceptibility to lung injury from ER stress[119]. Despite these abnormalities, their viability does suggest that systemic inhibition of other atg4b orthologs is unlikely lethal in other biological systems, making them candidate models for studying the effects of systemic loss of atg4b on human cancer growth and progression.

Pharmacological

Significant efforts have been made in the development of novel ATG4B inhibitors and investigating the potential of re-purposing existing compounds for ATG4B inhibition. The proposed binding sites and mechanism of action for some of these compounds are described in Table 1.1. It is important to note that, in addition to their effects on ATG4B, a number of these compounds also display some inhibitory activity against ATG4A. These include NSC18505877[120], LV320[121], S130[122], tioconazole[123], and ebelsen[124].

Table 1.1 Examples of novel and re-purposed compounds for ATG4B inhibition

Name	Proposed binding site	Mechanism of action
Novel		
NSC185058[120]	ATG4B active site	Inhibits LC3B and GABARAPL2 cleavage Inhibits autophagosome formation
UAMC-2526[125]	Not determined	Inhibits LC3 cleavage
LV320[121]	Secondary site near ATG4B regulatory loop or hinge of ATG4B n-terminal tail sequestering active site	Inhibits peptide substrate cleavage Inhibits LC3B delipidation Inhibits autophagosome-lysosome fusion
S130[122]	Binding pocket adjacent to ATG4B catalytic site	Inhibits LC3B and GABARAPL2 cleavage Inhibits LC3B delipidation

Compound 33[126]	ATG4B active site	Inhibits LC3B delipidation
Re-purposed		
Tioconazole[123]	ATG4B active site	Inhibits LC3B and GABARAPL2 cleavage Inhibits LC3B delipidation Inhibits autophagosome-lysosome fusion
Xanthium strumarium fruit extract[127]	Not determined	Inhibits LC3B and GABARAPL2 cleavage Inhibits LC3B delipidation
Ebelsen[124]	ATG4B active site	Inhibits GATE-16 and LC3B cleavage Inhibits autophagosome degradation

Partially adapted from Ho and Gorski, 2019[40]

1.6. Crosstalk between autophagy and cancer metabolism

1.6.1. Metabolic reprogramming is a hallmark of cancer

The alteration of metabolic processes in cancer cells to support tumor initiation and progression is recognized as a hallmark in cancer contexts.

Glucose metabolism

Glucose is a major carbon source in cells and is used to produce energy in the form of adenosine triphosphate (ATP) through cellular respiration under aerobic conditions. Cellular respiration involves 3 concerted steps, namely glycolysis, the tricarboxylic acid (TCA) cycle and oxidative phosphorylation (OXPHOS) [128]. Glycolysis produces 2 molecules of ATP per glucose molecule, and generates pyruvate, which enters OXPHOS to produce 32-34 ATP molecules per glucose. In the absence of oxygen, cells rely on glycolysis for ATP production, fermenting pyruvate to lactate, in a process termed anaerobic glycolysis[128].

One of the first instances of metabolic reprogramming in cancer was the observation that cancer cells preferentially undergo glycolysis under aerobic conditions. This was named the Warburg effect by Efraim Racker in 1972[129], and was first described by Otto Warburg and colleagues in the early 1920s[130]. Warburg observed that human and rat carcinomas presented with high glycolytic activity, characterized by increased

lactate production, under both aerobic and anaerobic conditions[130]. Glycolysis is an inherently inefficient process for producing ATP, and the basis for its preferential use by tumor cells to generate ATP remains a subject of great interest. It has been proposed that elevated glycolytic activity in cancer cells may aid in the generation and flux of glycolytic intermediates and electron carriers that can be utilized in key tumor-promoting anabolic pathways[131]. Although amino acids have been attributed as the main contributors to cell biomass[132], increased lactate production may also facilitate tumor cell proliferation through the incorporation of carbon into cellular biomass[131]. Reactive oxidative species is produced as a by-product of the OXPHOS electron transport chain (ETC) which occurs on the mitochondrial membrane. The reliance on glycolysis for energy production in both aerobic and anaerobic conditions in cancer cells has also been also been proposed as a means to reduce cellular levels of reactive oxidative species produced by OXPHOS[133], which may help mitigate tumor-suppressive oxidative stresses in some contexts[134].

Glutamine metabolism

Glutamine is a major source of both carbon and nitrogen, and contributes to metabolic processes, like the TCA cycle and nucleotide biosynthesis[135]. Studies have found that, in pancreatic cancer cells, a variant of the mitochondrial glutamine transporter, SLC1A5, which lacks exon 1, facilitates the catabolic breakdown of glutamine in the mitochondria to produce several key TCA intermediates and ATP, and promotes redox homeostasis by promoting glutathione synthesis and suppressing cellular reactive oxidative species[136]. This study presents an intriguing role for glutamine in sustaining mitochondrial respiration under the Warburg effect. While glucose is directed towards aerobic glycolysis in cancer cells, glutamine undergoes glutaminolysis to generate metabolites that feed into the TCA cycle and, subsequently, fuel OXPHOS to produce ATP[136].

Glutamine also contributes to the *de novo* synthesis of nucleotides, like purines and pyrimidines, through its role as an amide donor. In *de novo* purine biosynthesis, glutamine is used to generate inosine monophosphate (IMP) in two steps of the pathway, namely the conversion of phosphoribosyl pyrophosphate (PRPP) to phosphoribosylamine (PRA) and phosphoribosyl-N-formylglycineamide (FGAR) to 5′-phosphoribosylformylglycinamidine (FGAM). IMP can be converted to adenosine

triphosphate (ATP) or guanosine triphosphate (GTP) via two parallel and distinct pathways, and glutamine is utilized in GTP production during the conversion of xanthosine monosphate (XMP) to guanosine monophosphate (GMP). In *de novo* pyrimidine biosynthesis, glutamine is used to generate to carbamoyl phosphate, which facilitates the synthesis of the pyrimidine nucleotide, uridine monophosphate (UMP). Glutamine is also utilized in the conversion of uridine triphosphate (UTP) to the pyrimidine nucleotide cytidine triphosphate (CTP)[135].

The upregulation of *de novo* nucleotide biosynthesis is a feature observed in certain cancer contexts. Of note, studies have observed an increase in the *de novo* purine biosynthesis enzyme, PPAT, and a decrease in the glutaminolysis enzyme, GLS1, in human fibroblast cell line models of malignant progression[137]. These cells also presented with increased production of several key purine nucleotides, like IMP, AMP, GMP and UMP, and a decrease in the production of TCA intermediates, like alpha-ketoglutarate and fumarate. GLS1 overexpression was associated with an increase in alpha-ketoglutarate production, and a corresponding decrease in IMP, AMP, GMP, glutamate and aspartate production. Further, GLS1-overexpressing cells were not viable under glutamine-deprived media and formed significantly smaller tumors in mice. Knockdown of PPAT led to a decrease in AMP, IMP and GMP production, and an increase in alpha-ketoglutarate production. These metabolic changes were also associated with a significant reduction in proliferation and smaller tumors in mice[137]. *Together, these findings suggest that the metabolic fate of glutamine pivots from anaploresis to functioning as an amide donor in de novo nucleotide biosynthesis during tumor progression.*

Nucleotide metabolism

Purine and pyrimidine nucleotides in the cell can be produced by the *de novo* or the salvage pathways. Cell division is generally coupled with a substantial increase in nucleotide triphosphate levels. As such, the *de novo* pathway is required to meet the high nucleotide demands of proliferating cells[138], and is considered the primary pathway utilized to sustain nucleotide pools in proliferating cells, like cancer [139,140].

Indeed, studies have found that radiation-resistant glioblastoma cells possess elevated levels of purines and purine nucleotides and suppressing GTP biosynthesis by inhibiting the rate-limiting purine metabolic enzyme, IMPDH, using the pharmacological

agent, mycophenolic acid (MPA), increases the sensitivity of resistant glioblastoma cells to radiation therapy. Of note, inhibition of the *de novo* pyrimidine enzyme, DHODH, did not increase the sensitivity of resistant glioblastoma cells, suggesting that cellular purine levels are what confer resistance to radiation therapy in glioblastoma[141]. Independently, studies have found that treatment of TNBC cells with the chemotherapy agent, doxorubicin, is associated with an increase in the levels and production of pyrimidine nucleotides. Further, glutamine deprivation suppressed the observed increases in pyrimidine nucleotides upon doxorubicin treatment, suggesting that pyrimidine biosynthesis is upregulated in response to doxorubicin treatment in TNBC. Indeed, inhibition of *de novo* pyrimidine pathway enzymes, CAD and DHODH, increased the sensitivity of TNBC cells to doxorubicin[142], underscoring a potential importance of the de novo pyrimidine biosynthesis pathway in chemosensitivity. Studies in breast cancer cell lines also found that the expression of several key enzymes involved in nucleotide metabolism, including IMPDH1, IMPDH2 and GMPS, are promoted by gain-of-function mutant p53. Genetic knockdown of mutant p53 was associated with a reduction in ATP, GTP, and other deoxynucleotides[143]. Knockdown of GMPS, which facilitates the conversion of XMP to GMP, was associated with a reduction in GTP levels, and substantial decrease in cell invasion in vitro, and a decrease in tumor metastases *in vivo*[143]*.* Metabolite profiling of colorectal cancer patient derived xenografts (PDXs) revealed an increase in several metabolites involved in pyrimidine biosynthesis in metastatic PDXs. Further, inhibition of DHODH using the pharmacological inhibitor, leuflunomide, was associated with a significant impairment in colorectal cancer cell growth under conditions of hypoxia[144]. Genetic depletion of DHODH was also associated with colorectal cancer liver metastases[144]. *Together, these studies support roles for purine and pyrimidine biosynthesis in therapy resistance and metastases in cancer cells.*

Studies have also surfaced suggesting that the salvage pathway may also be important in modulating cancer cell growth. It was found that treatment of lung and breast cancer cell lines with oleanolic acid (OA) led to an impairment in cell growth and a significant reduction in purine salvage pathway metabolites *in vitro* and *in vivo*. This was proposed to be a result of OA treatment leading to the inactivation of the SOD1 superoxide dismutase, resulting in increased cellular reactive oxidative species and, consequently, the induction of autophagy-mediated degradation of HPRT1 and 5'NT[145]. These findings highlight a potential role for the purine salvage pathway in cancer growth,

and *a need for greater understanding of the roles of the nucleotide salvage pathway in cancer progression and survival.*

1.6.2. Autophagy as a source of metabolic substrates

It is well-established that autophagy is induced in response to various forms of nutrient stress and is essential for survival under such nutrient limiting conditions. Notably, genetic loss of core components of the autophagy conjugation machinery, like ATG5 and ATG7[146,147], have been associated with suckling defects in newborn mice and subsequent neonatal lethality, underscoring the importance of autophagy in the neonatal starvation period following the severance of nutrient supply from the maternal placenta[148]. The effect of autophagy modulation on levels and flux of metabolites, like amino acids, nucleotides, fatty acids, and NAD^+/NADH, have also been examined in eukaryotic model systems, and are described in this chapter.

Amino acids and nucleotides

Cancer cells

Previous studies in KRAS-driven lung cancers revealed that genetic loss of ATG7 led to a significant decrease in several metabolites involved in the TCA cycle and pentose phosphate pathway under conditions of starvation[149]. Glutamine supplementation was associated with a greater replenishment of the levels of several key TCA intermediates, like alpha-ketoglutarate and pyruvate, in ATG7-deficient cells compared to ATG7-proficient cells. Further, starved ATG7-deficient cells also presented with a significant decrease in adenylate energy charge, which was restored upon glutamine supplementation[149]. Total nucleotide pools were significantly lower in starved ATG7-deficient cells compared to wild-type cells, and this was associated with significantly higher levels of purine and pyrimidine bases, suggesting an increase in nucleotide catabolism. Indeed, supplementation of starved ATG7-defiicent cells with glutamine or purine and pyrimidine bases rescued growth defects, adenylate energy charge, and nucleotide levels[149]. *Together, these findings show that autophagy sustains cellular metabolite levels to support growth under nutrient stress conditions in lung cancer cells.*

The role of autophagy in sustaining amino acid and ATP levels during nutrient stress was also previously investigated in the TNBC cell line model, MDA-MB-231. Amino acid deprivation led to a significant reduction in cell proliferation and viability, and increase in cell death, and this was associated with an induction of autophagic flux. Of note, amino acid levels increased following short term amino acid deprivation but decreased substantially when amino acid deprivation was prolonged[68]. Inhibition of autophagy with bafilomycin A1 or genetic knockdown of ATG5 was associated with a significant decrease in amino acid and ATP levels during early time points of amino acid deprivation. Inhibition of the amino acid catabolism enzyme complex BCKDH led to a significant increase in branch-chained amino acid levels during early time points of amino acid starvation, which was reversed upon autophagy inhibition. Of note, free fatty acid levels also increased following short term amino acid starvation and were inhibited upon autophagy inhibition. Although glucose uptake also increased upon amino acid starvation, the effect of autophagy inhibition remains to be determined[68]. *Together, these findings show that autophagy provides metabolic substrates, like amino acids, during early stages of nutrient stress which are then catabolically broken down to generate ATP in TNBC cells.*

Interestingly, the genetic inhibition of autophagy in PDAC cells was also linked to a significant decrease in intracellular cysteine levels under nutrient-replete conditions[150]. This was associated with the translocation of the cysteine transporter, SLC7A11, away from the plasma membrane and to lysosomes in the cytosol, and a reduction in overall SLC7A11 activity. It was further determined that mTORC2 phosphorylates SLC7A11 to promote its localization with lysosomes when autophagy is inhibited. The significance of the localization of SLC7A11 to the lysosomes in the absence of functional autophagy remains to be determined[150]. *Findings from these studies show that autophagy is important for the proper localization and function of the cysteine transporter, SLC7A11, to maintain cysteine levels in pancreatic ductal adenocarcinoma cells.*

Yeast

Studies in yeast previously showed autophagy-defective Δ*atg7* yeast cells presented with an impaired ability to restore protein synthesis activity and total amino acid levels at later time points of nitrogen starvation. Supplementation of nitrogen starved Δ*atg7* cells with free amino acids restored defects in protein synthesis and

amino acid pools to levels comparable to wild type[151]. *These findings suggest that autophagy is important in sustaining amino acid levels for protein synthesis during conditions of nitrogen starvation in yeast.*

Subsequent studies in yeast also revealed that autophagy is important in facilitating the breakdown of RNA and subsequent excretion of superfluous nucleobases during nitrogen starvation. The transient increase in adenosine, guanosine, cytidine, and uridine under autophagy-inducing conditions in wild-type yeast cells was abolished following genetic perturbation of autophagy. Similarly, genetic deletion of the yeast vacuolar proteases, Pep4 and Prb1, was also associated with an impaired ability to increase nucleosides under nitrogen starvation[152]. It was determined that the vacuolar RNAse Rny1 and nucleotidase Pho8 are important for the degradation of RNA. Rny1 converts encapsulated RNA within vacuoles to 3'-NMPs, which are then subsequently broken down to nucleosides by Pho8. Indeed, nitrogen starvation was associated with an increase in Pho8 and Rny1 protein levels. Genetic deletion of Rny1 led to a significant accumulation of RNA-containing vacuoles, and further deletion of Atg2 prevented the accumulation of these RNA-containing vacuoles. It was proposed that the nucleosides generated from autophagy are then broken down further into nucleobases, like hypoxanthine and xanthine, in the cytosol by the nucleosidases Pnp1 and Urh1, and released into extracellular space[152]. Characterization of nucleoside and nucleobase changes revealed that the transient increase in nucleoside levels in nitrogen-starved yeast cells was associated with a subsequent increase in nucleobases, like hypoxanthine and xanthine, and not seen in Δ*atg2* yeast cells[152]. As ammonia is released during RNA catabolism[153], *these findings suggest that autophagy facilitates the catabolic breakdown of RNA to release ammonia as a nitrogen source and this is paired with the release of superfluous nucleobases to maintain cellular homeostasis under nitrogen starvation.*

Fatty acids

Cancer cells

The role of autophagy in the maintenance of free fatty acid levels was also previously described in acute myeloid leukemia cells. Genetic or pharmacological inhibition of autophagy was associated with accumulation of cytosolic lipids that resemble lipid droplets. Fatty acid oxidation (FAO) rates, oxygen consumption rates

(OCR) and mitochondrial ATP levels were also significantly reduced in autophagy-inhibited acute myeloid leukemia cells, suggesting a decrease in oxidative phosphorylation (OXPHOS)[154]. Inhibition of OXPHOS with metformin, a mitochondrial electron transfer chain (ETC) complex I inhibitor, was associated with a reduction in autophagy and mitochondria-endoplasmic reticulum contact sites (MERCS). Genetic knockdown of proteins involved in the formation of MERCS led to a significant decrease in autophagy and OXPHOS, and an accumulation of lipid droplets in acute myeloid leukemia cells. Genetic knockdown of VDAC1, which facilitates MERCS formation, in combination with the ETC complex I inhibitor, IACS-010759, was associated with a reduction in autophagy flux and cell proliferation *in vitro* and *in vivo*[154]. *Together, these findings suggest that autophagy is important in the catabolic breakdown of lipids for FAO and OXPHOS in acute myeloid leukemia cells.* Findings from these studies also revealed that mitochondrial oxidative phosphorylation regulates the formation of MERCS, which in turn promote autophagy to provide free fatty acids for FAO and OXPHOS.

NAD^+ and NADH

Murine fibroblast cell lines

Metabolite profiling studies on wild-type and $atg5^{-/-}$ murine embryonic fibroblast cells revealed that genetic inhibition of autophagy was associated with a significant depletion in cellular levels of NADH and NAD^+. Notably, growth of $atg5^{-/-}$ cells in galactose media to induce mitochondrial OXPHOS triggered caspase-mediated cell death, and could be rescued by hypoxia or treatment with the mitochondrial pyruvate carrier inhibiter, UK-5099[155]. NAM or NAM riboside supplementation restored NAD^+ and NADH levels and rescued the survival of $atg5^{-/-}$ cells. $Atg5^{-/-}$ cells also presented with increased mitochondrial defects and accumulation of damaged mitochondria, resulting in the hyperactivation of SIRT and PARP enzymes that catabolize NAD, thereby depleting cellular NAD^+ and NADH levels. Indeed, these observations could be recapitulated in mitophagy-deficient cells and rescued with NAM supplementation. *Together, these findings suggest that autophagy is important in actively respiring cells to mitigate the accumulation of mitochondrial defects and, consequently, cellular stresses that lead to the depletion of cellular NAD^+ and NADH levels.*

1.6.3. Metabolic regulation of autophagy in cancer

Energy sensors

Autophagy is activated in response to myriad of metabolic stresses. The AMPK and mTORC1 proteins are classic examples of cellular energy sensors that respond to varying nutrient levels in the cell by regulating autophagy.

AMPK

AMPK is a central energy sensor that plays important roles in the regulation of various metabolic processes in response to energy imbalances in the cell. Of note, AMPK is an important regulator of autophagy in response to nutrient stress. Under conditions of low energy levels or nutrient starvation, AMPK is phosphorylated and activated by upstream kinases, like LKB1. Activated AMPK inhibits mTORC1 activity by phosphorylating TSC2, which promotes GAP activity of the TSC1/2 complex, and results in inactive RHEB-GDP[156]. This prevents RHEB-mediated activation of mTORC1. The phosphorylation of RAPTOR by AMPK also prevents RAPTOR from binding to mTORC1, thereby further inhibiting mTORC1 activation. The inhibition of mTORC1 prevents mTOR-mediated phosphorylation and inhibition of ULK1, an important autophagy protein involved in the formation of the initiation complex of the autophagic machinery. Instead, ULK1 is phosphorylated and activated by AMPK, and this in turn promotes the formation and activation of the ULK1 initiation complex[156]. Additionally, AMPK also phosphorylates BECN1 to promote the activity of the VPS34 nucleation complex[157].

Of note, recent studies have also presented evidence suggesting that AMPK may also suppress autophagy under conditions of starvation[158]. It was found that the phosphorylation of ULK1 by AMPK at distinct sites stabilizes the interaction between ULK1 and AMPK to suppress autophagy, and this is proposed to allow for subsequent re-activation when cellular stress conditions are alleviated. The interaction between AMPK and ULK1 was found to confer protection of ULK1 from caspase-mediated degradation, thereby mitigating the induction of cellular apoptosis during glucose or amino acid starvation[158].

mTORC1

In the absence of nutrient stress, mTORC1 suppresses autophagy by phosphorylating and inactivating ULK1 at serine 758, thereby preventing ULK1 from interacting with AMPK[156]. mTORC1 also suppresses autophagy by phosphorylating and inactivating a number of other autophagy proteins, including ATG13[159], AMBRA1[160], and ATG14[161]. ATG13 and ATG14 are important components of the ULK1 complex and VPS34 nucleation complex respectively[16]. AMBRA1 is a BECN1 cofactor that helps regulate the activity of the VPS34 nucleation complex[16].

Metabolite deficiencies and surpluses

Autophagy can be regulated by deficiencies or surpluses in cellular metabolites. Through its roles in cellular recycling and degradation, autophagy helps counter these perturbations to maintain homeostasis under physiological conditions[162].

Glucose

Studies have found that AMPK is activated following glucose starvation and is associated with an induction in autophagy and increase in the formation of PI5P-positive autophagosomes. The autophagy protein ULK1 is activated by AMPK and was found to phosphorylate PIKfyve, a PI5P-producing lipid kinase, at its S1543 site to promote its activity[163]. Indeed, expression of a phosphomutant of PIKfyve (S1548A) in HeLa cells was associated with significantly reduced autophagosome and autolysosome formation compared to cells transfected with wild-type PIKfyve or PIKfyve with a phosphomimic mutation at its ULK1 phosphorylated site (S1548D) under both basal and glucose deprivation. Expression of wild-type or S1548D PIKfyve in cells was associated with an increase in autophagy, and pharmacological inhibition of ULK1 led to a blockade in autophagy induction following the expression of either vector [163]. *These findings suggest that autophagy is induced as a result of glucose deprivation through the activation of AMPK and ULK1, and the subsequent induction of PIKfyve-mediated autophagosome formation.*

Other studies have also found that glucose may promote autophagy flux in certain contexts. The induction of autophagy was observed following glucose supplementation in serum-free media in several cell line models, including HeLa and HEK-293 cells. Glucose supplementation was associated with dose-dependent

increases in cellular ATP, and the impairment of ATP production by pharmacological inhibition of lactate dehydrogenase was associated with a decrease in autophagosome formation[164]. Of note, supplementing cells with glucose did not activate AMPK or mTOR but did increase the activity of p38 MAPK and promote its translocation to nucleus. Indeed, genetic knockdown of p38 MAPK, or pharmacological inhibition of p38 MAPK or MK2, a kinase downstream of p38 MAPK, reduced the ability of glucose to upregulate autophagy in serum-deprived cells[164]. *These findings suggest that glucose may promote ATP production and p38 MAPK activity to induce autophagosome formation and autophagy in serum-deprived cells.*

Glutamine

Glutamine is an important amino acid utilized in cells for both the TCA cycle and nucleotide biosynthesis. Studies have found that pancreatic ductal adenocarcinoma cells deprived of glutamine presented with an increase in autophagy and a decrease in several TCA cycle intermediates. Of note, inhibition of glutamine synthetase did not increase autophagy, suggesting that the upregulation of autophagic flux in response to glutamine deprivation is likely a compensatory response to nutrient stress [165]. Indeed, treatment of glutamine deprived pancreatic ductal adenocarcinoma cells with the autophagy inhibitor, chloroquine, further decreased intracellular glutamine levels and was associated with a greater reduction of pancreatic ductal adenocarcinoma cell survival. *These findings suggest that low glutamine levels induce autophagy as a nutrient stress response to replenish cellular glutamine levels and TCA cycle intermediates and support pancreatic ductal adenocarcinoma cell survival.*

Studies have also found that autophagy is activated under glutamine deprivation to replenish serine levels for one-carbon metabolism in glioma cells. Glutamine deprivation was associated with an increase in glycine and serine levels in glioma cells, and genetic knockdown of the one-carbon metabolism enzyme MTHFD2 inhibited cell proliferation and increased cell death of glutamine-deprived glioblastoma cells[166]. It was found that cellular serine pools were not derived from glucose under glutamine deprivation, but rather through autophagy. Indeed, tracing experiments with 13C-labelled glucose-derived metabolites showed that glutamine deprivation alone was associated with a greater increase in 12C serine and glycine levels compared to 13C-labelled fractions. In contrast, inhibition of autophagy decreased unlabelled serine and glycine

levels, and induced cell death and reduced cell proliferation of glutamine-deprived cells. Further, the combination of autophagy inhibition and glutamine deprivation also led to a decrease in several enzymes involved in one carbon metabolism, including MTHFD2[166]. *These findings suggest that glutamine deprivation induces autophagy to help replenish levels of key amino acids, like serine and glycine, that are important for one carbon metabolism, to promote growth and survival of glutamine-deprived glioma cells.*

Ammonia

Metabolites that are generated from glutamine metabolism have also been implicated in the regulation of autophagy. Glutaminolysis, which catalyzes glutamine to glutamate, releases ammonia as a by-product[167]. Studies in immortalized and cancer cell line models revealed that ammonia induces autophagosome formation and promotes both the localization of dopamine receptor DRD3 to autophagosomes and the degradation of DRD3. Elevated DRD3 expression was associated with increased sensitivity to cellular ammonia levels and autophagy induction, suggesting that it may function as an ammonia sensor[168]. Ammonia inhibited mTORC1 activity and reduced mTOR lysosomal localization, while genetic inhibition of DRD3 impaired ammonia-induced autophagy and reduced mTOR localization to lysosomes upon ammonia treatment[168]. *These findings suggest that ammonia may stimulate autophagy by promoting the autophagosomal localization and degradation of DRD3, and subsequent suppression of mTOR lysosomal localization and activation.*

Of note, the authors also reported that ammonia treatment was associated with an increase in autophagosome pH levels[168], thereby perturbing lysosomal acidification. However, assessment of LC3B-II with bafilomycin A1 or chloroquine with increasing concentrations of ammonia confirmed that ammonia does indeed induce autophagic flux, suggesting, at least with the concentrations of ammonia tested, the potential autophagy-inhibitory effect of ammonia is masked by its other autophagy-promoting effects[168]. *This finding stresses the importance of evaluating both lysosomal pH levels and additional autophagy markers, like LC3B-II, when evaluating the effects of ammonia on autophagy.*

Glutamate

It has also been shown that glutamate suppresses autophagy in nutrient-deprived neuroblastoma cells, and this was associated with an increase in excitotoxic

necrosis, as determined by increased membrane damage and rupture, and cytoplasmic vacuolization which could be reversed following treatment with an NMDA inhibitor[169]. Glutamate also inhibited the activation of AMPK activity and increase in ULK1 levels under nutrient deprivation and was associated with transcriptional suppression of a number of autophagy genes. Expression of a catalytically active AMPK or treatment with an AMPK activator restored the growth of nutrient-deprived neuroblastoma cells exposed to glutamate. Further, induction of autophagy by expressing the transcription factor, TFEB, which promotes the transcription of autophagy genes also desensitized nutrient-deprived neuroblastoma cells to glutamate[169]. *Together, these findings suggest that glutamate suppresses AMPK activity and autophagy, and this contributes to increased cell death under conditions of nutrient deprivation.*

1.6.4. Autophagy and metabolism as therapeutic targets in cancer

The reliance of cancer cells on autophagy and metabolism to fuel growth and survival make the co-inhibition of both pathways an intriguing therapeutic avenue. Strategies to target glucose and glutamine utilization of cancer cells, through inhibition of glycolysis or glutaminolysis, in combination with autophagy in cancer have been a subject of great interest in pre-clinical studies (Table 1.2).

Table 1.2 Examples of pre-clinical studies evaluating the therapeutic benefits of combined inhibition of autophagy and metabolic pathways

Metabolic process	Targeted metabolic enzyme and mode	Mode of autophagy inhibition	Cancer type	Reference
Glycolysis	HK2 inhibition by 3-BrPa, 2-DG, Ionidamine	ATG5 shRNA	Liver cancer	[170]
Glycolysis	HK2 inhibition by 3-bromopyruvate	hydroxychloroquine	Ehrlich ascites carcinoma	[171]
Glycolysis	PKM2 shRNA	3-MA	Non-small cell lung cancer	[172]
Glycolysis	HK2 inhibition by 2-DG	chloroquine	Prostate cancer	[173]
Glutaminolysis	Glutaminase inhibition by compound 968	chloroquine	Non-small cell lung cancer	[174]
Glutaminolysis	Glutaminase inhibition by compound 968	chloroquine	Colon cancer	[175]
Glutaminolysis	Glutaminase inhibition by compound 968	chloroquine, bafilomycin A1	Triple-negative breast cancer Non-small cell lung cancer	[176]

The preferential use of glycolysis over oxidative phosphorylation is a hallmark of cancer. Hexokinases mediate the first and irreversible step of glycolysis, which involves the phosphorylation of glucose to glucose-6-phosphate[177]. Of the four hexokinase isoforms, hexokinase 2 (HK2) has been the target of choice for targeting the glycolytic pathway in cancer cells. In addition to being upregulated in several cancer types, HK2 also possesses higher binding affinity for glucose, greater access to mitochondria-generated ATP, and retention of two functional catalytic sites[177]. Indeed, studies in liver cancer showed that inhibition of HK2 using pharmacological inhibitors, like 3-bromopyruvate (3-BrPA), 2-deoxy-D-glucose (2-DG) or lonidamine, in combination with genetic knockdown of ATG5 was associated with a significant reduction in cell viability *in vitro*[170]. *In vivo* studies also revealed that the combination of HK2 and autophagy inhibition significantly impaired tumor growth[170]. Co-inhibition of autophagy with hydroxychloroquine and HK2 with 3-BrPA in Ehrlich ascites carcinoma cells was also associated with a significant decrease in ascitic volume and tumor cell viability[171]. Similarly, in prostate cancer, the combined inhibition of HK2 with 3-DG and autophagy with chloroquine also led to significant tumor regression and increased tumor cell apoptosis[173]. Pyruvate kinases mediate the catalysis of phosphoenolpyruvate to pyruvate, which is the final step of glycolysis. Of the four pyruvate kinase isoforms, studies have found that pyruvate kinase M2 (PKM2) is upregulated in certain cancers and important for tumorigenesis[178]. Studies previously found that combined inhibition of autophagy and glycolysis with the pharmacological autophagy inhibitor, 3-MA, and PKM2 knockdown induced apoptosis in non-small cell lung cancer cell lines[172]. *Together, these findings provide evidence for the therapeutic potential of combined inhibition of autophagy and glycolysis in mitigating tumor growth and survival.*

The rewiring of glutamine metabolism to feed various aspects of cellular metabolism is a feature in cancer cells, the catabolic conversion of glutamine to glutamate by glutamine synthetase (GLS) is a key step that feeds into the TCA cycle[135]. Indeed, a number of studies have found that combined perturbation of autophagy and glutamine metabolism, by targeting GLS, mitigates tumor growth, proliferation and metastases in various cancers types, like non-small cell lung cancer, TNBC, and colon cancer[174–176]. It is important to note that despite the importance of glutamine in nucleotide biosynthesis and evidence of altered nucleotide metabolism in promoting

cancer growth and proliferation, *the therapeutic potential of inhibiting autophagy in combination with nucleotide biosynthesis remains poorly investigated in cancer cells.*

1.7. The IMPDH family of proteins

1.7.1. Discovery of IMPDH proteins

Early work by Abrams and Bentley[179] was one of the first to isolate and report the enzymatic function of the inosine-5'-monophosphate dehydrogenase (IMPDH) protein in rabbit bone marrow tissues. Their work revealed that IMPDH facilitates GMP production by catalyzing the oxidation of inosine monophosphate (IMP) to xanthosine monophosphate (XMP) by diphosphopyridine nucleotide (DPN, otherwise known as NAD)[179]. The discovery of two distinct isoforms of IMPDH proteins in humans was the work of Natsumeda and colleagues who found that type I and II IMPDH cDNA clones from a human spleen cDNA library encoded proteins of the same molecular weight that shared 84% peptide sequence similarity[180]. Subsequent studies revealed that, in general, cancer cells present with elevated IMPDH activity compared to normal cells and levels of type II IMPDH (otherwise known as IMPDH2) are significantly higher in cancer cells than type I IMPDH (otherwise known as IMPDH1)[181,182].

1.7.2. Function of IMPDH proteins

Purine biosynthesis generates ATP and GTP in the cell. Purine nucleotides are derived from two main pathways, namely the *de novo* purine biosynthesis pathway and the purine salvage pathway[183,184]. The IMPDH proteins are key metabolic enzymes that catalyze the committed and rate-limiting step of guanine nucleotide biosynthesis. This step involves the oxidation of IMP to XMP, with the concomitant reduction of NAD^+ to NADH[185]. As part of this process, glutamine is an important amide donor in the early steps of *de novo* purine biosynthesis which generates IMP, and is also important in the catalysis of XMP to GMP[135] (Figure 1.6).

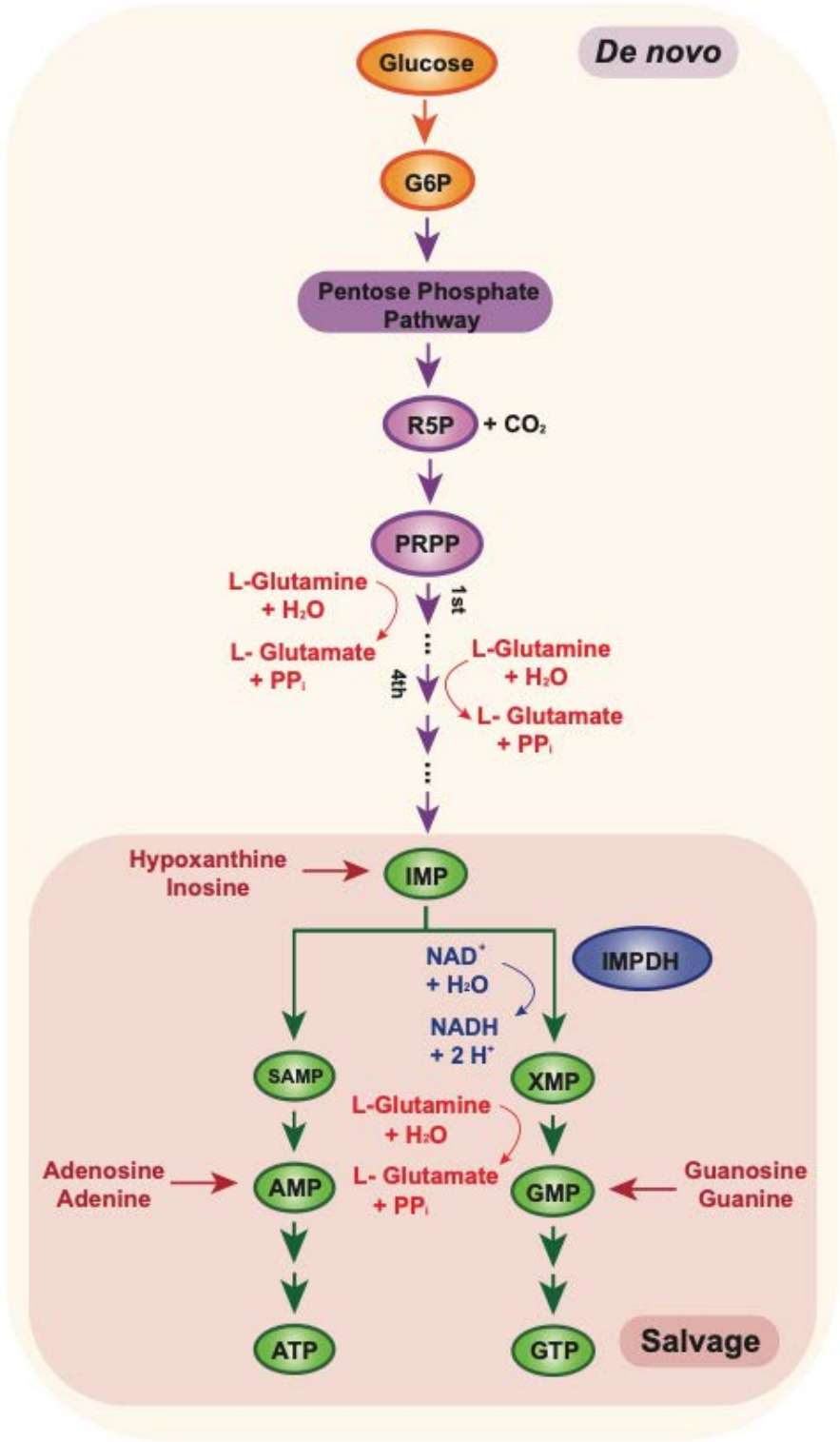

Figure 1.6 IMPDH in purine biosynthesis

Purine nucleotides can be generated through the de novo or the salvage pathways in the cell. Glutamine functions as an important amide donor in the de novo production of IMP, and in later

steps of XMP to GMP catalysis. IMPDH proteins mediates the oxidation of IMP to XMP, which concurrently reduces NAD^+ to NADH. This is a crucial, rate-limiting step of GTP biosynthesis. Derived from data and information from Mullen and Singh, 2023[138].

Our current understanding of the functional differences between the IMPDH proteins is limited due to the lack of isozyme-specific tools. Further, studies to date focus on recombinant homo-tetramers of IMPDH1 or IMPDH2 proteins, which overlook the potential cellular importance of hetero-tetramers of IMPDH1 and IMPDH2 that may also form in the cell as consequence of their high sequence similarity and conserved tetramer contact sites[185–187].

1.7.3. Structure and regulation of IMPDH proteins

The structure of IMPDH proteins consists of a catalytic domain and a regulatory domain. The catalytic domain is the site whereby the oxidation of IMP to XMP and concomitant reduction of NAD^+ to NADH occurs[186]. Studies have found that IMPDH proteins assemble into filaments, also known colloquially as rings-and-rods, in response to decreases in cellular guanine nucleotide levels. IMPDH filament assembly and aggregation are regulated by adenine and guanine nucleotides that differentially bind to three distinct sites on the IMPDH regulatory domain, also known as the Bateman domain[186].

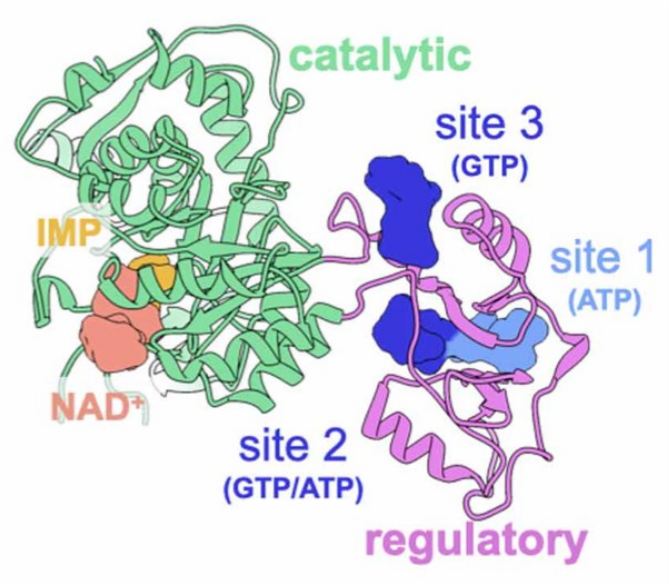

Figure 1.7 Structure of an IMPDH monomer
Each IMPDH monomer consists of a catalytic domain (green) and a regulatory domain (pink), also known as the Bateman domain. IMP is oxidized to XMP with the concomitant reduction of NAD+ to NADH at the catalytic domain. The binding of guanine and adenine nucleotides to distinct sites on the regulatory domain allosterically regulate the assembly of IMPDH monomers into stacked filaments. Schematic shown is representative of a GTP-bound IMPDH2 monomer (PDB: 6u9o). Image taken from Burrell and Kollman, 2022[186]. Licensed under CC BY-NC-ND.

ATP binding at the IMPDH1 and IMPDH2 Bateman domains is associated with the formation of active filaments in extended octameric conformations. In contrast, GTP binding results in the formation of compressed structures[186]. GTP-bound IMPDH2 results in the formation of stacked flat tetramers that are partially active[188]. Structural studies revealed that IMPDH2 proteins assemble into filaments as a means to resist GTP-mediated allosteric inhibition to maintain IMPDH2 activity under cellular conditions that present with high proliferative signals or deficiencies in guanine nucleotide levels[188]. In contrast, GTP binding of IMPDH1 is linked to the formation of stacked bowed tetramers that are inactive[187], and the physiological importance of these IMPDH1 structures remains to be determined.

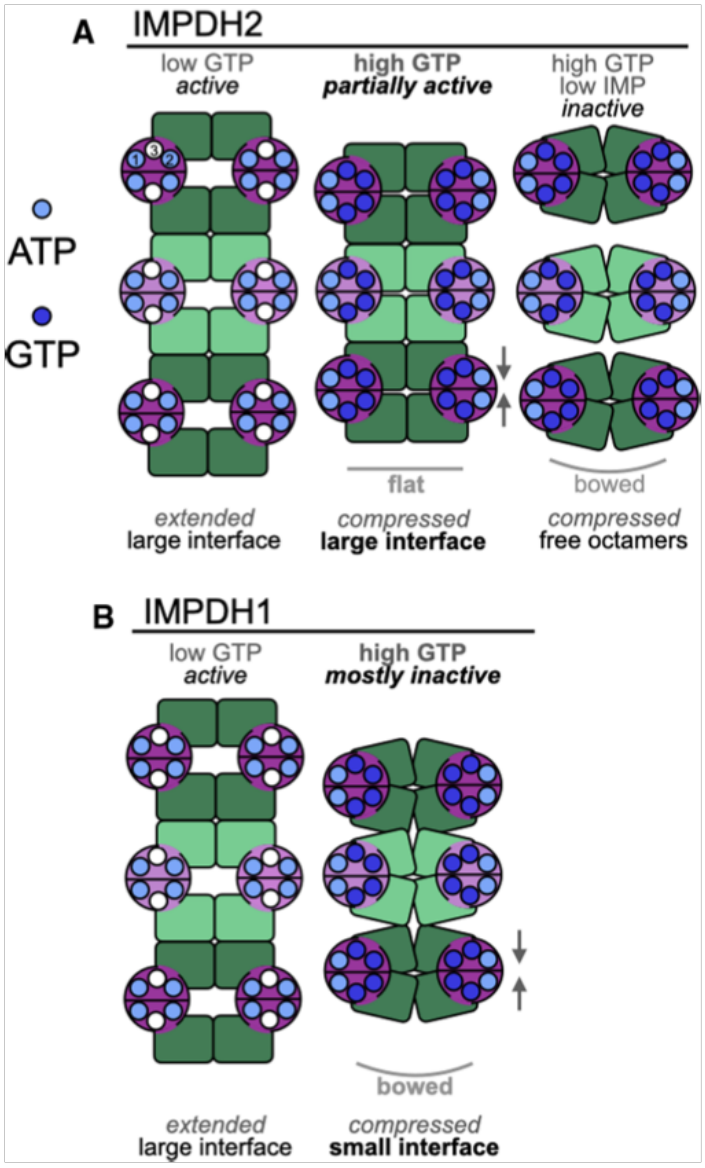

Figure 1.8 Allosteric regulation of IMPDH1 and IMPDH2 by adenine and guanine nucleotides

Under conditions of low cellular GTP, ATP binding to the Bateman domains of IMPDH1 and IMPDH2 proteins results in the formation of active IMPDH filaments in extended conformations that are identical. (a) When cellular GTP levels are elevated, IMPDH2 takes on a flat compressed conformation, which is partially active. Increasing GTP levels causes the conformation of IMPDH2 to shift towards a bowed compressed conformation where the protein exists as free inactive octamers. (b) In contrast, IMPDH1 forms inactive bowed compressed filaments under conditions of high cellular GTP because of their smaller assembly interfaces. It is proposed that the assembly of IMPDH1 into filaments does not result in allosteric regulation because of the lack of conformational constraints. Image taken from Burrell and Kollman, 2022[186]. Licensed under CC BY-NC-ND. Data and information derived from Burrell and Kollman, 2022[187], and Johnson and Kollman, 2020[188].

1.8. IMPDH filaments and nutrient stress

To date, several studies have reported formation of IMPDH rings-and-rods in response to a variety of stimuli. Notably, stresses that stem from the depletion of cellular glucose[189] and certain amino acids like glutamine[190] and serine[191] have been found to induce the formation of IMPDH2 rings-and-rods. To date, little is known about the formation of IMPDH1 rings-and-rods under nutrient-limiting conditions.

1.8.1. Glutamine

Glutamine is an important amide donor in the biosynthesis of purines. Studies in HeLa cells previously showed that IMPDH2 proteins assemble into structures of rings-and-rods in response to glutamine deprivation, and increase over time[190]. The formation of these IMPDH2 rings-and-rods was also associated with an increase in IMPDH2 mRNA and protein levels, which may suggest upregulation of IMPDH2 to form these rings-and-rods. Treatment with diazonorleucine (DON), a glutamine antagnonist[192], or methionine sulfoximine (MSOX), an inhibitor of glutamine synthetase, was also associated with the formation of IMPDH2 rings-and-rods[190]. Of note, guanosine supplementation to glutamine-deprived HeLa cells resulted in the disassembly of IMPDH2 rings-and-rods[190], *suggesting that IMPDH2 rings-and-rods form in response to depletion in cellular GTP levels because of limiting glutamine levels.*

1.8.2. Serine

Serine is an important amino acid utilized to produce 5,10-methylenetetrahydrofolate (N^5N^{10}-CH_2-THF) which feeds into the serine hydroxymethyltransferase (SHMT)-mediated reaction of the one-carbon folate cycle. N^5N^{10}-CH_2-THF is key to produce deoxythymidine monophosphate (dTMP), and this facilitates the formation of glycine and 10-formyltetrahydrofolate (N^{10}-formyl-THF)[191], which contribute to the *de novo* purine nucleotide biosynthesis pathway[193]. The serendipitous discovery of serine depletion as an inducer of IMPDH2 rings-and-rods stemmed from the observation that cells grown in Minimum Essential Medium (MEM) formed IMPDH2 rings-and-rods unlike cells grown in Dulbecco's Modified Eagle Medium (DMEM). MEM lacks amino acids like serine and glycine, and it was discovered that supplementation of serine depolymerized IMPDH2 rings-and-rods that formed in cells

grown in MEM[191]. Interestingly, supplementation of glycine, an amino acid generated from serine as part of the one-carbon folate pathway, increased the formation of IMPDH2 rings-and-rods in cells grown in MEM, which could suggest an induction of IMPDH2-mediated purine biosynthesis because of a surplus of cofactors available for the pathway. It was also shown that supplementing cells grown in MEM with guanosine or hypoxanthine also reversed the formation of IMPDH2 rings-and-rods, suggesting that these IMPDH2 rings-and-rods may form in response to reduced guanine nucleotide levels of the cell resulting from growth in less nutrient-rich conditions like MEM. Genetic or pharmacological inhibition of serine hydroxymethyltransferase 2 (SHMT2) or dihydrofolate reductase (DHFR), enzymes involved in the one-carbon folate cycle, was also associated with an induction of IMPDH2 rings-and-rods[191]. *These findings support a model whereby the depletion in one-carbon folate cycle metabolites resulting from serine deprivation or inhibition of enzymes involved in the one-carbon folate pathway promotes IMPDH2 rings-and-rods because of depletion of cellular GTP levels.*

1.8.3. Glucose

Glucose is an important metabolite involved in the generation of ribose-5-phoshate for nucleotide biosynthesis, and in the generation of serine for the folate cycle[189]. Previous studies have found that IMPDH2 forms rings-and-rods in response to glucose deprivation, and the frequency of the formation of these structures varied depending on cell line type[189]. It was reported that these IMPDH2 rings-and-rods that form under glucose deprivation co-localize with ARL2, a regulatory GTPase important for cellular processes like mitochondrial fusion and ATP production in the mitochondria. The formation of these IMPDH2 rings-and-rods increased over time in cells maintained in glucose-depleted media and, interestingly, increased in quantity but not size in cells[189]. Of note, guanosine supplementation reversed the formation of IMPDH2 rings-and-rods in glucose-deprived cells, *suggesting that they may form in response to depletion in guanine nucleotide levels because of limitations in glucose-derived metabolites like ribose-5-phosphate and serine.*

1.9. IMPDH in cancer

The importance of IMPDH proteins in malignant progression was later revealed by Weber and colleagues who found that IMPDH activity was positively correlated with growth rates, and was significantly elevated in rat hepatomas compared to normal liver[194]. In slow-growing hepatomas, IMPDH activity was found to be at least 2.5 to 3.5 times higher than normal liver tissues, and, in rapidly growing hepatomas, IMPDH activity was approximately twice as high as compared to non-malignant, proliferating hepatic tissues with similar growth rates. These findings suggest an oncogenic rewiring of the regulation of IMPDH activity in settings of malignancy[194].

1.9.1. The IMPDH proteins in cancer

Several pre-clinical studies have investigated the potential therapeutic benefit of pharmacological inhibitors that target both IMPDH1 and IMPDH2 in cancers. Although these studies do not discern between each isozyme, results thus far have provided promising evidence in support of the importance of IMPDH proteins and *de novo* purine biosynthesis in tumorigenesis.

Small cell lung cancer

Studies in small cell lung cancer (SCLC) previously found that the transcriptional levels of IMPDH1, IMPDH2, and several other key purine nucleotide enzymes were elevated in cell line and patient subsets that expressed low levels of the transcription factor ASCL1[195]. Metabolite tracing experiments also revealed that the *de novo* biosynthesis of purine nucleotides was significantly higher in ASCL1-low SCLC cells compared to ASCL1-high cells. Further transcriptomic analyses revealed that the MYC transcription factor inversely correlates with ASCL1, and is associated with high IMPDH1, IMPDH2 and other purine biosynthesis enzymes. Indeed, genetic knockout of MYC led to a decrease in IMPDH1 and IMPDH2 mRNA and protein levels and reduced de novo purine biosynthesis rates in ASCL-low cells[195]. Pharmacological inhibition of IMPDH with mycophenolic acid (MPA) or genetic knock-out of IMPDH1 was associated with a significant impairment *in vitro* lung cancer cell viability and growth, and in *in vivo* lung tumor growth*. Together, these findings suggest that IMPDH1 and IMPDH2 may support the tumorigenesis of ASCL-low SCLC subsets by sustaining the de novo purine biosynthesis pathway.*

Hepatocellular carcinoma

Transcriptomic analyses previously revealed that the levels of several core *de novo* purine biosynthesis genes, including IMPDH1 and IMPDH2, are elevated in hepatocellular carcinoma (HCC) patients compared to normal liver tissues[196]. Treatment with the IMPDH inhibitor, mycophenolate motefil, was associated with a reduction in the *in vitro* HCC cell proliferation and *in vivo* tumor growth. Genetic knockdown of IMPDH1 and IMPDH2 was also associated with a reduction in the *in vitro* cell proliferation, which was further augmented by treatment with the IMPDH inhibitor, mycophenolic acid (MPA). Studies in patient-derived xenograft (PDX) models of HCC found that response to MPA treatment is heterogenous and largely depends on levels of IMPDH1 and IMPDH2, and levels of guanosine nucleotides within a tumor[196]. A drug screen revealed that treatment with the PI3K inhibitor, PI-103, further reduced the growth of cells with genetic knock down of IMPDH1 and IMPDH2. Of note, treatment with rapamycin did not further reduce the growth of IMPDH1 and IMPDH2 knockdown HCC cells, suggesting a potential interplay between PI3K signaling and purine metabolism in supporting HCC growth independent of mTOR. Treatment with PI-103 or the AKT inhibitor, MK-2206, was associated with a reduction in the mRNA and protein levels of IMPDH1, IMPDH2 and other purine biosynthesis enzymes. TCGA analyses revealed a positive correlation between purine metabolism and PI3K pathway, and an association between tumors harboring deleterious PI3K mutations and high purine enzyme expression[196]. Further experiments found that PI3K hyper-phosphorylates the retinoblastoma (RB) protein, which promotes the activation of the transcription factor, E2F1, and expression of purine synthesis genes. MPA treatment or IMPDH1 and IMPDH2 knockdown was also associated with a decrease in the expression of genes involved in MAPK signaling. Indeed, combinatorial targeting of IMPDH and PI3K with MPA and PI-103, respectively, led a to a significant reduction of *in vivo* HCC tumor growth[196]. *Together, these findings suggest that the PI3K drives the expression of IMPDH proteins to promote purine metabolism and MAPK signaling to support HCC tumorigenesis by activating the E2F1 transcription factor.*

1.9.2. IMPDH1

Although few studies in the past have focused on targeting IMPDH1 to mitigate tumorigenesis, increasing evidence suggests that the IMPDH1 protein may indeed be important in tumor initiation and progression in certain cancer contexts.

Hepatocellular carcinoma

In HCC, elevated IMPDH1 protein levels were observed in tumors derived from HCC patients compared to matched normal liver tissues[197]. IMPDH1 inhibition was associated with a suppression of *in vitro* tumor cell colony formation and *in vivo* tumor initiation and growth[197]. Similar independent studies also found that IMPDH1 protein levels were elevated in HCC tumors compared to matched normal tissues[198]. Formation and growth of patient-derived tumors expressing high IMPDH1 protein levels in mice were significantly greater than low IMPDH1-expressing tumors. In this case, expression of IMPDH1 in HCC was found to be regulated by the transcription factor, MYBL2, which promotes the transcription and subsequent translation of IMPDH1, thereby supporting *de novo* purine biosynthesis. Indeed, genetic inhibition of MYBL2 was associated with a significant impairment in cellular levels of IMP, GMP and AMP, which are direct and indirect metabolites produced as a result of IMPDH activity during purine biosynthesis[198]. *These findings together support the importance of IMPDH1 in HCC initiation and progression*.

Clear cell renal cell carcinoma

In clear cell renal cell carcinoma (ccRCC) patients, high IMPDH1 mRNA levels were observed relative to normal tissues and associated with significantly reduced patient overall and disease-free survival[199]. Interestingly, it was also observed that metastatic cases of ccRCC patients bore tumors that presented with increased formation of IMPDH1 cytoophidia, which have been described as filamentous structures or “rings-and-rods” [199]. It was found that IMPDH1 stabilizes levels of the transcription factor, YB-1, which in turns promotes the expression of IMPDH1. IMPDH1 binds and stabilizes YB-1, and forms IMPDH1 cytoophidia to promote the nuclear translocation of YB-1. YB-1 is proposed to promote the transcription of IMPDH1, thereby resulting in an IMPDH1-YB-1 positive feedback loop. Suppression of tumor metastases by IMPDH1 knockdown was rescued by increased YB-1 expression, underscoring a role for YB-1 in promoting EMT.

Indeed, genetic knockdown of IMPDH1 led to a suppression of ccRCC migration and invasion in vitro, and impaired ccRCC tumor growth in vivo. The latter could be rescued by overexpression of YB-1, *further supporting the role of the YB-1/IMPDH1 axis in promoting ccRCC tumorigenesis*[199].

1.9.3. IMPDH2

Of the two isoforms, previous studies have predominantly focused on elucidating the potential tumorigenic importance of IMPDH2 in different cancer contexts. This interest stems from early findings in the literature that the expression of IMPDH2 is significantly higher in tumors compared to IMPDH1.

Colorectal cancer

In colorectal cancer (CRC) patients, high IMPDH2 mRNA and protein levels were observed in CRC tissues relative to matched normal tissues and associated with poor patient prognoses[200]. Overexpression of IMPDH2 in CRC cell lines was associated with increased *in vitro* cell proliferation and migration, and *in vivo* tumor growth. IMPDH2 overexpression was also associated with an increase in G1/S phase transition, and an increase in cyclin D1 and Ki-67 levels[200]. Further, genetic knockdown of IMPDH2 was also associated with a decrease in *in vitro* cell growth, proliferation and migration, and *in vivo* tumor growth, and associated with an impairment in G1/S phase transition, suggesting that IMPDH2 may facilitate CRC progression by promoting the cell cycle[200]. It was proposed that IMPDH2 overexpression activated PI3K/AKT signaling and promoted the phosphorylation of mTOR and FOXO1, resulting in increased colony formation and cell viability. Further, mTOR inhibition suppressed epithelial-to-mesenchymal (EMT) transition and cell invasiveness, highlighting a role for IMPDH2-mediated PI3K/AKT/mTOR signaling in EMT transition of CRC cells[200]. The functional significance of the IMPDH2-mediated PI3K/AKT/FOXO1 axis in this context remains to be determined. However, previous studies have implicated FOXO1 in negatively regulating the cell cycle and it is plausible that, in this instance, the phosphorylation of FOXO1 by AKT may similarly promote the cell cycle by suppressing FOXO1 activity[201]. *Together, these findings suggest that IMPDH2 is important for promoting PI3K/AKT signaling to upregulate the cell cycle and promote CRC progression.*

Glioblastoma

In glioblastoma (GBM) patients, high IMPDH2 protein expression was found to correlate with increased glioma malignancy and reduced patient survival[202]. In addition, genetic knockout of IMPDH2 or pharmacological inhibition of IMPDH by MPA was associated with a decrease in GTP biosynthesis and cell proliferation, suggesting that IMPDH2 may promote GBM progression via upregulating GTP biosynthesis[202]. Further studies revealed that GTP was largely used for the synthesis of rRNA and tRNA in contrast to DNA synthesis or GTP catabolism in GBM cells[202]. Indeed, pharmacological inhibition of IMPDH under conditions of low GTP and low Pol I and II activity induced features reminiscent of the nucleolar stress response and suppressed Pol I-mediated transcription. MPA treatment was associated with a reduction in nucleolar size and density, whereas overexpression of IMPDH2 was found to enlarge cellular nucleoli in GBM cells[202]. *Together, these findings suggest that IMPDH2 promotes GBM progression by upregulating GTP biosynthesis to drive rRNA and tRNA synthesis and nucleolar hypertrophy.*

Hepatocellular carcinoma

Increased mRNA and protein levels of IMPDH2 have been reported in HCC cell lines and HCC patient tissues compared to primary hepatocellular epithelial cell lines and matched patient adjacent tissue samples respectively[203]. High IMPDH2 protein expression in HCC patients was also associated with reduced median overall survival and inferior progression-free survival rates compared to HCC patients that expressed low levels of IMPDH2. Functional studies also revealed that overexpression of IMPDH2 in low-IMPDH2-expressing HCC cells was associated with increased proliferation, whereas the knockdown of IMPDH2 in high-IMPDH2-expressing HCC cells led to a significant reduction in cell proliferation[203]. *Together, these findings suggest that IMPDH2 is a potential prognostic factor in HCC patients and may be a potential therapeutic target in mitigating HCC cell proliferation.*

Non-small cell lung cancer

Studies in non-small cell lung cancer (NSCLC) previously found that IMPDH2 mRNA and protein levels were significantly elevated in NSCLC samples relative to adjacent normal tissues[204]. Similar observations at the mRNA level were also made in NSCLC cell lines compared to normal human bronchial epithelial cell lines. Of note,

genetic knockdown of IMPDH2 in NSCLC cell lines was associated with reduced cellular proliferation, increased apoptosis, and reduced migratory and invasive capacity. Increased E-cadherin and reduced N-cadherin and vimentin protein levels were also observed resulting from IMPDH2 knockdown, suggesting a suppression of EMT[204]. Further analyses also revealed an impairment of Wnt/B-catenin signaling resulting from genetic knockdown of IMPDH2, suggesting that IMPDH2 may promote EMT in NSCLC cells by activating Wnt/B-catenin signaling. Indeed, overexpression of IMPDH2 increased NSCLC cellular proliferation, migration, and invasion, and was also associated with an upregulation of EMT markers and increased Wnt/B-catenin signaling[204]. *These findings suggest that IMPDH2 promotes EMT in NSCLC cells by activating the Wnt/B-catenin pathway.*

1.9.4. Current tools for IMPDH inhibition

Genetic

Several studies have successfully employed the use of genetic approaches, like siRNAs[200,205,206], shRNAs[196,197,199,200], and CRISPR/Cas9[202,205,207], to modulate the expression of IMPDH1 and IMPDH2 in cell lines. Murine models presenting with homozygous loss of IMPDH1 have also been successfully generated, reportedly viable although presenting with vision impairments[208,209]. In contrast, mice with heterozygous IMPDH2 deletions present normally with no substantial defects, whereas homozygous IMPDH2 deletions were found to be embryonically lethal in mice, underscoring the importance of IMPDH2 in early development[210].

Pharmacological

The first IMPDH inhibitor, mycophenolic acid (MPA), was initially discovered by Bartolomio Gosio in 1893 who identified a fungal metabolite in spoiled corn[211], later rediscovered by Alsberg and Black and named MPA in 1913[212]. Since its discovery, numerous studies have found compelling evidence for therapeutic potential of MPA in cancer treatments[213]. Various pharmacological inhibitors of IMPDH proteins have since been identified and assessed for their potential therapeutic utility in the treatment of different cancer types[214], including mycophenolate motefil/MPA, ribavirin, tiazofurin and mizoribine (Table 1.3). It is important to note that many of these IMPDH inhibitors were re-purposed with known target proteins other than IMPDH, and few studies outlined in

Table 1.3 have validated their on-target efficacies on IMPDH activity via genetic approaches. Nevertheless, these studies present potentially promising findings regarding the anti-tumor potential for IMPDH inhibitors. To date, no IMPDH inhibitor has been approved for use in the treatment of cancers in the clinic.

Table 1.3 Examples of IMPDH inhibitors evaluated in pre-clinical cancer studies

Name	Proposed IMPDH binding site	Mechanism of action on IMPDH activity	Examples of evidence of anti-tumor effects
Mycophenolate Motefil (MMF) Pro-drug of mycophenolic acid (MPA)	NAD+ cofactor site	- Traps enzyme covalent intermediate (E-XMP*) - blocks enzyme flap closure and prevents XMP* hydrolysis[215]	ASCL^{low} SCLC[195] HCC[196] Glioblastoma[202] Breast cancer[216,217] Osteosarcoma[218] Gastric cancer[219] Multiple myeloma[220]
Ribavirin Pro-drug of Ribavirin-5'-monophosphate	Substrate binding site	- Blocks substrate processing[221]	Glioma[222] Breast cancer[223,224]
Tiazofurin Pro-drug of thiazole-4-carboxamide adenine dinucleotide (TAD)	NAD+ cofactor site	- Mimics NAD+ binding - blocks NAD+/NADH hydride transfer[225]	Leukemia[226–228]
Mizoribine Pro-drug of mizoribine-5'-phosphate	Substrate binding site	- Blocks substrate processing - Forms transition state analogue with E-XMP* and water[229,230]	ASCL^{low} SCLC[195] Leukemia[231] TSC1/2-associated cancers[206,232]

One drawback of IMPDH inhibitors outlined in Table 1.3 is their lack of isozyme specificity for the IMPDH1 and IMPDH2 proteins. Few compounds exist that selectively target either isozyme. Given the potential structural, functional, and potential oncogenic differences between the IMPDH proteins, isozyme specific inhibitors will certainly be

beneficial in helping elucidate these differences. One example is sappanone A (SA), which is a natural small molecule compound found to selectively inhibit only IMPDH2 by targeting the cysteine 140 residue of IMPDH2, resulting in an allosteric change that perturbs substrate processing[230]. To date, the anti-tumor potential of SA is yet to be determined. Another is the compound shikonin, which has been found to selectively inhibit the activity of IMPDH2 over IMPDH1. Shikonin was predicted to bind to the substrate binding pocket of IMPDH2, and shown to reduce growth and induce apoptosis of TNBC cell lines[233].

1.10. Rationale, aims, and hypotheses

Rationale

ATG4B is a core cysteine protease in the process of autophagy and has been associated with promoting the progression and survival of various types of cancers, as described in chapter 1.5.1. Notably, previous findings from our group highlight a potential functional importance of ATG4B in modulating the ability of HER2+ breast cancer cells to survive under conditions of nutrient stress[61]. Importantly, genetic knockdown of ATG4B did not have a significant effect on the viability of nutrient deprived HER2- breast cancer cells. These observations highlight a differential role of ATG4B in modulating the nutrient stress response of HER2+ vs. HER2- breast cancer cells[61]. *To date, little is known about the molecular mechanisms underlying ATG4B in modulating responses of HER2+ breast cancer cells to nutrient stress.* Additionally, findings by our group also revealed that genetic knockdown of ATG4B increased the sensitivity of HER2+ breast cancer cells to the anti-HER2 targeted agent, trastuzumab. This is significant given that resistance to trastuzumab in advanced and metastatic cases of HER2+ breast cancer patients, to date, remains an outstanding challenge[50,51]*. Additional studies investigating pharmacological and combinatorial approaches that may further improve the effects of ATG4B inhibition on augmenting trastuzumab efficacy are certainly warranted.*

As described in chapter 1.6.1, metabolic rewiring is a recognized hallmark of cancers. Glutamine functions as an important amide donor and carbon source in nucleotide biosynthesis and the TCA cycle respectively, and the reprogramming of glutamine metabolism to support cancer progression and survival has been reported in a number of cancer contexts. Notably, studies have found that glutamine deprivation

activates autophagy to promote growth and survival of cancers, like pancreatic ductal adenocarcinoma and gliomas[165,166]. Studies by Kim and colleagues previously observed elevated levels of enzymes involved in glutamine metabolism in HER2-enriched breast cancer cells in contrast to other molecular subtypes of breast cancers[234]. To date, current knowledge regarding the role of ATG4B in modulating responses of HER2+ breast cancer cells to glutamine deprivation remains limited.

The **overall aim** of this thesis was to elucidate how ATG4B is involved in the nutrient stress response of breast cancer cells to glutamine deprivation, and to leverage this axis to further improve the efficacies of HER2-targeted therapies, like trastuzumab, in HER2-positive breast cancer cells.

Aim 1: To investigate the molecular mechanisms underlying ATG4B in nutrient stress response in HER2+ breast cancer cells.

1. Identify candidate protein-protein interactors of ATG4B by immunoprecipitation-mass spectrometry (IP-MS)

2. Validate interactions between ATG4B and top candidate protein-protein interactor by immunoprecipitation-western blot (IP-WB)

3. Investigate the biological significance of interactions between ATG4B and the validated protein-protein interactor.

As part of the first aim of my thesis project, I discovered a new interaction between ATG4B and the metabolic enzyme, IMPDH2, by IP-MS. I validated this interaction between ATG4B and IMPDH2 in several independent breast cancer cell lines by IP-WB. I then investigated the biological significance of this interaction, focusing on HER2+ breast cancer cell lines as models, using a combination of cell and molecular biology approaches and metabolomics.

Hypothesis 1: ATG4B interacts with IMPDH2 to sustain growth by supporting de novo GTP biosynthesis in glutamine deprived HER2+ breast cancer cells.

Aim 2: To determine the effects of co-inhibition of ATG4 and IMPDH on the sensitivity of HER2+ breast cancer cells to existing anti-HER2 therapies.

1. Investigate the clinical significance of ATG4B and IMPDH2 in breast cancers.

2. Determine the effects of combined pharmacological inhibition of ATG4 and IMPDH on HER2+ breast cancer cell growth.

3. Determine the effects of combined genetic inhibition of ATG4 and IMPDH on HER2+ breast cancer cell growth.

4. Investigate the effects of combined genetic or pharmacological inhibition of ATG4 and IMPDH on sensitivity of HER2+ breast cancer cell lines to existing anti-HER2 agents.

As part of the second aim of my thesis project, I sought to leverage the newly discovered interaction between ATG4B and IMPDH2 to improve the efficacy of the HER2-targeted agent, trastuzumab, in HER2+ breast cancer cell lines. I examined the combinatorial effects of pharmacological or genetic inhibition of ATG4 and IMPDH proteins on the growth of the trastuzumab-resistant HER2+ breast cancer cell line, JIMT-1. I then investigated the potential therapeutic benefit of ATG4 inhibition on sensitivity to trastuzumab in JIMT-1 cells. *Future work will investigate the potential for this promising dual combination in improving the responses of HER2+ breast cancer cell lines to the HER2-targeted agent, trastuzumab.*

Hypothesis 2: Combined inhibition of ATG4B and IMPDH will increase the sensitivity of HER2+ breast cancer cells to trastuzumab.

Chapter 2. An ATG4B-IMPDH2 axis modulates cell growth in glutamine-deprived breast cancer cells

Portions of chapter 2 have been prepared as part of a manuscript tentatively entitled “An ATG4B-IMPDH2 axis modulates cell growth in glutamine-deprived breast cancer cells” (in preparation).

I designed and conceptualized these experiments under the mentorship of Dr. Sharon Gorski. I conducted all experiments in this manuscript, with the assistance of Nancy E. Go for select *in vitro* experiments and generation of stable shRNA knockdown cell lines, Drs. Gregg Morin, Vincent Chen, and Gian Negri for collaborations on IP-MS studies, and Jessica Koe and Dr. Seth Parker for collaborations on metabolomics experiments. Drs. Baofeng Jia and Kevin Yang assisted in breast cancer patient proteomic data analysis and protein-protein correlation studies.

2.1. Introduction

ATG4B is a core cysteine protease in the process of autophagy, and has been implicated in promoting the survival and progression of several cancer types[235,236]. Previous studies have found that ATG4B plays an important role in nutrient stress response in breast cancer cells of the HER2-positive subtype[61]. To date, the molecular mechanisms underlying the roles of ATG4B and nutrient stress in breast cancers remain poorly defined.

The human IMPDH proteins function as key rate-limiting metabolic enzymes that partake in the production of cellular GTP levels in the purine biosynthetic pathway. General IMPDH inhibitors, like MPA, that target both isozymes have revealed promising results in tumor models in pre-clinical studies (Table 1.3). An increasing amount of evidence in recent years present potential roles for the IMPDH1 protein in cancer progression[197–199], but much of the literature to date has been centered around IMPDH2 inhibition as a therapeutic avenue for mitigating tumor growth and survival [200,202–204,237] . This interest stems primarily from past studies that revealed elevated levels of IMPDH2 in cancer models, in contrast to IMPDH1[180–182,237,238]. Although some pre-clinical studies have found anti-tumor potential for IMPDH inhibitors, like MPA[216,217] and ribavirin[223,224],

in breast cancers, *the molecular mechanisms underlying the regulation of IMPDH2 in breast tumorigenesis remain poorly defined.*

IMPDH2 has also been directly shown to form polymers of ring-and-rod structures in the cell in response to certain nutrient stresses, like serine[191], glucose[189] or glutamine[190] deprivation. Structural studies have suggested this occurs in response to depletion of cellular GTP levels in the cell or in response to an increase in proliferative signaling, characterized by an increase in ATP and IMP levels[188] *. However, to my current knowledge, the biological significance of these IMPDH2 structures have not yet been studied under nutrient stress conditions in cancers, and further studies are warranted.*

In this chapter, I describe my discovery of a novel protein-protein interaction between ATG4B and IMPDH2, and my investigations into the functional role of this axis in mediating breast cancer cell growth under conditions of glutamine deprivation through a crosstalk between ATG4B and *de novo* purine biosynthesis.

2.2. Materials and methods

2.2.1. Cell lines and culture conditions

Human breast cancer cell lines were grown in a cell culture incubator at 37◦C and under 5% CO_2. The JIMT-1 cell line was obtained from the German Collection of Microorganisms and Cell Culture (Deutsche Sammlung von Mikroorganismen und Zellkulturen GmbH). The MDA-MB-231 cell line was obtained from the American Type Culture Collection (ATCC). The MCF-7/HER2 and MCF-7/NEO cell lines were a kind gift from the labs of Dr. M. Alaoui-Jamali (McGill University) and Dr. Marcel Bally (BC Cancer Research Centre). In brief, the generation of MCF-7/HER2 and MCF-7/NEO cell lines involved the transfection of MCF-7 cells with plasmids containing the HER2 cDNA or a neomycin cassette as previously described[239]. Expression of HER2 in the MCF-7/HER2 line used in this chapter was previously characterized by Warburton and colleagues[240]. All cell lines were cultured in DMEM (Gibco, 11995-065) supplemented with 10% fetal bovine serum, 5ug/mL insulin (Sigma, I0516 or Sigma, I1882 dissolved in 1N HCl (pH 3.5-3.7)), 10 mM HEPES (Gibco, 15630-080) and 1X MEM non-essential

amino acids (Gibco, 1140-050). Cell lines were checked with the e-Myco Mycoplasma PCR Detection Kit (Version 2.0, Lilif Diagnostics) to rule out mycoplasma contamination.

2.2.2. Generation of ATG4B-knockout (KO) cell lines by CRISPR/Cas9

The JIMT-1 cell line was transfected with a pSpCas9(BB)-2A-GFP (PX458) plasmid containing a single guide RNA (sgRNA) targeting exon 5 of the ATG4B gene (sgRNA sequence: TCCTGTCGATGAATGCGTTG). Monoclonal cell lines were derived by FACS sorting GFP-positive cells into single-cell wells of a 96-well plate 48 hours later. ATG4B KO monoclonal cell lines were verified by western blot for absence of ATG4B protein expression and accumulation of pro-LC3B protein.

2.2.3. Immunofluorescence (IF)

JIMT-1 parental and ATG4B KO cell lines were grown on coverslips in 6-well plates for the indicated durations of time in full media or glutamine-deprived media. For guanosine rescue experiments, cells were treated with 1mM guanosine (Sigma, G6264) or DMSO 1 hour before harvest. Cells were fixed with 4% paraformaldehyde solution for 12 minutes and washed twice with 1X PBS for 10 minutes per wash. Cells were then permeabilized using 0.2% Triton X-100 for 5 minutes and washed thrice with 1X PBS for 10 minutes per wash. Cells were then blocked with 10% goat serum for 1 hour at room temperature, and then washed twice with 1X PBS for 10 minutes per wash before an overnight incubation at 4◦C rotating in primary antibody (1:500) diluted in 1% goat serum. Cells were then washed three times with 1X PBS for 10 minutes per wash and incubated with secondary antibody (1:2500) diluted in 1% goat serum for 2 hours at room temperature. Cells were washed three times with 1X PBS for 10 minutes per wash before being stained with DAPI for 6 minutes. Cells were washed three times with 1X PBS for 10 minutes per wash before mounting with Mowiol-488 (Sigma, 81,381). Fluorescence microscopy images were acquired using the Zeiss Axio Observer (Z1/7) inverted fluorescence microscope equipped with Apotome and an AxioCam MRm R3 camera (Zeiss). Images were acquired at 63X magnification (oil immersion) with the Zen Blue Software (Zeiss).

2.2.4. Immunoprecipitation (IP)

Cells were grown in 15cm^2 cell culture dishes in full media or glutamine-deprived media. Cells were then washed twice with 1X PBS and trypsinized. Cells were syringed 10 times with a 21-gauge needle and lysed for 30 minutes on ice with IP lysis buffer (25mM Tris-HCl, 150mM NaCl, 1X PhosSTOP (Roche, 04906837001), 1X complete protease inhibitor cocktail (Roche, 46416400), 5% glycerol, 0.1% NP-40, water) in protein lo-bind tubes. Lysates were cleared at 13,000 rpm for 15 minutes at 4◦C and transferred to fresh protein lo-bind tubes. Protein concentrations of cell lysates were determined using a BCA assay. Cell lysates were incubated with primary antibody (5ug antibody per 1mg protein) overnight at 4◦C rotating. ProG Dynabeads (Invitrogen/ThermoFisher, 10004D) were washed twice with IP wash buffer (1X complete protease inhibitor cocktail (Roche, 46416400), 1X PhosSTOP (Roche, 04906837001), 0.1% NP-40, water) and once with IP lysis buffer before incubation with lysate-antibody mixtures for 2 hours at 4◦C rotating. Supernatants were then removed using a magnetic stand and beads were washed thrice with IP wash buffer before being transferred to fresh protein lo-bind tubes and resuspended with elution buffer (2X Bolt LDS buffer, 1X reducing agent, water). IP samples were heated at 65◦C for 5 minutes, and then eluted using a magnetic stand.

2.2.5. Proteomics

ATG4B IP samples were prepared as described and subjected to proteomics analysis. MS data were acquired on the Orbitrap Fusion in data-dependent mode. 2.4 kV was applied to the nanoelectrospray source to generate ions, and ion transfer tube temperature was 275 °C. MS1 scans were acquired in the Orbitrap with the following parameters: (1) resolution: 120,000 over a mass range of 400–1200 m/z with an RF lens setting of 60%, (2) an automatic gain control (AGC) target value: 4 x 105, (3) maximum ion injection time: 120 ms. MS2 scans were acquired with the following parameters: (1) monoisotopic precursor selection: peptides, (2) charge state filtering: 2–4, (3) undetermined charge states: included. Dynamic exclusion of selected masses was enabled after 1 observation for 20 seconds with a tolerance of 20 ppm. High energy collision-induced dissociation fragmentation was performed with a quadrupole isolation window of 1.4 m/z and a collision energy of 33%. Data were acquired in the Iontrap in

the normal scan range with a fixed first mass of 120 m/z, an AGC target of 1 x 104, and a max injection time of 45 ms with 1 microscan in centroid mode.

Raw MS data were analyzed by searching SequestHT (Proteome Discoverer (v2.4; Thermo Fisher Scientific)) against the UniProt Swissprot Human Proteome database (2020/02/18). Precursor mass tolerance was set at 10ppm and fragment mass tolerance was set at 0.6 Da. Modifications included were as follows: (1) Dynamic: methionine oxidation (+15.995), N-terminal acetylation (+42.011), (2) Static: cysteine carbamidomethylation (+57.021,C). Peptide spectrum match (PSM) identification false discovery rates were calculated using Percolator by searching the results against a decoy sequence set and only PSMs with FDR < 1% were retained in the analysis. Proteins that were not cytoskeletal or ribosomal proteins, and were associated with at least 2 razor and unique peptides were prioritized as candidates.

2.2.6. siRNA transfections

The following siRNAs and controls were used: 1) hs.Ri.IMPDH1.13.1 (IDT), 2) hs.Ri.IMPDH1.13.2 (IDT), 3) hs.Ri.IMPDH2.13.1 (IDT), 4) Negative Control (NC) DsiRNA (IDT, 56532). Sequences for IMPDH1 and IMPDH2 siRNAs are located in the Appendix (Table A1). Cells were seeded onto 6-well plates and allowed to adhere overnight before the initiation of experiments. The following day, cells were transfected with the indicated amounts of siRNA using Lipofectamine RNAiMAX (Invitrogen, 13778150) as per manufacturer's recommendations. A second transfection was then performed after 72 hours. Cells were harvested 72 hours after the second transfection and subjected to western blot analyses.

2.2.7. Western blot analyses

Cell pellets were harvested and suspended in RIPA lysis buffer (Santa Cruz, SC24948) supplemented with complete protease inhibitor (Roche, 11836153001), 1X PhosSTOP (Roche, 04906837001), 1mM sodium orthovanadate (Santa Cruz) and 2mM PMSF (Santa Cruz). Cells were lysed for 1 hour at 4◦C rotating, and protein concentration was determined using a BCA assay (Thermo Scientific, 23225). Gel electrophoresis were performed using 10% or 4-12% Bis-Tris gels under reducing conditions. Protein gels were then transferred onto PVDF membranes using the Mini

Trans-Blot cell system (Bio-Rad). Membranes were blocked with 5% skim milk/PBST for 1 hour at room temperature and incubated with primary antibody diluted in Intercept (TBS) blocking buffer (Li-Cor, 927-60001) for overnight at 4◦C rotating. Membranes were then washed thrice with 1X PBST for 5 min per wash and incubated in secondary antibody diluted in 2.5% skim milk/PBST. Protein signals were detected using the Clarity Western ECL Substrate (Bio-Rad, 1705061) and quantified by ImageJ.

2.2.8. Cell growth assessment by Incucyte

Cells were seeded onto 48-well plates and allowed to adhere overnight before the initiation of experiments. Media were replaced the next day with full or glutamine-deprived media in the absence or presence of the indicated amounts of DMSO, small molecule inhibitors and/or drugs. Plates were then placed in the Incucyte machine (Model S3, Sartorius) to measure change in cell phase confluence per well over time. Four images per well were captured every 4 hours using a 10x objective unless otherwise indicated and analyzed using the Incucyte Zoom software. Growth curves were established by plotting the raw percent phase confluence at each time point or normalizing to phase confluence of wells at the start of the experiment (day 0 and hour 0 (0d0h)) as indicated.

2.2.9. Metabolite profiling and 13C-tracing experiments

Sample preparation: Cells were seeded onto 6-well plates and allowed to adhere overnight. Fresh full or glutamine-deprived media was replaced daily for 48 hours prior to harvesting and metabolite extraction. For guanosine rescue experiments, cells were incubated with 1mM guanosine (Sigma, G6264) or DMSO 1 hour before harvesting and metabolite extraction. For 13C-tracing experiments, cells were incubated in DMEM media (Sigma, D5030-10X1L) supplemented with 3.7g/L 13C-sodium bicarbonate (Sigma, 372382-1G) and 1g/L glucose (Gibco, A24940-01), with/without 0.584g/L L-glutamine (Gibco, 25030081) and with/without 1mM guanosine (Sigma, G6264) or DMSO for 1 hour before harvesting and metabolite extraction. Prior to metabolite extraction, cell culture media were aspirated and cells were washed once with cold 0.9% NaCl solution. Metabolites were extracted from cells by scraping following addition of cold extraction buffer containing 80% methanol (VWR) and uniformly (13Cx, 15Ny) isotope-labelled amino acid standards: 2.5 nmol of L-alanine, L-lysine, L-histidine, L-

arginine, L-aspartic acid, L-leucine, L-isoleucine, L-valine, L-threonine, L-proline, L-serine, L-asparagine, and glycine; 4 nmol of L-glutamine, and 1.25 nmol of cystine (Cambridge Isotope Laboratories)). Samples were stored at -80oC at this stage for 1-3 weeks prior to further processing at the LC-MS facility. Samples were centrifuged at 21300 x G at 4oC for 15 minutes, and supernatant were collected and dried using a SpeedVac (ThermoFisher). Dried metabolite samples were then reconstituted in 25-30uL of HPLC-grade water (Sigma) and vortexed at 1500 rpm for 30 minutes. Samples were further centrifuged at 21300 x G at 4oC for 15 minutes and supernatants were collected for LC-MS.

Liquid chromatography mass spectrometry (LC-MS): LC-MS was performed using a Thermo Orbitrap Exploris 240 mass spectrometer operating in heated electrospray ionization mode. MS1 and MS2 data were obtained using a hybrid orbitrap in positive and negative polarity switching mode. For each analysis, 2 µL was injected. Ion-source parameters were as follows: (1) spray voltage: 3.4 kV for positive ion and 2 kV for negative ion, (2) ion transfer tube temperature: 320 °C, (3) vaporizer temperature: 75 °C, (4) sheath flow rate: 25, (5) aux gas flow rate: 5, (6) sweep gas flow rate: 0.5. MS1 parameters for positive and negative modes were as follows: (1) resolution: 120k, (2) scan range: 67-1000 m/z, (3) normalized automatic gain control (AGC) target: 300%, (4) RF lens: 70%, (5) maximum injection time (IT): auto. Data from MS1 scans were acquired in profile mode. The top 5 positive and top 3 negative precursor ions were then fragmented in MS2 in a data-dependent manner. MS2 parameters for positive and negative modes were as follows: (1) resolution: 30k, (2) isolation window: 1.5 m/z, (3) AGC target: “standard”, (4) intensity threshold: 5 x 104, (5) dynamic exclusion: 10s, 5 ppm, (6) maximum IT: auto, (7) multiplexed higher-energy C-trap dissociation (HCD) collision energy: 10%, 30%, 80%. Data from MS2 scan was acquired in centroid mode, with a flow rate of 0.1mL/min (25oC oven temperature). Mobile phase A contained 10 mM ammonium carbonate (pH 9) and mobile phase B contained 100% acetonitrile. The following gradients were used: (1) 0 – 30 minutes: 80% to 20% solvent B, (2) 30-40 minutes: 20% solvent B held, (3) 40-40.5 minutes: 20% to 80% solvent B, (4) 40.5- 52 minutes: 80% solvent B.

Data acquisition and analysis: Acquisition and analyses for metabolite profiling experiments were performed using TraceFinder (ThermoFisher). The highest peaks were quantified using the ICIS detection algorithm, and metabolite annotation was

performed using an in-house library based on retention time and accurate mass generated with chemical standards (IROA Technologies, Sigma). Detection algorithm parameters applied on TraceFinder were as follows: (1) peak area threshold: 5e4, (2) retention time window: 60-180 seconds, (3) minimum peak height: 2 (S/N), (4) area noise factor: 5, (5) peak noise factor: 10, (6) baseline window: 100, (7) peak height: 5%, (8) tailing factor: 1, (9) noise method: “repetitive”, (10) multiplet resolution: 10, (11) area tail extension: 20. Data were normalized to cell count from each experiment. Acquisition and analyses for 13C-bicarbonate tracing experiments were performed using El-MAVEN (Elucidata). Raw files were converted to mzXML file format using msConvert (ProteoWizard). Peak areas were manually integrated, and data were normalized to cell count from each experiment. Peak areas with ion counts that were less than $5x10^4$ were below the threshold of detection.

2.3. Results

2.3.1. Identification and validation of IMPDH2 as a novel protein-protein interactor of ATG4B

The molecular mechanisms underlying ATG4B in nutrient stress response remain poorly defined in HER2-positive (HER2+) breast cancer cells. To this end, a single immunoprecipitation-mass spectrometry (IP-MS) experiment was performed to identify potential protein-protein interactors of ATG4B in MCF-7/HER2 breast cancer cell lines. Endogenous and FLAG IPs were initially performed in MCF-7/HER2 cells transfected with an empty vector (FLAG-EV) or FLAG-tagged ATG4B (FLAG-ATG4B) vector. The immunoprecipitation of endogenous ATG4B (anti-ATG4B IP) in both FLAG-EV and FLAG-ATG4B cell lines revealed more candidate interactors by MS compared to the immunoprecipitation of FLAG-ATG4B. As such, candidates from only the endogenous ATG4B IP-MS experiments performed in both FLAG-EV and FLAG-ATG4B cell lines were considered.

Razor peptides are peptides that can be mapped to more than one protein, but have a higher probability of being derived from one based on the greatest total number of peptides identified or highest scoring peptides[241,242]. Unique peptides are peptides that only be mapped to a single protein group[241,242]. Candidate protein-protein interactors of ATG4B, excluding ribosomal and cytoskeletal proteins, with at least 2 razor and unique

peptides (PEP) in either or both FLAG-ATG4B and FLAG-EV cell lines were prioritized. NME2 was included as an exception to the PEP cut-off as two NME isoforms, NME1 and NME3, met the PEP cut-off and were shortlisted. Spectral counts (SPC) refer to the total number of spectra identified for peptides associated with a protein. Spectral counting is a label-free approach to quantify protein abundance. Higher protein abundance translates to greater number of tryptic peptides and, consequently, higher number of spectral counts [243]. Prioritized candidate protein-protein interactors of ATG4B interactors and associated spectral counts (SPC) and razor and unique peptides (PEP) are shown in Table 2.1.

Table 2.1 Candidate ATG4B protein-protein interactors identified from pilot ATG4B immunoprecipitation -mass spectrometry experiment.

UniProt ID	Symbol	anti-ATG4B IP				IgG IP			
		FLAG-ATG4B		FLAG-EV		FLAG-ATG4B		FLAG-EV	
		SPC	PEP	SPC	PEP	SPC	PEP	SPC	PEP
Q9Y4P1	ATG4B	26	11	28	16	0	0	0	0
P20839	IMPDH1	3	3	2	2	0	0	0	0
P12268	IMPDH2	9	8	8	8	0	0	0	0
P15531	NME1	3	2	2	1	0	0	0	0
P22392	NME2	1	1	1	1	0	0	0	0
Q13232	NME3	5	4	9	6	0	0	0	0
P19474	TRIM21	1	1	7	7	0	0	0	0

SPC: Spectral counts; PEP: peptides

Of the candidate ATG4B protein-protein interactors that were identified, IMPDH2 was prioritized as the top candidate as it was associated with the greatest SPC. To validate the interaction between ATG4B and IMPDH2 independently, forward ATG4B and reciprocal IMPDH2 immunoprecipitation-western blots (IP-WBs) were performed in the HER2+ breast cancer cell lines, JIMT-1 and MCF-7/HER2. Additionally, IP-WBs were also performed in HER2- breast cancer cell lines, MDA-MB-231 and MCF-7/NEO to determine if the interaction was specific to the HER2 setting. IP-WB findings successfully validated the interaction between ATG4B and IMPDH2 in the HER2+ breast cancer cell lines examined and, additionally, revealed that the interaction was not specific to the HER2+ setting (Figure 2.1). *To date, this study is the first to identify and validate an interaction between ATG4B and IMPDH2.*

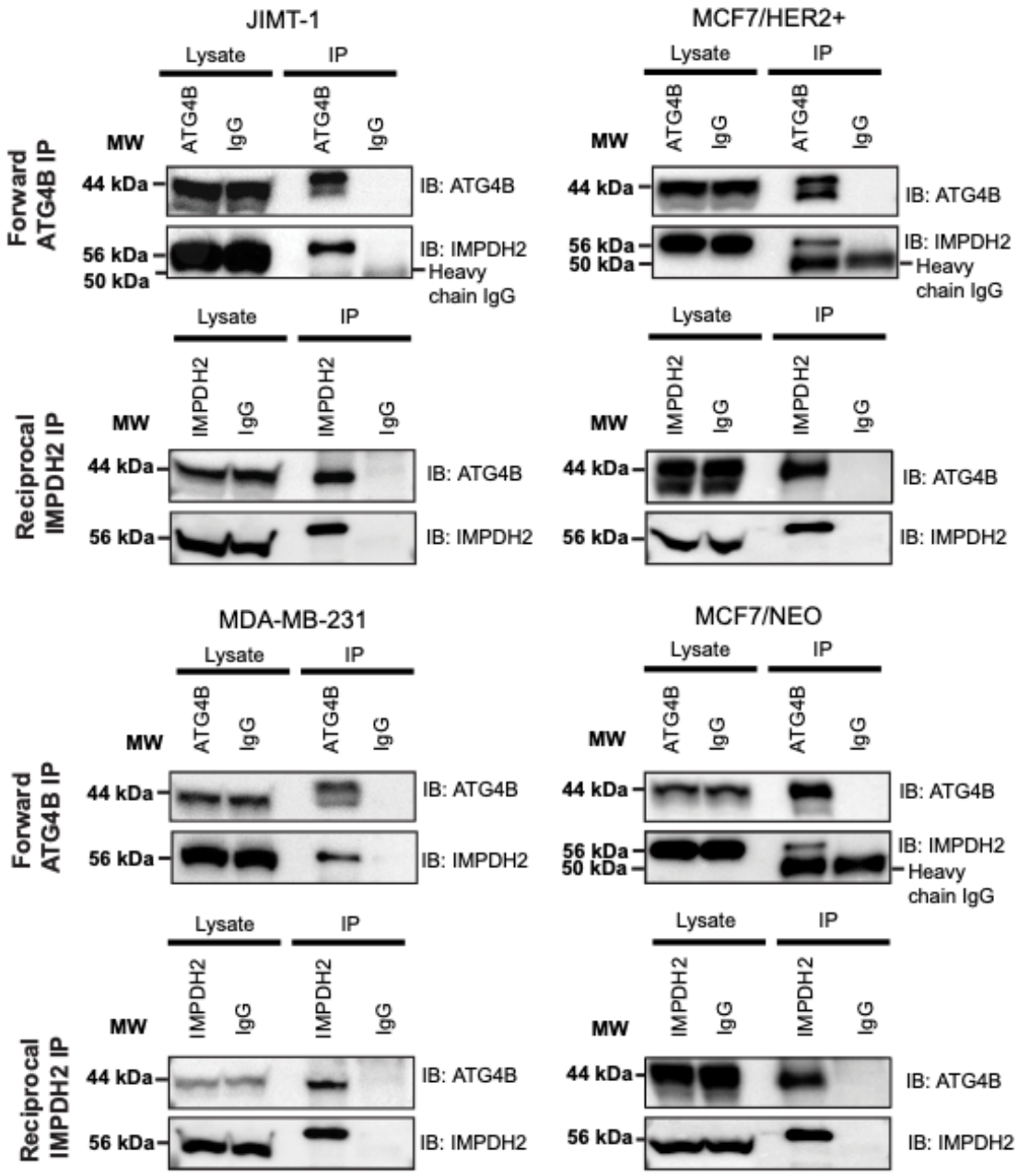

Figure 2.1 Validation of the interaction between ATG4B and IMPDH2 in several independent breast cancer cell lines.

IP-WB experiments were performed in two HER2+ breast cancer cell lines (JIMT-1, MCF7/HER2) and in two HER2- breast cancer cell lines (MDA-MB-231, MCF7/NEO). Forward ATG4B IPs were performed using cells grown in full media, and immunoprecipitated samples were subjected to WB for IMPDH2. Reciprocal IMPDH2 IPs were performed using cells grown in full media, and immunoprecipitated samples were subjected to WB for ATG4B. At least 2 biological replicates were performed for each forward and reciprocal IP. Representative blots are shown. 44 kDa bands correspond to ATG4B. 56 kDa bands correspond to IMPDH2. 50 kDa bands correspond to heavy chain IgG and are as labelled. Heavy chain IgG bands were more prominent in forward ATG4B IPs done on MCF7/NEO, MCF7/HER2 and JIMT-1 cell lines as gels were run for a shorter time during initial technique optimizations.

2.3.2. ATG4B and IMPDH2 are significantly correlated at the protein level in independent breast cancer patient cohorts

Genes and proteins that are involved in similar biological processes are frequently co-regulated and co-expressed[244]. To investigate the potential functional relationship between ATG4B and IMPDH2, the transcript and protein levels of ATG4B and IMPDH2 in publicly available breast cancer patient cohorts were examined by pearson correlation irrespective of their subtype. In general, correlation coefficients of 0.39 or less are considered weak, 0.40 to 0.69 are considered moderate, and 0.70 and above are considered strong[245]. P-values in this case test the likelihood of the null hypothesis that the pearson correlation coefficient derived is zero[245]. From the TCGA PanCancer Atlas Breast Invasive Carcinoma cohort[246,247], ATG4B and IMPDH2 presented with a weak positive correlation at the mRNA level (Figure 2.2A) and modest positive correlation at the protein level (Figure 2.2B). To validate the observations at the protein level, a larger and independent patient proteomics data from a recently published cohort was analyzed[248] and a weak positive correlation between ATG4B and IMPDH2 protein levels was observed in breast cancer patients as well (Figure 2.2C). A modest positive correlation was also observed in the normal breast samples available in this cohort despite the small sample size. Together, these findings *support a potential functional interplay between ATG4B and IMPDH2 in breast cancers that may bridge a crosstalk between the two pathways.*

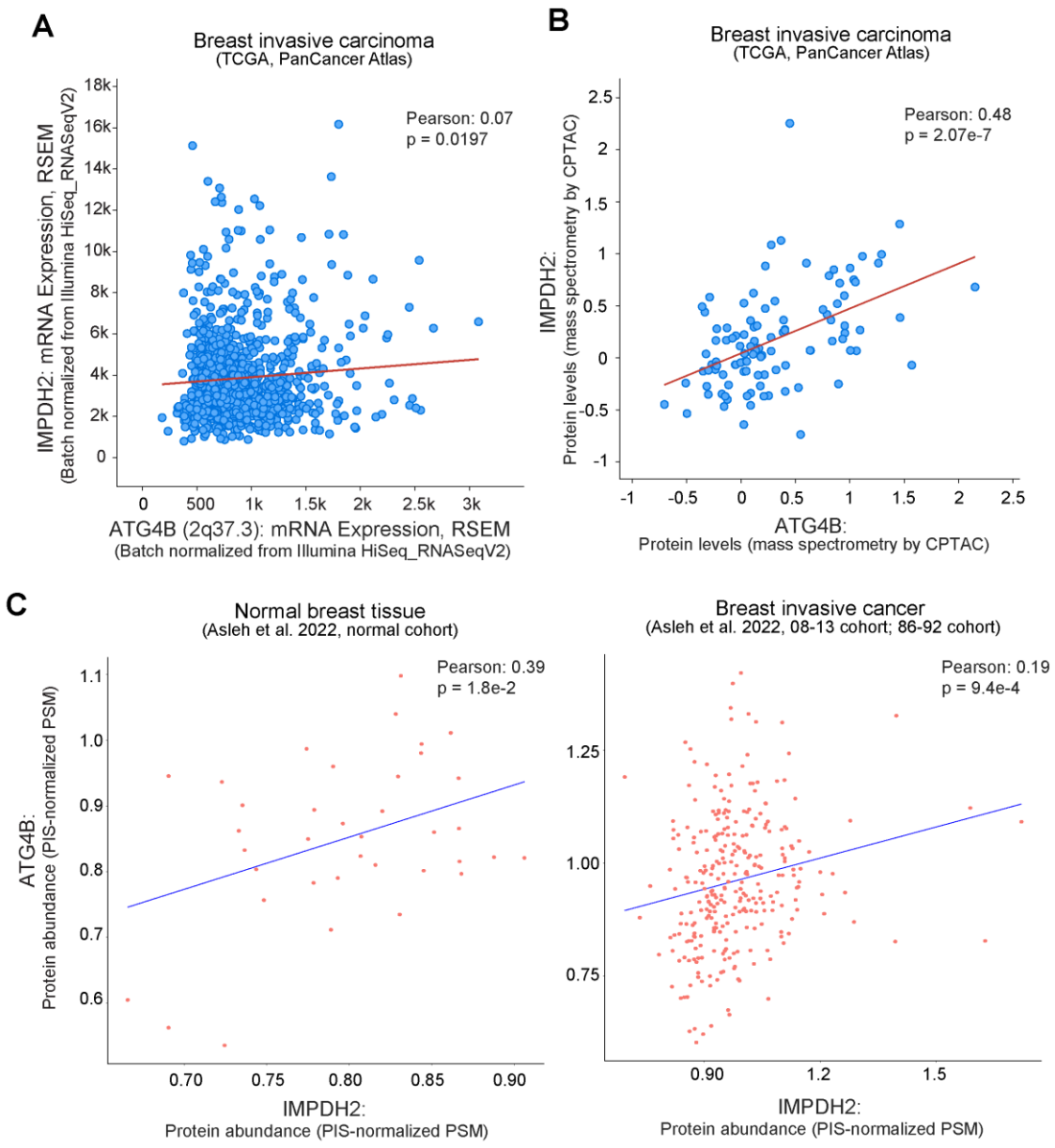

Figure 2.2 Analyses of independent breast cancer patient cohorts reveal a positive correlation between ATG4B and IMPDH2 at the protein level

Pearson correlations were performed to determine the significance of the correlation between ATG4B and IMPDH2 mRNA and protein levels. Analyses revealed weak to modest correlations beween ATG4B and IMPDH2 at the mRNA and protein level in independent breast cancer patient datasets: (A, B) TCGA PanCancer Atlas cohort (C) Asleh et al. 2022 08-13, 86-92 cohort.

2.3.3. Genetic inhibition of ATG4B does not substantially alter IMPDH protein levels

Given the modest correlation between ATG4B and IMPDH2 protein levels, I next asked whether ATG4B regulates the levels of the IMPDH proteins. To generate a tool for evaluating the effects of loss of ATG4B, I used CRISPR/Cas9 gene editing to generate ATG4B knock-out (KO) JIMT-1 cell lines. Since the IMPDH proteins are important metabolic enzymes in purine biosynthesis, and glutamine is an important amino acid in this process[135,138], I evaluated the effect of ATG4B KO on IMPDH1 and IMPDH2 protein levels in glutamine-replete or -depleted media. Parental and ATG4B KO JIMT-1 cells were validated for loss of ATG4B and LC3B processing, and IMPDH1 and IMPDH2 protein levels were examined following growth in full or glutamine-deprived media for 48 hours. Findings from these experiments revealed that glutamine deprivation had a negligible effect on IMPDH1 and IMPDH2 protein levels regardless of ATG4B status (Figure 2.3). Given the high variability of absolute protein quantifications between biological replicates (Figure 2.3B), protein quantifications were normalized to full media parental JIMT-1 controls (Figure 2.3C) and used to draw conclusions. Genetic loss of ATG4B was associated with a modest reduction in IMPDH1 protein levels under both full and glutamine-deprived media conditions in JIMT-1 ATG4B KO#1, but not in JIMT-1 ATG4B KO#2 (Figure 2.3C-i). IMPDH2 protein levels were not statistically altered in the ATG4B KO lines (Figure 2.3C-ii)

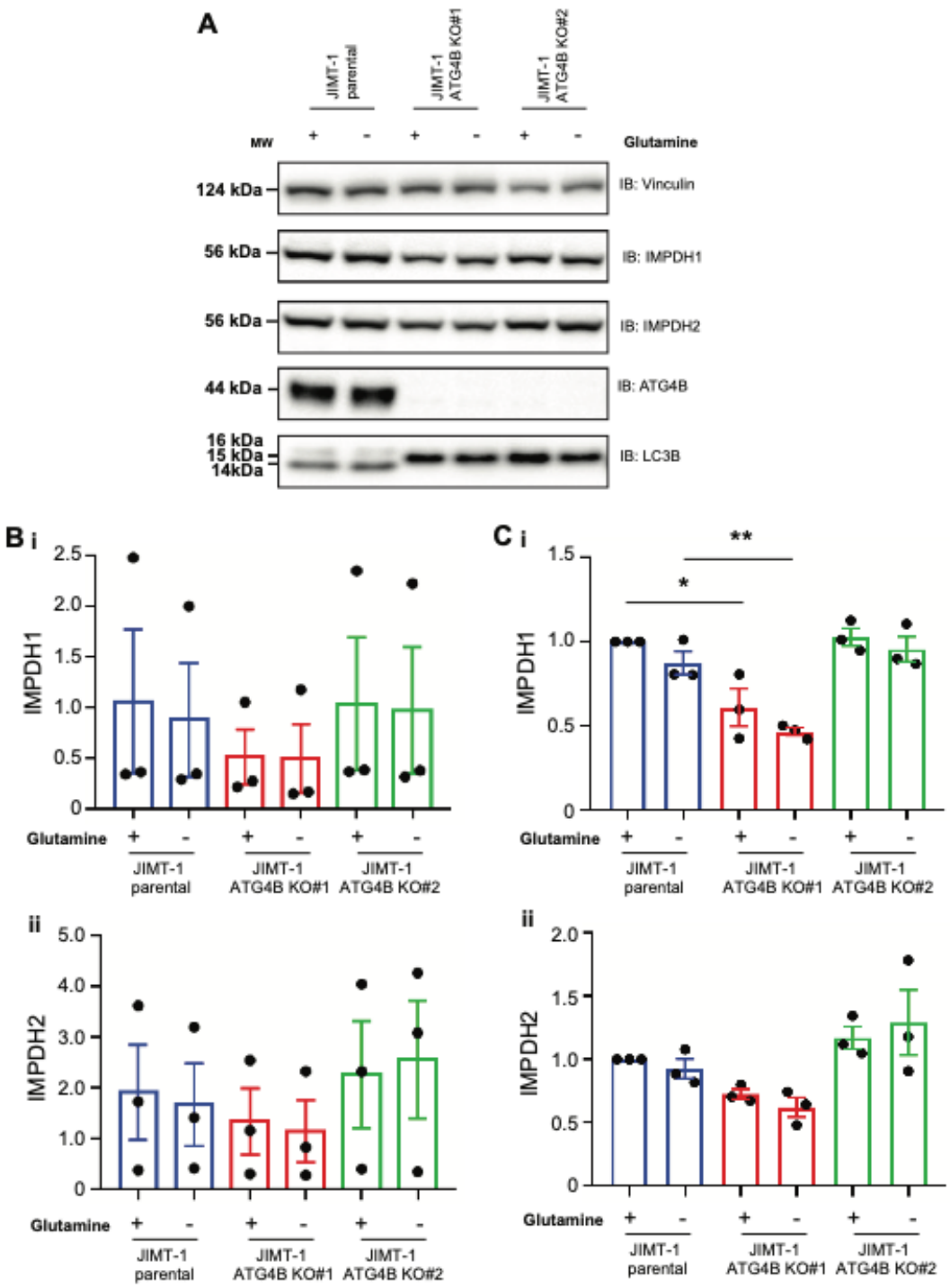

Figure 2.3 Genetic loss of ATG4B is associated with little to no changes in IMPDH protein levels in cells grown in culture for 48 hours

(A)Parental and JIMT-1 ATG4B KO cell lines were subjected to 48 hours of growth in full or glutamine-deprived media. Cells were harvested and evaluated for levels of IMPDH1, IMPDH2, ATG4B and LC3B by western blot. Accumulation of pro-LC3B (15kDa) reflects a loss of ATG4B-

mediated LC3B processing. A total of 3 biological replicates were performed. (B) Absolute quantifications of IMPDH1 and IMPDH2 protein levels were determined relative to vinculin loading controls and are shown to depict variability of absolute values between biological replicates. (C) Normalized quantifications of IMPDH1 and IMPDH2 protein levels were first determined relative to vinculin loading controls and then normalized to parental JIMT-1 full media conditions to control for variabilities in absolute values between biological replicates. For B and C, one way ANOVA with Tukey's multiple comparisons test was used to evaluate statistical differences, and error bars represent SEM. 3 biological replicates were performed.

To determine if prolonging the duration of glutamine deprivation would affect IMPDH1 and IMPDH2 protein levels, glutamine-deprived conditions were extended, and cells were harvested for western blot analyses following 120 hours (Figure 2.4). To control for the variability of the absolute protein quantifications (Figure 2.4B), protein levels were normalized to parental JIMT-1 full media controls to compare differences in IMPDH1 and IMPDH2 protein levels. No significant changes in IMPDH1 or IMPDH2 protein levels were detected (Figure 2.4C).

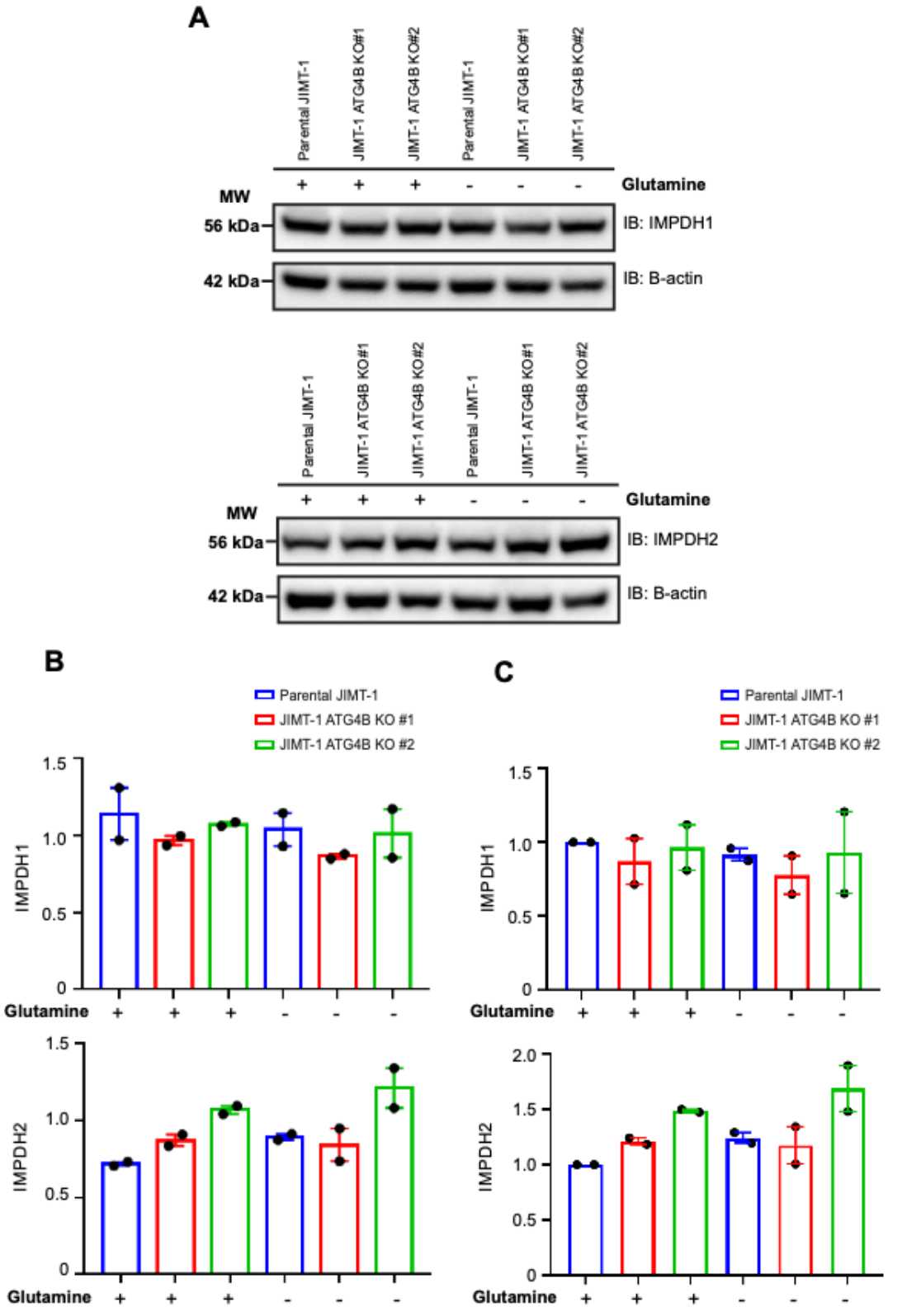
A
Parental JIMT-1
JIMT-1 ATG4B KO#1
JIMT-1 ATG4B KO#2
Parental JIMT-1
JIMT-1 ATG4B KO#1
JIMT-1 ATG4B KO#2
Glutamine
+ + + - - -
MW
56 kDa
IB: IMPDH1
42 kDa
IB: B-actin
Parental JIMT-1
JIMT-1 ATG4B KO#1
JIMT-1 ATG4B KO#2
Parental JIMT-1
JIMT-1 ATG4B KO#1
JIMT-1 ATG4B KO#2
Glutamine
+ + + - - -
MW
56 kDa
IB: IMPDH2
42 kDa
IB: B-actin
B
Parental JIMT-1
JIMT-1 ATG4B KO #1
JIMT-1 ATG4B KO #2
IMPDH1
1.5
1.0
0.5
0
Glutamine + + + - - -
IMPDH2
1.5
1.0
0.5
0
Glutamine + + + - - -
C
Parental JIMT-1
JIMT-1 ATG4B KO #1
JIMT-1 ATG4B KO #2
IMPDH1
1.5
1.0
0.5
0
Glutamine + + + - - -
IMPDH2
2.0
1.5
1.0
0.5
0
Glutamine + + + - - -

Figure 2.4 Genetic loss of ATG4B is not associated with significant changes in IMPDH1 or IMPDH2 protein in cells grown in culture for 120 hours

(A) Parental and ATG4B KO JIMT-1 cells were harvested for western blot analyses of IMPDH1, IMPDH2 and B-actin after growth in full media for 120 hours. Western blots were performed as described in methods. (B) Absolute quantifications of IMPDH1 and IMPDH2 protein levels were determined relative to B-actin loading controls and are shown to depict variability of absolute values between biological replicates. (C) Normalized quantifications of IMPDH1 and IMPDH2 protein levels were first determined relative to B-actin loading controls and then normalized to parental JIMT-1 full media conditions to control for variabilities in absolute values between biological replicates. For B and C, one way ANOVA with Tukey's multiple comparisons test was used to evaluate statistical differences, and no statistically significant changes were observed. 2 biological replicates were performed.

Since genetic loss of ATG4B may have induced compensatory mechanisms that aided in the maintenance of IMPDH protein levels, a genetic knockdown approach was explored next. To determine if genetic knockdown of ATG4B would alter IMPDH1 and IMPDH2 protein levels, a stable ATG4B knockdown JIMT-1 cell line was generated by shRNA and used to evaluate levels of IMPDH1 and IMPDH2 compared to a scramble control line following 48 hours of glutamine deprivation (Figure 2.5). To control for the variability of absolute protein quantifications between biological replicates (Figure 2.5B), protein quantifications were further normalized to shRNA scramble (shSCR) JIMT-1 controls (Figure 2.5C) and used to draw conclusions. Findings revealed that genetic knockdown of ATG4B was associated with a modest but significant increase in IMPDH2 protein levels under conditions of glutamine deprivation (Figure 2.5C-ii). No significant changes in IMPDH1 protein levels resulting from knockdown of ATG4B were observed in full or glutamine-deprived media (Figure 2.5C-i). These findings support data from Figure 2.4 where genetic loss of ATG4B was associated with a modest trend on increasing IMPDH protein levels in cells grown in culture for 120 hours and suggests that ATG4B may negatively regulate IMPDH2 protein levels to a small degree.

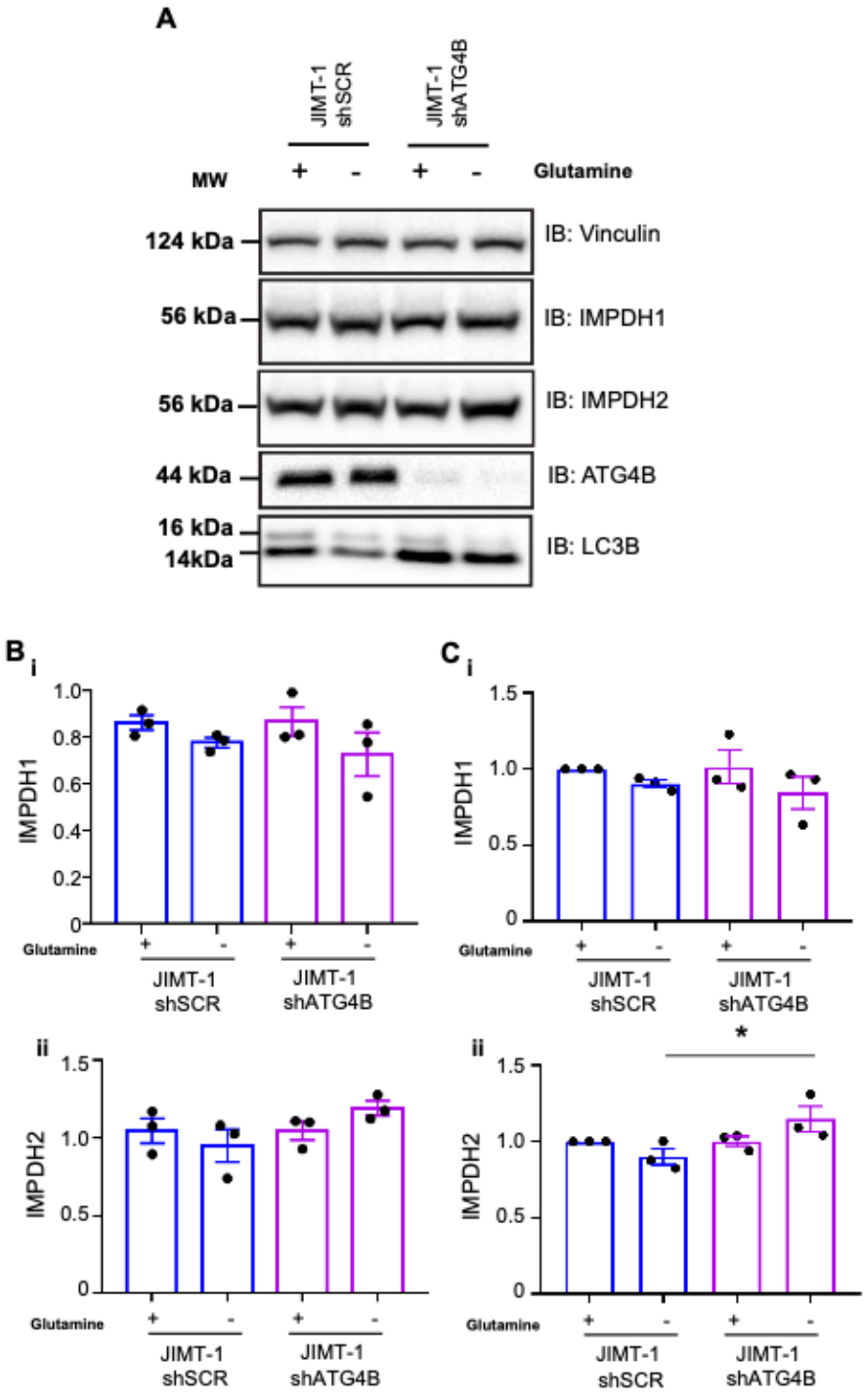

Figure 2.5 Genetic knockdown of ATG4B does not reduce IMPDH protein levels
(A) Stable shATG4B and shSCRAMBLE (shSCR) JIMT-1 cell lines were generated by Nancy E. Go. JIMT-1 cells were stably transfected with shSCR control or shATG4B, and subjected to 48 hours of growth in full or glutamine-deprived media. Cells were harvested and evaluated for levels of IMPDH1, IMPDH2, ATG4B and LC3B by western blot. A total of 3 biological replicates were performed. (B) Absolute quantifications of IMPDH1 and IMPDH2 protein levels were determined relative to vinculin loading controls and are shown to depict variability of absolute values between

biological replicates. (C) Normalized quantifications of IMPDH1 and IMPDH2 protein levels were determined relative to vinculin loading controls and then normalized to shSCR JIMT-1 full media conditions to control for variabilities in absolute values between biological replicates. For B and C, one way ANOVA with Tukey's multiple comparisons test was used to evaluate statistical differences, and error bars represent SEM. 3 biological replicates were performed.

2.3.4. Inhibition of IMPDH does not affect ATG4B protein levels but is associated with reduced processing or stabilization of ATG8 proteins

IMPDH2 facilitates the oxidation of IMP to XMP, with the concomitant reduction of NAD^+ to NADH[185]. Previous studies have reported that ATG4B is redox regulated, and the reduction of ATG4B promotes its activity[105]. As such, I hypothesized that the premise for the ATG4B-IMPDH2 interaction may stem from IMPDH2's role in indirectly promoting the reduced state of ATG4B and, consequently, ATG4B activity (Figure 2.6).

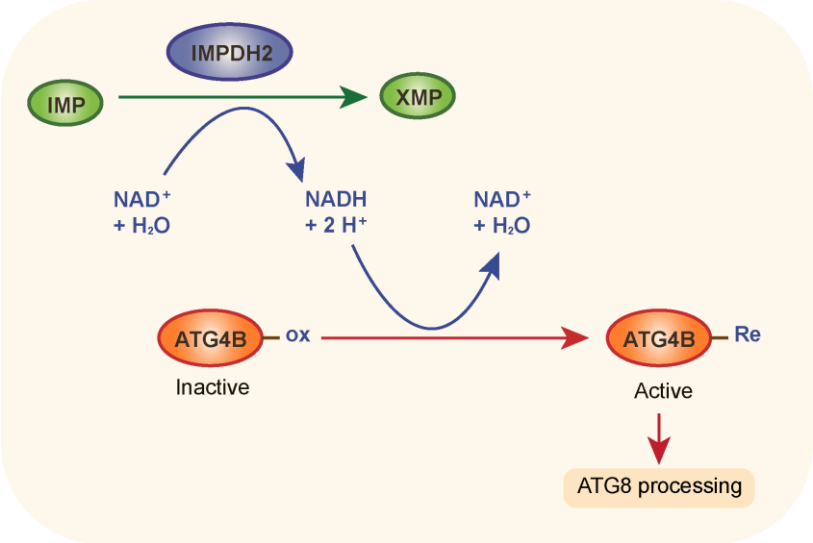

Figure 2.6 Proposed model for IMPDH2 regulation of ATG8 protein processing
The oxidation of IMP to XMP by IMPDH2 results in the production of cellular NADH. The close proximity of ATG4B to IMPDH2 may prime it as a target of reductive modification by NADH to promote its activity.

To first determine if ATG4B activity is regulated by IMPDH2, the ATG8 proteins, MAP1LC3B (also known as LC3B) and GABARAP, were examined following the treatment of parental JIMT-1 cells with MPA. An ATG4B KO JIMT-1 cell line was included as a control for impaired LC3B processing[115] or GABARAP stabilization[93].

Given the high variability of absolute protein quantifications between biological repliates (Figure 2.7B), protein quantifications were normalized to 0 μM MPA controls to control for variability (Figure 2.7C) and used to draw conclusions.

Pharmacological inhibition of IMPDH led to a significant accumulation of lipidated LC3B (LC3B-II), suggesting an impairment in the de-lipidation of LC3B (Figure 2.7C-i). IMPDH inhibition did not have an apparent effect on the processing of GABARAP, but was associated with a reduction in GABARAP protein levels, which could suggest an impairment in the stabilization of GABARAP (Figure 2.7C-ii). Previous studies have shown that ATG4B stabilizes unlipidated forms of GABARAP through by interacting with GABARAP via its C-terminal LC3-interacting region motif[93]. The decrease in unlipidated GABARAP protein levels resulting from IMPDH inhibition could suggest a decrease in the function of ATG4B to interact with GABARAP and stabilize its unlipidated form in the cell. *These findings suggest that IMPDH proteins may promote the processing or stabilization of the ATG8 proteins, LC3B and GABARAP, by, regulating ATG4B activity or function.*

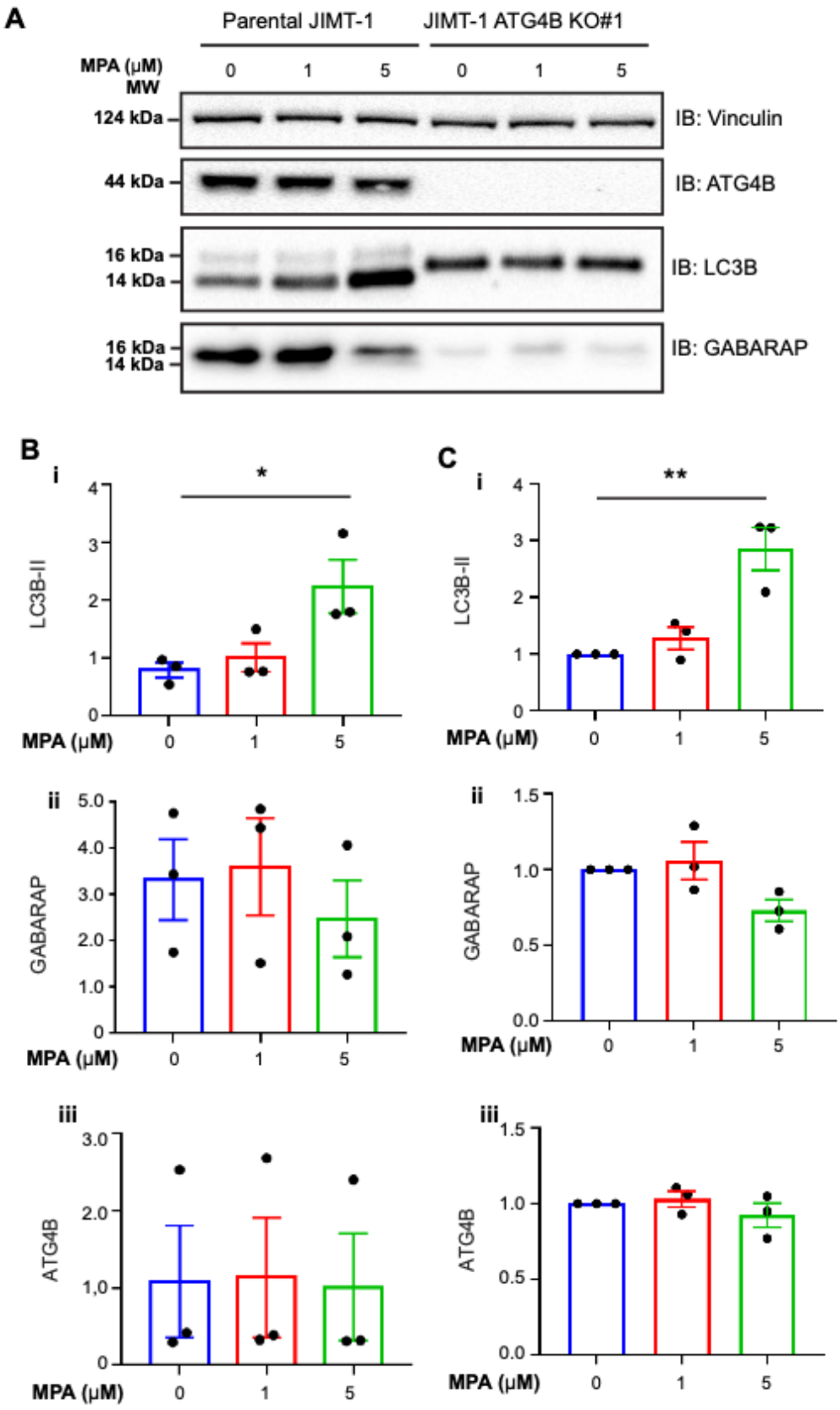
A
Parental JIMT-1
JIMT-1 ATG4B KO#1
MPA (μM)
0
1
5
0
1
5
MW
124 kDa
IB: Vinculin
44 kDa
IB: ATG4B
16 kDa
14 kDa
IB: LC3B
16 kDa
14 kDa
IB: GABARAP
B
i
*
LC3B-II
MPA (μM)
ii
GABARAP
iii
ATG4B
C
i
**
LC3B-II
ii
GABARAP
iii
ATG4B

Figure 2.7 Pharmacological inhibition of IMPDH impairs LC3B processing and GABARAP stabilization

(A) Parental and ATG4B KO JIMT-1 cells were treated with 0, 1, or 5 μM of MPA for 120 hours, and harvested for western blot analyses of vinculin, ATG4B, LC3B and GABARAP protein levels. Representative western blots are shown. Accumulation of pro-LC3B (15kDa) reflects a loss of ATG4B-mediated LC3B processing. (B) Absolute quantifications of ATG4B, LC3B-II and GABARAP protein levels were determined relative to vinculin loading controls and are shown to depict variability between biological replicates. (C) Normalized quantifications of ATG4B, LC3B-II and GABARAP levels were determined relative to vinculin loading controls and then normalized to 0 μM MPA controls to control for variabilities in absolute values between biological replicates. For B and C, one way ANOVA with Tukey's multiple comparisons test was used to evaluate statistical differences, and error bars represent SEM.3 biological replicates were performed.

To investigate if the IMPDH2 regulates ATG4B protein levels, I evaluated ATG4B protein levels following pharmacological inhibition of IMPDH by mycophenolic acid (MPA). I found no significant changes in ATG4B protein levels in parental JIMT-1 cells treated with MPA (Figure 2.7C-iii). To validate these findings, I examined the effect of genetic knockdown of both IMPDH1 and IMPDH2 by siRNA in parental JIMT-1 cells. Similarly, genetic knockdown of IMPDH proteins did not significant alter ATG4B protein levels (Figure A1). *These findings suggest that the IMPDH proteins unlikely regulate protein levels of ATG4B.*

2.3.5. Glutamine deprivation modestly reduces cellular growth and induces IMPDH2 rings-and-rod structures in response to depletion in cellular guanine nucleotide levels

Glutamine is an important amide donor in *de novo* purine biosynthesis and guanine nucleotide production[135]. Previous studies by Kim et al. 2013 reported increased expression of enzymes involved in glutamine metabolism in breast tumors of the HER2 molecular subtype[234]. As such, the HER2-positive breast cancer cell line, JIMT-1, was selected as a cell line model to examine the effects of glutamine deprivation on breast cancer cell growth. Changes in the phase confluence of parental JIMT-1 cells under full or glutamine-deprived media were measured for 48 hours, and a modest reduction in cellular growth was observed from short-term glutamine deprivation (Figure 2.8). *These findings suggest that glutamine contributes to the growth of HER2-positive breast cancer cells.*

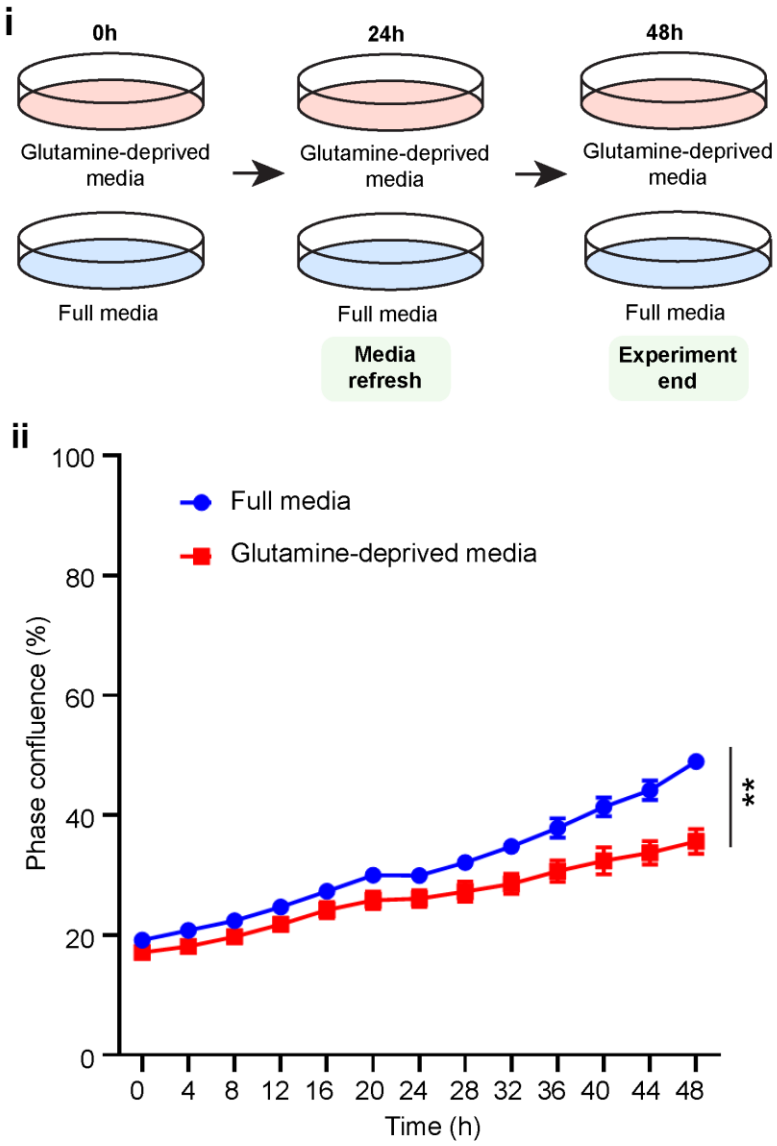

Figure 2.8 Short-term glutamine leads to a modest reduction in cellular growth. (i) Schematic of experimental set-up for short-term glutamine deprivation experiments (ii) Parental JIMT-1 cells were subjected to full or glutamine-deprived media for a total of 48 hours. Growth of cells was measured every 4 hours by evaluating the phase confluence of cells using an Incucyte. A total of 3 biological replicates were performed. Error bars represent SEM, and an unpaired t-test was performed to evaluate statistical difference.

Glutamine deprivation has been previously shown to induce the polymerization of IMPDH2 into ring-and-rod structures in HeLa cells[190]. IMPDH2 facilitates GTP production in the cell[185] (Figure 2.9A) and it has been proposed that the formation of IMPDH2 ring-and-rod structures occurs in response to depletion in guanine nucleotide levels[190]. To investigate if breast cancer cells also have the ability to form IMPDH2 rings-and-rods

under glutamine deprivation, IMPDH2 was stained for and evaluated by immunofluorescence microscopy. Following 48 hours of glutamine deprivation, IMPDH2 presented as four distinct phenotypes in glutamine-deprived breast cancer cells: i) diffuse, ii) vesicle-like or puncta (0.5-1 μm diameter), iii) short rods (1-10 μm diameter), iv) long rods (>10 μm diameter) and rings (Figure 2.9B). Interestingly, cells that tended to form one of four distinct phenotypes often were clustered together in certain regions of the tissue culture plate well. This observation may suggest that different regions of a tissue culture plate may present with differing nutrient availabilities, thereby modulating the ability of cells that reside in these regions to form different IMPDH2 ring-and-rod structures. To determine if purine and guanine nucleotide levels are affected by glutamine deprivation, cellular levels of IMP, XMP, GMP, GDP and GTP were examined by metabolomics in JIMT-1 cells grown in full or glutamine-deprived media. 48 hours of glutamine deprivation led to a reduction in levels of XMP, GMP, GDP and GTP, *suggesting a correlation between the formation of IMPDH2 rings-and-rods occurs and reduced cellular guanine nucleotide levels* (Fig. 2.9C)

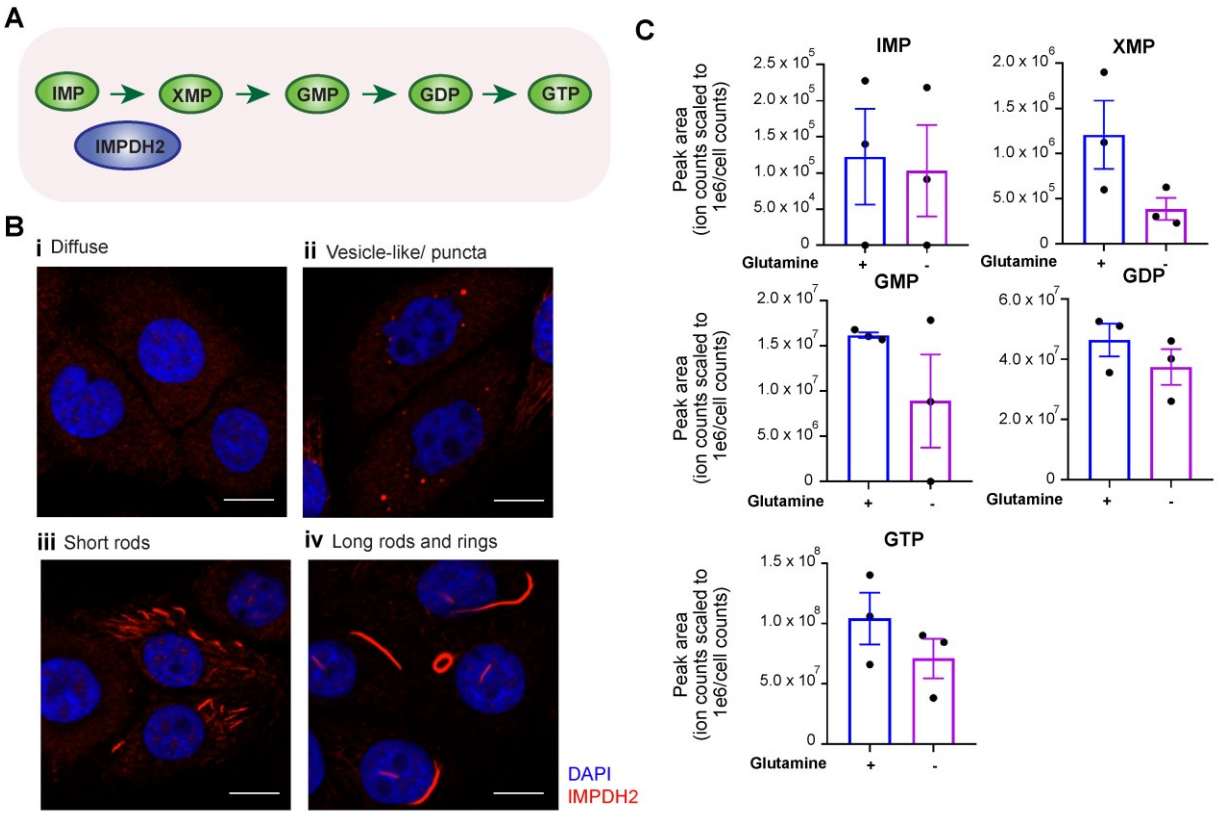

Figure 2.9 Glutamine deprivation induces IMPDH2 ring-and-rod formation and leads to a reduction in cellular XMP and guanine nucleotide levels

(A) IMPDH2 is involved in the oxidation of IMP to XMP, which facilitates the downstream generation of key purine nucleotides that are important for GTP production. Derived from information provided in Mullen and Singh, 2023[138]. (B) IMPDH2 exists in 4 distinct phenotypes under glutamine deprivation: i) diffuse, ii) vesicle-like/puncta, iii) short rods, and iv) long rods and rings. Parental JIMT-1 cells were subjected to full or glutamine-deprived conditions for 48 hours prior to immunofluorescence staining and microscopy. Representative images of cells are shown. Scale bar = 10 um. (C) Parental JIMT-1 cells were subjected to growth in full or glutamine deprived media and harvested for untargeted metabolite profiling studies as described in methods. Targeted analyses of IMP, XMP, GMP, GDP, and GTP were performed to compare levels of these metabolites in fed- vs. glutamine-deprived cells. Unpaired t-tests were performed to evaluate statistical differences and error bars represent SEM. A total of 3 independent biological replicates were performed.

2.3.6. Guanosine supplementation depolymerizes IMPDH2 ring-and-rod structures by restoring cellular GTP levels in glutamine-deprived cells

Previous studies have shown that supplementation of glutamine-deprived cells with guanosine leads to depolymerization of IMPDH2 rings-and-rods[190]. This is because, through the purine salvage pathway, guanosine can be converted to guanine, enter the purine biosynthesis pathway as GMP, and be catalyzed to GTP[138] (Figure 2.10A). To determine if increasing GTP levels through the purine salvage pathway can lead to IMPDH2 ring-and-rod depolymerization in glutamine-deprived breast cancer cells, JIMT-1 cells were supplemented with guanosine following 48 hours of glutamine deprivation. Immunofluorescence microscopy revealed that IMPDH2 ring-and-rod structures completely depolymerized in glutamine-deprived cells supplemented with guanosine (Figure 2.10B).

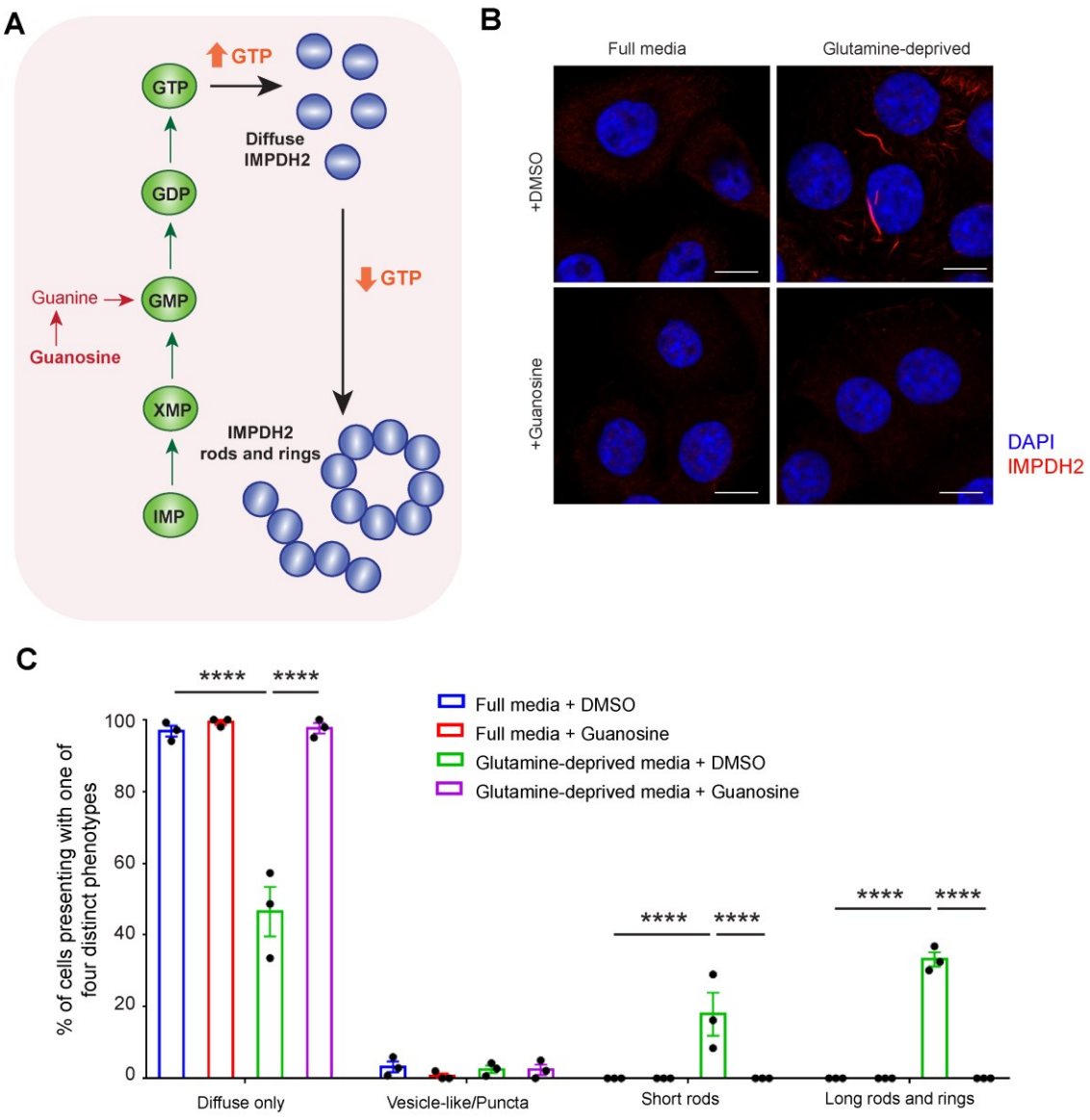

Figure 2.10 Guanosine supplementation leads to the complete depolymerization of IMPDH2 ring-and-rod structures in glutamine-deprived cells

(A) Guanosine can be converted through the purine salvage pathway through the concerted activities of salvage pathway enzymes to replenish cellular GTP levels. (B) Guanosine supplementation reverses IMPDH2 ring and rod formation in glutamine-deprived parental JIMT-1 cells. Parental JIMT-1 cells were subjected to full or glutamine-deprived conditions for 48 hours. Media was supplemented with guanosine or 0.56% DMSO 1 hour prior to immunofluorescence. Representative immunofluorescence images are shown. Scale bar = 10 um. (C) Quantitative comparison of parental JIMT-1 cells subjected to full media or glutamine-deprived conditions in the absence or presence of guanosine for 1 hour. Cells were scored based on the presentation of one of four distinct phenotypes: (i) diffuse only, (ii) vesicle-like/puncta, (iii) short rods, and (iv) long rods and rings. A total of 3 biological replicates were performed, and at least 140 cells were scored per replicate. Two-way ANOVA with Tukey's multiple comparisons test was performed (**** $p \leq 0.0001$). Error bars represent SEM.

To confirm that guanosine supplementation increased cellular production of GTP, a pilot 13C-bicarbonate metabolite tracing experiment was performed on parental JIMT-1 cells following 48 hours of growth in full media or glutamine deprived conditions, with or without guanosine supplementation. Turnover of guanine, GMP, GDP and GTP were significantly increased following guanosine supplementation. Of note, turnover of these metabolites following guanosine supplementation was significantly higher in glutamine-deprived cells, suggesting their increased cellular demand under glutamine deprivation (Figure 2.11). *Together, these findings provide evidence that the formation of IMPDH2 rings-and-rods occurs in response to depletion of GTP levels in breast cancer cells.*

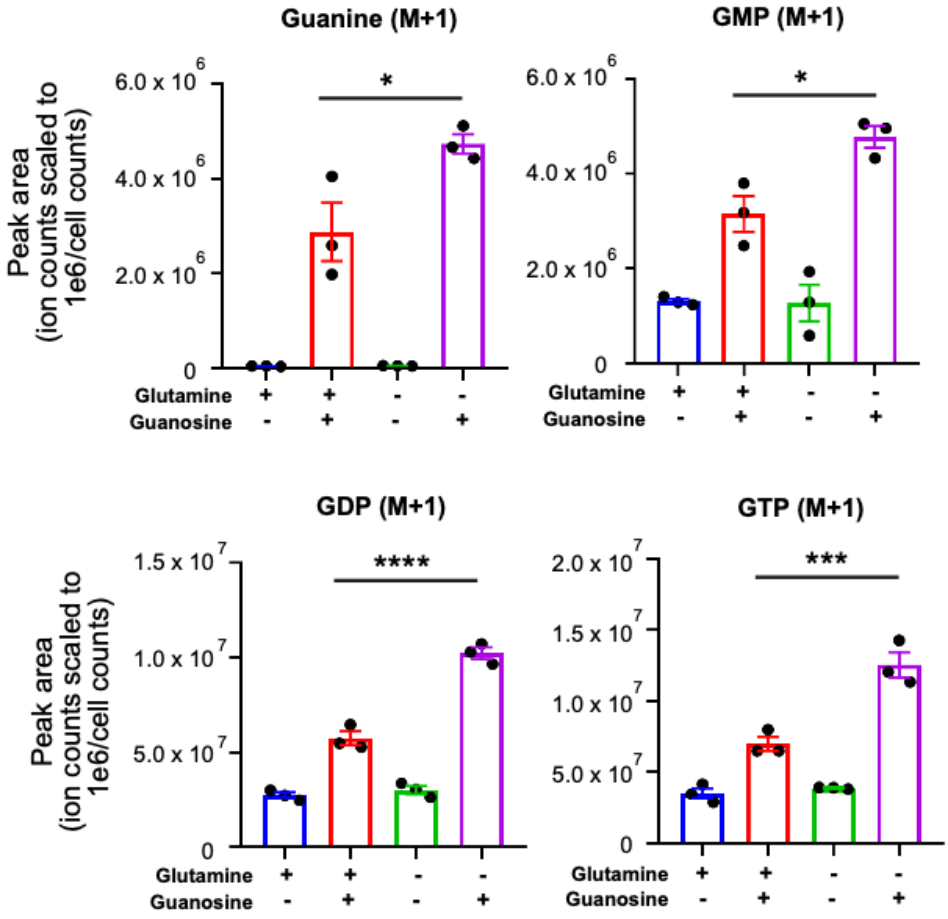

Figure 2.11 Guanosine supplementation increases cellular turnover of guanine nucleotides

Parental JIMT-1 cells were grown in full or glutamine-deprived media, prior to harvesting for 13C-bicarbonate tracing experiments by LC-MS. Peak area in the unit of ion counts for each metabolite was scaled to the cell counts for each condition. Increased cellular turnover of

guanine, GMP, GDP and GTP was observed following guanosine supplementation. Turnover of guanine and guanine nucleotides was significantly greater in glutamine-deprived breast cancer cells when supplemented with guanosine. A total of 3 technical replicates were performed. One way ANOVA with Tukey's multiple comparisons tests were performed to evaluate statistical differences. Error bars represent SEM.

2.3.7. Genetic loss of ATG4B impairs IMPDH2 ring-and-rod formation and is associated with an increase in guanine nucleotide levels under glutamine deprivation

To determine if ATG4B is important for IMPDH2 ring-and-rod formation in glutamine-deprived breast cancer cells, parental and ATG4B KO JIMT-1 cells were subjected to glutamine deprivation to induce IMPDH2 rings-and-rods. Genetic loss of ATG4B was associated with a significant impairment in the ability of glutamine-deprived cells to form IMPDH2 ring-and-rod structures (Figure 2.12A). Previous studies have reported that GTP allosterically inhibits the ability of IMPDH proteins to form ring-and-rod structures[188]. To determine if the impaired ability of ATG4B KO cells to form IMPDH2 rings-and-rods correlates to changes in cellular XMP and guanine nucleotide levels, levels of XMP, GMP, GDP and GTP were evaluated in glutamine-deprived parental and ATG4B KO cells by metabolite profiling. Findings revealed that the guanine nucleotides, GMP, GDP and GTP, were elevated in ATG4B KO cells compared to parental cells under glutamine deprivation (Figure 2.12B). *These findings support the utilization of an alternate pathway in ATG4B KO cells to generate guanine nucleotides in glutamine-deprived settings.*

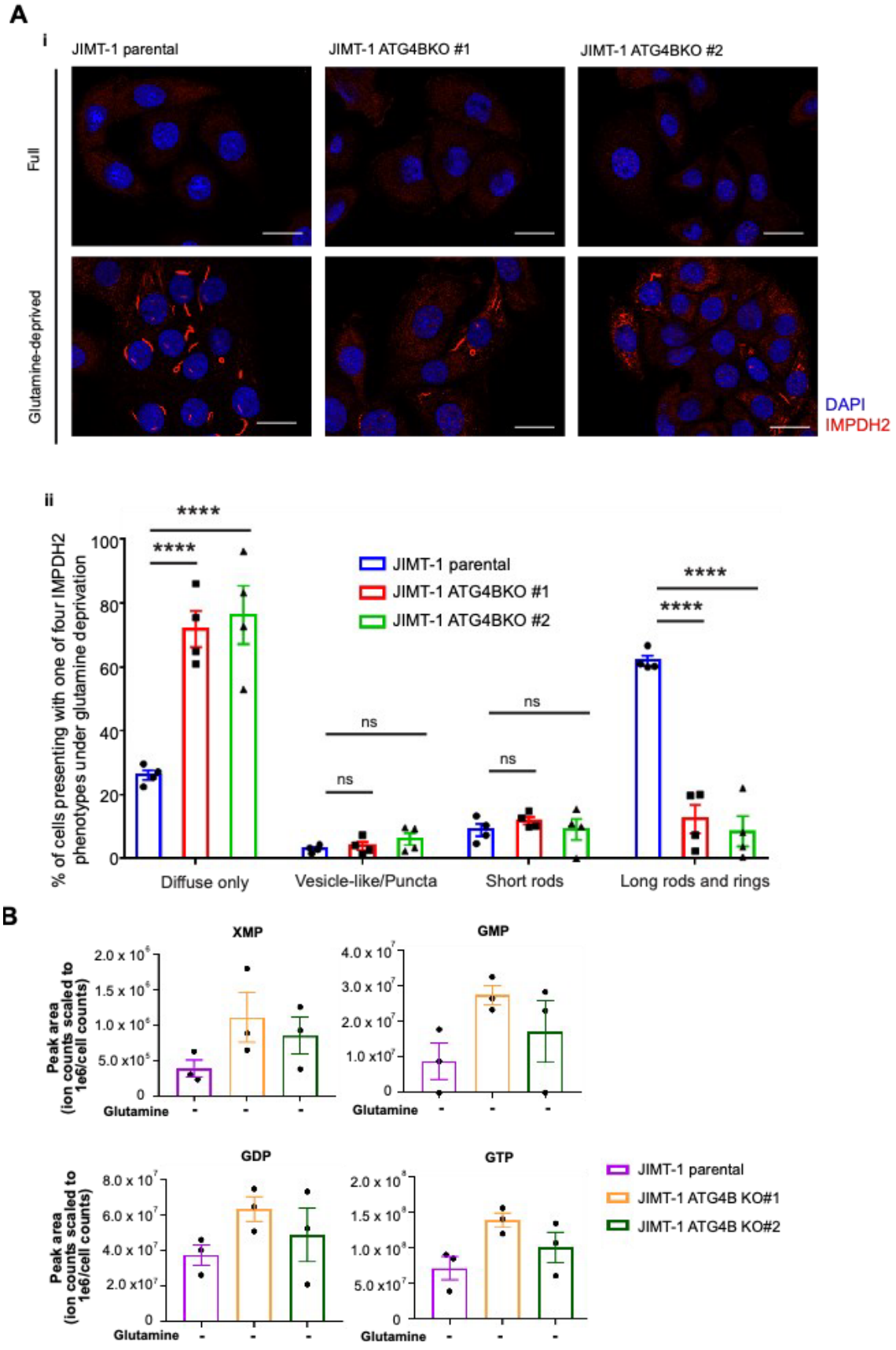
A
i
JIMT-1 parental
JIMT-1 ATG4BKO #1
JIMT-1 ATG4BKO #2
Full
Glutamine-deprived
DAPI
IMPDH2
ii
% of cells presenting with one of four IMPDH2 phenotypes under glutamine deprivation
JIMT-1 parental
JIMT-1 ATG4BKO #1
JIMT-1 ATG4BKO #2
****
ns
Diffuse only
Vesicle-like/Puncta
Short rods
Long rods and rings
B
XMP
GMP
GDP
GTP
Peak area (ion counts scaled to 1e6/cell counts)
Glutamine
JIMT-1 parental
JIMT-1 ATG4B KO#1
JIMT-1 ATG4B KO#2

Figure 2.12 Genetic loss of ATG4B impairs IMPDH2 ring-and-rod formation and is associated with an increase in guanine nucleotides in glutamine-deprived cells

(A) Parental and ATG4B KO JIMT-1 cells were subjected to full or glutamine- deprived media conditions for 48 hours. i) IMPDH2 immunofluorescence was performed, and cells were scored based on the presentation of one of four distinct IMPDH2 phenotypes: diffuse, vesicle-like puncta, short rods, or long rods and rings. Representative immunofluorescence images are shown. Scale bar = 20 um. (ii) Quantification of parental and ATG4B KO JIMT-1 cells presenting with one of four distinct IMPDH2 phenotypes under glutamine deprivation. Percent mean (%) of 4 biological replicates are shown in bar graphs. Two-way ANOVA with Dunnett's multiple comparisons test was performed (**** $P \leq 0.0001$). Error bars represent SEM. (B) Parental and ATG4B KO JIMT-1 cells were subjected to growth in glutamine deprived media and harvested for untargeted metabolite profiling studies as described in methods. A targeted analyses of XMP, GMP, GDP and GTP was performed to compare cellular levels of these metabolites between cell lines. A total of 3 biological replicates were performed. One way ANOVA with Tukey's multiple comparisons tests were performed to evaluate statistical differences. No statistically significant changes were observed. Error bars represent SEM.

2.3.8. Genetic loss of ATG4B is associated with an enrichment in metabolites involved in purine metabolism

To understand the metabolic consequences of glutamine deprivation, untargeted metabolite profiling studies were performed on parental JIMT-1 cells following 48 hours of growth in full or glutamine-deprived media. Pathway enrichment analyses were separately performed on metabolites that were downregulated or upregulated under glutamine deprivation relative to full media conditions. Notably, these analyses revealed an over-representation of metabolites involved in purine metabolism that are altered following glutamine deprivation (Figure 2.13A). Several key metabolites involved in purine metabolism, like the adenine and guanine nucleotides were reduced upon glutamine deprivation. Interestingly, some purine metabolism metabolites, like adenosine, guanosine and PRPP, were increased under conditions of glutamine deprivation. This may be a result of increased adenosine, guanosine, and glucose uptake by cells under conditions of glutamine deprivation in response to glutamine deprivation. *Results from these analyses highlight the importance of glutamine in purine metabolism.*

A

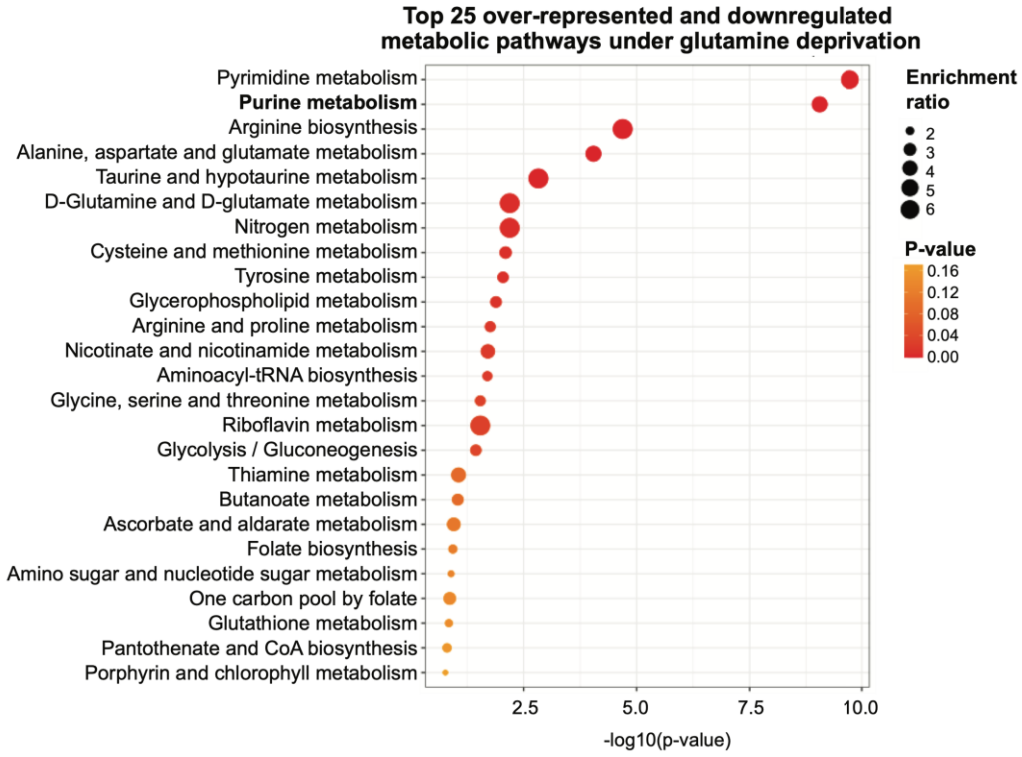
Top 25 over-represented and downregulated metabolic pathways under glutamine deprivation
Pyrimidine metabolism
Purine metabolism
Arginine biosynthesis
Alanine, aspartate and glutamate metabolism
Taurine and hypotaurine metabolism
D-Glutamine and D-glutamate metabolism
Nitrogen metabolism
Cysteine and methionine metabolism
Tyrosine metabolism
Glycerophospholipid metabolism
Arginine and proline metabolism
Nicotinate and nicotinamide metabolism
Aminoacyl-tRNA biosynthesis
Glycine, serine and threonine metabolism
Riboflavin metabolism
Glycolysis / Gluconeogenesis
Thiamine metabolism
Butanoate metabolism
Ascorbate and aldarate metabolism
Folate biosynthesis
Amino sugar and nucleotide sugar metabolism
One carbon pool by folate
Glutathione metabolism
Pantothenate and CoA biosynthesis
Porphyrin and chlorophyll metabolism
2.5
5.0
7.5
10.0
-log10(p-value)
Enrichment ratio
2
3
4
5
6
P-value
0.16
0.12
0.08
0.04
0.00

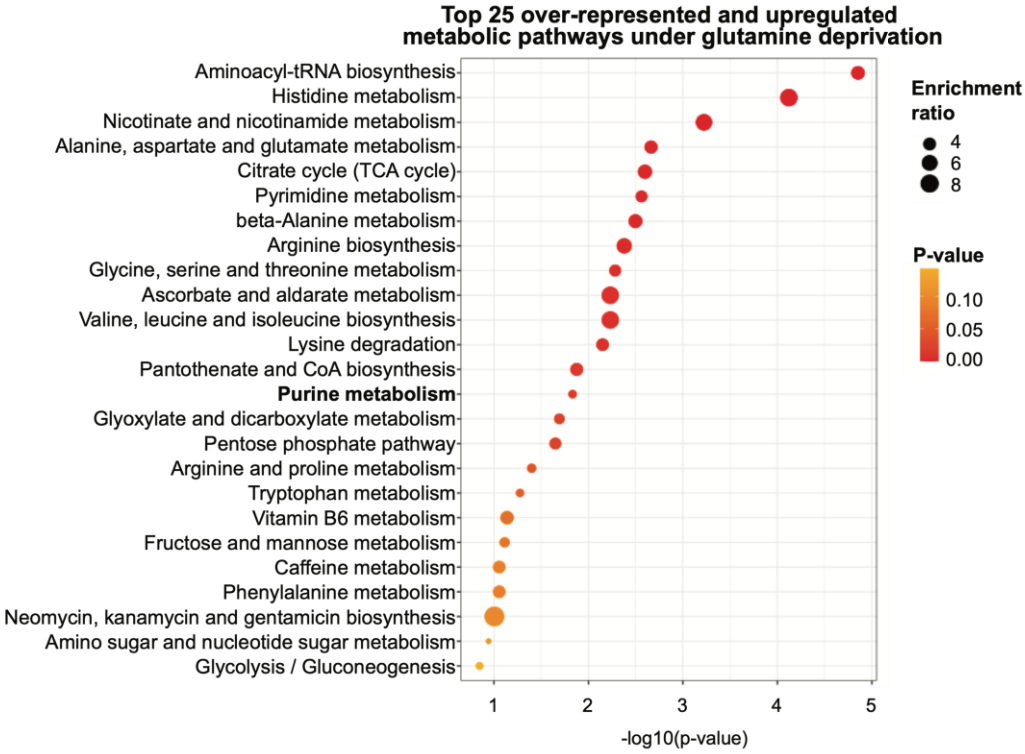
Top 25 over-represented and upregulated metabolic pathways under glutamine deprivation
Aminoacyl-tRNA biosynthesis
Histidine metabolism
Nicotinate and nicotinamide metabolism
Alanine, aspartate and glutamate metabolism
Citrate cycle (TCA cycle)
Pyrimidine metabolism
beta-Alanine metabolism
Arginine biosynthesis
Glycine, serine and threonine metabolism
Ascorbate and aldarate metabolism
Valine, leucine and isoleucine biosynthesis
Lysine degradation
Pantothenate and CoA biosynthesis
Purine metabolism
Glyoxylate and dicarboxylate metabolism
Pentose phosphate pathway
Arginine and proline metabolism
Tryptophan metabolism
Vitamin B6 metabolism
Fructose and mannose metabolism
Caffeine metabolism
Phenylalanine metabolism
Neomycin, kanamycin and gentamicin biosynthesis
Amino sugar and nucleotide sugar metabolism
Glycolysis / Gluconeogenesis
1
2
3
4
5
-log10(p-value)
Enrichment ratio
4
6
8
P-value
0.10
0.05
0.00

B

Purine metabolism metabolites altered by glutamine deprivation	
Downregulated	Upregulated
Adenine	**Adenosine**
ADP	Allantoin
ADP ribose	dAMP
AICAR	Deoxyadenosine
ATP	**Guanosine**
Cyclic GMP	**PRPP**
dATP	Xanthosine
Deoxyguanosine	
GDP	
GMP	
GTP	
Guanine	
Hypoxanthine	
IDP	
Inosine	
Inosinic acid (IMP)	
ITP	
L-glutamine	
Uric acid	
Xanthine	
Xanthylic acid	

Figure 2.13 Glutamine is an important effector of purine metabolism in breast cancer cells

Parental JIMT-1 cells were grown in full or glutamine-deprived media for 48 hours, prior to harvesting for metabolite profiling experiments by LC-MS. Peak area in the unit of ion counts for each metabolite was scaled to the cell counts for each condition and averaged to determine log2-fold change values between full and glutamine-deprived conditions. A total of 3 biological replicates were performed. Metabolites with an average fold change of <0.9 were classified as downregulated, and metabolites with a fold change of >1.1 were classified as upregulated. Milder cut-offs were used to avoid eliminating potentially important metabolites of interest. **(a)** Pathway enrichment analyses were separately performed on metabolites that were downregulated (top) or upregulated (bottom) using MetaboAnalyst 5.0 to elucidate over-represented pathways. **(b)** List of metabolites involved in purine metabolism that were downregulated or upregulated under glutamine deprivation. Metabolites in bold were specifically examined in Figure 2.14.

To understand the metabolic consequences of genetic loss of ATG4B, metabolite profiling studies were performed on parental and ATG4B KO cells following 48 hours of growth in full or glutamine-deprived media to evaluate changes in purine bases and nucleotides. An enrichment in the pentose phosphate pathway intermediate[249], phosphoribosyl pyrophosphate (PRPP), and metabolites involved in the purine salvage pathway was observed in ATG4B KO cells compared to parental cells (Figure 2.14A). In addition, purine nucleotides were also noticeably enriched in ATG4B KO cells under glutamine deprivation (Figure 2.14A). To validate these findings, an independent

metabolomic dataset comparing metabolites in wild-type and atg4b$^{-/-}$ mice[250] was examined. Metabolites involved in the purine salvage pathway were similarly found enriched in atg4b$^{-/-}$ mice compared to wild-type mice, specifically in the heart and muscle (Fig 2.14B). *These findings suggest that genetic loss of ATG4B is associated with an enrichment in purine nucleotides and metabolites involved in the purine salvage pathway, an alternate pathway for cellular GTP production.*

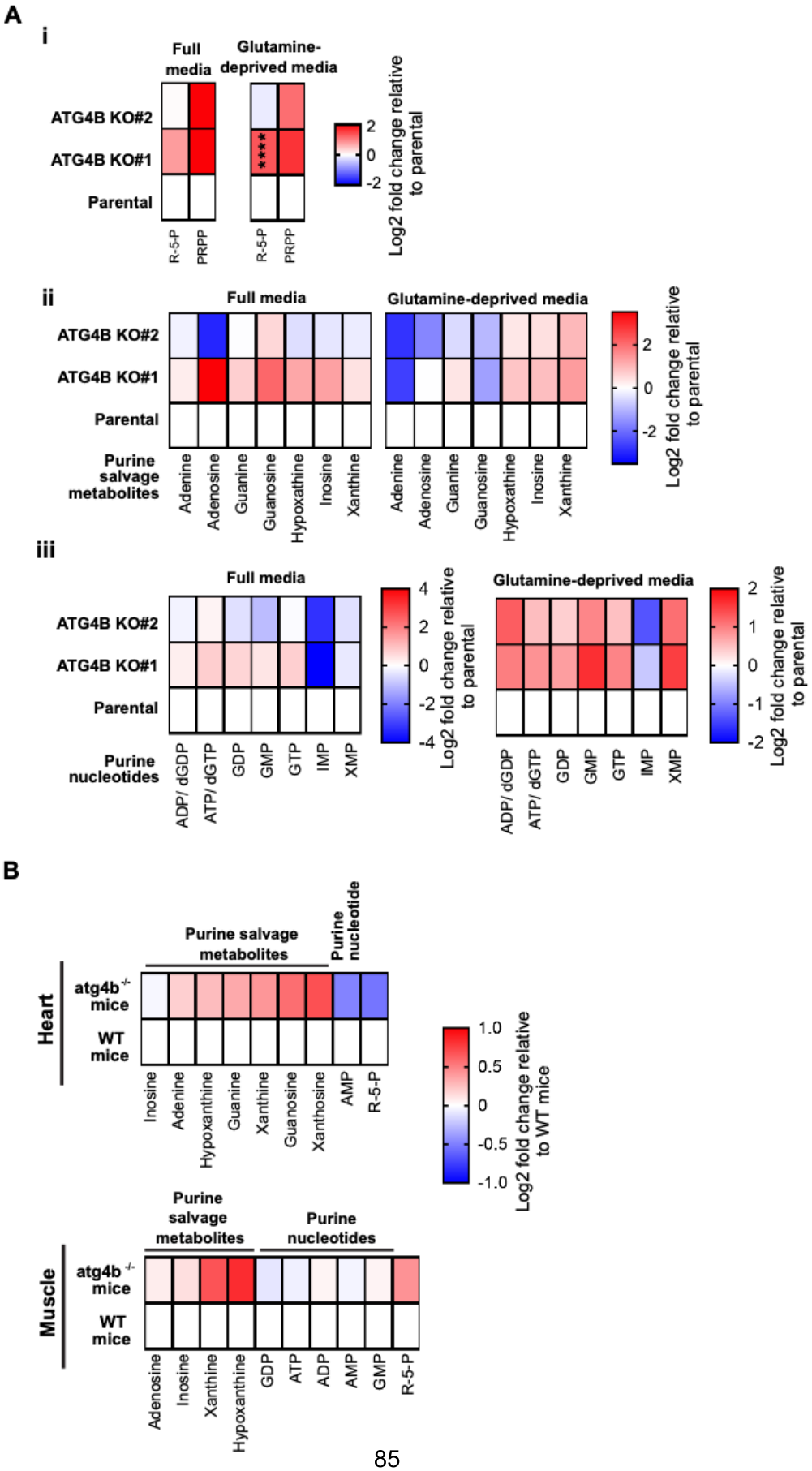
A
i
Full media
Glutamine-deprived media
ATG4B KO#2
ATG4B KO#1
Parental
****
R-5-P
PRPP
Log2 fold change relative to parental
ii
Full media
Glutamine-deprived media
Purine salvage metabolites
Adenine
Adenosine
Guanine
Guanosine
Hypoxathine
Inosine
Xanthine
iii
Purine nucleotides
ADP/ dGDP
ATP/ dGTP
GDP
GMP
GTP
IMP
XMP
B
Heart
atg4b -/- mice
WT mice
Purine salvage metabolites
Purine nucleotide
Inosine
Adenine
Hypoxanthine
Guanine
Xanthine
Guanosine
Xanthosine
AMP
R-5-P
Log2 fold change relative to WT mice
Muscle
Purine salvage metabolites
Purine nucleotides
Adenosine
Inosine
Xanthine
Hypoxanthine
GDP
ATP
ADP
AMP
GMP
R-5-P

Figure 2.14 Genetic loss of ATG4B is associated with an enrichment in purine salvage metabolites and purine nucleotides

(A) Heat map of log2 fold change values of metabolites involved in purine metabolism in parental, ATG4B KO#1 and aTG4B KO#2 JIMT-1 cells. Parental JIMT-1 and ATG4B KO cells were grown in full or glutamine-deprived media for 48 hours, prior to harvesting for metabolite profiling experiments by LC-MS. Peak area in the unit of ion counts for each metabolite was scaled to the cell counts for each condition and averaged to determine log2-fold change values in ATG4B KO cells relative to parental cells in full or glutamine-deprived conditions. A total of 3 biological replicates were performed. One-way ANOVA with Tukey's multiple comparisons tests were performed on normalized peak areas of each metabolite to evaluate statistical differences. (B) Heat map of log2 fold change values of metabolites involved in purine metabolism in wild-type (WT) and atg4b$^{-/-}$ mice. Normalized peak area intensities of purine salvage metabolites and purine nucleotides from an independent and publicly available metabolomic dataset comparing WT and atg4b$^{-/-}$ mice were analyzed (Martínez-García, G., *et al.* 2021). Normalized peak area intensities for each metabolite were averaged to determine the log2-fold change between WT and atg4b$^{-/-}$ mice. Data comprised of metabolite profiles from 12 WT and 12 atg4b$^{-/-}$ mice, and analyses were performed independent of sex. Multiple unpaired t-tests with the original FDR method of Benjamini and Hochberg (Q = 5%) were used to evaluate statistical differences. No statistically significant changes were noted.

2.3.9. Prolonged glutamine deprivation leads to a significantly greater reduction in cellular growth in ATG4B KO cells compared to parental cells

To determine if genetic loss of ATG4B is important for cellular growth under prolonged glutamine deprivation, changes in the percent phase confluence of parental and ATG4B KO cells under full or glutamine-deprived conditions were measured for 120 hours. Interestingly, the growth of parental and ATG4B KO cells were similar up to 48 hours of glutamine deprivation, where differences in IMPDH2 ring-and-rod and purine metabolite profiles were observed. Extended glutamine deprivation up to 120 hours, importantly, was associated with a greater reduction in cellular growth under glutamine-limiting conditions in the ATG4B KO cells (Figure 2.15). Given metabolomic findings from chapter 2.3.8, these growth differences suggest a model whereby the *purine salvage pathway is utilized predominantly by ATG4B KO cells but is limited in its capacity to sustain cellular growth under prolonged glutamine deprivation.*

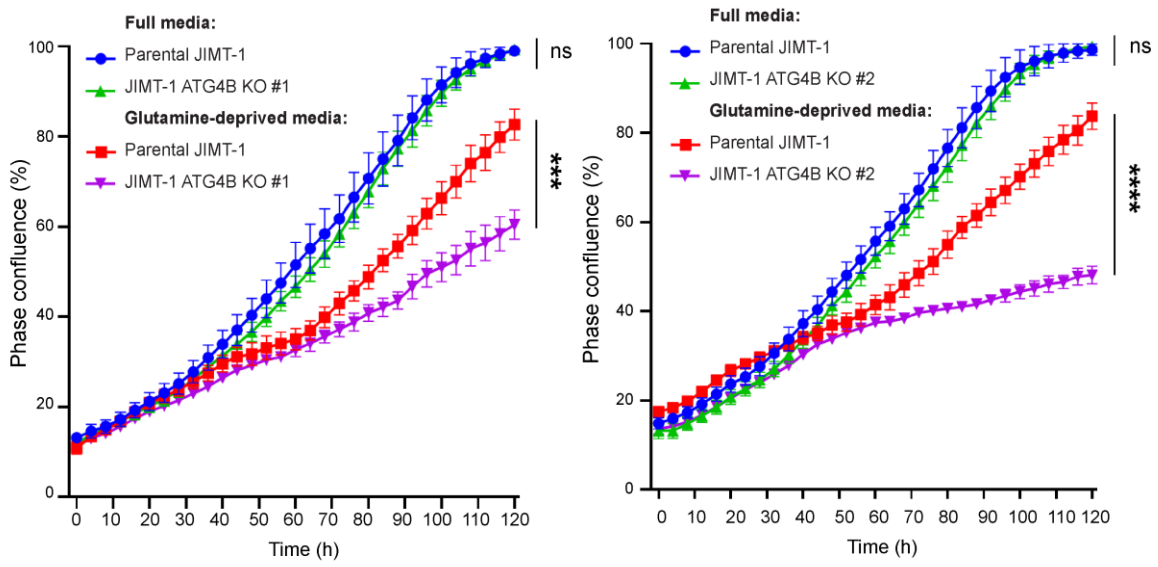

Figure 2.15 ATG4B KO cells are sensitive to extended glutamine deprivation
Parental and ATG4B KO JIMT-1 cells were grown in full or glutamine-deprived media, and changes in phase confluence were measured by Incucyte every 4 hours for a total of 120 hours. Error bars represent SEM. One-way ANOVA with Tukey's multiple comparisons tests were performed to determine the statistical differences in phase confluence at the 120-hour endpoint. A total of 4 biological replicates were performed.

2.3.10. IMPDH inhibition is associated with little to no further reduction in growth of glutamine-deprived ATG4B KO cells

To determine if glutamine deprivation would increase the sensitivity of cells to IMPDH inhibition, the percent phase confluence of parental JIMT-1 cells was measured following 120 hours of growth in full or glutamine deprived media, and treatment with or without increasing concentrations of the IMPDH inhibitor, mycophenolic acid (MPA). Glutamine deprivation did not increase the sensitivity of JIMT-1 cells to IMPDH inhibition (Figure 2.16), suggesting *that alternate pathways for purine nucleotide production, like the purine salvage pathway, may also sustain growth when IMPDH is inhibited.*

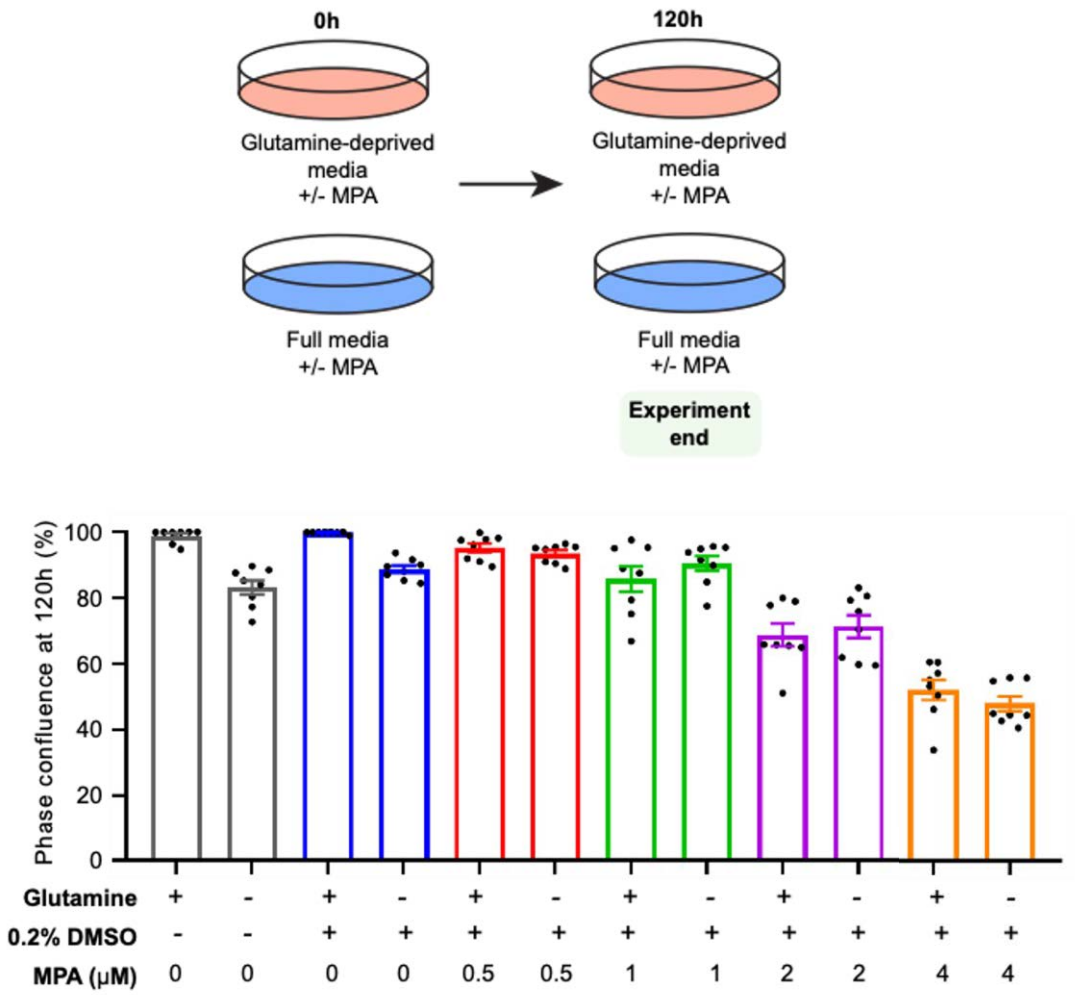

Figure 2.16 Glutamine deprivation does not increase sensitivity to IMPDH inhibition

Parental JIMT-1 cells were subjected to growth in full or glutamine-deprived media with DMSO or the IMPDH inhibitor, MPA. Percent phase confluences of cells were measured after 120 hours using the Incucyte. A total of 8 biological replicates were performed. One-way ANOVA with Tukey's multiple comparisons tests were performed to evaluate statistical differences. No statistically significant changes were observed. Error bars represent SEM.

To determine if ATG4B KO cells rely on IMPDH-mediated *de novo* purine biosynthesis for growth, the end point percent phase confluence of parental and ATG4B KO JIMT-1 cells was measured following 120 hours of growth in glutamine-deprived media, with or without MPA. MPA treatment was associated with a dose-dependent reduction in cellular growth in glutamine-deprived parental JIMT-1 cells. In contrast, MPA treatment resulted in little to no further reduction in the percent phase confluence of glutamine deprived ATG4B KO cells (Figure 2.17A). To evaluate growth over time of

glutamine-deprived cells treated with MPA, changes in the percent phase confluence were measured over 120 hours. IMPDH inhibition by MPA was associated with a significant reduction in growth of parental JIMT-1 cells. In contrast, MPA treatment led to modest decreases in the growth of glutamine deprived ATG4B KO cells (Figure 2.17B). *This suggests ATG4B KO cells may have acquired the ability to grow in extended glutamine-deprived conditions through IMPDH-independent pathways.*

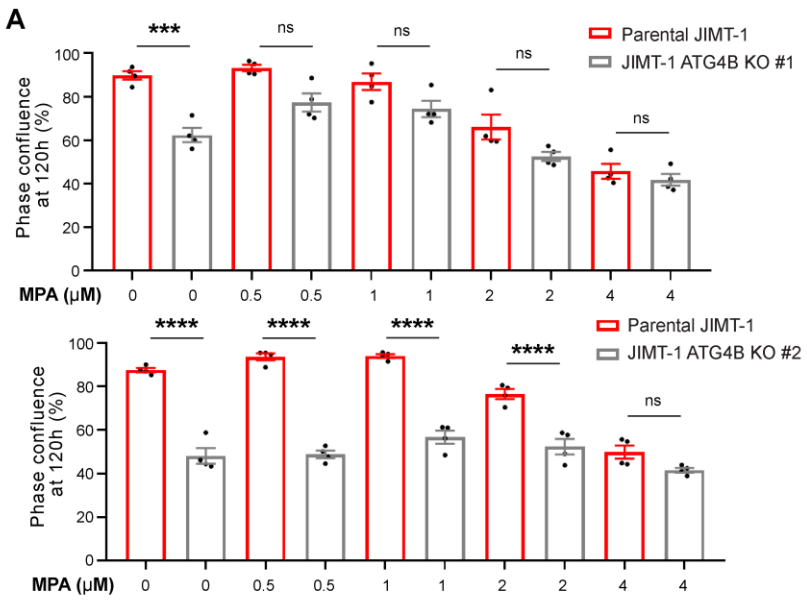
A
Parental JIMT-1
JIMT-1 ATG4B KO #1
Phase confluence at 120h (%)
MPA (μM)
***
ns
Parental JIMT-1
JIMT-1 ATG4B KO #2
****

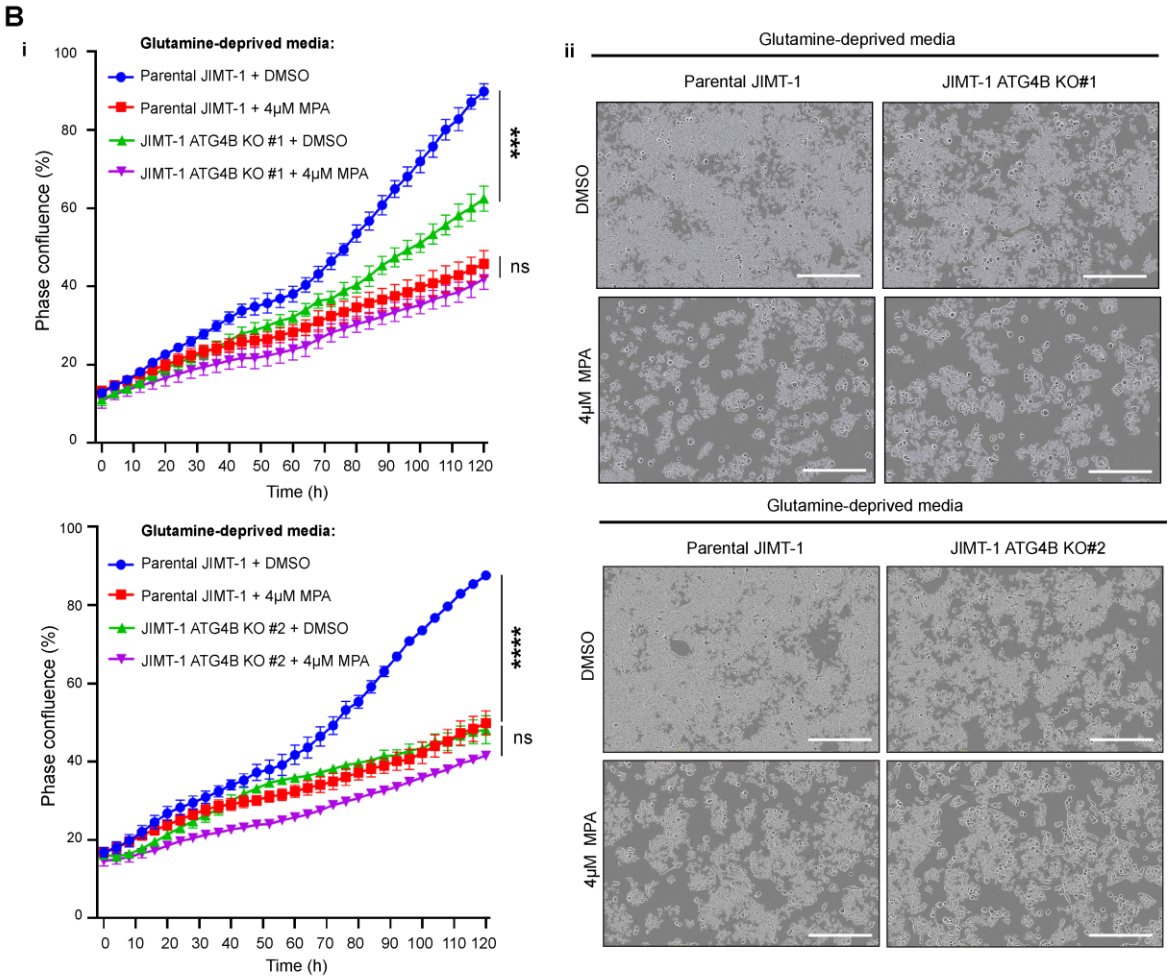
B
i
Glutamine-deprived media:
Parental JIMT-1 + DMSO
Parental JIMT-1 + 4μM MPA
JIMT-1 ATG4B KO #1 + DMSO
JIMT-1 ATG4B KO #1 + 4μM MPA
JIMT-1 ATG4B KO #2 + DMSO
JIMT-1 ATG4B KO #2 + 4μM MPA
Phase confluence (%)
Time (h)
ii
Glutamine-deprived media
Parental JIMT-1
JIMT-1 ATG4B KO#1
JIMT-1 ATG4B KO#2
DMSO
4μM MPA

Figure 2.17 Genetic loss of ATG4B does not increase sensitivity to IMPDH inhibition under glutamine deprivation

Parental and ATG4BKO JIMT-1 cells were subjected to growth in glutamine-deprived media with 0.4% DMSO or the IMPDH inhibitor, MPA. (A) Percent phase confluences of cells were measured after 120 hours using the Incucyte. A total of 4 independent biological replicates were performed. One-way ANOVA with Tukey's multiple comparisons tests were performed to evaluate statistical differences. Error bars present SEM. (B) (i) Growth curves of glutamine-deprived parental and ATG4BKO JIMT-1 cells treated with DMSO or 4uM of MPA. Varying concentrations of MPA were screened and data for the concentration of MPA (4uM) that revealed the greatest difference in growth between parental and ATG4B KO cells is shown. Changes in phase confluence were measured by Incucyte every 4 hours for a total of 120 hours. One-way ANOVA with Tukey's multiple comparisons tests were performed to determine the statistical differences in phase confluence at the 120-hour endpoint. A total of 4 biological replicates were performed. (ii) Representative images of cells captured by Incucyte. Scale bars = 400um.

2.3.11. Genetic loss of ATG4B does not lead to signficant changes in the protein levels of core *de novo* and salvage pathway enzymes

Current findings suggest that ATG4B KO cells may rely on pathways independent of IMPDH-mediated de novo purine biosynthesis to sustain growth. Current metabolomic findings also suggest a potential role for the purine salvage pathway in purine nucleotide production in glutamine deprived ATG4B KO cells. Adenine phosphoribysoltransferase (APRT) and hypoxanthine phosphoribosyltransferase (HPRT1) are important purine salvage enzymes that facilitate the conversion of purine nucleobases to their cognate nucleoside monophosphates[138] (Figure 2.18).

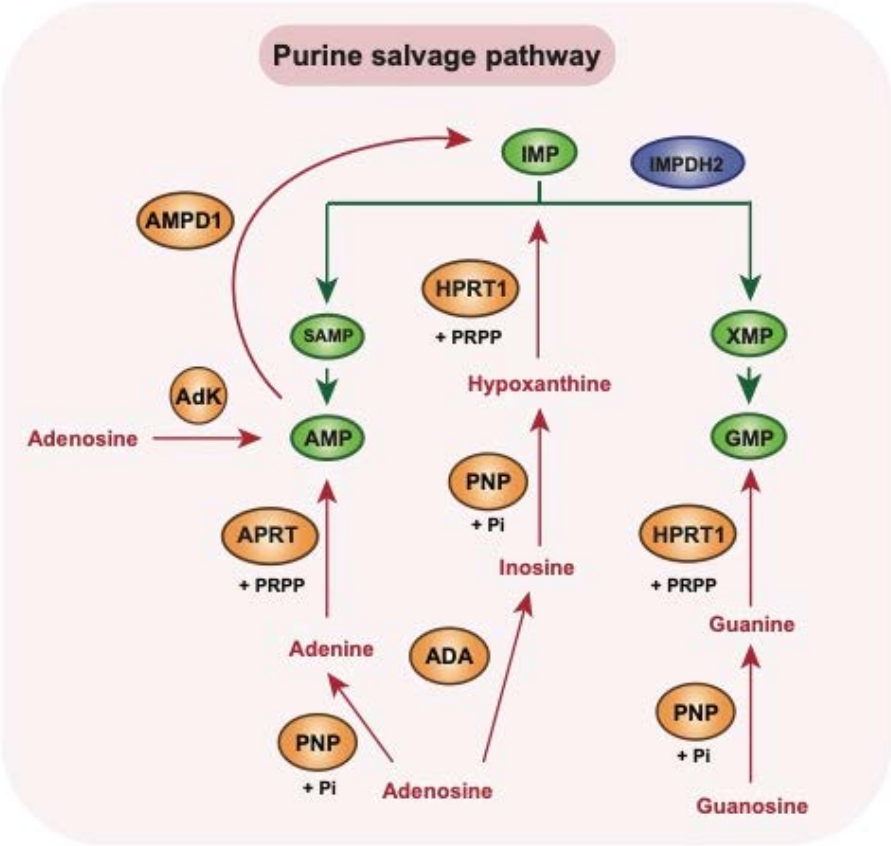

Figure 2.18 The purine salvage pathway
The purine salvage pathway converts purine nucleobases and nucleosides to their cognate nucleoside monophosphates. Purine nucleosides cannot be directly salvaged and require the activity of purine nucleoside phosphorylases (PNP) to facilitate the conversion to their respective nucleobases. Purine nucleobases are converted to their cognate purine nucleoside monophoshates through phosphorribosyltransferase reactions mediated by adenine phosphoribysoltransferase (APRT) and hypoxanthine phosphoribosyltransferase (HPRT1). Derived from data and information from Mullen and Singh, 2023[138].

To determine if ATG4B KO cells express elevated protein levels of APRT and HPRT1, western blot analyses in parental and ATG4B KO cells following growth in full or glutamine-deprived media were performed (Figure 2.19). To control for variability of absolute protein quantifications between biological replicates (Figure 2.19B), absolute protein levels were normalized to parental JIMT-1 full media controls to compare differences in HPRT1 and APRT between cell lines and conditions (Figure 2.19C). Genetic loss of ATG4B did not lead to substantial changes in the protein levels of APRT nor HPRT1 (Figure 2.19C), *suggesting that the enrichments in purine nucleotides and metabolites involved in purine salvage in ATG4B KO cells (Figure 2.14) are unlikely through upregulation of levels of the purine salvage enzymes, APRT and HPRT1.*

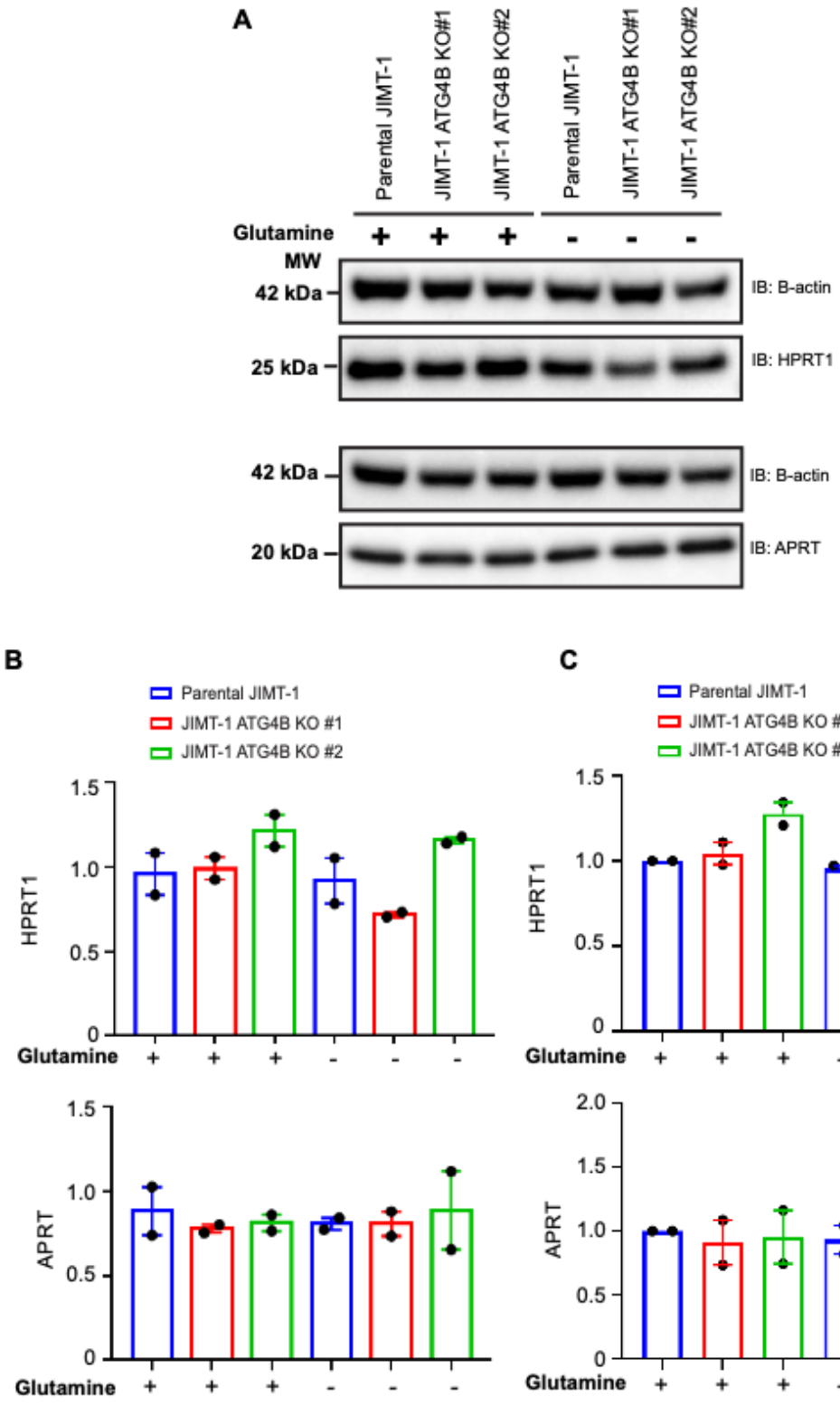
A
Parental JIMT-1
JIMT-1 ATG4B KO#1
JIMT-1 ATG4B KO#2
Parental JIMT-1
JIMT-1 ATG4B KO#1
JIMT-1 ATG4B KO#2
Glutamine + + + - - -
MW
42 kDa
IB: B-actin
25 kDa
IB: HPRT1
42 kDa
IB: B-actin
20 kDa
IB: APRT
B
Parental JIMT-1
JIMT-1 ATG4B KO #1
JIMT-1 ATG4B KO #2
HPRT1
1.5
1.0
0.5
0
Glutamine + + + - - -
APRT
1.5
1.0
0.5
0
Glutamine + + + - - -
C
Parental JIMT-1
JIMT-1 ATG4B KO #1
JIMT-1 ATG4B KO #2
HPRT1
1.5
1.0
0.5
0
Glutamine + + + - - -
APRT
2.0
1.5
1.0
0.5
0
Glutamine + + + - - -

Figure 2.19 APRT and HPRT1 protein levels are not altered by genetic loss of ATG4B

(A) Parental and ATG4B KO JIMT-1 cells were grown in full or glutamine-deprived media for 120 hours and harvested for western blot analyses of HPRT1 and APRT protein levels as described in methods. (B) Absolute quantifications of HPRT1 and APRT protein levels were determined relative to B-actin loading controls and are shown to depict variability between biological replicates. (C) Normalized quantifications of HPRT1 and APRT protein levels were determined relative to B-actin loading controls and then normalized to parental JIMT-1 full media conditions to control for variabilities in absolute values between biological replicates. For B and C, one way ANOVA with Tukey's multiple comparisons test was used to evaluate statistical differences, and no statistically significant changes were observed. 2 biological replicates were performed.

To determine if genetic loss of ATG4B decreases levels of *de novo* purine pathway enzymes, the protein levels of PPAT, ATIC, ADSL and GART were also examined (Figure 2.20). Given the variability of absolute protein quantifications between biological replicates (Figure 2.20B), absolute protein levels were normalized to the parental full media conditions to compare differences in levels of *de novo* purine metabolism enzymes between cell lines and conditions (Figure 2.20C). Western blot findings revealed that genetic loss of ATG4B was not associated with any striking changes in protein levels of these *de novo* purine pathway enzymes (Figure 2.20C). Intriguingly, protein levels of ATIC modestly increased in ATG4B KO#2 following glutamine deprivation. Protein levels of the 46kDa isoform of GART was also significantly higher in ATG4B KO#2 compared to parental cells under conditions of glutamine deprivation. It remains to be determined if these changes are true, or an artifact of the evidently lower B-actin levels in ATG4B KO#2 under conditions of glutamine deprivation. *In general, these findings suggest that protein levels of enzymes involved in de novo purine biosynthesis are not substantially affected by genetic loss of ATG4B.*

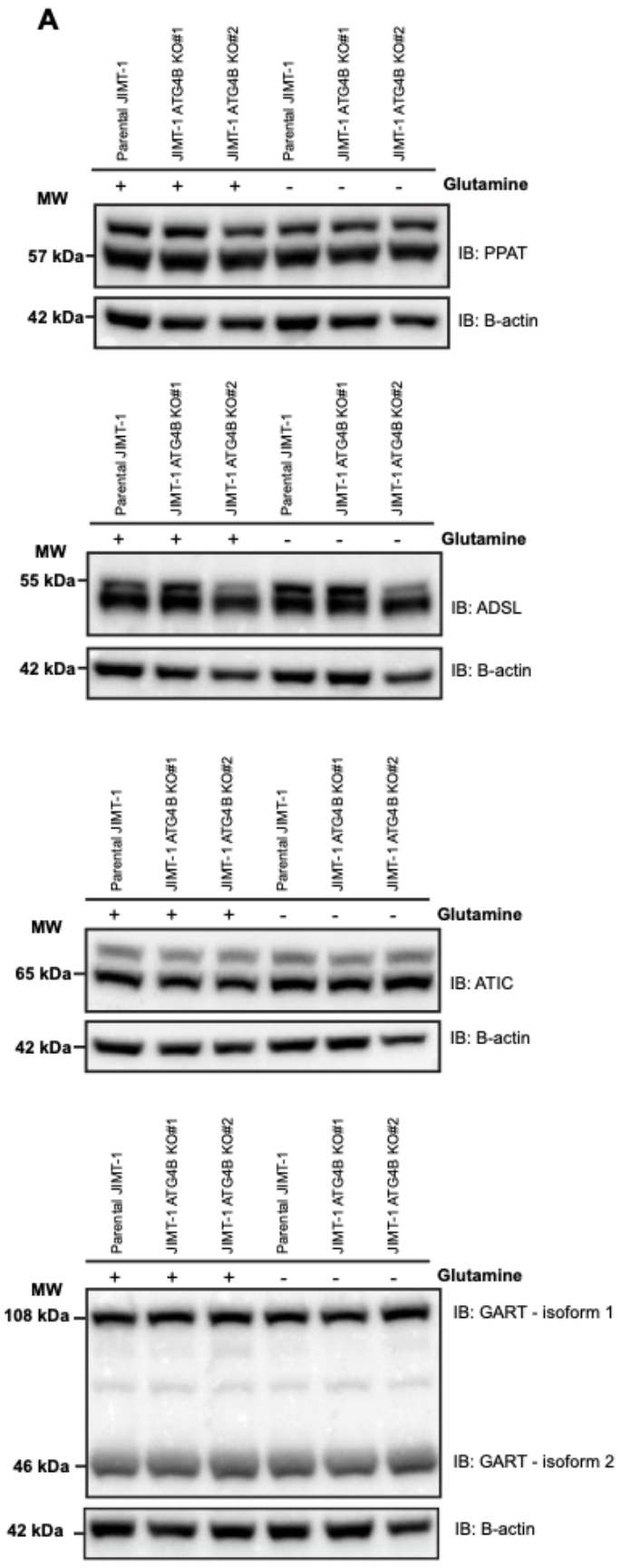
A
Parental JIMT-1
JIMT-1 ATG4B KO#1
JIMT-1 ATG4B KO#2
Parental JIMT-1
JIMT-1 ATG4B KO#1
JIMT-1 ATG4B KO#2
Glutamine
+ + + - - -
MW
57 kDa
IB: PPAT
42 kDa
IB: B-actin
Parental JIMT-1
JIMT-1 ATG4B KO#1
JIMT-1 ATG4B KO#2
Parental JIMT-1
JIMT-1 ATG4B KO#1
JIMT-1 ATG4B KO#2
Glutamine
+ + + - - -
MW
55 kDa
IB: ADSL
42 kDa
IB: B-actin
Parental JIMT-1
JIMT-1 ATG4B KO#1
JIMT-1 ATG4B KO#2
Parental JIMT-1
JIMT-1 ATG4B KO#1
JIMT-1 ATG4B KO#2
Glutamine
+ + + - - -
MW
65 kDa
IB: ATIC
42 kDa
IB: B-actin
Parental JIMT-1
JIMT-1 ATG4B KO#1
JIMT-1 ATG4B KO#2
Parental JIMT-1
JIMT-1 ATG4B KO#1
JIMT-1 ATG4B KO#2
Glutamine
+ + + - - -
MW
108 kDa
IB: GART - isoform 1
46 kDa
IB: GART - isoform 2
42 kDa
IB: B-actin

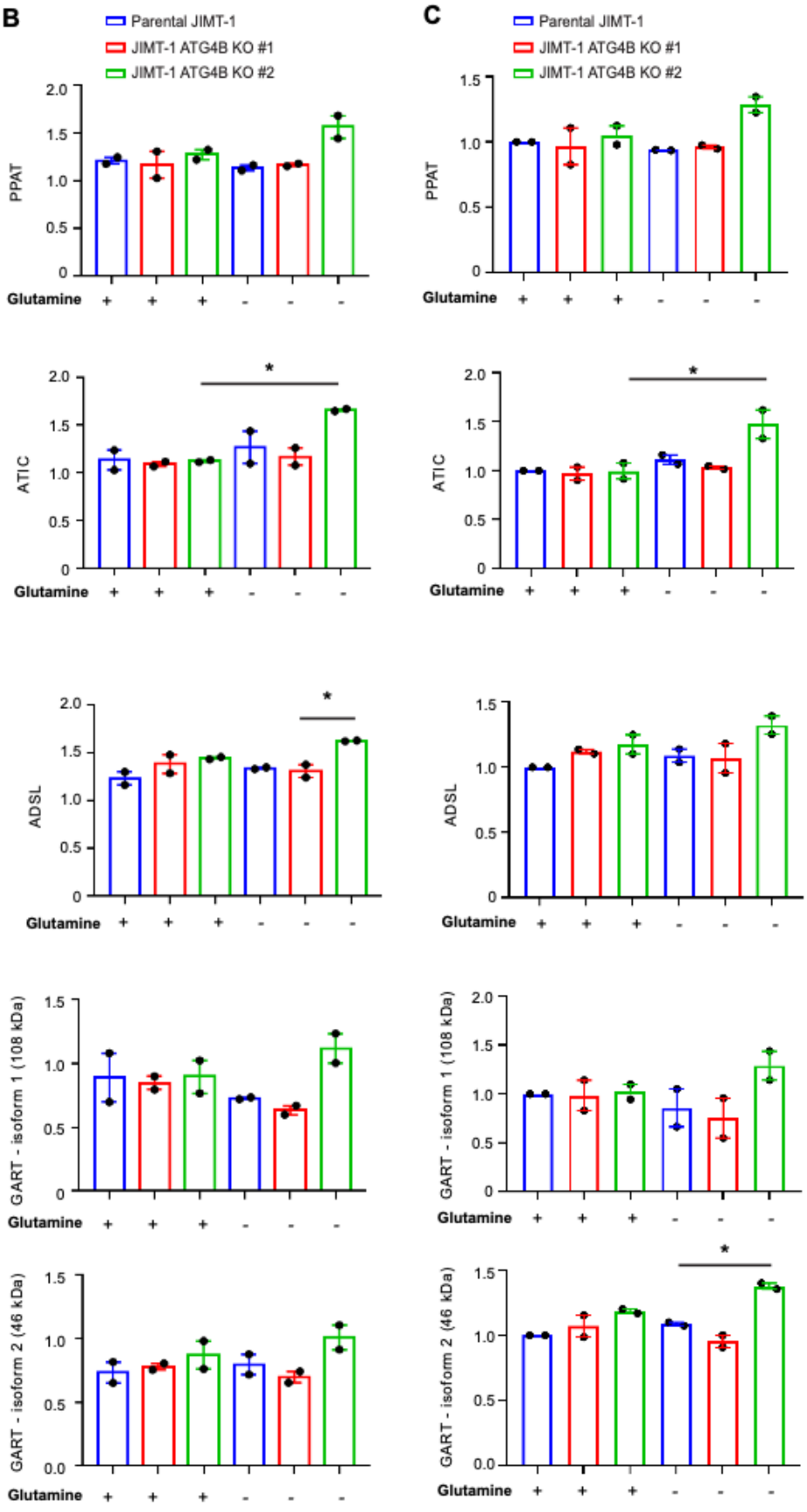
B
C
Parental JIMT-1
JIMT-1 ATG4B KO #1
JIMT-1 ATG4B KO #2
PPAT
ATIC
ADSL
GART - isoform 1 (108 kDa)
GART - isoform 2 (46 kDa)
Glutamine
+
-
*

Figure 2.20 Genetic loss of ATG4B is associated with little to no changes in the protein levels of *de novo* purine pathway enzymes

(A) Parental and ATG4B KO JIMT-1 cells were grown in full or glutamine-deprived media for 120 hours and harvested for western blot analyses of PPAT, ATIC, ADSL and GART protein levels as described in methods. (B) Absolute quantifications of PPAT, ATIC, ADSL and GART protein levels were determined relative to B-actin loading controls and are shown to depict variability between biological replicates. (C) Normalized quantifications of PPAT, ATIC, ADSL and GART protein levels were determined relative to B-actin loading controls and then normalized to parental JIMT-1 full media conditions to control for variabilities in absolute values between biological replicates. For B and C, one way ANOVA with Tukey's multiple comparisons test was used to evaluate statistical differences, and error bars represent SEM. 2 biological replicates were performed.

2.3.12. Glutamine-deprived ATG4B KO cells have an impaired ability to restore cellular growth under purine depleted conditions

Although APRT and HPRT1 protein levels were not significantly altered by ATG4B loss, it is plausible that ATG4B KO cells may depend on the many purine nucleosides and nucleobases that feed the purine salvage pathway instead (Figure 2.18). To determine if ATG4B KO cells rely on purines under glutamine deprivation**,** growth of parental and ATG4B KO cells were examined in glutamine-deprived and purine-depleted or purine-replete media. Depletion of exogenous purines that feed the purine salvage pathway resulted in an initial reduction of growth in parental JIMT-1 cells, but growth was seemingly restored over time. In contrast, ATG4B KO cells were significantly more sensitive to combined glutamine- and purine-depletion and growth is not as efficiently restored as compared to parental cells (Figure 2.21). *This suggests that ATG4B KO cells rely on the purine salvage pathway for growth under glutamine deprivation, and that the purine salvage pathway alone may not be sufficient to sustain growth following extended periods of glutamine deprivation (Figure 2.22)*

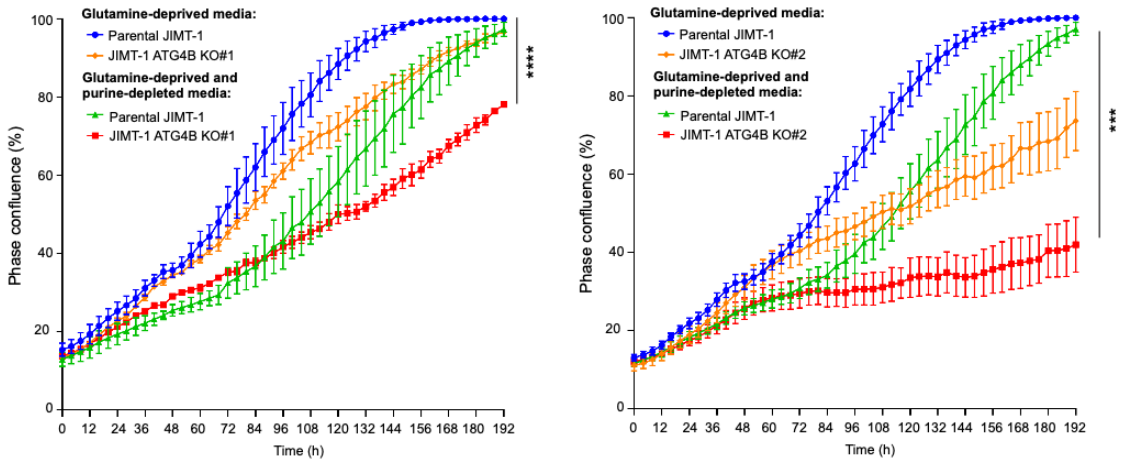

Figure 2.21 ATG4B KO cells are significantly more sensitive to combined glutamine- and purine-depletion compared to parental cells

Parental and ATG4B KO JIMT-1 cells were grown in glutamine-deprived media or glutamine-deprived and purine-depleted media. Changes in phase confluence were measured by Incucyte every 4 hours for a total of 192 hours. Error bars represent SEM. One-way ANOVA with Tukey's multiple comparisons tests were performed to determine the statistical differences in phase confluence at the 120-hour endpoint. A total of 3 biological replicates were performed.

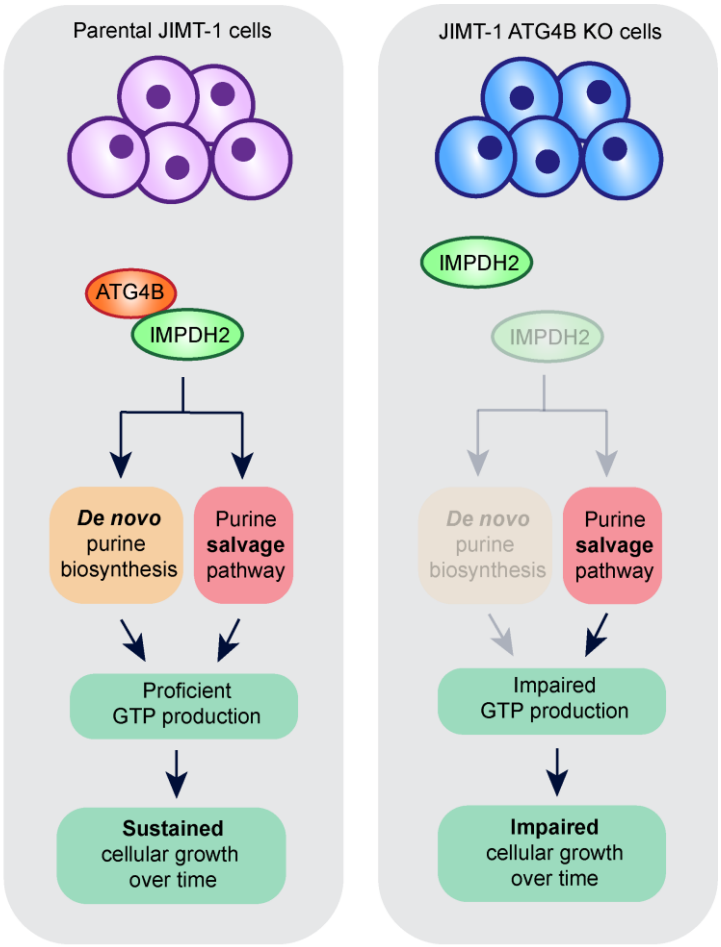

Figure 2.22 ATG4B KO cells rely on the purine salvage pathway for cellular growth under glutamine deprivation

Under conditions of nutrient stress, like glutamine deprivation, cells may rely on both the *de novo* purine biosynthesis and purine salvage pathway to generate important guanine nucleotides required to sustain growth. It is plausible that cells utilize the more energy-efficient purine salvage first, and switch to the de novo purine biosynthetic pathway when the cellular purine demands can no longer be met by the salvage pathway alone. In cells that do not express ATG4B, the lack of an ATG4B-IMPDH2 interaction may hamper the ability of cells to utilize the *de novo* purine biosynthesis when the purine demands can no longer be met by the salvage pathway alone, thereby resulting in significantly impaired cellular growth over time.

2.4. Discussion

It is well reported in the literature that autophagy is induced in response to nutrient stresses in the cell, serving to replenish and maintain levels of metabolites to sustain cellular growth, as described in chapters 1.6.2 and 1.6.3 of this thesis. Previous studies have identified an importance for the core autophagy cysteine protease, ATG4B, in modulating the responses of HER2-positive breast cancer cell lines to nutrient

deprivation[61]. To date, the molecular mechanism underlying how ATG4B may regulate nutrient stress responses of HER2-positive breast cancer cells remains poorly described.

In collaboration with Drs. Gregg Morin and Gian Negri, I performed a pilot IP-MS study and identified a new protein-protein interactor of ATG4B, the metabolic enzyme IMPDH2. I validated this interaction in several independent breast cancer cell lines and found that this interaction was not dependent on the HER2 status of breast cancer cells. To date, this is the first study to identify and validate a novel protein-protein interaction between ATG4B and IMPDH2. Given the importance of the IMPDH2 in metabolism, in particular GTP biosynthesis, I predicted that functional investigations into the significance of this interaction may shed light on how ATG4B is involved in the nutrient stress response of breast cancer cells. With assistance from Drs. Baofeng Jia and Kevin Yang, I evaluated the relationship between ATG4B and IMPDH2 protein levels in independent breast cancer patient proteomic datasets by Pearson correlation. The pearson correlation is a common technique for evaluating the linear relationship between two quantitative sets of data, and is used to derive a coefficient that represents the direction and magnitude of the correlation between the datasets[251]. From these analyses, I found a positive correlation between ATG4B and IMPDH2 protein levels in the independent breast cancer patient proteomic cohorts examined. It should be noted that these protein-protein correlations were modest. Pearson correlations require the two datasets in examination to possess a linear and a normal distribution, and deviations may misrepresent the direction and/or magnitude of the correlations[252]. In this case, one caveat is that both requisites were assumed for the Pearson correlations performed. Another caveat is that large variations in the protein levels between different subgroups within each cohort examined may also mask or misrepresent the relationship between the datasets[251]. To address the possibility that the ATG4B-IMPDH2 relationship may be stronger in certain breast cancer subtypes than others, I further stratified patients according to their known PAM50 status to examine ATG4B-IMPDH2 protein-protein relationship by Pearson correlation in the different PAM50 subtypes in chapter 3. Additionally, outliers present in either datasets may also skew the magnitude and/or direction of the derived correlation coefficient[251]. Additional enquiries into the protein-protein correlation between ATG4B and IMPDH2 in other independent and larger cohorts are certainly warranted. Nevertheless, this correlation does support a potential

functional interplay between autophagy and purine metabolism that may be bridged by the ATG4B-IMPDH2 interaction.

Interestingly, I found that pharmacological inhibition or genetic knockdown of the IMPDH proteins did not alter levels of ATG4B protein. Similarly, genetic knockdown or genetic loss of ATG4B also did not strongly alter levels of the IMPDH proteins. These findings suggest that the main purpose of the ATG4B-IMPDH2 interaction is unlikely the regulation of levels of these proteins despite the weak positive correlations observed from breast cancer patient cohorts. As part of next steps, I then explored the possibility that the ATG4B-IMPDH2 interaction may function to regulate their activity. With assistance from Nancy E. Go, I found that pharmacological inhibition of IMPDH was associated with an impairment in the processing of LC3B and stabilization GABARAP proteins. The observed impairments in LC3B processing[115] and GABARAP stabilization[93] could suggest a suppression in the catalytic or protein-stabilizing functions of ATG4B, as reported in previous studies[93,115]. Given that this association is correlative and does not directly address the activity of ATG4B, ongoing studies using a tandem reporter LC3B construct[253] to assess ATG4B activity following IMPDH inhibition are underway. In addition, to explore the potential of ATG4B regulating activity of the IMPDH proteins, metabolomics experiments in collaboration with the Victoria Proteomics Centre are also currently underway.

Given that ATG4B functions as a cysteine protease, I also explored the possibility that IMPDH2 may be cleaved by ATG4B. I hypothesized that IMPDH2 will likely share sites of homology with the ATG8 proteins, which are known substrates of ATG4B, if IMPDH2 is also cleaved by ATG4B. In collaboration with Dr. Baofeng Jia, I performed a multiple sequence alignment of IMPDH2 and the human ATG8 proteins. I found several regions of homology between IMPDH2 and the ATG8 proteins (Figure A2). Of note, IMPDH2 shares a homologous region with the ATG8 C-terminal region, which consists of a glycine residue that is cleaved by ATG4B prior to conjugation to phosphatidylethanolamine on the surface of autophagosomes[254]. I next hypothesized that if IMPDH2 is indeed cleaved by ATG4B, then genetic loss of ATG4B should result in a molecular weight shift or the loss of smaller IMPDH2 band fragments. I investigated this in parental and ATG4B KO cells, grown in the full or glutamine-deprived media, but found no obvious differences in the molecular weight or banding patterns of IMPDH2 in

parental and ATG4B KO cells in either condition (Figure A3). This finding suggests that ATG4B unlikely cleaved IMPDH2 in the conditions tested.

Glutamine is an important amide donor in GTP biosynthesis[135]. Previous studies have reported that under conditions of glutamine deprivation, HeLa cells form structures of IMPDH2, termed rings-and-rods, which disassemble upon guanosine supplementation[190]. I showed that this biological phenomenon also occurs in glutamine-deprived HER2-positive breast cancer cell line, JIMT-1, and was associated with a reduction in guanine nucleotide levels in this cell line. Additionally, I found that guanosine supplementation significantly increased cellular GTP production and depolymerized these IMPDH2 ring-and-rod structures in glutamine-deprived JIMT-1 cells. To date, this is the first study to our knowledge providing metabolomic evidence that the formation of IMPDH2 rings-and-rods occurs because of reduced guanine nucleotide levels and the disassembly of these structures upon guanosine supplementation is a result of increased GTP production in HER2-positive breast cancer cells. Given the implication of ATG4B in modulating nutrient stress responses in HER2-positive breast cancer cells, I next hypothesized that ATG4B may contribute to IMPDH2 ring-and-rod formation given my discovery that the two proteins interact. I discovered that genetic loss of ATG4B was associated with a significant impairment in the ability of JIMT-1 cells to form IMPDH2 ring-and-rod structures. Seeing that IMPDH2 rings-and-rods form in response to depletion in guanine nucleotide levels, this not only suggested that ATG4B is important in IMPDH2 ring-and-rod formation but also that ATG4B may be important in regulating GTP levels in the cell. It will be of interest to examine the effects of glutamine deprivation on the stability of the interaction between ATG4B and IMPDH2 as part of future work.

In collaboration with Jessica Koe and Dr. Seth Parker, I found that glutamine deprivation was associated with an over-representation of downregulated metabolites involved in purine metabolism in parental JIMT-1 cells. Interestingly, a number of purine metabolites, like adenosine, guanosine and PRPP were increased in glutamine-deprived cells. I posit that this may be attributed to an increase in the cellular uptake of adenine, guanosine, and glucose to replenish adenine and guanine nucleotides in response to limited glutamine availability. Adenosine and guanosine are amino acids that can be utilized through the purine salvage pathway to generate adenine and guanine nucleotides[138]. Increased glucose uptake would similarly fuel adenine and guanine

nucleotide production by entering the pentose phosphate pathway and generating PRPP which can be utilized in both the *de novo* purine and purine salvage pathways[138]. Future studies evaluating the uptake of these metabolites would certainly clarify this and support the importance and cellular utilization of both the *de novo* and purine salvage pathways under conditions of nutrient stress, like glutamine deprivation.

I next investigated the metabolic consequences of genetic loss of ATG4B and discovered that ATG4B KO cells presented with elevated guanine nucleotide levels compared to parental JIMT-1 cells. This finding was intriguing as it suggested that ATG4B KO cells may upregulate certain pathways to increase cellular guanine nucleotide levels, explaining why ATG4B KO cells formed significantly less IMPDH2 rings-and-rods under glutamine deprivation. I further evaluated the metabolite profiles of parental and ATG4B KO cells and found that ATG4B KO cells were enriched in metabolites involved in the purine salvage pathway and in purine nucleotides. The lack of statistically significant changes, with the exception of the observed significantly higher ribose-5-phosphate (R-5-P) in glutamine-deprived ATG4B KO#1 JIMT-1 cells, could be due to a number of factors.

Firstly, I investigated levels of the different metabolites involved in purine metabolism by untargeted metabolite profiling, which was based on the normalized peak areas of each metabolite in the unit of ion counts. Untargeted metabolomics was performed to enable a comprehensive view of metabolite profiles that could be altered between the cell lines and conditions examined in this chapter, which would aid in hypothesis generation[255–257]. However, such relative quantitative methods for metabolomics are generally considered less sensitive than absolute quantification by targeted metabolomics. This aspect may have been a contributing factor toward outliers, variability in ion counts between samples, or metabolite levels that were not quantified if present below the threshold of $5x10^4$ ion counts in some samples and replicate, thereby impacting the statistical significance of the metabolite changes.

Secondly, it is likely that ATG4B KO#1 and KO#2 harbor underlying genetic differences that were not addressed as part of this thesis. Such genetic heterogeneity between ATG4B KO clones could explain the observed differences in the metabolite profiles between ATG4B KO#1 and KO#2 (Figure 2.14). An example would be the metabolite adenosine, which was enriched in ATG4B KO#1 but depleted in ATG4B

KO#2. These differences warrant further investigation by evaluating metabolite profiles in additional ATG4B KO cell lines and/or ATG4B knockdown models. In addition, the observation that, compared to parental JIMT-1 cells, IMPDH1 protein levels were significantly lower in ATG4B KO#1, but not in ATG4B KO#2, when cells were grown in culture for 48 hours could have also contributed to the differences in their metabolite profiles which were also examined following 48 hours of growth (Figure 2.3). While IMPDH1 was not the central focus of this chapter, IIMPDH1 was also identified as a candidate protein-protein interactor of ATG4B (Table 2.1). Both IMPDH1 and IMPDH2 have similar functions in guanine nucleotide biosynthesis[138]. It plausible that reduced IMPDH1 protein levels decreased overall IMPDH activity in ATG4B KO#1, resulting in a negative feedback loop that slowed purine salvage of metabolites like adenosine, hypoxanthine, and inosine when cells were not stressed. In contrast, such a defect may not have existed in ATG4B KO#2, given that their IMPDH1 protein levels were similar to parental cells. At least in the context of full media conditions, this may explain why adenosine, inosine and hypoxanthine were enriched in ATG4B KO#1 but depleted in ATG4B KO#2. Further, although both ATG4B KO#1 and KO#2 were similarly sensitive to glutamine-deprivation with or without purine-depletion (Figure 2.15, Figure 2.21), and showed modest growth reductions in response to IMPDH inhibition under glutamine-limiting conditions (Figure 2.17), the degree to which their growths are affected by these stresses are noticeably different. It remains to be determined if and what genetic factors contributed to these growth differences between ATG4B KO#1 and ATG4B KO#2, and if these differences were a consequence of their different metabolite profiles. It is also plausible that the enrichment in purine salvage metabolites occurs at an earlier time point in ATG4B KO#2 and is depleted sooner, which would explain why ATG4B KO#2 was found to be more sensitive to glutamine- and purine-depletion than ATG4B KO#1. Future work examining the temporal changes in profiles and turnover of metabolites in each of the ATG4B KO cells compared to parental cells may clarify this.

Monoclonal ATG4B KO cell lines were generated as models for the metabolomic experiments executed in chapter 2 to evaluate the effect of complete loss of ATG4B on metabolite profiles under conditions of glutamine deprivation. I did not select genetic ATG4B knockdown models for these experiments as I anticipated that were would have been milder differences and changes to metabolite profiles, given that there was still detectable LCB processing in ATG4B KD cells as evident in figure 2.5. Given the current

findings from this chapter, it now seems plausible that the potential activation of compensatory mechanisms that may have occurred heterogeneously in these monoclonal ATG4B KO cells lines. Future work may consider validating these findings in additional ATG4B KO or knockdown cell line models and examining the effect of genetic loss of ATG4B in polyclonal KO populations or through the use of more than one CRISPR/Cas9 guide RNA to perturb different exons of ATG4B.

In spite of the differences in metabolite profiles, I found that both ATG4B KO cells still presented with a clear enrichment in purine nucleotides under conditions of glutamine deprivation. Further, I also examined an independent and publicly available metabolomic dataset[250] , and found a similar enrichment in purine salvage metabolites in atg4b$^{-/-}$ mice compared to wild-type mice. In investigating the biological consequence of these metabolic alterations, I found that prolonged glutamine deprivation was associated with a significant reduction in cell growth in both ATG4B KO#1 and KO#2 compared to parental cells. Notably, treatment of glutamine-deprived ATG4B KO#1 and KO#2 with the pharmacological inhibitor, MPA, was associated with modest reductions in cell growth, suggesting that the reliance of ATG4B KO cells on IMPDH-independent pathways for growth under glutamine deprivation. Given that MPA is a pharmacological non-competitive inhibitor of both IMPDH1 and IMPDH2[258], future work validating these findings through genetic knockdown or knockout approaches that modulate levels of the IMPDH1 or IMPDH2 protein will be important in clarifying the contributions of either or both isoforms to this axis. Given the metabolomic findings and the ability of the purine salvage pathway to also contribute to purine nucleotide production[138], I hypothesized that the purine salvage pathway may play an important role in growth of glutamine-deprived ATG4B KO cells. Indeed, I found that depletion of exogenous purines further significantly reduced the growth of ATG4B KO cells compared to parental cells under conditions of glutamine deprivation. Together, these findings suggest a potential metabolic pivot towards utilization of the purine salvage pathway, an alternate pathway for GTP production in cells, as a consequence of genetic loss of ATG4B. It is important to note that the *de novo* purine pathway metabolites were not detected in these experiments, and detection for these metabolites are currently being optimized to fully understand the metabolic consequence of ATG4B loss. In this case, I expect that levels of *de novo* purine metabolites will be lower in ATG4B KO cells compared to parental

cells if the hypothesis that ATG4B KO cells predominantly utilize the purine salvage pathway for purine nucleotide production is true.

Although the purine salvage pathway is a more energy-efficient route for purine biosynthesis, the purine requirement in cells is often greater than the capacity of the purine salvage pathway to provide, requiring activation of *de novo* purine biosynthesis[183]. As such, I hypothesized that the genetic loss of ATG4B creates a metabolic reliance on the purine salvage pathway because it perturbs the ATG4B-IMPDH2 interaction may contribute to *de novo* production of purines, like guanine nucleotides. In situations of prolonged nutrient stress resulting in severe depletion of guanine nucleotides, I postulate that the purine salvage pathway alone will not suffice in proving cells with purines required to maintain cellular growth. I found that ATG4B KO cells are significantly more sensitive to glutamine deprivation that parental JIMT-1 cells, supporting the importance of ATG4B in nutrient stress response, in this case, to glutamine deprivation. I found that IMPDH inhibition with the pharmacological IMPDH inhibitor, MPA, was associated with a significant reduction in growth of glutamine-deprived JIMT-1 cells. I discovered that IMPDH inhibition only led to a modest decrease in growth of glutamine deprived ATG4B KO cells. This suggested that ATG4B KO cells rely on IMPDH-independent pathways to sustain growth in prolonged glutamine-deprived settings. Given the metabolomic findings, I postulated that ATG4B KO cells rely on the purine salvage pathway for growth in glutamine-deprived conditions. Indeed, I found that depleting exogenous purine supply of glutamine deprived ATG4B KO cells was associated with a significantly greater reduction in growth compared to parental cells. These findings reveal a novel mechanism whereby genetic loss of ATG4B metabolically reprograms HER2+ breast cancer cells to rely on the purine salvage pathway for growth. I must note that depletion of exogenous purines was performed using a dialyzed FBS approach, and therefore depletion was not specific to just purines. Future studies investigating if supplementation of ATG4B KO cells with purines, like hypoxanthine or guanosine, would restore growth defects seen under glutamine- and purine-depleted media will help support these findings. To date, pharmacological inhibitors that specifically target the purine salvage pathway have not yet been identified and remains a clear gap in the field. Although genetic tools, like siRNA or shRNA, that target purine salvage enzymes exist, this approach is not straightforward because of how the purine salvage pathway is heavily interconnected with crosstalk that allows for compensation for the inhibition in any one

salvage enzyme. My survey of enzymes involved in *de novo* purine biosynthesis pathway and purine salvage pathway also did not reveal any strong effect on their protein levels following genetic loss of ATG4B. This suggests that the protein levels of these metabolic enzymes are unlikely regulated by ATG4B, and these protein levels do not necessarily reflect their cellular activity and involvement in purine biosynthetic pathways.

Studies by Mimura et al. 2021 showed that purine depletion in HEK293T cells results in the activation of autophagy via a mTOR-dependent mechanism, whereas autophagy induction in response to pyrimidine depletion occurs in a mTOR-independent manner[259]. These findings are in support of a role for autophagy in maintaining cellular nucleotide levels and suggests that the underlying mechanisms regulating the autophagic response to cellular deficiencies in either purine nucleotides or pyrimidine nucleotides differs. Defects in autophagy were also associated with decreases in adenylate energy charge and metabolites involved in the TCA cycle and pentose phosphate pathway in KRAS-driven lung cancers under conditions of nutrient stress[149]. Notably, ATG7-deficient KRAS-driven lung cancer cells presented with an accumulation of purine and pyrimidine bases and a substantial depletion in nucleotide pools under conditions of starvation, which may suggest an increase in nucleotide catabolism to maintain cellular energy charge and generate carbon sources for the TCA cycle and pentose phosphate pathway[149]. I similarly discovered that genetic loss of ATG4B was associated with an enrichment in purine bases but, interestingly, discovered that glutamine-deprived ATG4B KO cells instead presented with an enrichment in adenine and guanine nucleotides. This difference could be owing to the distinct roles of ATG4B and ATG7 in nucleotide metabolism, or the type of nutrient stress cells are exposed to. My findings suggest that the elevated purine bases in ATG4B KO cells may serve to replenish levels of purine nucleotides under conditions of glutamine deprivation, which would explain the enrichment in adenine and guanine nucleotides. This notion is supported by my findings which revealed an increased reliance on the purine salvage pathway in glutamine deprived ATG4B KO cells. It is plausible that the increase in purine bases may be attributed to increased uptake of exogenous purines, and future work examining the effect of inhibiting key nutrient transporters on levels of purine bases and purine nucleotides in ATG4B KO cells under glutamine deprivation will clarify this. It will also be interesting to see if ATG7-deficient cells may also present with a similar reliance

on the nucleotide salvage pathway over the *de novo* nucleotide biosynthesis pathway under conditions of glutamine deprivation.

Questions still remain: Can we reverse the metabolic reliance of ATG4B KO cells on the purine salvage pathway by re-expressing ATG4B? Does ATG4B regulate IMPDH activity and, if so, is this through autophagy? Is the ATG4B-IMPDH2 interaction important for the *de novo* purine biosynthesis pathway? The function of IMPDH2 rings-and-rods in glutamine-deprived settings, and potential implications of ATG4B in the formation of these structures in breast cancers remains to be determined. Although studies have suggested that rings-and-rods may serve to maintain IMPDH activity through mitigating feedback allosteric inhibition of activity by GTP[188], these findings were not performed on cells deprived of nutrients like glutamine to induce rings-and-rods nor investigated in cancer contexts. It is also important to mention that the functional investigations in this study were performed primarily in the HER2-positive breast cancer cell line, JIMT-1, and subsequent studies evaluating if similar biological mechanisms described in this chapter exist in other breast cancer cell lines should be performed.

In total, this study is the first to describe the discovery and validation of a novel protein-protein interaction between ATG4B and IMPDH2 in breast cancer cells. This study is also the first to describe a novel metabolic reprogram where cells predominantly utilize the purine salvage pathway for growth as a consequence of genetic loss of ATG4B. This is significant given the quantity of pre-clinical studies evaluating the potential therapeutic benefit of ATG4B inhibition in cancers[235,236]. Sustained loss of ATG4B or inhibition of ATG4B activity may lead to compensatory utilization of pathways like the purine salvage pathway for growth. In these cases, findings from this study suggest that depletion of exogenous purines may augment the therapeutic efficacy of ATG4B inhibition in cancer therapies by addressing potential compensatory utilization of the purine salvage pathway. Additionally, findings from this study suggest a potential new role for an ATG4B-IMPDH2 axis in modulating *de novo* purine biosynthesis, given that perturbation of this interaction through ATG4B loss seems to shift cells towards utilization of the purine salvage pathway. To date, there is an abundance of literature in support of the importance of purine metabolism in cancers[138,184]. Given the interplay between the autophagy machinery and nucleotide metabolism, the new discovery that the ATG4B-IMPDH2 axis could contribute to *de novo* purine biosynthesis in breast

cancers opens up the potential of ATG4B and/or IMPDH2 inhibition in mitigating breast cancer growth and progression.

Chapter 3. Investigating the potential therapeutic applications of ATG4B and IMPDH in breast cancer

3.1. Introduction

Breast cancer is the top commonly diagnosed form of cancer amongst Canadian women and is the 2nd leading cause of cancer-related deaths[43] . Approximately 15-20% of breast cancer cases are of the HER2-positive subtype, meaning that they overexpress the human epidermal growth factor receptor 2 (HER2) protein[44,45]. HER2 overexpression is associated with aberrant activation of various downstream pathways that promote breast tumorigenesis[260]. Although significant improvement in HER2-positive breast cancer patient outcomes have been achieved since the development and approval of HER2-targeted agents, like trastuzumab [261], the issue of treatment resistance still remains an outstanding challenge in advanced and metastatic cases of HER2-positive breast cancers[50,51].

Pre-clinical studies have found that autophagy inhibition may be beneficial in potentiating the efficacy of trastuzumab and mitigating tumorigenesis of HER2-positive breast cancer cells[59–61,262]. Of note, studies by our group found that genetic knockdown of the core autophagy cysteine protease, ATG4B, in combination with trastuzumab was associated with a significant reduction in cell viability in HER2-positive cell lines[61]. *These findings suggest that ATG4B may be important in modulating the responses of HER2-positive breast cancers to trastuzumab.*

Findings from chapter 2 of this thesis report of a novel interaction between ATG4B and the metabolic enzyme, IMPDH2, that may support *de novo* purine production in breast cancer cells. Recent transcriptomic studies have found elevated IMPDH2 mRNA levels in breast invasive carcinomas and a significant reduction in percent survival of high IMPDH2-expressing TNBC patients[233]. However, the clinical significance of IMPDH1 and IMPDH2 at the protein level remains to be defined. IMPDH inhibitors, like MPA[216,217] and ribavirin[223,224], have also been found to reduce the growth and viability of breast cancer cell lines, supporting a potential role for IMPDHs in breast tumorigenesis. However, the molecular mechanisms underlying how IMPDH proteins, especially IMPDH2, are involved in breast cancer growth and treatment responses remains to be determined. As part of chapter 3, I sought to investigate the potential

therapeutic applications of combined inhibition of ATG4B and IMPDH2 in improving the responses of a cell line model of HER2-positive and trastuzumab-resistant breast cancer, JIMT-1, to trastuzumab.

3.2. Materials and methods

3.2.1. Cell lines and culture conditions

The JIMT-1 cell line was obtained from the German Collection of Microorganisms and Cell Culture (Deutsche Sammlung von Mikroorganismen und Zellkulturen GmbH), and grown in a cell culture incubator at 37◦C and under 5% CO_2.

3.2.2. Generation of JIMT-1 ATG4B KO cell lines by CRISPR/Cas9

Generation of JIMT-1 ATG4B KO cell lines were as described in Chapter 2.2.2. methods.

3.2.3. Assessment of cell growth by Incucyte

Incucyte experiments to assess changes in cell growth were performed as described in Chapter 2.2.8.

3.2.4. Assessment of cell viability by crystal violet

$2x10^5$ cells were seeded in 6-well plates and allowed to adhere overnight prior to treatment with indicated concentrations of trastuzumab and/or LV320. Following 72 hours of treatment, cell culture media were removed, and cells were fixed onto each well with 4% paraformaldehyde for at least 30 minutes at room temperature or overnight at 4°C. Fixed cells were then stained by crystal violet dye for at least 30 minutes at room temperature with gentle agitation. Crystal violet dye were removed from each well and plates were washed with water and left to dry overnight. The next day, 2mL of acetic acid were added to each well and left to incubate for at least 30 minutes at room temperature with gentle agitation. Approximately 100uL of resuspended crystal violet solution was removed from each well and placed into 96 well plates for measurement of absorbance at 590nm using a VersaMax plate reader. 3 technical replicates of readings

were performed for each condition, and the average absorbances were normalized to parental and/or untreated controls as indicated to examine differences in cell viability.

3.3. Results

3.3.1. IMPDH1 and IMPDH2 protein levels are significantly elevated in breast cancers compared to normal breast tissues

The clinical significance of IMPDH1 and IMPDH2 in breast cancers has been limited primarily to studies at the transcriptomic level. To evaluate the potential clinical importance of IMPDH1 and IMPDH2 proteins in breast tumors, protein levels in breast tumors and normal breast tissues were examined in two independent and publicly available proteomic patient cohorts[248,263]. Proteomic analyses of IMPDH1 and IMPDH2 protein levels revealed significantly higher levels of these proteins in breast tumors compared to normal breast tissues (Figure 3.1). This suggests *that IMPDH1 and IMPDH2 proteins may be important in breast cancer progression and survival.*

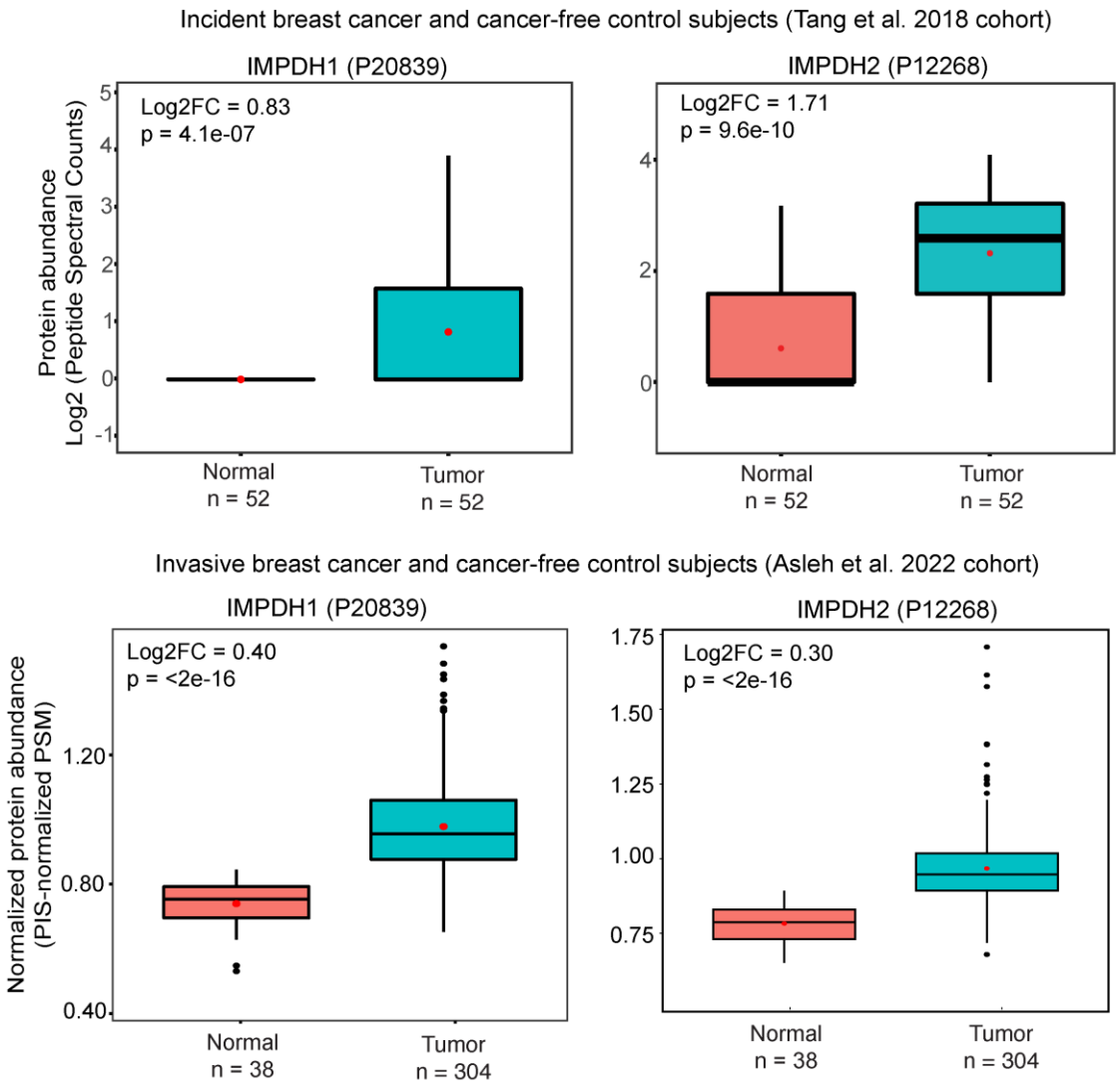

Figure 3.1 IMPDH protein levels are significantly elevated in breast tumors
IMPDH1 and IMPDH2 protein levels were evaluated in two independent breast cancer patient cohorts as indicated. Protein abundances were normalized and log base 2 transformed. Data were visualized using R and the ggplot2 library. Log2 fold changes (Log2FC) were calculated to compare differences in IMPDH protein levels in normal breast tissues versus breast tumor samples. Unpaired t-tests were performed to evaluate statistical differences in protein levels between normal breast tissues versus breast tumors samples.

To determine if elevated IMPDH protein levels may exist in certain subtypes of breast cancers, breast tumors were further stratified according to their reported PAM50-subtype. Proteomic analyses revealed that IMPDH1 and IMPDH2 protein levels are significantly elevated compared to normal breast tissues in all four PAM50 subtypes of

tumors examined (Figure 3.2). *This suggests that high IMPDH1 and IMPDH2 protein levels may be a feature in breast cancers irrespective of their PAM50 subtype.*

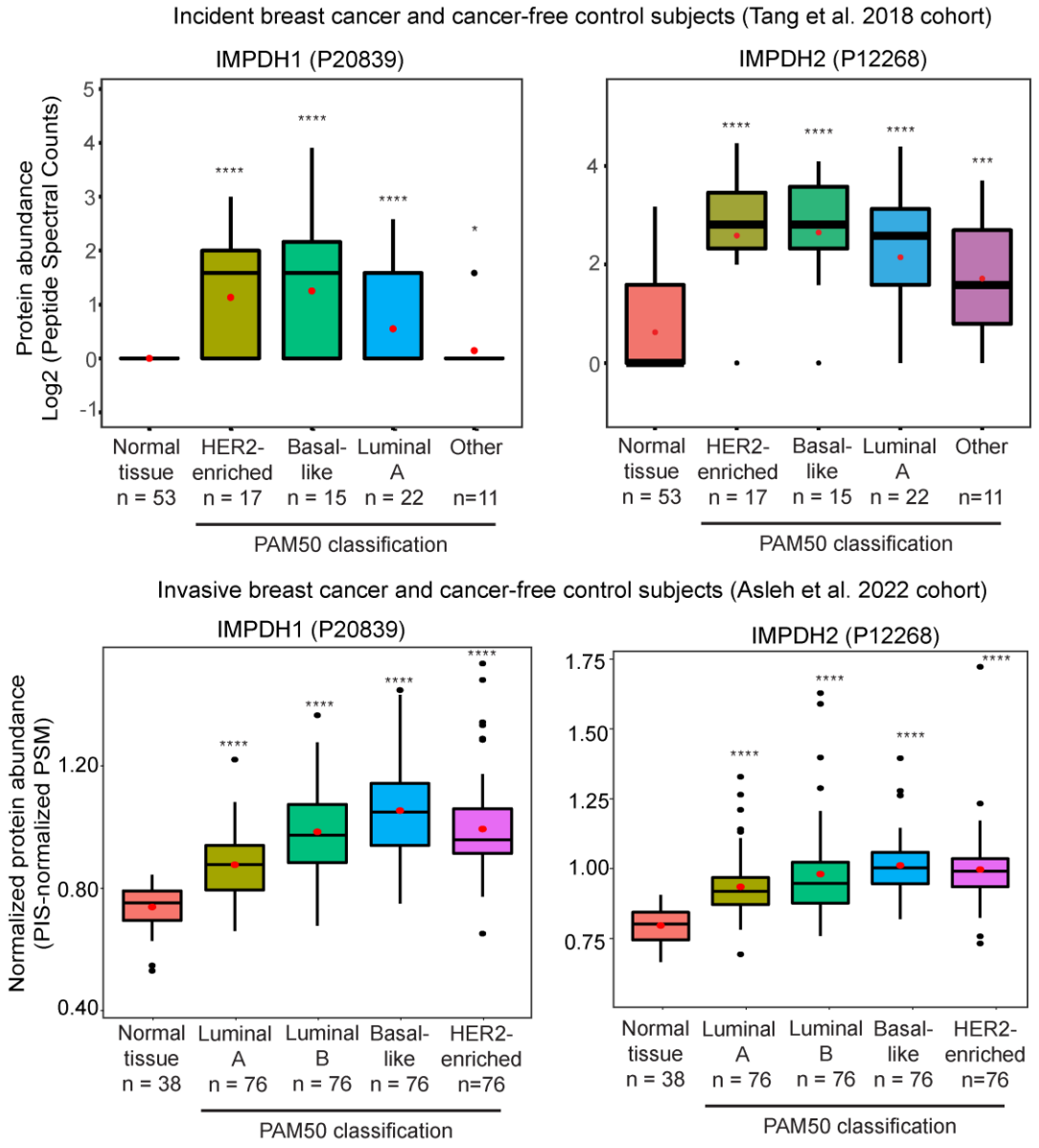

Figure 3.2 Stratification of breast tumors reveal elevated IMPDH protein levels in all breast tumors regardless of known PAM-50 subtype status

IMPDH1 and IMPDH2 protein abundances of normal and tumor breast tissues from two independent breast cancer patient cohorts were stratified according to PAM50 subtypes. Protein abundances were normalized and log base 2 transformed prior to visualization via R and the ggplot2 library. Log2 fold change (Log2FC) values were calculated to compare protein abundances between subtypes relative to normal tissues, and the statistical significance between the group means were calculated using an unpaired t-test and false discovery rate corrected using the Benjamini-Hochberg procedure. Labelled significance represents post adjusted p-values.

3.3.2. High IMPDH2 protein levels are associated with inferior prognoses in breast cancer patients

To investigate the potential prognostic value of IMPDH protein levels in breast cancers, correlations between IMPDH1 and IMPDH2 protein levels and overall patient survival probability were evaluated in a publicly available breast cancer patient cohort[263] using KMPlotter[264]. Breast cancer patients with high IMPDH1 protein expression were not associated with a significantly reduced overall survival probability compared to patients with low IMPDH1 protein expression. In contrast, breast cancer patients that presented with high IMPDH2 protein levels were associated with significantly reduced overall breast cancer patient survival probability (Figure 3.3), *suggesting that high IMPDH2 protein levels are a potential negative prognostic marker in breast cancer patients.*

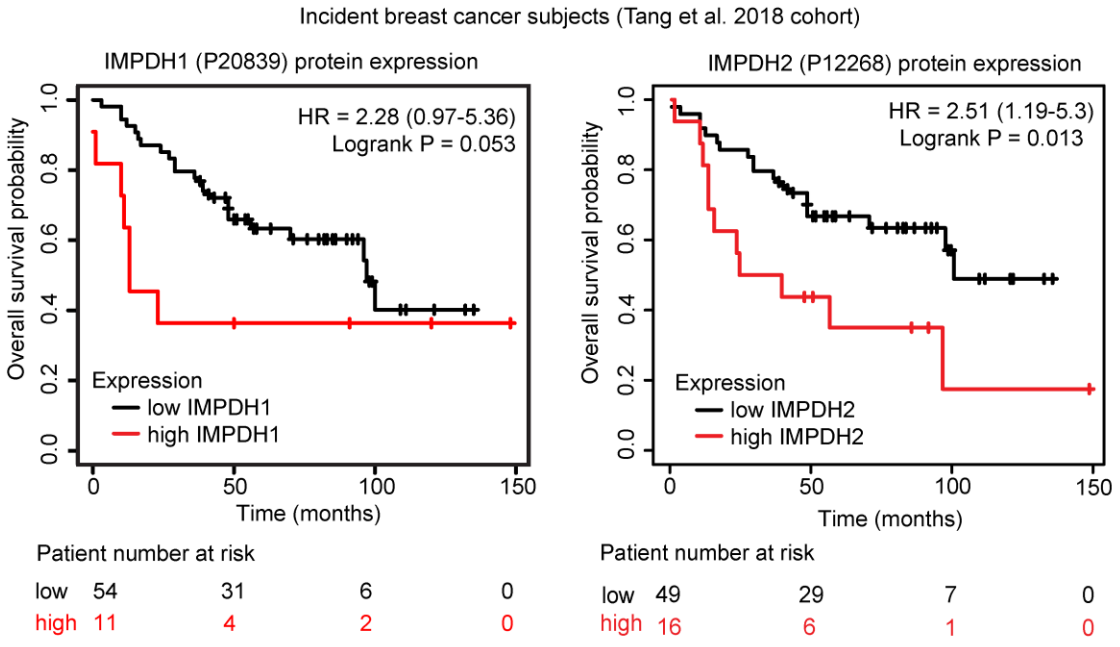

Figure 3.3 High IMPDH protein levels are associated with significantly reduced overall breast cancer patient survival probability

Breast cancer patient data were obtained from a cohort recruited between 1993 and 2003, and consisted of patients with pathologically confirmed breast cancers that were diagnosed within 6 months prior to recruitment [263,265]. Breast cancer patients were stratified based on high or low IMPDH1 and IMPDH2 by an upper quartile cut-off using KMPlotter, independent of tumor grade, stage and receptor status. Hazard ratios were determined and Logrank tests were performed by

KMPlotter to evaluate the magnitudes and statistical differences of overall survival probability between the two groups.

Of note, ATG4B protein levels were not part of this current dataset[263] and, as such, the associations between high or low ATG4B protein levels and overall patient survival probability could not be examined.

3.3.3. ATG4B protein levels are elevated in luminal B, basal-like and HER2-enriched breast tumors compared to normal tissues

To investigate the clinical significance of the ATG4B protein in breast cancers, levels were evaluated in one of the breast cancer cohorts described in chapter 3.3.1 that contained proteomic data for ATG4B[248]. Proteomic analyses revealed that ATG4B protein levels are elevated in breast tumors compared to normal breast tissues, and stratification of tumors according to PAM50 subtype statuses revealed that ATG4B levels were significantly higher in luminal B, basal-like and HER2-enriched subtypes (Figure 3.4). *These findings present supporting evidence for the role of ATG4B in breast tumorigenesis in subtypes like luminal B, basal-like and HER2-enriched.*

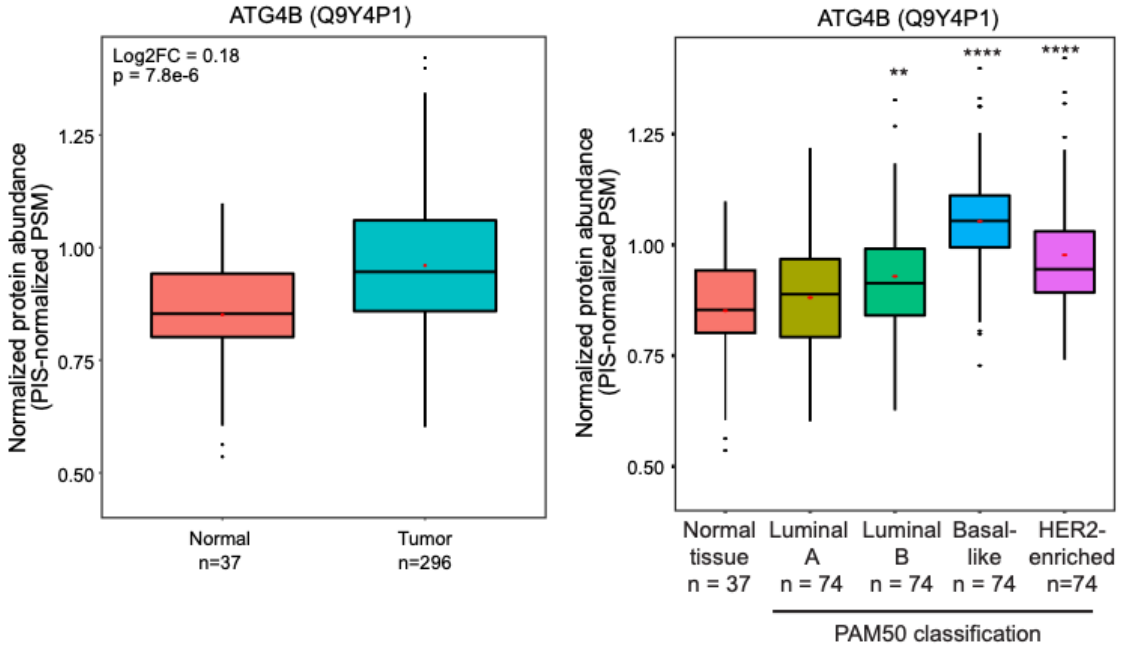

Figure 3.4 ATG4B protein levels are elevated in breast tumors compared to normal tissues

ATG4B protein levels were evaluated in a publicly available breast cancer patient cohort. Protein abundance were normalized and log base 2 transformed prior to visualization via R and ggplot2 library. Breast cancer samples were further stratified according to their known PAM-50 subtypes. Log2 fold changes (Log2FC) were calculated to compare differences in ATG4B protein levels in normal breast tissues versus breast tumor samples. The statistical significance between the group means were calculated using an unpaired t-test and false discovery rate corrected using the Benjamini-Hochberg procedure. Labelled significance represents post adjusted p-values.

3.3.4. ATG4B and IMPDH2 protein levels do not show substantial correlations in PAM50 subtypes of breast cancers

Analyses from chapter 2.3.2 revealed a significant positive correlation between ATG4B and IMPDH2 in breast tumors. To better understand the significance of ATG4B and IMPDH2 in different subtypes of breast cancers, protein-protein correlations were performed on breast cancer patient proteomic data from Asleh et al. 2022 cohort[248] following stratification of breast tumors according to respective PAM50 subtypes. Although no significant correlations between ATG4B and IMPDH2 were observed in any of the PAM50 subtypes of breast cancers, HER2-enriched and luminal B subtype patients did present with a positive ATG4B-IMPDH2 correlation trend (Figure 3.5). *Analyses of other datasets to verify these trends are certainly warranted. Given that a significant positive correlation between ATG4B and IMPDH2 was observed when breast tumors were unstratified, this suggests that PAM50 subtyping may not be an effective way to identify breast cancer contexts whereby both ATG4B and IMPDH2 are co-expressed.*

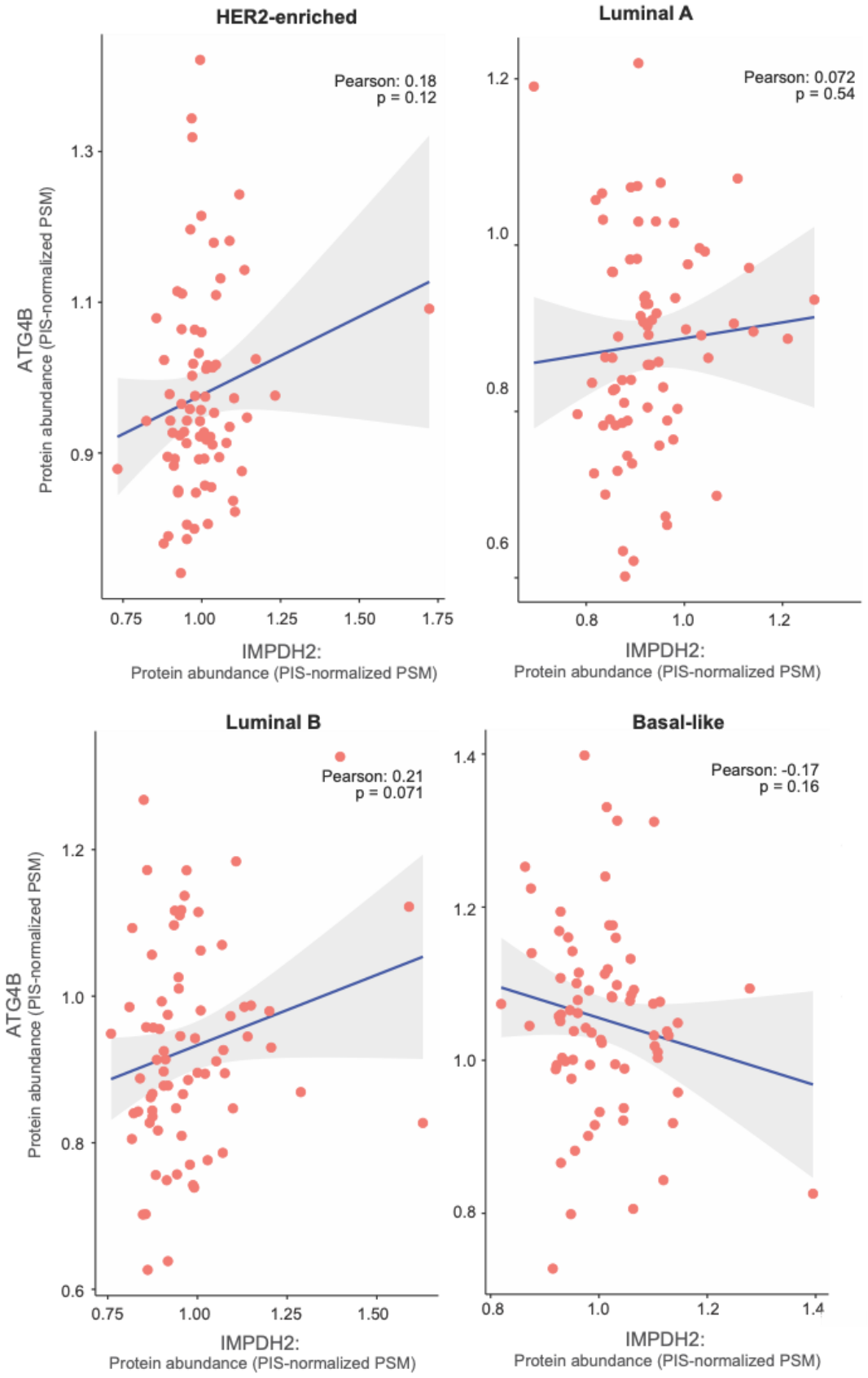
HER2-enriched
Pearson: 0.18
p = 0.12
Luminal A
Pearson: 0.072
p = 0.54
Luminal B
Pearson: 0.21
p = 0.071
Basal-like
Pearson: -0.17
p = 0.16
ATG4B
Protein abundance (PIS-normalized PSM)
IMPDH2:
Protein abundance (PIS-normalized PSM)

Figure 3.5 ATG4B and IMPDH2 protein levels are not significantly correlated in PAM50 subtypes of breast cancers

Breast cancer patients were stratified according to known PAM50-subtype statuses. Pearson correlation was performed to evaluate the statistical significance of ATG4B-IMPDH2 correlations in each subtype of breast cancer by log2 transforming the pooled internal standard (PIS)-normalized peptide spectral counts and plotting each sample with both ATG4B and IMPDH2 abundances on an X-Y scatter plot using R and ggplot2.

ATG4B was previously associated with modulating the responses of HER2-positive breast cancer cells to nutrient stress and trastuzumab treatment[61]. This study sought to leverage the ATG4B-IMPDH interplay to mitigate breast cancer growth and progression. Intra-tumoral heterogeneity of the HER2 protein exists in approximately 40% of breast cancers, and is a potential mechanism for resistance to HER2 targeted therapies[266]. To first determine if ATG4B and HER2 protein levels are correlated in certain subtypes of breast cancers, protein levels were analyzed in tumor samples of breast cancer patients stratified according to their known PAM50 subtype. Comparative analyses revelated that ATG4B and HER2 are not significantly correlated at the protein level in any PAM50-subtype of breast cancer in the cohort examined (Figure 3.6). However, a positive correlation trend was observed between ATG4B and HER2 in breast cancers of the HER2-enriched subtype*, suggesting that both proteins may be correlated in certain subpopulations of HER2-enriched breast tumors.*

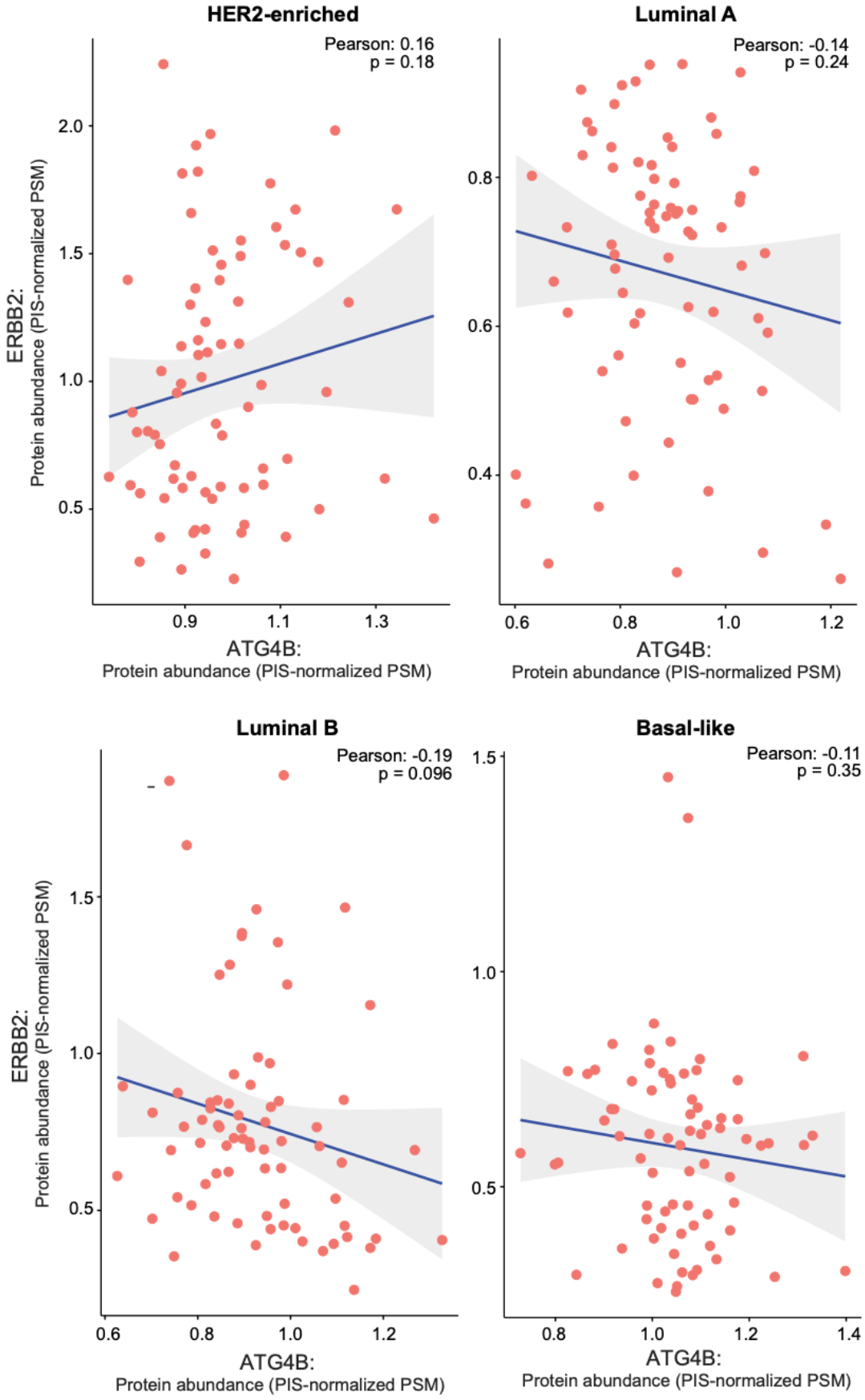
HER2-enriched
Pearson: 0.16
p = 0.18
Luminal A
Pearson: -0.14
p = 0.24
Luminal B
Pearson: -0.19
p = 0.096
Basal-like
Pearson: -0.11
p = 0.35
ERBB2:
Protein abundance (PIS-normalized PSM)
ATG4B:
Protein abundance (PIS-normalized PSM)

Figure 3.6 ATG4B and HER2 protein levels are not signifcantly correlated in breast cancer patients stratified according to PAM50 subtype

Breast cancer patients were stratified according to known PAM50-subtype statuses. Pearson correlation was performed to evaluate the statistical significance of ATG4B-ERBB2 (also known as HER2) correlations in each subtype of breast cancer by log2 transforming the pooled internal standard (PIS)-normalized peptide spectral counts and plotting each sample with both ATG4B and ERBB2 abundances on an X-Y scatter plot using R and ggplot2.

Next, to determine if IMPDH2 and HER2 are correlated in certain subtypes of breast cancers, protein-protein correlations studies were again performed in the different PAM50 subtypes of breast cancers. Analyses revealed a positive, though weak, correlation between IMPDH2 and HER2 only in the HER2-enriched subtype (Figure 3.7). Overall, *these findings suggest that there is no substantial correlation between IMPDH2 and HER2 in breast tumors.*

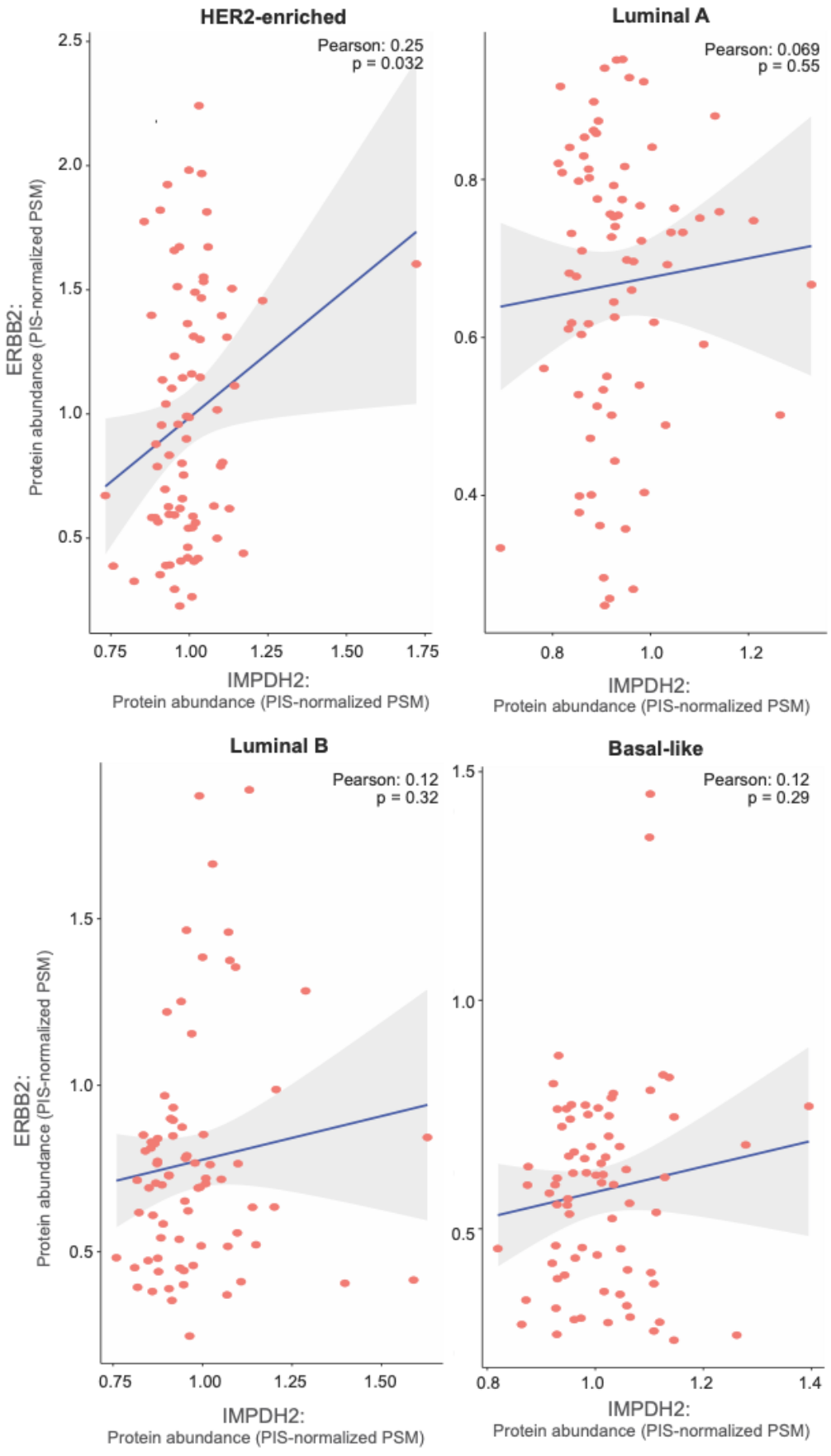
HER2-enriched
Pearson: 0.25
p = 0.032
Luminal A
Pearson: 0.069
p = 0.55
Luminal B
Pearson: 0.12
p = 0.32
Basal-like
Pearson: 0.12
p = 0.29
ERBB2:
Protein abundance (PIS-normalized PSM)
IMPDH2:
Protein abundance (PIS-normalized PSM)

Figure 3.7 IMPDH2 and HER2 protein levels are positively correlated in HER2-enriched breast tumors

Breast cancer patients were stratified according to known PAM50-subtype statuses. Pearson correlation was performed to evaluate the statistical significance of IMPDH2-ERBB2 (also known as HER2) correlations in each subtype of breast cancer by log2 transforming the pooled internal standard (PIS)-normalized peptide spectral counts and plotting each sample with both ATG4B and IMPDH2 abundances on an X-Y scatter plot using R and ggplot2.

3.3.5. Pharmacological inhibition of ATG4 and IMPDH results in a modest but synergistic reduction in JIMT-1 cell growth

Findings from Chapter 2 suggest that the ATG4B-IMPDH2 interplay may play an important role in breast cancer growth under nutrient stresses, like glutamine deprivation, in JIMT-1 cells. To determine if this protein-protein interaction axis may also modulate the responses of JIMT-1 cells to trastuzumab, the effect of genetic loss of ATG4B on the sensitivity of HER2+ breast cancer cells to IMPDH inhibition was first examined. ATG4B KO cells were treated with increasing concentrations of the pharmacological inhibitor, mycophenolic acid (MPA), which is a non-competitive inhibitor of IMPDH that targets the NAD^+ site of the enzyme[258]. Growth was monitored over a course of 120 hours, and the best-fit IC50 values for parental JIMT-1, JIMT-1 ATG4B KO#1, and JIMT-1 ATG4B KO#2 were 1.92 μM, 3.14 μM and 1.569 μM respectively. These findings suggest that genetic loss of ATG4B does not substantially reduce the IC50 of MPA in JIMT-1 cells (Figure 3.8).

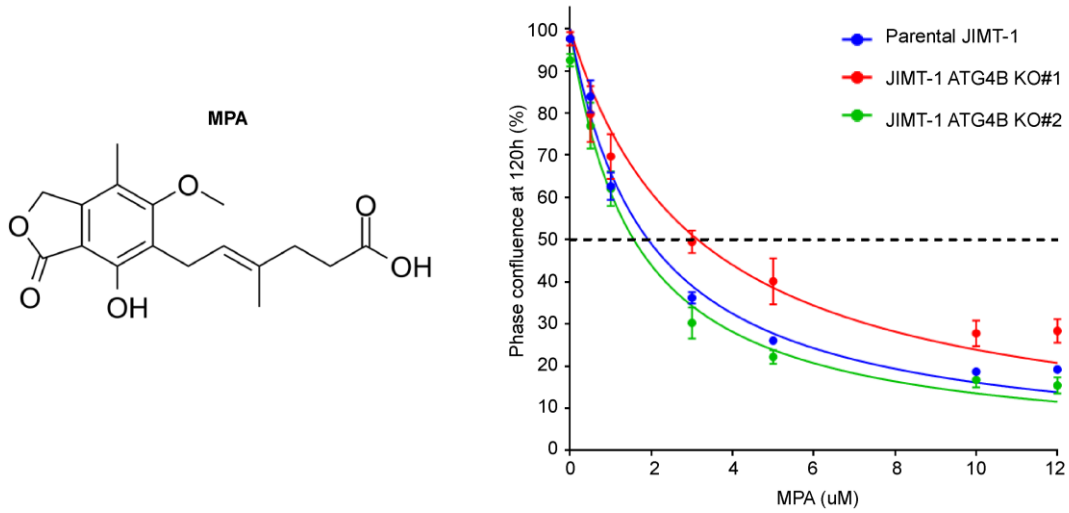

Figure 3.8 Genetic loss of ATG4B does not increase sensitivity to IMPDH inhibition

Parental and ATG4B KO cells were treated with increasing concentrations of MPA (0-12uM; 0.6% DMSO) as described in methods. Percent phase confluence after 120 hours was measured by

Incucyte. IC50 of each cell line for each concentration of MPA was determined using GraphPad. One-way ANOVA with Dunnett's multiple comparisons test was performed to evaluate statistical differences in the IC50 values of parental JIMT-1 cells to ATG4B KO#1 and KO#2 across 3 biological replicates. No statistically significant differences were found. Error bars represent SEM.

Next, to determine if pharmacological inhibition of ATG4 and IMPDH would lead to a greater reduction in growth compared to single treatments alone, the growth of parental JIMT-1 cells treated with LV320 and MPA were monitored after 120 hours. LV320 is a pharmacological inhibitor of ATG4A and ATG4B, and *in silico* predictions suggest that it elicits its inhibitory activity on ATG4B by binding near the regulatory loop or to the N-terminal tail of the ATG4B protein[121]. Combined treatment with 20μM LV320 and 0.5μM or 1.0μM MPA led to a synergistic but modest reduction in growth as determined by CompuSyn (Figure 3.9A), *supporting a potential therapeutic value for combining ATG4 and IMPDH inhibition in the treatment of HER2-positive breast cancers.*

To assess the growth of parental JIMT-1 cells in the absence or presence of LV320 or MPA over time, the change in the percent phase confluence of cells treated with the best synergistic combination was measured by Incucyte. Growth of cells treated with LV320 or MPA remained similar to control DMSO-treated cells, whereas growth of cells treated with a combination of LV320 and MPA decreased around the 72-hour time mark (Figure 3.9B). Given the importance of IMPDH proteins in de novo purine biosynthesis and ATG4B in nutrient recycling through autophagy, it is plausible that delayed growth reduction may be due to a depletion of core metabolites required for metabolic pathways as a result of blunting both autophagy and purine biosynthesis. *Together, these findings suggest that combined inhibition of ATG4 and IMPDH may be a potential therapeutic avenue that can be leveraged to improve efficacies of current breast cancer treatments.* These findings additionally suggest that ATG4B KO cells may not be suitable for evaluating the potential therapeutic value of IMPDH inhibition, given the possibility of compensatory mechanisms activated in response to genetic loss of ATG4B.

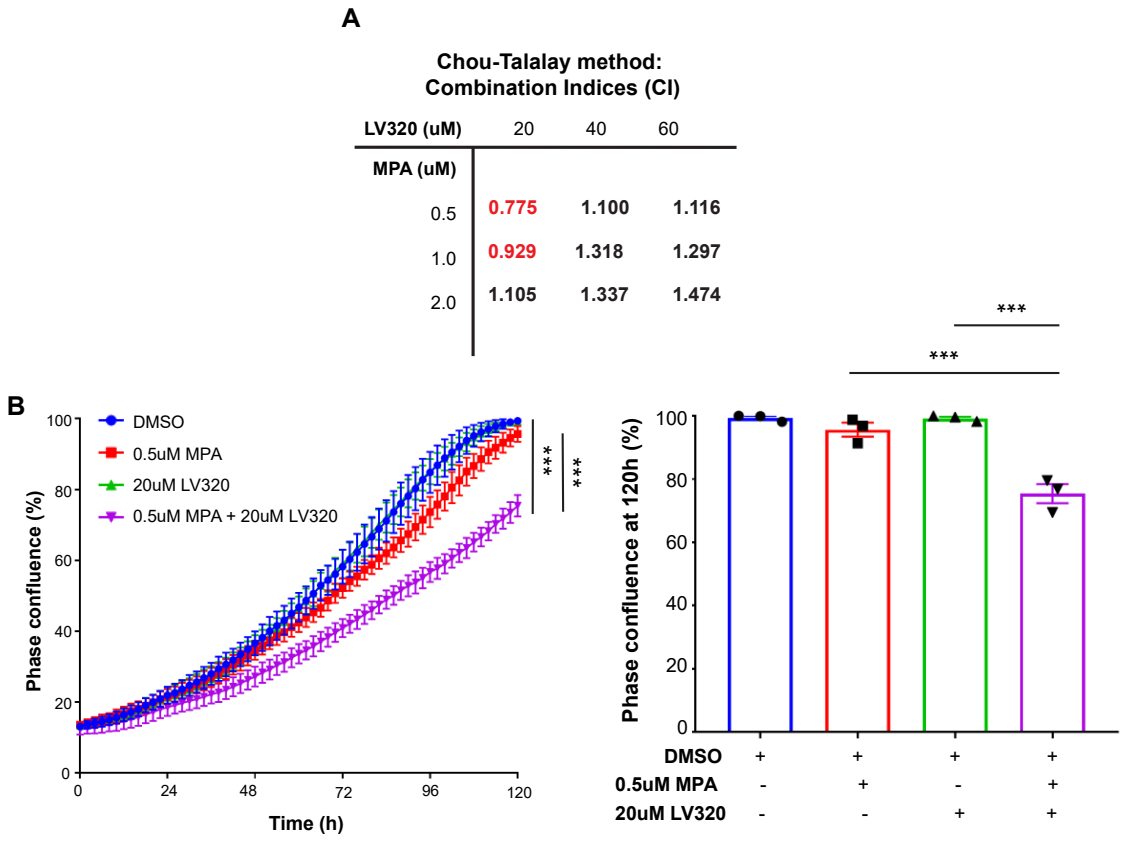

Figure 3.9 Combined LV320 and MPA treatment leads to a modest but synergistic reduction in growth

(A) Parent JIMT-1 cells were treated with different concentrations of LV320 and MPA (0.4% DMSO control) for 120 hours as described in methods. The percent phase confluence of cells after 120 hours was measured by Incucyte and used to calculate combination indices (CI) for synergy by the Chou-Talalay method using CompuSyn. CI values equivalent to 1 are considered additive, greater than 1 are considered antagonistic and less than 1 are considered synergistic[267]. CI values of synergistic combinations are indicated in red. (B) Growth curves (left) and bar graph of end point phase confluence (right) of parental JIMT-1 cells treated with 20μM LV320 and/or 0.5μM MPA. Growth of cells was evaluated every 2 hours by measurement of the percent phase confluence of cells using Incucyte. A total of 3 biological replicates was performed. One way ANOVA with Tukey's multiple comparisons tests were performed to evaluate statistical differences. Error bars represent SEM.

3.3.6. Pharmacological inhibition of ATG4B with LV320 increases the trastuzumab sensitivity of JIMT-1 breast cancer cells

Previous studies have found that genetic knockdown of ATG4B increases the sensitivity of HER2-positive breast cancer cells to the anti-HER2 targeted agent, trastuzumab, *in vitro*[61]. As part of efforts to develop tools that may allow us to translate these findings to an *in vivo* setting, cells with genetic loss of ATG4B and the ATG4 inhibitor LV320 were separately evaluated to determine if they may recapitulate previous

findings. The JIMT-1 cell line is a HER2+ breast cancer cell line model characterized by resistance to trastuzumab. To determine if genetic loss of ATG4B may increase the sensitivity of JIMT-1 cells to trastuzumab, parental and ATG4B KO JIMT-1 cells were treated with trastuzumab for 72 hours. A trastuzumab-sensitive cell line, BT-474, was included as a positive control for trastuzumab response. Findings revealed that genetic loss of ATG4B did not increase the sensitivity of JIMT-1 cells to trastuzumab (Figure 3.10A), *suggesting the presence of potential compensatory mechanisms that may be activated in response to ATG4B KO.*

To evaluate an alternate tool for ATG4B inhibition, the pharmacological ATG4 inhibitor, LV320, was utilized in combination with trastuzumab in parental JIMT-1 cells. Pharmacological inhibition of ATG4 with LV320 led to a modest but significant reduction in cell viability in combination with trastuzumab (Figure 3.10B), *supporting the potential utility of LV320 as a pharmacological tool for ATG4 inhibition in combination with trastuzumab.*

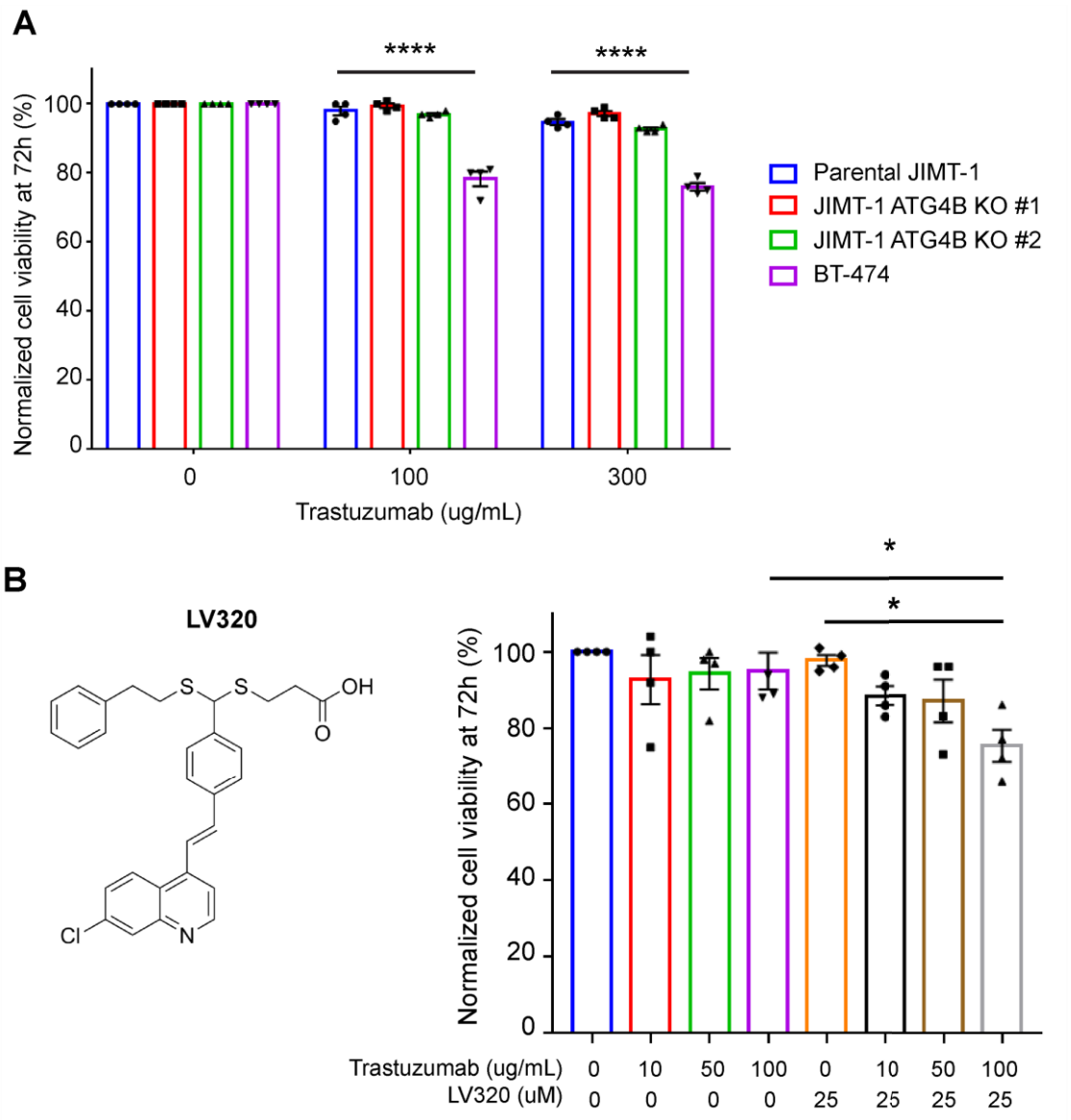

Figure 3.10 LV320 is a potential tool for ATG4B inhibition in combination with trastuzumab

(A) Parental and ATG4B KO JIMT-1 cells were treated with trastuzumab for 72 hours. BT-474, a trastuzumab-sensitive HER2-positive breast cancer cell line, was included as a positive control. Cell viabilities following trastuzumab treatment were evaluated by crystal violet as described in methods. A total of 4 biological replicates were performed. Two-way ANOVA with Tukey's multiple comparisons tests were performed to evaluate statistical differences, and error bars represent SEM. (B) Parental JIMT-1 cells were treated with increasing concentrations of trastuzumab in the absence or presence of LV320 for 72 hours. Cell viabilities were evaluated by crystal violet as described in methods. A total of 4 biological replicates were performed. One-way ANOVA with Tukey's multiple comparison's tests were performed to evaluate statistical differences, and error bars represent SEM. Statistical significance for comparisons of cells treated with 100µg/ml trastuzumab versus 100µg/ml trastuzumab and 25µM LV320, and 25µM LV320 versus 100µg/ml trastuzumab and 25µM LV320 are shown.

To determine if the effects of combined LV320 and trastuzumab treatment are augmented over time, changes in percent phase confluence of parental JIMT-1 cells treated with combined trastuzumab and LV320 were monitored for 120 hours. Findings revealed a significantly greater reduction in growth over time (Figure 3.11), *further supporting the potential utility of LV320 as a pharmacological tool for ATG4 inhibition in combination with trastuzumab.*

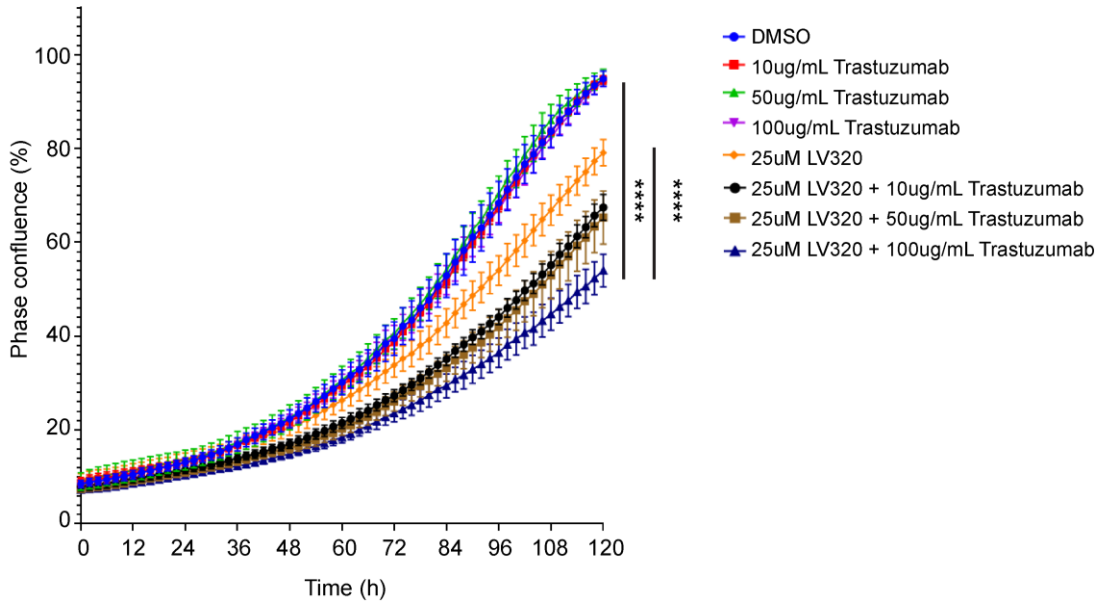

Figure 3.11 Combined LV320 and trastuzumab treatment leads to a significant reduction in growth over time

Parental JIMT-1 cells were treated with increasing concentrations of trastuzumab, with or without LV320. Growth of cells was evaluated every 2 hours by measurement of the percent phase confluence of cells using Incucyte. A total of 4 biological replicates were performed. One-way ANOVA with Tukey's multiple comparisons tests were performed to evaluate statistical differences. Error bars represent SEM.

3.4. Discussion

Current knowledge regarding the clinical significance of IMPDH1 and IMPDH2 expression at the protein level remains poorly defined in breast cancers. Similarly, the clinical importance of protein levels of both ATG4B and IMPDH2 in breast cancer subtypes also remains elusive. In addressing these gaps, I performed proteomic data analysis on independent and publicly available breast cancer patient cohorts in collaboration with Drs. Baofeng Jia and Kevin Yang. I found that IMPDH1 and IMPDH2

protein levels are significantly elevated in breast tumors compared to normal breast tissues in two independent breast cancer patient cohorts. I observed that the levels of both IMPDH proteins were significantly elevated in all PAM50 subtypes of breast cancers relative to normal tissues. This suggests that elevated levels of the IMPDH protein may not be specific to certain PAM50 subtypes of breast cancer, and that the PAM50 subtype stratification may not be an effective way in identifying breast cancer types where high IMPDH protein levels are important. Interestingly, I also discovered that only high IMPDH2 protein levels were associated with significantly reduced overall breast cancer patient survival probabilities. High IMPDH1 protein levels were not associated with significantly reduced overall breast cancer patient survival probabilities. This finding suggests a greater clinical importance of the IMPDH2 protein in breast cancer progression and survival, in contrast to IMPDH1.

Additionally, I leveraged available ATG4B protein data from one of the publicly available patient cohorts analyzed and found that breast tumors present with high ATG4B protein levels compared to normal breast tissues. In addition, I also found that, of the four PAM50 subtypes that the breast cancer samples were stratified to, ATG4B protein levels were significantly higher in the luminal B, basal-like and HER2-enriched subtypes compared to normal tissues, supporting potential clinical importance for ATG4B in these subtypes of breast cancers. Interestingly, independent studies by Bortnik *et al.* 2020 have found that ATG4B protein expression was highest in luminal A breast cancer subtypes and lowest in basal-like breast cancer subtypes[268]. These observations differ from findings from this chapter where amongst the four PAM50 subtypes, basal-like breast cancer subtypes had the highest ATG4B expression and luminal A subtypes had the lowest (Figure 3.4). Differences could be owing to different study population cohorts, discrepancies in independent subtype stratification criteria, and differences in methodologies for assessing protein expression and/or levels.

Findings from chapter 2 revealed a positive but modest correlation between ATG4B and IMPDH2 in breast cancer patients, which could suggest a functional interplay between the two proteins. I expanded on these findings by next examining the protein-protein correlations between ATG4B and IMPDH2 in different subtypes of breast cancers from the Asleh et al. 2022 cohort[248] which contained proteomic data for ATG4B and IMPDH2 and characterized PAM50 subtype statuses for the different tumor samples. I found no significant correlations between ATG4B and IMPDH2 in any of the

PAM50 subtypes of breast cancer, suggesting that the PAM50 subtype stratification may not be effective in identifying breast cancers that present with co-elevated ATG4B and IMPDH2 protein levels.

The central aim of this chapter was to examine if combined ATG4 and IMPDH inhibition could augment responses of HER2-positive breast cancer cells to trastuzumab. As such, I narrowed my focus next on whether the ATG4B-IMPDH2 relationship could be dependent on the HER2 status of breast cancers. I expected to find a positive correlation between ATG4B and IMPDH2 in HER2-enriched breast cancers, given that both proteins interacted and high ATG4B and IMPDH2 protein levels were independently observed in HER2-enriched breast cancer patients compared to normal breast tissues (Figure 3.2, 3.4). The lack of statistically significant nor strong pearson correlations in this case may be owing to intra-tumoral heterogeneity of breast tumors classified as of the HER2-enriched molecular subtype[269]. HER2-positive breast tumors are characterized by amplification of the ERBB2 gene and/or overexpression of the HER2 protein[269]. This is in contrast to breast tumors classified as HER2-enriched, which is based on molecular/transcriptional signatures as defined by the PAM50 classification. Notably, it has been proposed that not all HER2-enriched breast tumors are HER2-positive, and subpopulations can be HER2-negative [269]. To determine if HER2 overexpression could be a criterion for breast tumors to present with a strong ATG4B-IMPDH2 protein-protein correlation, I performed examine the relationship between ATG4B and HER2, and IMPDH2 and HER2. Notably, I found a weak positive correlation between IMPDH2 and HER2 protein levels in HER2-enriched breast cancer patients. This observation supports the potential clinical importance of IMPDH2 in HER2-positive breast cancers and warrants further validation in independent cohorts. Although I did not find a significant positive correlation between ATG4B and HER2 in any PAM50 subtype of breast cancer, HER2-enriched breast cancers did present with a trend of positive ATG4B and IMPDH2 correlation. This could suggest that only certain subpopulations of HER2-enriched breast cancers are characterized by high ATG4B and HER2 protein levels. In general, the observation that the correlations between ATG4B, IMPDH2 and/or HER2 were modest or weak regardless of if breast cancer cohorts were examined as a whole (Chapter 2.3.2) or classified according to their PAM50 subtypes (Chapter 3.3.4) does call into question the clinical importance of the ATG4B-IMPDH2 axis in breast cancer samples. The identification of alternate biomarkers for stratifying breast cancer

patients that may have stronger likelihood of relying on an interplay between ATG4B, IMPDH2 and/or HER2 will be important.

I next postulated that both the ATG4B and IMPDH proteins are important for growth of HER2-positive breast cancer cells. I aimed to investigate and leverage this potential therapeutic vulnerability to improve the responses of HER2-positive breast cancers to HER2-targeted agents. As such, I selected the trastuzumab-resistant HER2-positive breast cancer cell line, JIMT-1, as a cell line model for subsequent experiments. I found that pharmacological inhibition of both ATG4 and IMPDH with LV320 and MPA was associated with a modest but synergistic reduction in cell growth. Notably, some inhibitor combinations were found to be antagonistic, meaning that the effect that these combinations had on cellular growth were less than expected given their individual effects alone. The observed antagonistic combinations may be a result of a buffering effect, whereby the effect of one drug or inhibitor masks the effect of the other, or a suppressive effect, whereby one drug suppresses the effect of the other[270,271]. Unexpectedly, genetic loss of ATG4B did not increase the sensitivity of cells to IMPDH inhibition. Given that the pharmacological ATG4 inhibitor utilized, LV320, targets both ATG4B and ATG4A[121], it is plausible that ATG4A may also contribute to the ATG4B-IMPDH2 functional interplay and genetic loss of ATG4B results in compensation by ATG4A. Future work will involve evaluating the effect of combined genetic knockdown of ATG4A and ATG4B on IMPDH sensitivity. Nevertheless, the modest but significant reduction in growth resulting from combined ATG4 and IMPDH inhibition suggests that this inhibitor duo is a promising combination that warrants further investigation to improve responses to trastuzumab in HER2-positive breast cancer cells. Given findings from Chapter 2, it will be of interest to examine if targeting the purine salvage pathway by glutamine- and/or purine-depletion could augment the efficacy of pharmacological inhibition of ATG4 and IMPDH. Previous studies found that genetic knockdown of ATG4B was associated with increased sensitivity to trastuzumab in HER2-positive breast cancer cells[61]. I independently investigated this avenue using the ATG4 inhibitor, LV320, and found that LV320 treatment was associated with a significant reduction in cell growth when combined with trastuzumab. These findings support the importance of ATG4 in modulating trastuzumab responses in HER2-positive breast cancers and suggest that combined ATG4 and IMPDH inhibition may further augment the growth reduction observed from ATG4 inhibition alone.

In total, this study is the first to describe the potential clinical significance of IMPDH protein levels in breast cancer patients. Additionally, this study is the first to show that combined ATG4 and IMPDH inhibition synergistically reduces cellular growth and the first to validate LV320 as a promising tool to improve trastuzumab responses in resistant HER2-positive breast cancer cells. Future investigations evaluating the effect of combined ATG4 and IMPDH inhibition on trastuzumab responses in resistant HER2-positive breast cancer cell lines have the potential to identify a new therapeutic avenue that can be leveraged to improve trastuzumab efficacy. This is imperative given that advanced and metastatic cases of HER2-positive breast cancer patients often experience resistance to trastuzumab[50,51].

.

Chapter 4. General discussion

As part of my thesis, I sought to discover molecular mechanisms underlying how ATG4B is involved in the nutrient stress response to glutamine deprivation in HER2-positive breast cancer cells through a combination of proteomics, metabolomics and cell and molecular biology approaches. In identifying how ATG4B may modulate nutrient stress responses, I aimed to leverage this novel relationship to improve the responses of HER2-positive breast cancer cells to the HER2-targeted agent, trastuzumab.

4.1. A novel ATG4B-IMPDH2 interaction and consequences on purine metabolism

4.1.1. Study summary and significance

To investigate the molecular mechanisms underlying ATG4B in nutrient stress response, I performed a pilot IP-MS study and discovered a novel protein-protein interaction between ATG4B and the metabolic enzyme, IMPDH2. To understand the potential clinical importance of the ATG4B-IMPDH2 interaction in breast cancers, I performed protein-protein correlation studies using publicly available patient cohorts and discovered a significant positive correlation between ATG4B and IMPDH2 in breast cancers. Given the positive correlation between ATG4B and IMPDH2, I next investigated if reducing protein levels of one binding partner would affect protein levels of the other. I found that genetic inhibition of IMPDH proteins did not affect protein levels of ATG4B, and genetic inhibition of the ATG4B protein was associated with modest effects on IMPDH protein levels. This suggested that protein level regulation of interaction partners is unlikely the primary biological purpose of the ATG4B-IMPDH2 interaction. To explore the possibility that regulation of enzyme activity is the function of the ATG4B-IMPDH2 interaction, I utilized a pharmacological IMPDH inhibitor and found that inhibition of IMPDH activity reduced the processing of LC3B and stabilization of GABARAP, which could suggest an impairment in ATG4B activity and/or function[93,115]. It is important to note that the accumulation of lipidated LC3B could suggest either an increase in autophagosome formation or a defect in the autophagosome-lysosome fusion step[272]. As such, it remains to be determined if IMPDH inhibition by MPA promotes or suppresses autophagic flux. Studies in glioma cells previously showed that

pharmacological inhibition of IMPDH with the inhibitor ribavirin results in a dose-dependent increase in lipidated LC3[273], which could suggest a similar block in ATG4B activity. In this case, the authors found that the accumulation in lipidated LC3 was correlated with a decrease in p62[273], suggesting autophagy induction and that the increase in lipidated LC3 could be in part of due to increased autophagosome formation.

Previous studies have reported the formation of IMPDH2 ring-and-rod structures under conditions of nutrient stress, as described in chapter 1.8. To investigate if and why this biological phenomenon also occurs in glutamine-deprived breast cancer cells, I performed a combination of immunofluorescence microscopy and metabolomics in the HER2-positive breast cancer cell line, JIMT-1. I observed four distinct phenotypes of IMPDH2 in glutamine-deprived JIMT-1 cells, namely, diffuse, vesicle-like, short rods, and long rods and rings, and a correlation with reduced guanine nucleotide levels in these cells under glutamine-limiting conditions. I hypothesized that the formation of IMPDH2 structures occurs in response to depletion in guanine nucleotide levels and confirmed this with guanosine supplementation experiments that increased GTP production in glutamine-deprived cells. Notably, cellular growth reduction under these short-term glutamine deprivation experiments was only modest, and it remains to be determined if perturbing the ability of cells to form these IMPDH2 ring-and-rod structures would exacerbate the growth reduction in these glutamine-deprived cells.

Given the interaction between ATG4B and IMPDH2, I postulated that ATG4B may contribute to IMPDH2 ring-and-rod formation. I discovered that genetic loss of ATG4B was associated with significantly reduced IMPDH2 ring-and-rod structures and increased guanine nucleotide levels in glutamine-deprived cells. To better understand the metabolic consequences of genetic loss of ATG4B, I performed metabolite profiling studies and examined levels of purine bases and nucleotides in parental and ATG4B KO JIMT-1 cells. I found that ATG4B KO cells were enriched in purine nucleotides and metabolites involved in the purine salvage pathway, suggesting a metabolic shift towards utilization of the purine salvage pathway to produce adenine and guanine nucleotides. To validate this, I examined an independent and publicly available metabolomic dataset, and found that in heart and muscle of atg4b$^{-/-}$ mice[250], purine salvage metabolites were also enriched, supporting a potential metabolic shift towards utilization of the purine salvage pathway as a consequence of genetic loss of ATG4B. To date, this study is the

first to describe a potential metabolic reprogram in nucleotide metabolism resulting from genetic loss of an autophagy protein.

Cells generally upregulate the *de novo* purine pathway to meet elevated purine demands that cannot be met by the purine salvage pathway alone[183]. I hypothesized that prolonged glutamine deprivation will activate the *de novo* pathway because of depletion of purine metabolites and purine nucleotides over the capacity within which the purine salvage pathway can provide. I further postulated that ATG4B KO cells rely predominantly on the purine salvage pathway because of an impairment in *de novo* purine biosynthesis owing to the lack of an ATG4B-IMPDH2 interplay. Under conditions of glutamine deprivation, I expect that growth of ATG4B KO cells will be significantly reduced because of the inability to activate *de novo* purine biosynthesis. Indeed, I found that glutamine deprivation was associated with a significant reduction in growth of glutamine-deprived ATG4B KO JIMT-1 cells compared to parental JIMT-1. I hypothesized that the impaired ability of ATG4B KO cells to form rings-and-rods under glutamine deprivation could have a consequence on the ability of these cells to grow under nutrient stress conditions. Differences in growth between parental and ATG4B KO cells were not apparent during earlier time points of glutamine deprivation when the ability of these cells to form IMPDH2 rings-and-rods were assessed. In this case, it would be interesting to examine if the ATG4B KO cells are still impaired in their ability to form IMPDH2 rings-and-rods under conditions of prolonged glutamine deprivation where growth differences were more apparent.

I postulated that the loss of an ATG4B-IMPDH2 interaction in ATG4B KO cells would mean that these cells would be less dependent on the *de novo* purine biosynthesis pathway for growth under conditions of nutrient stress. Indeed, growth of parental JIMT-1 cells was significantly reduced upon IMPDH inhibition in glutamine-deprived media, whereas growth of glutamine-deprived ATG4B KO cells was reduced only modestly when IMPDH was inhibited. Given that the next major pathway for purine nucleotide biosynthesis is the purine salvage pathway, I next postulated that these ATG4B KO cells would be more reliant on purine bases that feed the purine salvage pathway for growth under glutamine deprived conditions. I found that depletion of exogenous purine bases using dialyzed FBS led to significant further reductions in growth of glutamine-deprived ATG4B KO JIMT-1 cells compared to glutamine-deprived parental cells. This finding suggests an increased reliance on low molecular weight

metabolites, like purine bases, as their concentrations are significantly reduced in dialyzed FBS, and which supports an increased reliance on the purine salvage pathway in the absence of ATG4B. As noted, concentrations of other small metabolites are also reduced in dialyzed FBS, and their potential importance to ATG4B KO growth cannot be excluded at this point. Future studies restoring purine bases in glutamine-deprived media supplemented with dialyzed FBS will be important in validating the significance of exogenous purines in sustaining growth of ATG4B KO cells under conditions of glutamine deprivation. It also remains to be determined if the increased sensitivity to glutamine- and purine-depleted conditions of ATG4B KO cells could also be a result of defects in autophagy. Studies in HEK293K cells previously showed that genetic loss of the core *de novo* purine enzyme, phosphoribosylformylglycinamidine synthase (PFAS), was associated with activation of autophagy under similar purine-depleted conditions with dialyzed FBS[259]. This finding suggests that the autophagy machinery may function as an alternate source of replenishing purine nucleotides in contexts whereby cells are defective in both the *de novo* purine biosynthesis and purine salvage pathways. It will be intriguing to investigate if treatment of ATG4B KO cells with pharmacological inhibitors of autophagy, like chloroquine, to inhibit the IMPDH-mediated *de novo* purine biosynthesis pathway and to further suppress the autophagy machinery would augment their sensitivity to glutamine- and purine-depleted conditions. Notably, I found that protein levels of core *de novo* purine enzymes and purine salvage enzymes were not affected by genetic loss of ATG4B. This suggests that the mechanisms underlying this newly described metabolic reprogram may not occur through regulation of enzyme protein levels and may occur through regulation of enzyme activity.

Together, these findings reveal a novel protein-protein interaction between ATG4B and IMPDH2 in breast cancers and are in support of a metabolic reprogram in ATG4B KO cells that shift towards reliance on IMPDH-independent pathways, like the purine salvage pathway, for growth under glutamine deprivation (Figure 4.1). These findings also suggest an importance for the ATG4B-IMPDH2 interaction in *de novo* purine biosynthesis. These results are significant given the plentiful studies investigating ATG4B inhibition as a therapeutic strategy in cancers[235]. In such cases, including glutamine- and purine-depletion as nutrient stressors may further augment the efficacy of ATG4B inhibition in mitigating cancer progression or augmenting treatment efficacy. Further, findings here also provide premise for combined inhibition of ATG4B and

IMPDH2 as a therapeutic approach in cancer settings where the *de novo* purine pathway may be utilized to facilitate cancers by promoting progression and treatment resistance.

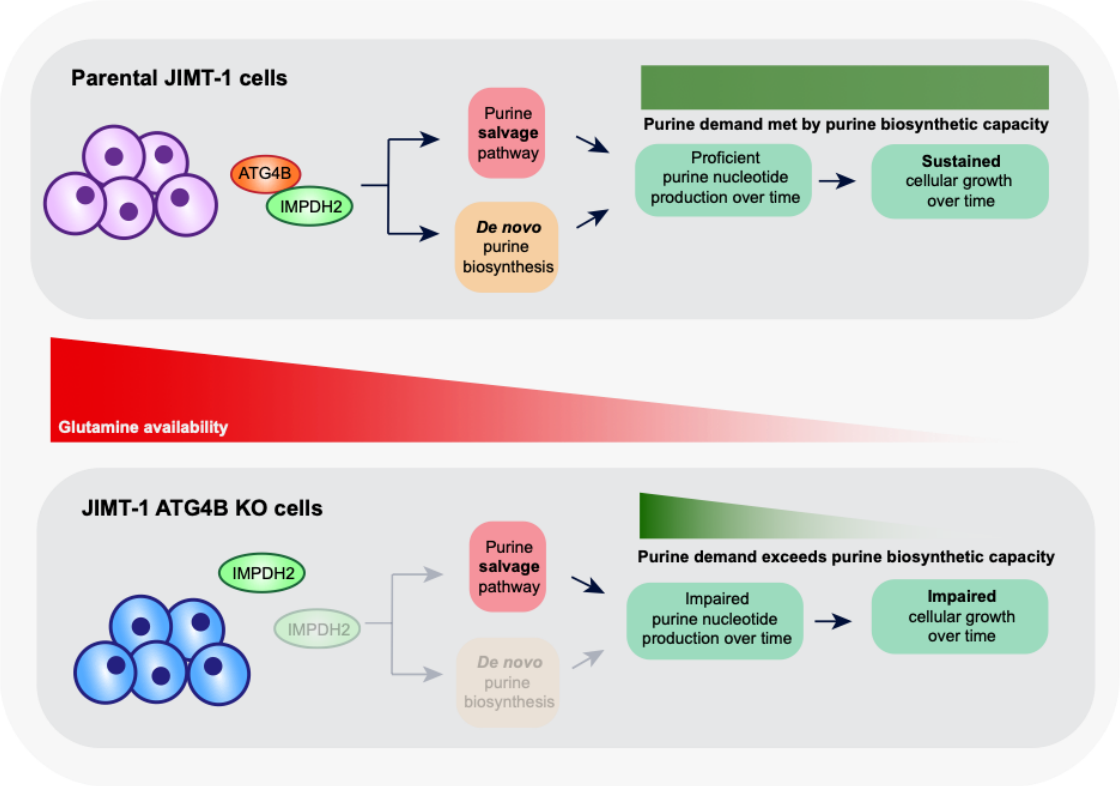

Figure 4.1 Proposed model for the metabolic consequences of genetic loss of ATG4B on purine metabolism in breast cancer cells.

The *de novo* purine biosynthesis and purine salvage pathways are important in maintaining purine nucleotide pools in the cell. The purine salvage pathway is more energetically efficient and is the primary pathway used to generate purine nucleotides in the cell. However, purine demands often exceed the capacity in which the purine salvage pathway can provide under nutrient stress conditions, like glutamine deprivation. In response, cells activate the de novo purine biosynthesis pathway to need these purine demands for survival. In the case of ATG4B KO cells, loss of ATG4B perturbs an ATG4B-IMPDH2 interaction that results in a metabolic reprogram towards utilization of IMPDH-independent purine salvage pathways to sustain growth. The purine salvage pathway is not sustainable over extended periods of nutrient stress, impairing the growth of ATG4B KO cells over time.

4.1.2. Limitations and future avenues

Although the ATG4B-IMPDH2 interaction was validated in several independent breast cancer cell lines, the downstream functional studies were performed solely in the JIMT-1 cell line. Further, IP-WB and protein-protein correlation studies suggested that the ATG4B-IMPDH2 interaction itself is independent of HER2 status and may be a pan-

breast cancer occurrence. However, this does not indicate that the functional importance of this interplay will be independent of the HER2 status. It remains to be determined if similar consequences resulting from genetic loss of ATG4B will be true in other cell line types and subtypes of breast cancer, and future work validating some of the key functional studies, like the IMPDH inhibition and glutamine- and purine-depletion experiments, in other contexts will be important. Protein-protein correlation studies between ATG4B and IMPDH2 reflected weak to modest Pearson correlation values, which could suggest that the interaction may not be direct or exists only in certain subsets of the cohort. Future studies exploring this correlation in larger cohorts and exploring the possibility of an intermediate protein bridging the ATG4B-IMPDH2 interaction will be important and interesting avenues to explore.

Genetic studies examining the effect of genetic loss or knockdown of ATG4B on IMPDH protein levels yielded temporal differences in results. Genetic loss of ATG4B was associated with modest decreases in IMPDH protein levels following 48 hours of growth in culture, whereas modest increases in IMPDH protein levels were observed following 120 hours of growth in culture. It remains unclear why this was the case, but it is probable that IMPDH protein levels are lower in ATG4B KO cells initially because of the loss of their interaction, and increased growth duration in culture might limit nutrient availability and trigger feedback upregulation of IMPDH protein levels in response. However, this notion is not supported given the observation that glutamine deprivation, regardless of ATG4B status, had no substantial effect on IMPDH protein levels. Future work investigating the temporal changes in IMPDH protein levels in response to ATG4B loss and nutrient stress will certainly clarify this. Additionally, genetic knockdown of ATG4B by shRNA was not associated with changes in IMPDH protein levels. This could suggest that minimal amounts of ATG4B are sufficient to maintain consistent IMPDH protein levels, but this conclusion requires further validation using additional shRNAs given that only one shRNA cell line was used.

The pharmacological tool employed to examine the effects of IMPDH inhibition, MPA, targets both IMPDH1 and IMPDH2[274]. It remains to be determined if the effects resulting from MPA treatment on ATG8 processing are a result of inhibition of IMPDH1, IMPDH2 or both IMPDH proteins. Genetic approaches investigating this relationship are limited in that good knockdown of IMPDH proteins was difficult to achieve in JIMT-1 in my experience. Prolonged and additional siRNA transfections had to be performed to

achieve approximately 75% knockdown, which run the risk of activation of compensatory mechanisms and feedback loops. Additionally, compensatory mechanisms have been reported resulting from genetic inhibition of IMPDH2[202], which makes studying the functional importance of this protein challenging. In studying the effects of IMPDH inhibition on ATG4B activity, assessment of ATG8 proteins do not necessarily reflect only the activity of ATG4B. This is because the ATG8 proteins can be processed by other ATG4 proteins as well[88,97] as described in chapter 1.4.3. Future studies examining the potential regulation of ATG4B by IMPDH proteins through *in vitro* recombinant protein enzymatic assays will be important in clarifying this relationship. Further, this study has not yet examined the effect of IMPDH inhibition on autophagy, which begets the question of whether the proposed regulation of ATG4B by IMPDH2 will have a consequent effect on autophagy. Studies in glioma cells have found that autophagy is induced following treatment with the IMPDH inhibitors, ribavirin and tiazofurin[273], suggesting that IMPDH proteins may negatively regulate the autophagic machinery. Interestingly, studies by Fang *et al.* 2017 revealed that treatment of hepatoma cells with MPA is associated with a block in autophagy, and reduced mRNA and protein expression of ATG proteins, like ATG3, ATG5, and ATG7[275]. These findings suggest that, at least in the context of MPA-mediated IMPDH inhibition, IMPDH proteins may function to promote autophagy by regulating the expression of key ATG proteins. Future studies examining the effects of genetic knockdown of IMPDH1/2 will be important in clarifying the role of IMPDH proteins in the regulation of autophagic flux. Although I did not see any effect of genetic knockdown of IMPDH (Figure A.1.) or MPA treatment on ATG4B protein levels (Figure 2.7), I found that MPA-mediated IMPDH inhibition impairs LC3B processing and GABARAP stabilization (Figure 2.7), supporting a potential role for IMPDH proteins in regulating ATG4B activity and function. Future studies investigating if genetic knockdown of IMPDH1 and/or IMPDH2 will have the same effect on the ATG8 proteins will be important in clarifying the role of IMPDH proteins in regulation of ATG4B activity and function.

Additionally, at this time, I have not yet determined if ATG4B may also regulate IMPDH activity. Previous attempts using commercially available IMPDH activity kits have not yielded consistent results, even with IMPDH inhibitor controls, and this may be owing to the fact that these kits rely on NADH generated as part of the IMPDH reaction as an output in cell lysates. The caveat to such kits is that they do not delineate between

NADH generated as a result of IMPDH activity and NADH generated by other metabolic or cellular processes in the cell either basally or in response to experimental conditions imposed. At the time of this thesis preparation, I await results from collaborators for experiments that seek to evaluate IMPDH activity by examining metabolites generated directly and downstream by IMPDH through metabolomics/MS.

The observation that IMPDH2 presents itself as four distinct phenotypes in breast cancer cells is intriguing, and is reminiscent of the formation of cytoophidia, which are long filament-like structures, by the metabolic enzyme CTPS1[276–278]. Although this study found that genetic loss of ATG4B primarily affected the formation of long rods and rings, it remains to be determined why other IMPDH2 phenotypes, like vesicles and short rods, also form in certain subpopulations of cells subjected to the same stress. Are they simply intermediates leading to long rods and rings? Future work investigating the functional significance of the different phenotypes of IMPDH2 formed under nutrient stress conditions will certainly shed insight as to why these structures form heterogeneously in populations of cells all subjected to the same stress.

It is important to note that, although guanosine supplementation experiments do support the model that IMPDH2 ring-and-rod structures form in response to guanine nucleotide depletions, the metabolite findings only show a trend where these guanine nucleotide levels are reduced upon glutamine deprivation and are not statistically significant. This may be because of technical reasons resulting from the sample preparations or mass spectrometry runs, or biological reasons resulting from the cells being of different cell passage numbers and experimented on at different times. Future work may be directed towards performing more biological replicates to confirm, at the metabolite level, that the reduction in guanine nucleotides like GTP does indeed coincide with the induction of IMPDH2 ring-and-rod structures in cells.

Further, this study has yet to identify the functional significance of these IMPDH2 ring-and-rod structures. Although structural studies suggest that they may serve to maintain IMPDH activity by preventing GTP-mediated allosteric inhibition[188], these studies were done primarily in cell-free assays and have not been performed in nutrient stress conditions nor in cancer cells. Future work investigating the functional significance of these IMPDH2 structures under glutamine deprivation will shed insights into the biological role of these structures under nutrient stress. Additionally, glutamine deprived

conditions that induce IMPDH2 ring-and-rod structures were only associated with modest reductions in growth. It remains to be determined if IMPDH2 rings-and-rods may play an importance in sustaining growth and if so through what mechanisms. Although genetic loss of ATG4B had significantly reduced IMPDH2 ring-and-rod formation compared to parental cells but did not result in greater reduction of growth from the glutamine-deprived conditions set up, this may be because of the upregulated guanine nucleotide levels observed in these cells as a result of their metabolic shift to purine salvage as a consequence of ATG4B loss. Future studies examining the effect on cell growth from perturbing the formation of IMPDH2 rings-and-rods through genetic approaches under nutrient stress conditions that induce these structures will provide new insights regarding their function.

In this study, I have also not examined the ability of ATG4B KO cells to form IMPDH2 structures following extended periods of glutamine deprivation that did result in a significant reduction in their growth compared to parental cells. I hypothesize that the reason why growth changes were not apparent in ATG4B KO cells following short periods of glutamine deprivation is because of the generation of purine nucleotides by the purine salvage pathway. I expect that prolonging the glutamine-deprived state resulted in growth reduction because the purine demand at these time points exceeds the capacity of the purine salvage pathway to provide. The loss of ATG4B impairs the ATG4B-IMPDH interplay, which I suspect contributes to *de novo* purine biosynthesis. Future studies determining if prolonged glutamine deprivation increases IMPDH2 ring-and-rod formation in ATG4B KO cells will clarify this. To date, I have also not examined the effect of autophagy inhibition or genetic loss of other ATGs on IMPDH2 ring-and-rod formation. Future work examining this will clarify if this mechanism is a result of solely the interplay of ATG4B with IMPDH2 and purine metabolism, or if autophagy is also involved.

In this study, I was unable to detect *de novo* purine metabolites from the metabolomics experiments performed in collaboration with the Parker lab. Given that these metabolite profiling experiments were untargeted and semi-quantitative relative to library standards, future work utilizing targeted approaches with in-run standards will improve detection and quantification. Although the ATG4B KO cells presented with an enrichment in purine salvage metabolites and purine nucleotides relative to parental cells, a number of these metabolite level differences were not statistically significant.

This could be owing to similar technical or biological errors, as mentioned in earlier portions of this subchapter, and future work could be directed towards performing more biological replicates to better verify this trend. Nevertheless, an independent metabolomic dataset did support the observation that genetic loss of ATG4B enriches purine salvage metabolites, and so the high p-values do not negate the significance of my cell line metabolomics findings.

I also performed a series of western blot studies examining the effect of genetic loss of ATG4B on protein levels of enzymes involved in the de novo purine pathway and purine salvage pathway[138]. Although I did not find any strong changes in the levels of these enzymes, this does not necessarily reflect on their activity in parental and ATG4B KO cells. Further, one of the ATG4B KO cells (ATG4B KO#2) appeared to present with a modest increase in some of these enzyme levels, and this was statistically significant. I infer this to be a result of slightly lower B-actin protein levels in this KO cell line compared to the parental cell line. Future work examining the effect of ATG4B loss on the activity of these enzymes, through enzymatic activity assay kits or metabolomics, will help determine if the effect of ATG4B loss on purine metabolism involves regulation of the activity of enzymes involved in these pathways.

Finally, it is important to note that the purine depletion experiments I performed were not specific to depletion of only purines as it was performed using dialyzed FBS in place of regular FBS. Dialysed FBS (Thermofisher, catalog number 26400044) removes metabolites that are smaller than approximately 10kDa, which means that they are not exclusive to purines. Future work verifying the reliance of ATG4B KO cells on the purine salvage pathway through alternate approaches are certainly warranted. Studies determining if supplementation with purine bases, like guanosine and hypoxanthine, that feed the purine salvage pathway will restore growth of glutamine- and purine-depleted ATG4B KO cells are currently in progress. I must note that the field currently faces a lack in efficient tools for investigating the functional importance of the purine salvage pathway. To date, there are no inhibitors that specifically inhibit the purine salvage pathway, and genetic approaches targeting enzymes are not efficient given that compensation can happen from parallel pathways. At the time of this thesis preparation, studies investigating the effect of genetic knockdown of APRT and HPRT[138], enzymes involved in the purine salvage pathway, on growth of glutamine-deprived ATG4B KO cells are currently underway.

4.2. Therapeutic applications of the ATG4B-IMPDH interplay in breast cancer cells

4.2.1. Study summary and significance

Findings from the first portion of my thesis present a potential importance for the ATG4B-IMPDH2 in *de novo* purine biosynthesis in breast cancer cells. Alterations in purine metabolism are known to drive different aspects of tumorigenesis, including treatment resistance in cancers[138]. In the second portion of my thesis, I sought to leverage this newly proposed role for ATG4B and IMPDH2 in *de novo* purine metabolism to improve the responses of HER2-positive breast cancer cells to trastuzumab.

The clinical significance of protein levels of IMPDH in breast cancers remains poorly defined. With assistance from Drs. Baofeng Jia and Kevin Yang, I examined protein levels of IMPDH1 and IMPDH2 in breast cancers compared to normal breast tissues. I found that IMPDH proteins were significantly elevated in breast tumors compared to normal breast tissues. I further stratified these breast tumors based on their reported PAM50 subtypes and found that all subtypes presented with significantly elevated IMPDH protein levels compared to normal breast tissues. To examine the potential prognostic value of these elevated IMPDH protein levels in breast cancers, I examined overall patient survival probabilities in high vs. low IMPDH protein-expressing cohorts and found that only high IMPDH2 protein levels were associated with inferior breast cancer patient prognoses. These findings support the potential clinical importance of IMPDH proteins, in particular IMPDH2, in breast cancers. To also investigate the clinical importance of ATG4B independently in breast cancers, I analyzed ATG4B protein levels from the Asleh *et al.* 2022[248] cohort which contained ATG4B proteomic data. I found that ATG4B protein levels were significantly elevated in breast tumors, specifically luminal B, basal-like and HER2-enriched subtypes, compared to normal tissues. As noted in chapter 3.4, previous studies in an independent cohort found that ATG4B protein expression was highest in the luminal A subtype and lowest in the basal-like subtype[268], which could be due to differences in study cohort, stratification criteria, and methods for evaluating protein levels or expression. Of note, in the case of the latter, the Asleh et al. 2022[248] study examined protein levels based on mass spectrometry methods whereas Bortnik et al. 2020[268] study examined protein expression based on immunohistochemical methods. Future studies could benefit from combining

the use of both methodologies for evaluating protein levels and expression to examine proteins of interest, like ATG4B, more accurately. Nevertheless, these findings in total support the potential clinical importance of ATG4B in breast cancers.

To identify contexts whereby high ATG4B and IMPDH2 protein levels may be important, I expanded on findings from chapter 2.3.2 by stratifying and examining protein-protein correlations between ATG4B and IMPDH2 in breast tumors according to their reported PAM50 subtypes. I found that, although there was a significant positive correlation between ATG4B and IMPDH2 protein levels in the breast tumor cohort as a whole, there was no significant correlation between ATG4B and IMPDH2 protein levels in any one subtype of breast cancer. I hypothesized that this may be a result of HER2 intra-tumoral heterogeneity, and so examined the protein-protein correlations between HER2 and ATG4B, and HER2 and IMPDH2 across the breast cancer subtypes. I observed a significant positive correlation between HER2 and IMPDH2 proteins only in the HER2-enriched subtype. I also found that although there were no significant correlations between HER2 and ATG4B protein levels in any of subtypes, there was a clear positive correlation trend between these two proteins in the HER2-enriched subtype. These findings suggest that ATG4B and IMPDH2 may be important in breast cancers that have high HER2 protein levels, which may only include subpopulations of HER2-enriched breast tumors given the intra-tumoral heterogeneity.

In investigating the potential therapeutic applications of combined ATG4B and IMPDH2 inhibition in improving the responses of HER2-positive breast cancer cells to trastuzumab, I utilized the trastuzumab-resistant HER2-positive breast cancer cell line, JIMT-1, as a model. I first examined the effects of pharmacological inhibition of both ATG4 and IMPDH using LV320 and MPA and found that combination treatment resulted in a synergistic but modest reduction in growth of JIMT-1 cells. Unexpectedly, I found that genetic loss of ATG4B did not increase the sensitivity of JIMT-1 cells to MPA, which could suggest potential compensation by ATG4A given that LV320 targets both ATG4B and ATG4A. Nevertheless, results from the LV320 and MPA pharmacological combination are promising and suggest that both ATG4 and IMPDH proteins contribute to growth of HER2-positive breast cancer cells. Previous studies found that genetic knockdown of ATG4B increased the sensitivity of HER2-positive breast cancer cells, like JIMT-1, to trastuzumab[61]. I found that pharmacological inhibition of ATG4 using LV320

also increased the sensitivity of JIMT-1 cells to trastuzumab, supporting the utility of LV320 as pharmacological tool for ATG4 inhibition.

In summary, this study is the first to describe the clinical importance of an ATG4B-IMPDH2 axis in breast cancers, with supporting evidence that this axis may be of greater clinical importance in subpopulations that overexpress HER2. This study is also the first to examine the potential combinatorial effects of combined IMPDH inhibition with ATG4 inhibitors, in this case the combination of MPA and LV320, on growth of breast cancer cells. The modest but synergistic effects observed from this combination are promising and I envision that future work dedicated towards testing the effect of combined LV320 and MPA on trastuzumab sensitivity could identify a new therapeutic approach for improving responses of HER2-positive breast cancers to trastuzumab, especially cases that present with resistance against HER2-targeted agents.

4.2.2. Limitations and future avenues

Experiments in this study were performed primarily using the JIMT-1 cell line, which is a characterized by trastuzumab resistance and HER2 overexpression. Future work verifying if the combinatorial effects of LV320 and MPA on growth, and effects of LV320 on increased trastuzumab sensitivity will hold in other cell line models of trastuzumab-resistant and HER2-positive breast cancers will be important. Future studies examining the molecular effects of these different inhibitor combinations on proteins involved in HER2 signaling, autophagy, and purine metabolism will also be important in providing insight towards the molecular mechanisms underlying why certain combinations result in synergistic and/or better augmented effects while others do not.

The breast cancer patient cohorts I examined in this study were relatively small, and future studies validating the reported correlations in other independent and larger patient proteomic cohorts will certainly be important. Further, HER2 protein levels can vary in the HER2-enriched breast cancer subtype, as supported by previous reports of HER2 intra-tumoral heterogeneity and discrepancies between HER2 overexpression and HER2 gene amplification in breast cancers[266,279]. This in itself limits the accuracy of studies that aim to identify protein biomarkers that could be of clinical importance in certain subtypes of breast cancers. For example, in the breast cancer cohort examined, IMPDH2 and ATG4B protein levels were both elevated in the HER2-enriched subtype,

but no significant protein-protein correlation between the two proteins were observed in the HER2-enriched breast tumor sample, suggesting that they may not have been elevated in the same tumor samples. However, protein-protein correlation studies between IMPDH2 and HER2 revealed a significant positive correlation between the two proteins only in the HER2-enriched subtype. Similarly, a statistically insignificant but positive correlation trend was observed between ATG4B and HER2 in the HER2-enriched subtypes. These analyses also revealed a clear spread of HER2-enriched breast tumors that have both high and low HER2 protein levels. It is clear that better stratification of breast cancer patients and more strictly defining clinical classifications of breast cancer subtypes, especially those of the HER2-enriched group, will be important.

Intriguingly, the observation that genetic loss of ATG4B did not increase the sensitivity of cells to MPA suggests that potential compensatory mechanisms may be activated in response to ATG4B loss. Given that MPA and LV320 did result in a synergistic reduction in growth, it is plausible that this synergism may be because both ATG4A and ATG4B are inhibited by LV320. Future studies determining if genetic inhibition of both ATG4A and ATG4B will increase the sensitivity of cells to MPA will clarify if ATG4A could also be important in this axis. Further, findings from chapter 2 also suggest a potential metabolic shift towards growth independent of IMPDH-mediated pathways and reliance on the purine salvage pathway. Future studies examining if inhibition of the purine salvage pathway in combination with MPA and LV320 will further augment cellular growth reduction or examining if glutamine- and purine-depletion in combination with LV320 will increase sensitivity to trastuzumab will be interesting avenues to explore.

Finally, given the synergistic growth reduction from combined MPA and LV320 treatment, I hypothesize inhibiting IMPDH in addition to ATG4 will further increase the sensitivity of JIMT-1 cells to trastuzumab. Future studies examining if combined MPA and LV320 treatment will synergistically increase the sensitivity of HER2-positive breast cancer cells to trastuzumab are warranted.

References

1. Lu, G. *et al.* Autophagy in health and disease: From molecular mechanisms to therapeutic target. *MedComm* **3**, e150 (2022).
2. Harnett, M. M. *et al.* From Christian de Duve to Yoshinori Ohsumi: More to autophagy than just dining at home. *Biomed. J.* **40**, 9–22 (2017).
3. Ohsumi, Y. Historical landmarks of autophagy research. *Cell Res.* **24**, 9–23 (2014).
4. Levine, B. & Klionsky, D. J. Autophagy wins the 2016 Nobel Prize in Physiology or Medicine: Breakthroughs in baker's yeast fuel advances in biomedical research. *Proc. Natl. Acad. Sci.* **114**, 201–205 (2017).
5. Wen, X. & Klionsky, D. J. An overview of macroautophagy in yeast. *J. Mol. Biol.* **428**, 1681–1699 (2016).
6. Three Distinct Types of Microautophagy Based on Membrane Dynamics and Molecular Machineries - Oku - 2018 - BioEssays - Wiley Online Library. https://onlinelibrary.wiley.com/doi/full/10.1002/bies.201800008.
7. Parzych, K. R. & Klionsky, D. J. An Overview of Autophagy: Morphology, Mechanism, and Regulation. *Antioxid. Redox Signal.* **20**, 460–473 (2014).
8. Yang, K. C., Sathiyaseelan, P., Ho, C. & Gorski, S. M. Evolution of tools and methods for monitoring autophagic flux in mammalian cells. *Biochem. Soc. Trans.* **46**, 97–110 (2018).
9. Kumar, A. V. & Mills, J. Non-canonical autophagy in aging and age-related diseases. *Front. Cell Dev. Biol.* **11**, 1137870 (2023).

10. Durgan, J. & Florey, O. Many roads lead to CASM: Diverse stimuli of noncanonical autophagy share a unifying molecular mechanism. *Sci. Adv.* **8**, eabo1274 (2022).

11. Leidal, A. *et al.* The LC3-conjugation machinery specifies the loading of RNA-binding proteins into extracellular vesicles. *Nat. Cell Biol.* **22**, (2020).

12. Sanjuan, M. A. *et al.* Toll-like receptor signalling in macrophages links the autophagy pathway to phagocytosis. *Nature* **450**, 1253–1257 (2007).

13. Heckmann, B. L. *et al.* LC3-Associated Endocytosis Facilitates β-Amyloid Clearance and Mitigates Neurodegeneration in Murine Alzheimer's Disease. *Cell* **178**, 536-551.e14 (2019).

14. Martinez, J. *et al.* Microtubule-associated protein 1 light chain 3 alpha (LC3)-associated phagocytosis is required for the efficient clearance of dead cells. *Proc. Natl. Acad. Sci.* **108**, 17396–17401 (2011).

15. Martinez, J. *et al.* Molecular characterization of LC3-associated phagocytosis reveals distinct roles for Rubicon, NOX2 and autophagy proteins. *Nat. Cell Biol.* **17**, 893–906 (2015).

16. Galluzzi, L. *et al.* Molecular definitions of autophagy and related processes. *EMBO J.* **36**, 1811–1836 (2017).

17. Mizushima, N. The ATG conjugation systems in autophagy. *Curr. Opin. Cell Biol.* **63**, 1–10 (2020).

18. Lőrincz, P. & Juhász, G. Autophagosome-Lysosome Fusion. *J. Mol. Biol.* **432**, 2462–2482 (2020).

19. Tsuboyama, K. *et al.* The ATG conjugation systems are important for degradation of the inner autophagosomal membrane. *Science* **354**, 1036–1041 (2016).

20. Lahiri, V., Hawkins, W. D. & Klionsky, D. J. Watch What You (Self-) Eat: Autophagic Mechanisms that Modulate Metabolism. *Cell Metab.* **29**, 803–826 (2019).

21. Mizushima, N. & Levine, B. Autophagy in Human Diseases. *N. Engl. J. Med.* **383**, 1564–1576 (2020).

22. Galluzzi, L. *et al.* Autophagy in malignant transformation and cancer progression. *EMBO J.* **34**, 856–880 (2015).

23. Li, X., He, S. & Ma, B. Autophagy and autophagy-related proteins in cancer. *Mol. Cancer* **19**, 12 (2020).

24. Bustos, S. O., Antunes, F., Rangel, M. C. & Chammas, R. Emerging Autophagy Functions Shape the Tumor Microenvironment and Play a Role in Cancer Progression - Implications for Cancer Therapy. *Front. Oncol.* **10**, (2020).

25. Dagogo-Jack, I. & Shaw, A. T. Tumour heterogeneity and resistance to cancer therapies. *Nat. Rev. Clin. Oncol.* **15**, 81–94 (2018).

26. Hanahan, D. & Weinberg, R. A. Hallmarks of cancer: the next generation. *Cell* **144**, 646–674 (2011).

27. Wang, J., Seebacher, N., Shi, H., Kan, Q. & Duan, Z. Novel strategies to prevent the development of multidrug resistance (MDR) in cancer. *Oncotarget* **8**, 84559–84571 (2017).

28. Hansen, E., Woods, R. J. & Read, A. F. How to Use a Chemotherapeutic Agent When Resistance to It Threatens the Patient. *PLOS Biol.* **15**, e2001110 (2017).

29. Hawkes, N. Drug resistance: the next target for cancer treatment. *BMJ* **365**, l2228 (2019).

30. Greene, J. M., Gevertz, J. L. & Sontag, E. D. A mathematical approach to differentiate spontaneous and induced evolution to drug resistance during cancer treatment. *bioRxiv* 235150 (2018) doi:10.1101/235150.

31. Hasan, S., Taha, R. & Omri, H. E. Current Opinions on Chemoresistance: An Overview. *Bioinformation* **14**, 80–85 (2018).

32. Panda, M. & Biswal, B. K. Cell signaling and cancer: a mechanistic insight into drug resistance. *Mol. Biol. Rep.* (2019) doi:10.1007/s11033-019-04958-6.

33. Zheng, H.-C. The molecular mechanisms of chemoresistance in cancers. *Oncotarget* **8**, 59950–59964 (2017).

34. Zahreddine, H. & Borden, K. Mechanisms and insights into drug resistance in cancer. *Front. Pharmacol.* **4**, (2013).

35. Parseghian, C. M., Napolitano, S., Loree, J. M. & Kopetz, S. Mechanisms of Innate and Acquired Resistance to anti-EGFR therapy: A Review of Current Knowledge with a Focus on Rechallenge Therapies. *Clin. Cancer Res.* clincanres.0823.2019 (2019) doi:10.1158/1078-0432.CCR-19-0823.

36. Salgia, R. & Kulkarni, P. The Genetic/Non-genetic Duality of Drug 'Resistance' in Cancer. *Trends Cancer* **4**, 110–118 (2018).

37. Hammerlindl, H. & Schaider, H. Tumor cell-intrinsic phenotypic plasticity facilitates adaptive cellular reprogramming driving acquired drug resistance. *J. Cell Commun. Signal.* **12**, 133–141 (2018).

38. Nikolaou, M., Pavlopoulou, A., Georgakilas, A. G. & Kyrodimos, E. The challenge of drug resistance in cancer treatment: a current overview. *Clin. Exp. Metastasis* **35**, 309–318 (2018).

39. Chatterjee, N. & Bivona, T. G. Polytherapy and Targeted Cancer Drug Resistance. *Trends Cancer* **5**, 170–182 (2019).

40. Ho, C. J. & Gorski, S. M. Molecular Mechanisms Underlying Autophagy-Mediated Treatment Resistance in Cancer. *Cancers* **11**, 1775 (2019).

41. Battista, R. A. *et al.* Autophagy mediates epithelial cancer chemoresistance by reducing p62/SQSTM1 accumulation. *PloS One* **13**, e0201621 (2018).

42. Fitzwalter, B. E. *et al.* Autophagy Inhibition Mediates Apoptosis Sensitization in Cancer Therapy by Relieving FOXO3a Turnover. *Dev. Cell* **44**, 555-565.e3 (2018).

43. Canadian Cancer Statistics Advisory in collaboration with, the Canadian Cancer Society, Statistics Canada and the, & Public Health Agency of Canada. Canadian Cancer Statistics: A 2022 special report on cancer prevalence. *2022*.

44. Szymiczek, A., Lone, A. & Akbari, M. R. Molecular intrinsic versus clinical subtyping in breast cancer: A comprehensive review. *Clin. Genet.* **99**, 613–637 (2021).

45. Nascimento, R. G. do & Otoni, K. M. Histological and molecular classification of breast cancer: what do we know? *Mastology* **30**, e20200024 (2020).

46. Fallahpour, S., Navaneelan, T., De, P. & Borgo, A. Breast cancer survival by molecular subtype: a population-based analysis of cancer registry data. *Can. Med. Assoc. Open Access J.* **5**, E734–E739 (2017).

47. van Maaren, M. C. *et al.* Ten-year recurrence rates for breast cancer subtypes in the Netherlands: A large population-based study. *Int. J. Cancer* **144**, 263–272 (2019).

48. Nedeljković, M. & Damjanović, A. Mechanisms of Chemotherapy Resistance in Triple-Negative Breast Cancer—How We Can Rise to the Challenge. *Cells* **8**, 957 (2019).

49. da Silva, J. L., Cardoso Nunes, N. C., Izetti, P., de Mesquita, G. G. & de Melo, A. C. Triple negative breast cancer: A thorough review of biomarkers. *Crit. Rev. Oncol. Hematol.* **145**, 102855 (2020).

50. Rexer, B. N. & Arteaga, C. L. Intrinsic and Acquired Resistance to HER2-Targeted Therapies in HER2 Gene-Amplified Breast Cancer: Mechanisms and Clinical Implications. *Crit. Rev. Oncog.* **17**, 1–16 (2012).

51. Wynn, C. S. & Tang, S.-C. Anti-HER2 therapy in metastatic breast cancer: many choices and future directions. *Cancer Metastasis Rev.* **41**, 193–209 (2022).

52. Parker, J. S. *et al.* Supervised Risk Predictor of Breast Cancer Based on Intrinsic Subtypes. *J. Clin. Oncol.* **27**, 1160–1167 (2009).

53. Liang, X. H. *et al.* Induction of autophagy and inhibition of tumorigenesis by beclin 1. *Nature* **402**, 672–676 (1999).

54. Vega-Rubín-de-Celis, S. *et al.* Increased autophagy blocks HER2-mediated breast tumorigenesis. *Proc. Natl. Acad. Sci.* 201717800 (2018) doi:10.1073/pnas.1717800115.

55. Marsh, T. *et al.* Autophagic Degradation of NBR1 Restricts Metastatic Outgrowth during Mammary Tumor Progression. *Dev. Cell* **52**, 591-604.e6 (2020).

56. Li, M. *et al.* Autophagy-related 7 modulates tumor progression in triple-negative breast cancer. *Lab. Invest.* **99**, 1266–1274 (2019).

57. Chittaranjan, S. *et al.* Autophagy Inhibition Augments the Anticancer Effects of Epirubicin Treatment in Anthracycline-Sensitive and -Resistant Triple-Negative Breast Cancer. *Clin. Cancer Res.* **20**, 3159–3173 (2014).

58. Wu, C.-L. *et al.* BECN1-knockout impairs tumor growth, migration and invasion by suppressing the cell cycle and partially suppressing the epithelial-mesenchymal transition of human triple-negative breast cancer cells. *Int. J. Oncol.* **53**, 1301–1312 (2018).

59. Vazquez-Martin, A., Oliveras-Ferraros, C. & Menendez, J. A. Autophagy Facilitates the Development of Breast Cancer Resistance to the Anti-HER2 Monoclonal Antibody Trastuzumab. *PLOS ONE* **4**, e6251 (2009).

60. Cufí, S. *et al.* Autophagy-related gene 12 (ATG12) is a novel determinant of primary resistance to HER2-targeted therapies: utility of transcriptome analysis of the autophagy interactome to guide breast cancer treatment. *Oncotarget* **3**, 1600–1614 (2012).

61. Bortnik, S. *et al.* Identification of breast cancer cell subtypes sensitive to ATG4B inhibition. *Oncotarget* **7**, 66970–66988 (2016).

62. Dragowska, W. H. *et al.* Induction of autophagy is an early response to gefitinib and a potential therapeutic target in breast cancer. *PloS One* **8**, e76503 (2013).

63. Liu, Z. *et al.* Autophagy inhibitor facilitates gefitinib sensitivity in vitro and in vivo by activating mitochondrial apoptosis in triple negative breast cancer. *PLoS ONE* **12**, (2017).

64. Kim, H. M. & Koo, J. S. The Role of Autophagy in Breast Cancer Metastasis. *Biomedicines* **11**, 618 (2023).

65. Vera-Ramirez, L., Vodnala, S. K., Nini, R., Hunter, K. W. & Green, J. E. Autophagy promotes the survival of dormant breast cancer cells and metastatic tumour recurrence. *Nat. Commun.* **9**, 1944 (2018).

66. Lock, R., Kenific, C. M., Leidal, A. M., Salas, E. & Debnath, J. Autophagy-Dependent Production of Secreted Factors Facilitates Oncogenic RAS-Driven Invasion. *Cancer Discov.* **4**, 466–479 (2014).

67. He, L. *et al.* Autophagy: The Last Defense against Cellular Nutritional Stress. *Adv. Nutr.* **9**, 493–504 (2018).

68. Thomas, M. *et al.* Autophagy is essential for the maintenance of amino acids and ATP levels during acute amino acid starvation in MDAMB231 cells. *Cell Biochem. Funct.* **36**, 65–79 (2018).

69. Lee, M. J., Park, J.-S., Jo, S. B. & Joe, Y. A. Enhancing Anti-Cancer Therapy with Selective Autophagy Inhibitors by Targeting Protective Autophagy. *Biomol. Ther.* **31**, 1–15 (2023).

70. Salimi-Jeda, A. *et al.* Autophagy Modulation and Cancer Combination Therapy: A Smart Approach in Cancer Therapy. *Cancer Treat. Res. Commun.* **30**, 100512 (2022).

71. Arnaout, A. *et al.* A randomized, double-blind, window of opportunity trial evaluating the effects of chloroquine in breast cancer patients. *Breast Cancer Res. Treat.* **178**, 327–335 (2019).

72. Espina, V. A. *et al.* Abstract CT140: PINC trial: Preventing invasive breast neoplasia with chloroquine. *Cancer Res.* **77**, CT140 (2017).

73. Anand, K. *et al.* A Phase II Study of the Efficacy and Safety of Chloroquine in Combination With Taxanes in the Treatment of Patients With Advanced or Metastatic Anthracycline-refractory Breast Cancer. *Clin. Breast Cancer* **21**, 199–204 (2021).

74. Chen, X. & Geiger, J. D. Janus sword actions of chloroquine and hydroxychloroquine against COVID-19. *Cell. Signal.* **73**, 109706 (2020).

75. Abdel-Aziz, A. K. *et al.* A Critical Review of Chloroquine and Hydroxychloroquine as Potential Adjuvant Agents for Treating People with Cancer. *Future Pharmacol.* **2**, 431–443 (2022).

76. Lim, J. & Murthy, A. Targeting Autophagy to Treat Cancer: Challenges and Opportunities. *Front. Pharmacol.* **11**, (2020).

77. Kirisako, T. *et al.* The reversible modification regulates the membrane-binding state of Apg8/Aut7 essential for autophagy and the cytoplasm to vacuole targeting pathway. *J. Cell Biol.* **151**, 263–276 (2000).

78. Lang, T. Aut2p and Aut7p, two novel microtubule-associated proteins are essential for delivery of autophagic vesicles to the vacuole. *EMBO J.* **17**, 3597–3607 (1998).

79. Zhang, S., Hama, Y. & Mizushima, N. The evolution of autophagy proteins – diversification in eukaryotes and potential ancestors in prokaryotes. *J. Cell Sci.* **134**, jcs233742 (2021).

80. Maruyama, T. & Noda, N. N. Autophagy-regulating protease Atg4: structure, function, regulation and inhibition. *J. Antibiot. (Tokyo)* **71**, 72–78 (2018).

81. Wesch, N., Kirkin, V. & Rogov, V. V. Atg8-Family Proteins—Structural Features and Molecular Interactions in Autophagy and Beyond. *Cells* **9**, 2008 (2020).

82. Agrotis, A. *et al.* Human ATG4 autophagy proteases counteract attachment of ubiquitin-like LC3/GABARAP proteins to other cellular proteins. *J. Biol. Chem.* **294**, 12610–12621 (2019).

83. Weidberg, H. *et al.* LC3 and GATE-16/GABARAP subfamilies are both essential yet act differently in autophagosome biogenesis. *EMBO J.* **29**, 1792–1802 (2010).

84. Nguyen, T. N. *et al.* Atg8 family LC3/GABARAP proteins are crucial for autophagosome–lysosome fusion but not autophagosome formation during PINK1/Parkin mitophagy and starvation. *J Cell Biol* **215**, 857–874 (2016).

85. Zhang, L., Li, J., Ouyang, L., Liu, B. & Cheng, Y. Unraveling the roles of Atg4 proteases from autophagy modulation to targeted cancer therapy. *Cancer Lett.* **373**, 19–26 (2016).

86. Betin, V. M. S. & Lane, J. D. Caspase cleavage of Atg4D stimulates GABARAP-L1 processing and triggers mitochondrial targeting and apoptosis. *J. Cell Sci.* **122**, 2554–2566 (2009).

87. Betin, V. M. S., MacVicar, T. D. B., Parsons, S. F., Anstee, D. J. & Lane, J. D. A cryptic mitochondrial targeting motif in Atg4D links caspase cleavage with mitochondrial import and oxidative stress. *Autophagy* **8**, 664–676 (2012).

88. Kauffman, K. J. *et al.* Delipidation of mammalian Atg8-family proteins by each of the four ATG4 proteases. *Autophagy* **14**, 992–1010 (2018).

89. Sathiyaseelan, P. Deciphering the expression and function of the autophagy cysteine protease, ATG4B, in pancreatic cancer. https://summit.sfu.ca/item/36061 (2022).

90. Kumanomidou, T. *et al.* The Crystal Structure of Human Atg4b, a Processing and De-conjugating Enzyme for Autophagosome-forming Modifiers. *J. Mol. Biol.* **355**, 612–618 (2006).

91. Sugawara, K. *et al.* Structural basis for the specificity and catalysis of human Atg4B responsible for mammalian autophagy. *J. Biol. Chem.* **280**, 40058–40065 (2005).

92. Satoo, K. *et al.* The structure of Atg4B–LC3 complex reveals the mechanism of LC3 processing and delipidation during autophagy. *EMBO J.* **28**, 1341–1350 (2009).

93. Skytte Rasmussen, M. *et al.* ATG4B contains a C-terminal LIR motif important for binding and efficient cleavage of mammalian orthologs of yeast Atg8. *Autophagy* **13**, 834–853 (2017).

94. Fujita, N. *et al.* An Atg4B Mutant Hampers the Lipidation of LC3 Paralogues and Causes Defects in Autophagosome Closure. *Mol. Biol. Cell* **19**, 4651–4659 (2008).

95. Yu, Z.-Q. *et al.* Dual roles of Atg8-PE deconjugation by Atg4 in autophagy. *Autophagy* **8**, 883–892 (2012).

96. Choy, A. *et al.* The Legionella Effector RavZ Inhibits Host Autophagy Through Irreversible Atg8 Deconjugation. *Science* **338**, 1072–1076 (2012).

97. Li, M. *et al.* Kinetics comparisons of mammalian Atg4 homologues indicate selective preferences toward diverse Atg8 substrates. *J. Biol. Chem.* **286**, 7327–7338 (2011).

98. Park, N. Y., Jo, D. S. & Cho, D.-H. Post-Translational Modifications of ATG4B in the Regulation of Autophagy. *Cells* **11**, 1330 (2022).

99. Huang, T. *et al.* MST4 Phosphorylation of ATG4B Regulates Autophagic Activity, Tumorigenicity, and Radioresistance in Glioblastoma. *Cancer Cell* **32**, 840-855.e8 (2017).

100. Ni, Z. *et al.* AKT-mediated phosphorylation of ATG4B impairs mitochondrial activity and enhances the Warburg effect in hepatocellular carcinoma cells. *Autophagy* 1–17 (2018) doi:10.1080/15548627.2017.1407887.

101. Pengo, N. *et al.* Identification of Kinases and Phosphatases That Regulate ATG4B Activity by siRNA and Small Molecule Screening in Cells. *Front. Cell Dev. Biol.* **6**, (2018).

102. Li, X., Sun, L., Yan, G. & Yan, X. PFKP facilitates ATG4B phosphorylation during amino acid deprivation-induced autophagy. *Cell. Signal.* **82**, 109956 (2021).

103. Pengo, N., Agrotis, A., Prak, K., Jones, J. & Ketteler, R. A reversible phospho-switch mediated by ULK1 regulates the activity of autophagy protease ATG4B. *Nat. Commun.* **8**, 294 (2017).

104. Jo, Y. K. *et al.* O-GlcNAcylation of ATG4B positively regulates autophagy by increasing its hydroxylase activity. *Oncotarget* **7**, 57186–57196 (2016).

105. Zheng, X. *et al.* The protease activity of human ATG4B is regulated by reversible oxidative modification. *Autophagy* 1–13 (2020) doi:10.1080/15548627.2019.1709763.

106. Kuang, E. *et al.* Regulation of ATG4B Stability by RNF5 Limits Basal Levels of Autophagy and Influences Susceptibility to Bacterial Infection. *PLoS Genet.* **8**, (2012).

107. Sun, L. *et al.* Deacetylation of ATG4B promotes autophagy initiation under starvation. *Sci. Adv.* **8**, eabo0412 (2022).

108. Norman, J. M., Cohen, G. M. & Bampton, E. T. W. The in vitro cleavage of the hAtg proteins by cell death proteases. *Autophagy* **6**, 1042–1056 (2010).

109. Zhang, L. *et al.* Systems biology-based discovery of a potential Atg4B agonist (Flubendazole) that induces autophagy in breast cancer. *Mol. Biosyst.* **11**, 2860–2866 (2015).

110. Dower, C. M., Bhat, N., Wang, E. W. & Wang, H.-G. Selective reversible inhibition of autophagy in hypoxic breast cancer cells promotes pulmonary metastasis. *Cancer Res.* **77**, 646–657 (2017).

111. Liu, P.-F. *et al.* ATG4B promotes colorectal cancer growth independent of autophagic flux. *Autophagy* **10**, 1454–1465 (2014).

112. Rothe, K. *et al.* The core autophagy protein ATG4B is a potential biomarker and therapeutic target in CML stem/progenitor cells. *Blood* **123**, 3622–3634 (2014).

113. Toshima, T. *et al.* Autophagy enhances hepatocellular carcinoma progression by activation of mitochondrial β-oxidation. *J. Gastroenterol.* **49**, 907–916 (2014).

114. Peng, W. *et al.* Egr-1 regulates irradiation-induced autophagy through Atg4B to promote radioresistance in hepatocellular carcinoma cells. *Oncogenesis* **6**, e292 (2017).

115. Agrotis, A., Pengo, N., Burden, J. J. & Ketteler, R. Redundancy of human ATG4 protease isoforms in autophagy and LC3/GABARAP processing revealed in cells. *Autophagy* **15**, 976–997 (2019).

116. Yang, A. *et al.* Autophagy Sustains Pancreatic Cancer Growth through Both Cell-Autonomous and Nonautonomous Mechanisms. *Cancer Discov.* **8**, 276–287 (2018).

117. Mariño, G. *et al.* Autophagy is essential for mouse sense of balance. *J. Clin. Invest.* **120**, 2331–2344 (2010).

118. Read, R., Savelieva, K., Baker, K., Hansen, G. & Vogel, P. Histopathological and neurological features of Atg4b knockout mice. *Vet. Pathol.* **48**, 486–494 (2011).

119. Maciel, M. *et al.* Impaired autophagic activity and ATG4B deficiency are associated with increased endoplasmic reticulum stress-induced lung injury. *Aging* **10**, 2098–2112 (2018).

120. Akin, D. *et al.* A novel ATG4B antagonist inhibits autophagy and has a negative impact on osteosarcoma tumors. *Autophagy* **10**, 2021–2035 (2014).

121. Bosc, D. *et al.* A new quinoline-based chemical probe inhibits the autophagy-related cysteine protease ATG4B. *Sci. Rep.* **8**, 11653 (2018).

122. Fu, Y. *et al.* Discovery of a small molecule targeting autophagy via ATG4B inhibition and cell death of colorectal cancer cells in vitro and in vivo. *Autophagy* **0**, 1–17 (2018).

123. Liu, P.-F. *et al.* Drug Repurposing Screening Identifies Tioconazole as an ATG4 Inhibitor that Suppresses Autophagy and Sensitizes Cancer Cells to Chemotherapy. *Theranostics* **8**, 830–845 (2018).

124. Xie, H. *et al.* Discovery and mechanism studies of a novel ATG4B inhibitor Ebselen by drug repurposing and its anti-colorectal cancer effects in mice. *Cell Biosci.* **12**, 206 (2022).

125. Kurdi, A. *et al.* ATG4B inhibitors with a benzotropolone core structure block autophagy and augment efficiency of chemotherapy in mice. *Biochem. Pharmacol.* **138**, 150–162 (2017).

126. Quintana, M., Bilbao, A., Comas-Barceló, J., Bujons, J. & Triola, G. Identification of benzo[cd]indol-2(1H)-ones as novel Atg4B inhibitors via a structure-based virtual screening and a novel AlphaScreen assay. *Eur. J. Med. Chem.* **178**, 648–666 (2019).

127. Chang, H.-W. *et al.* Xanthium strumarium Fruit Extract Inhibits ATG4B and Diminishes the Proliferation and Metastatic Characteristics of Colorectal Cancer Cells. *Toxins* **11**, (2019).

128. Bose, S., Zhang, C. & Le, A. Glucose Metabolism in Cancer: The Warburg Effect and Beyond. in *The Heterogeneity of Cancer Metabolism* (ed. Le, A.) 3–15 (Springer International Publishing, 2021). doi:10.1007/978-3-030-65768-0_1.

129. Racker, E. Bioenergetics and the Problem of Tumor Growth: An understanding of the mechanism of the generation and control of biological energy may shed light on the problem of tumor growth. *Am. Sci.* **60**, 56–63 (1972).

130. Warburg, O. The Metabolism of Carcinoma Cells1. *J. Cancer Res.* **9**, 148–163 (1925).

131. Vander Heiden, M. G., Cantley, L. C. & Thompson, C. B. Understanding the Warburg Effect: The Metabolic Requirements of Cell Proliferation. *Science* **324**, 1029–1033 (2009).

132. Hosios, A. M. *et al.* Amino Acids Rather than Glucose Account for the Majority of Cell Mass in Proliferating Mammalian Cells. *Dev. Cell* **36**, 540–549 (2016).

133. Ghanbari Movahed, Z., Rastegari-Pouyani, M., Mohammadi, M. hossein & Mansouri, K. Cancer cells change their glucose metabolism to overcome increased

ROS: One step from cancer cell to cancer stem cell? *Biomed. Pharmacother.* **112**, 108690 (2019).

134. Perillo, B. *et al.* ROS in cancer therapy: the bright side of the moon. *Exp. Mol. Med.* **52**, 192–203 (2020).

135. Yoo, H. C., Yu, Y. C., Sung, Y. & Han, J. M. Glutamine reliance in cell metabolism. *Exp. Mol. Med.* **52**, 1496–1516 (2020).

136. Yoo, H. C. *et al.* A Variant of SLC1A5 Is a Mitochondrial Glutamine Transporter for Metabolic Reprogramming in Cancer Cells. *Cell Metab.* **31**, 267-283.e12 (2020).

137. Kodama, M. *et al.* A shift in glutamine nitrogen metabolism contributes to the malignant progression of cancer. *Nat. Commun.* **11**, 1320 (2020).

138. Mullen, N. J. & Singh, P. K. Nucleotide metabolism: a pan-cancer metabolic dependency. *Nat. Rev. Cancer* 1–20 (2023) doi:10.1038/s41568-023-00557-7.

139. Lane, A. N. & Fan, T. W.-M. Regulation of mammalian nucleotide metabolism and biosynthesis. *Nucleic Acids Res.* **43**, 2466–2485 (2015).

140. Tong, X., Zhao, F. & Thompson, C. B. The molecular determinants of de novo nucleotide biosynthesis in cancer cells. *Curr. Opin. Genet. Dev.* **19**, 32–37 (2009).

141. Zhou, W. *et al.* Purine metabolism regulates DNA repair and therapy resistance in glioblastoma. *Nat. Commun.* **11**, 3811 (2020).

142. Brown, K. K., Spinelli, J. B., Asara, J. M. & Toker, A. Adaptive Reprogramming of De Novo Pyrimidine Synthesis Is a Metabolic Vulnerability in Triple-Negative Breast Cancer. *Cancer Discov.* **7**, 391–399 (2017).

143. Kollareddy, M. *et al.* Regulation of nucleotide metabolism by mutant p53 contributes to its gain-of-function activities. *Nat. Commun.* **6**, 7389 (2015).

144. Yamaguchi, N. *et al.* PCK1 and DHODH drive colorectal cancer liver metastatic colonization and hypoxic growth by promoting nucleotide synthesis. *eLife* **8**, e52135 (2019).

145. Liu, D. *et al.* Oleanolic acid blocks the purine salvage pathway for cancer therapy by inactivating SOD1 and stimulating lysosomal proteolysis. *Mol. Ther. - Oncolytics* **23**, 107–123 (2021).

146. Komatsu, M. *et al.* Impairment of starvation-induced and constitutive autophagy in Atg7-deficient mice. *J. Cell Biol.* **169**, 425–434 (2005).

147. Kuma, A. *et al.* The role of autophagy during the early neonatal starvation period. *Nature* **432**, 1032–1036 (2004).

148. Kuma, A., Komatsu, M. & Mizushima, N. Autophagy-monitoring and autophagy-deficient mice. *Autophagy* **13**, 1619–1628 (2017).

149. Guo, J. Y. *et al.* Autophagy provides metabolic substrates to maintain energy charge and nucleotide pools in Ras-driven lung cancer cells. *Genes Dev.* **30**, 1704–1717 (2016).

150. Mukhopadhyay, S. *et al.* Autophagy is required for proper cysteine homeostasis in pancreatic cancer through regulation of SLC7A11. *Proc. Natl. Acad. Sci. U. S. A.* **118**, e2021475118 (2021).

151. Onodera, J. & Ohsumi, Y. Autophagy Is Required for Maintenance of Amino Acid Levels and Protein Synthesis under Nitrogen Starvation*. *J. Biol. Chem.* **280**, 31582–31586 (2005).

152. Huang, H. *et al.* Bulk RNA degradation by nitrogen starvation-induced autophagy in yeast. *EMBO J.* **34**, 154–168 (2015).

153. Xu, Y.-F. *et al.* Nucleotide degradation and ribose salvage in yeast. *Mol. Syst. Biol.* **9**, 665 (2013).

154. Bosc, C. *et al.* Autophagy regulates fatty acid availability for oxidative phosphorylation through mitochondria-endoplasmic reticulum contact sites. *Nat. Commun.* **11**, 4056 (2020).

155. Kataura, T. *et al.* Autophagy promotes cell survival by maintaining NAD levels. *Dev. Cell* **57**, 2584-2598.e11 (2022).

156. Li, Y. & Chen, Y. AMPK and Autophagy. *Adv. Exp. Med. Biol.* **1206**, 85–108 (2019).

157. Kim, J. *et al.* Differential Regulation of Distinct Vps34 Complexes by AMPK in Nutrient Stress and Autophagy. *Cell* **152**, 290–303 (2013).

158. Park, J.-M., Lee, D.-H. & Kim, D.-H. Redefining the role of AMPK in autophagy and the energy stress response. *Nat. Commun.* **14**, 2994 (2023).

159. Puente, C., Hendrickson, R. C. & Jiang, X. Nutrient-regulated Phosphorylation of ATG13 Inhibits Starvation-induced Autophagy. *J. Biol. Chem.* **291**, 6026–6035 (2016).

160. Nazio, F. *et al.* mTOR inhibits autophagy by controlling ULK1 ubiquitylation, self-association and function through AMBRA1 and TRAF6. *Nat. Cell Biol.* **15**, 406–416 (2013).

161. Yuan, H.-X., Russell, R. C. & Guan, K.-L. Regulation of PIK3C3/VPS34 complexes by MTOR in nutrient stress-induced autophagy. *Autophagy* **9**, 1983–1995 (2013).

162. Galluzzi, L., Pietrocola, F., Levine, B. & Kroemer, G. Metabolic Control of Autophagy. *Cell* **159**, 1263–1276 (2014).

163. Karabiyik, C., Vicinanza, M., Son, S. M. & Rubinsztein, D. C. Glucose starvation induces autophagy via ULK1-mediated activation of PIKfyve in an AMPK-dependent manner. *Dev. Cell* **56**, 1961-1975.e5 (2021).

164. Moruno-Manchón, J. F., Pérez-Jiménez, E. & Knecht, E. Glucose induces autophagy under starvation conditions by a p38 MAPK-dependent pathway. *Biochem. J.* **449**, 497–506 (2012).

165. Seo, J.-W. *et al.* Autophagy is required for PDAC glutamine metabolism. *Sci. Rep.* **6**, 37594 (2016).

166. Tanaka, K. *et al.* Glioma cells require one-carbon metabolism to survive glutamine starvation. *Acta Neuropathol. Commun.* **9**, 16 (2021).

167. Fares, H. M. *et al.* Autophagy in cancer: The cornerstone during glutamine deprivation. *Eur. J. Pharmacol.* **916**, 174723 (2022).

168. Li, Z. *et al.* Ammonia Induces Autophagy through Dopamine Receptor D3 and MTOR. *PLOS ONE* **11**, e0153526 (2016).

169. Vucicevic, L. *et al.* Transcriptional block of AMPK-induced autophagy promotes glutamate excitotoxicity in nutrient-deprived SH-SY5Y neuroblastoma cells. *Cell. Mol. Life Sci.* **77**, 3383–3399 (2020).

170. Jiao, L. *et al.* Regulation of glycolytic metabolism by autophagy in liver cancer involves selective autophagic degradation of HK2 (hexokinase 2). *Autophagy* **14**, 671–684 (2017).

171. Mansour, M. A., Ibrahim, W. M., Salama, M. M. & Salama, A. F. Dual inhibition of glycolysis and autophagy as a therapeutic strategy in the treatment of Ehrlich ascites carcinoma. *J. Biochem. Mol. Toxicol.* **34**, e22498 (2020).

172. Chu, B., Wang, J., Wang, Y. & Yang, G. Knockdown of PKM2 induces apoptosis and autophagy in human A549 alveolar adenocarcinoma cells. *Mol. Med. Rep.* **12**, 4358–4363 (2015).

173. Wang, L. *et al.* Co-targeting hexokinase 2-mediated Warburg effect and ULK1-dependent autophagy suppresses tumor growth of PTEN- and TP53-deficiency-driven castration-resistant prostate cancer. *eBioMedicine* **7**, 50–61 (2016).

174. Han, T. *et al.* A novel glutaminase inhibitor-968 inhibits the migration and proliferation of non-small cell lung cancer cells by targeting EGFR/ERK signaling pathway. *Oncotarget* **8**, 28063–28073 (2016).

175. Li, J. *et al.* Synthetic lethality of glutaminolysis inhibition, autophagy inactivation and asparagine depletion in colon cancer. *Oncotarget* **8**, 42664–42672 (2017).

176. Halama, A. *et al.* Accelerated lipid catabolism and autophagy are cancer survival mechanisms under inhibited glutaminolysis. *Cancer Lett.* **430**, 133–147 (2018).

177. Roberts, D. J. & Miyamoto, S. Hexokinase II integrates energy metabolism and cellular protection: Akting on mitochondria and TORCing to autophagy. *Cell Death Differ.* **22**, 248–257 (2015).

178. Hsu, M.-C. & Hung, W.-C. Pyruvate kinase M2 fuels multiple aspects of cancer cells: from cellular metabolism, transcriptional regulation to extracellular signaling. *Mol. Cancer* **17**, 35 (2018).

179. Abrams, R. & Bentley, M. TRANSFORMATION OF INOSINIC ACID TO ADENYLIC AND GUANYLIC ACIDS IN A SOLUBLE ENZYME SYSTEM1. *J. Am. Chem. Soc.* **77**, 4179–4180 (1955).

180. Natsumeda, Y. *et al.* Two distinct cDNAs for human IMP dehydrogenase. *J. Biol. Chem.* **265**, 5292–5295 (1990).

181. Konno, Y. *et al.* Expression of human IMP dehydrogenase types I and II in Escherichia coli and distribution in human normal lymphocytes and leukemic cell lines. *J. Biol. Chem.* **266**, 506–509 (1991).

182. Nagai, M. *et al.* Selective Up-Regulation of Type II Inosine 5′-Monophosphate Dehydrogenase Messenger RNA Expression in Human Leukemias1. *Cancer Res.* **51**, 3886–3890 (1991).

183. Pareek, V., Pedley, A. M. & Benkovic, S. J. Human de novo Purine Biosynthesis. *Crit. Rev. Biochem. Mol. Biol.* **56**, 1–16 (2021).

184. Yin, J. *et al.* Potential Mechanisms Connecting Purine Metabolism and Cancer Therapy. *Front. Immunol.* **9**, (2018).

185. Hedstrom, L. IMP Dehydrogenase: Structure, Mechanism and Inhibition. *Chem. Rev.* **109**, 2903–2928 (2009).

186. Burrell, A. L. & Kollman, J. M. IMPDH dysregulation in disease: a mini review. *Biochem. Soc. Trans.* **50**, 71–82 (2022).

187. Burrell, A. L. *et al.* IMPDH1 retinal variants control filament architecture to tune allosteric regulation. *Nat. Struct. Mol. Biol.* **29**, 47–58 (2022).

188. Johnson, M. C. & Kollman, J. M. Cryo-EM structures demonstrate human IMPDH2 filament assembly tunes allosteric regulation. *eLife* **9**, e53243 (2020).

189. Schiavon, C. R. *et al.* Compositional complexity of rods and rings. *Mol. Biol. Cell* **29**, 2303–2316 (2018).

190. Calise, S. J. *et al.* Glutamine deprivation initiates reversible assembly of mammalian rods and rings. *Cell. Mol. Life Sci. CMLS* **71**, 2963–2973 (2014).

191. Calise, S. J. *et al.* 'Rod and ring' formation from IMP dehydrogenase is regulated through the one-carbon metabolic pathway. *J. Cell Sci.* **129**, 3042–3052 (2016).

192. Lemberg, K. M., Vornov, J. J., Rais, R. & Slusher, B. S. We're Not "DON" Yet: Optimal Dosing and Prodrug Delivery of 6-Diazo-5-oxo-L-norleucine. *Mol. Cancer Ther.* **17**, 1824–1832 (2018).

193. Villa, E., Ali, E. S., Sahu, U. & Ben-Sahra, I. Cancer Cells Tune the Signaling Pathways to Empower de Novo Synthesis of Nucleotides. *Cancers* **11**, (2019).

194. Jackson, R. C., Weber, G. & Morris, H. P. IMP dehydrogenase, an enzyme linked with proliferation and malignancy. *Nature* **256**, 331–333 (1975).

195. Huang, F. *et al.* Inosine Monophosphate Dehydrogenase Dependence in a Subset of Small Cell Lung Cancers. *Cell Metab.* **28**, 369-382.e5 (2018).

196. Chong, Y. C. *et al.* Targeted Inhibition of Purine Metabolism Is Effective in Suppressing Hepatocellular Carcinoma Progression. *Hepatol. Commun.* **4**, 1362–1381 (2020).

197. Jia, X. *et al.* Inosine monophosphate dehydrogenase type1 sustains tumor growth in hepatocellular carcinoma. *J. Clin. Lab. Anal.* **36**, e24416 (2022).

198. Zhao, J.-Z. *et al.* MYBL2 regulates de novo purine synthesis by transcriptionally activating IMPDH1 in hepatocellular carcinoma cells. *BMC Cancer* **22**, 1290 (2022).

199. Ruan, H. *et al.* IMPDH1/YB-1 Positive Feedback Loop Assembles Cytoophidia and Represents a Therapeutic Target in Metastatic Tumors. *Mol. Ther.* **28**, 1299–1313 (2020).

200. Duan, S. *et al.* IMPDH2 promotes colorectal cancer progression through activation of the PI3K/AKT/mTOR and PI3K/AKT/FOXO1 signaling pathways. *J. Exp. Clin. Cancer Res. CR* **37**, 304 (2018).

201. Yuan, C., Wang, L., Zhou, L. & Fu, Z. The function of FOXO1 in the late phases of the cell cycle is suppressed by PLK1-mediated phosphorylation. *Cell Cycle* **13**, 807–819 (2014).

202. Kofuji, S. *et al.* IMP dehydrogenase-2 drives aberrant nucleolar activity and promotes tumorigenesis in glioblastoma. *Nat. Cell Biol.* **21**, 1003–1014 (2019).

203. He, Y. *et al.* Over-expression of IMPDH2 is associated with tumor progression and poor prognosis in hepatocellular carcinoma. *Am. J. Cancer Res.* **8**, 1604–1614 (2018).

204. Xu, H. *et al.* IMPDH2 promotes cell proliferation and epithelial-mesenchymal transition of non-small cell lung cancer by activating the Wnt/β-catenin signaling pathway. *Oncol. Lett.* **20**, 1–1 (2020).

205. Keppeke, G. D. *et al.* IMP/GTP balance modulates cytoophidium assembly and IMPDH activity. *Cell Div.* **13**, 5 (2018).

206. Valvezan, A. J. *et al.* mTORC1 Couples Nucleotide Synthesis to Nucleotide Demand Resulting in a Targetable Metabolic Vulnerability. *Cancer Cell* **32**, 624-638.e5 (2017).

207. Pua, K. H., Stiles, D. T., Sowa, M. E. & Verdine, G. L. IMPDH2 Is an Intracellular Target of the Cyclophilin A and Sanglifehrin A Complex. *Cell Rep.* **18**, 432–442 (2017).

208. Aherne, A. *et al.* On the molecular pathology of neurodegeneration in IMPDH1-based retinitis pigmentosa. *Hum. Mol. Genet.* **13**, 641–650 (2004).

209. Gu, J. J. *et al.* Targeted Disruption of the Inosine 5′-Monophosphate Dehydrogenase Type I Gene in Mice. *Mol. Cell. Biol.* **23**, 6702–6712 (2003).

210. Gu, J. J. *et al.* Inhibition of T lymphocyte activation in mice heterozygous for loss of the *IMPDH II* gene. *J. Clin. Invest.* **106**, 599–606 (2000).

211. Gosio, B. Sperimentate su culture pure di bacilli del carbonchio demonstrarano notevole potere antisettica. *CR Acad Med Torino* 484 (1893).

212. Alsberg, C. & Black, O. F. *Contributions to the Study of Maize Deterioration: Biochemical and Toxicological Investigations of Penicillium Puberulum and Penicillium Stoloniferum*. (U.S. Government Printing Office, 1913).

213. Benjanuwattra, J., Chaiyawat, P., Pruksakorn, D. & Koonrungsesomboon, N. Therapeutic potential and molecular mechanisms of mycophenolic acid as an anticancer agent. *Eur. J. Pharmacol.* **887**, 173580 (2020).

214. Naffouje, R. *et al.* Anti-Tumor Potential of IMP Dehydrogenase Inhibitors: A Century-Long Story. *Cancers* **11**, (2019).

215. Freedman, R., Yu, R., Sarkis, A. W. & Hedstrom, L. A structural determinant of mycophenolic acid resistance in eukaryotic inosine 5′-monophosphate dehydrogenases. *Protein Sci.* **29**, 686–694 (2020).

216. Zheng, Z.-H. *et al.* Mycophenolic acid induces adipocyte-like differentiation and reversal of malignancy of breast cancer cells partly through PPARγ. *Eur. J. Pharmacol.* **658**, 1–8 (2011).

217. Sidi, Y. *et al.* Growth inhibition and induction of phenotypic alterations in MCF-7 breast cancer cells by an IMP dehydrogenase inhibitor. *Br. J. Cancer* **58**, 61–63 (1988).

218. Klangjorhor, J. *et al.* Mycophenolic acid is a drug with the potential to be repurposed for suppressing tumor growth and metastasis in osteosarcoma treatment. *Int. J. Cancer* **146**, 3397–3409 (2020).

219. Dun, B. *et al.* Mycophenolic Acid Inhibits Migration and Invasion of Gastric Cancer Cells via Multiple Molecular Pathways. *PLOS ONE* **8**, e81702 (2013).

220. Takebe, N. *et al.* IMP dehydrogenase inhibitor mycophenolate mofetil induces caspase-dependent apoptosis and cell cycle inhibition in multiple myeloma cells. *Mol. Cancer Ther.* **5**, 457–466 (2006).

221. Thomas, E., Ghany, M. G. & Liang, T. J. The application and mechanism of action of ribavirin in therapy of hepatitis C. *Antivir. Chem. Chemother.* **23**, 1–12 (2012).

222. Casaos, J. *et al.* Ribavirin as a potential therapeutic for atypical teratoid/rhabdoid tumors. *Oncotarget* **9**, 8054–8067 (2018).

223. Kökény, S. *et al.* Ribavirin Acts via Multiple Pathways in Inhibition of Leukemic Cell Proliferation. *Anticancer Res.* **29**, 1971–1980 (2009).

224. De la Cruz-Hernandez, E. *et al.* Ribavirin as a tri-targeted antitumor repositioned drug. *Oncol. Rep.* **33**, 2384–2392 (2015).

225. *Inosine Monophosphate Dehydrogenase: A Major Therapeutic Target*. vol. 839 (American Chemical Society, 2003).

226. Harrison, S. D., Jr., O'Dwyer, P. J. & Trader, M. W. Therapeutic Synergism of Tiazofurin and Selected Antitumor Drugs against Sensitive and Resistant P388 Leukemia in Mice1. *Cancer Res.* **46**, 3396–3400 (1986).

227. Colovic, M. *et al.* In vitro sensitivity of hematopoietic progenitors to Tiazofurin in refractory acute myeloid leukemia and in the blast crisis of chronic myeloid leukemia. *Cancer Lett.* **195**, 153–159 (2003).

228. Malek, K., Boosalis, M. S., Waraska, K., Mitchell, B. S. & Wright, D. G. Effects of the IMP-dehydrogenase inhibitor, Tiazofurin, in bcr-abl positive acute myelogenous leukemia: Part I. In vivo studies. *Leuk. Res.* **28**, 1125–1136 (2004).

229. Gan, L. *et al.* The Immunosuppressive Agent Mizoribine Monophosphate Forms a Transition State Analogue Complex with Inosine Monophosphate Dehydrogenase. *Biochemistry* **42**, 857–863 (2003).

230. Liao, L.-X. *et al.* Highly selective inhibition of IMPDH2 provides the basis of antineuroinflammation therapy. *Proc. Natl. Acad. Sci.* **114**, E5986–E5994 (2017).

231. Tzoneva, G. *et al.* Clonal evolution mechanisms in NT5C2 mutant-relapsed acute lymphoblastic leukaemia. *Nature* **553**, 511–514 (2018).

232. Valvezan, A. J. *et al.* IMPDH inhibitors for antitumor therapy in tuberous sclerosis complex. *JCI Insight* **5**, e135071.

233. Wang, W. *et al.* Shikonin is a novel and selective IMPDH2 inhibitor that target triple-negative breast cancer. *Phytother. Res.* **35**, 463–476 (2021).

234. Kim, S., Kim, D. H., Jung, W.-H. & Koo, J. S. Expression of glutamine metabolism-related proteins according to molecular subtype of breast cancer. *Endocr. Relat. Cancer* **20**, 339–348 (2013).

235. Agrotis, A. & Ketteler, R. On ATG4B as Drug Target for Treatment of Solid Tumours—The Knowns and the Unknowns. *Cells* **9**, 53 (2019).

236. Fu, Y. *et al.* Targeting ATG4 in Cancer Therapy. *Cancers* **11**, (2019).

237. Kofuji, S. & Sasaki, A. T. GTP metabolic reprogramming by IMPDH2: unlocking cancer cells' fuelling mechanism. *J. Biochem. (Tokyo)* **168**, 319–328 (2020).

238. Hedstrom, L. IMP Dehydrogenase: Structure, Mechanism and Inhibition. *Chem. Rev.* **109**, 2903–2928 (2009).

239. Benz, C. C. *et al.* Estrogen-dependent, tamoxifen-resistant tumorigenic growth of MCF-7 cells transfected with HER2/neu. *Breast Cancer Res. Treat.* **24**, 85–95 (1992).

240. Warburton, C. *et al.* Treatment of HER-2/neu overexpressing breast cancer xenograft models with trastuzumab (Herceptin) and gefitinib (ZD1839): drug combination effects on tumor growth, HER-2/neu and epidermal growth factor receptor expression, and viable hypoxic cell fraction. *Clin. Cancer Res. Off. J. Am. Assoc. Cancer Res.* **10**, 2512–2524 (2004).

241. Tyanova, S., Temu, T. & Cox, J. The MaxQuant computational platform for mass spectrometry-based shotgun proteomics. *Nat. Protoc.* **11**, 2301–2319 (2016).

242. Kole, K. *et al.* Proteomic landscape of the primary somatosensory cortex upon sensory deprivation. *GigaScience* **6**, gix082 (2017).

243. Zhu, W., Smith, J. W. & Huang, C.-M. Mass Spectrometry-Based Label-Free Quantitative Proteomics. *BioMed Res. Int.* **2010**, e840518 (2009).

244. Kustatscher, G. *et al.* Co-regulation Map of the Human Proteome Enables Identification of Protein Functions. *Nat. Biotechnol.* **37**, 1361–1371 (2019).

245. Schober, P., Boer, C. & Schwarte, L. A. Correlation Coefficients: Appropriate Use and Interpretation. *Anesth. Analg.* **126**, 1763 (2018).

246. Cerami, E. *et al.* The cBio Cancer Genomics Portal: An Open Platform for Exploring Multidimensional Cancer Genomics Data. *Cancer Discov.* **2**, 401–404 (2012).

247. Gao, J. *et al.* Integrative analysis of complex cancer genomics and clinical profiles using the cBioPortal. *Sci. Signal.* **6**, pl1 (2013).

248. Asleh, K. *et al.* Proteomic analysis of archival breast cancer clinical specimens identifies biological subtypes with distinct survival outcomes. *Nat. Commun.* **13**, 896 (2022).

249. LeClair, R. J. Pentose Phosphate Pathway (PPP), Purine and Pyrimidine Metabolism. (2021).

250. Martínez-García, G. G. *et al.* Autophagy Deficiency by Atg4B Loss Leads to Metabolomic Alterations in Mice. *Metabolites* **11**, 481 (2021).

251. Aggarwal, R. & Ranganathan, P. Common pitfalls in statistical analysis: The use of correlation techniques. *Perspect. Clin. Res.* **7**, 187–190 (2016).

252. Miot, H. A. Correlation analysis in clinical and experimental studies. *J. Vasc. Bras.* **17**, 275–279 (2018).

253. Kimura, S., Noda, T. & Yoshimori, T. Dissection of the autophagosome maturation process by a novel reporter protein, tandem fluorescent-tagged LC3. *Autophagy* **3**, 452–460 (2007).

254. Tanida, I., Ueno, T. & Kominami, E. Human light chain 3/MAP1LC3B is cleaved at its carboxyl-terminal Met121 to expose Gly120 for lipidation and targeting to autophagosomal membranes. *J. Biol. Chem.* **279**, 47704–47710 (2004).

255. Cajka, T. & Fiehn, O. Toward Merging Untargeted and Targeted Methods in Mass Spectrometry-Based Metabolomics and Lipidomics. *Anal. Chem.* **88**, 524–545 (2016).

256. Kapoore, R. V. & Vaidyanathan, S. Towards quantitative mass spectrometry-based metabolomics in microbial and mammalian systems. *Philos. Transact. A Math. Phys. Eng. Sci.* **374**, 20150363 (2016).

257. Roberts, L. D., Souza, A. L., Gerszten, R. E. & Clish, C. B. Targeted Metabolomics. *Curr. Protoc. Mol. Biol.* **CHAPTER**, Unit30.2 (2012).

258. Cholewiński, G., Iwaszkiewicz-Grześ, D., Prejs, M., Głowacka, A. & Dzierzbicka, K. Synthesis of the inosine 5′-monophosphate dehydrogenase (IMPDH) inhibitors. *J. Enzyme Inhib. Med. Chem.* **30**, 550–563 (2015).

259. Mimura, K. *et al.* Genome-wide CRISPR screening reveals nucleotide synthesis negatively regulates autophagy. *J. Biol. Chem.* **296**, (2021).

260. Iqbal, N. & Iqbal, N. Human Epidermal Growth Factor Receptor 2 (HER2) in Cancers: Overexpression and Therapeutic Implications. *Mol. Biol. Int.* **2014**, e852748 (2014).

261. Wang, J. & Xu, B. Targeted therapeutic options and future perspectives for HER2-positive breast cancer. *Signal Transduct. Target. Ther.* **4**, 1–22 (2019).

262. Cufí, S. *et al.* The anti-malarial chloroquine overcomes Primary resistance and restores sensitivity to Trastuzumab in HER2-positive breast cancer. *Sci. Rep.* **3**, 2469 (2013).

263. Tang, W. *et al.* Integrated proteotranscriptomics of breast cancer reveals globally increased protein-mRNA concordance associated with subtypes and survival. *Genome Med.* **10**, (2018).

264. Lánczky, A. & Győrffy, B. Web-Based Survival Analysis Tool Tailored for Medical Research (KMplot): Development and Implementation. *J. Med. Internet Res.* **23**, e27633 (2021).

265. Boersma, B. J. *et al.* Association of Breast Cancer Outcome With Status of p53 and MDM2 SNP309. *JNCI J. Natl. Cancer Inst.* **98**, 911–919 (2006).

266. Hou, Y., Nitta, H. & Li, Z. HER2 Intratumoral Heterogeneity in Breast Cancer, an Evolving Concept. *Cancers* **15**, 2664 (2023).

267. Chou, T.-C. Drug combination studies and their synergy quantification using the Chou-Talalay method. *Cancer Res.* **70**, 440–446 (2010).

268. Bortnik, S. *et al.* Differential expression and prognostic relevance of autophagy-related markers ATG4B, GABARAP, and LC3B in breast cancer. *Breast Cancer Res. Treat.* **183**, 525–547 (2020).

269. Godoy-Ortiz, A. *et al.* Deciphering HER2 Breast Cancer Disease: Biological and Clinical Implications. *Front. Oncol.* **9**, 1124 (2019).

270. Yin, N. *et al.* Synergistic and Antagonistic Drug Combinations Depend on Network Topology. *PLoS ONE* **9**, e93960 (2014).

271. Yeh, P., Tschumi, A. I. & Kishony, R. Functional classification of drugs by properties of their pairwise interactions. *Nat. Genet.* **38**, 489–494 (2006).

272. Mizushima, N. & Yoshimori, T. How to interpret LC3 immunoblotting. *Autophagy* **3**, 542–545 (2007).

273. Isakovic, A. M. *et al.* Autophagy suppression sensitizes glioma cells to IMP dehydrogenase inhibition-induced apoptotic death. *Exp. Cell Res.* **350**, 32–40 (2017).

274. Carr, S. F., Papp, E., Wu, J. C. & Natsumeda, Y. Characterization of human type I and type II IMP dehydrogenases. *J. Biol. Chem.* **268**, 27286–27290 (1993).

275. Fang, S. *et al.* Suppression of autophagy by mycophenolic acid contributes to inhibition of HCV replication in human hepatoma cells. *Sci. Rep.* **7**, 44039 (2017).

276. Liu, J.-L. The enigmatic cytoophidium: Compartmentation of CTP synthase via filament formation. *BioEssays* **33**, 159–164 (2011).

277. Liu, J.-L. The Cytoophidium and Its Kind: Filamentation and Compartmentation of Metabolic Enzymes. *Annu. Rev. Cell Dev. Biol.* **32**, 349–372 (2016).

278. Liu, J.-L. Intracellular compartmentation of CTP synthase in Drosophila. *J. Genet. Genomics* **37**, 281–296 (2010).

279. Nassar, A., Khoor, A., Radhakrishnan, R., Radhakrishnan, A. & Cohen, C. Correlation of HER2 overexpression with gene amplification and its relation to chromosome 17 aneuploidy: a 5-year experience with invasive ductal and lobular carcinomas. *Int. J. Clin. Exp. Pathol.* **7**, 6254–6261 (2014).

Appendix A.

Supplementary tables and figures

Table A.1. Sequences of IDT DsiRNAs to genetically knockdown IMPDH1 and IMPDH2

Name:	Sequences (5'-3'):	
hs.Ri.IMPDH1.13.1	Sequence 1	rCrUrU rGrGrG rArUrC rArCrA rGrUrU rGrCrG rUrCrA rUrUG T
	Sequence 2	rArCrA rArUrG rArCrG rCrArA rCrUrG rUrGrA rUrCrC rCrArA rGrUrG
hs.Ri.IMPDH1.13.2	Sequence 1	rGrUrG rArGrG rArUrG rArCrA rArArU rArCrC rGrUrC rUrGG A
	Sequence 2	rUrCrC rArGrA rCrGrG rUrArU rUrUrG rUrCrA rUrCrC rUrCrA rCrGrG
hs.Ri.IMPDH2.13.1	Sequence 1	rArUrG rGrUrU rUrCrU rGrCrG rGrUrA rUrCrC rCrArA rUrCA C
	Sequence 2	rGrUrG rArUrU rGrGrG rArUrA rCrCrG rCrArG rArArA rCrCrA rUrGrC

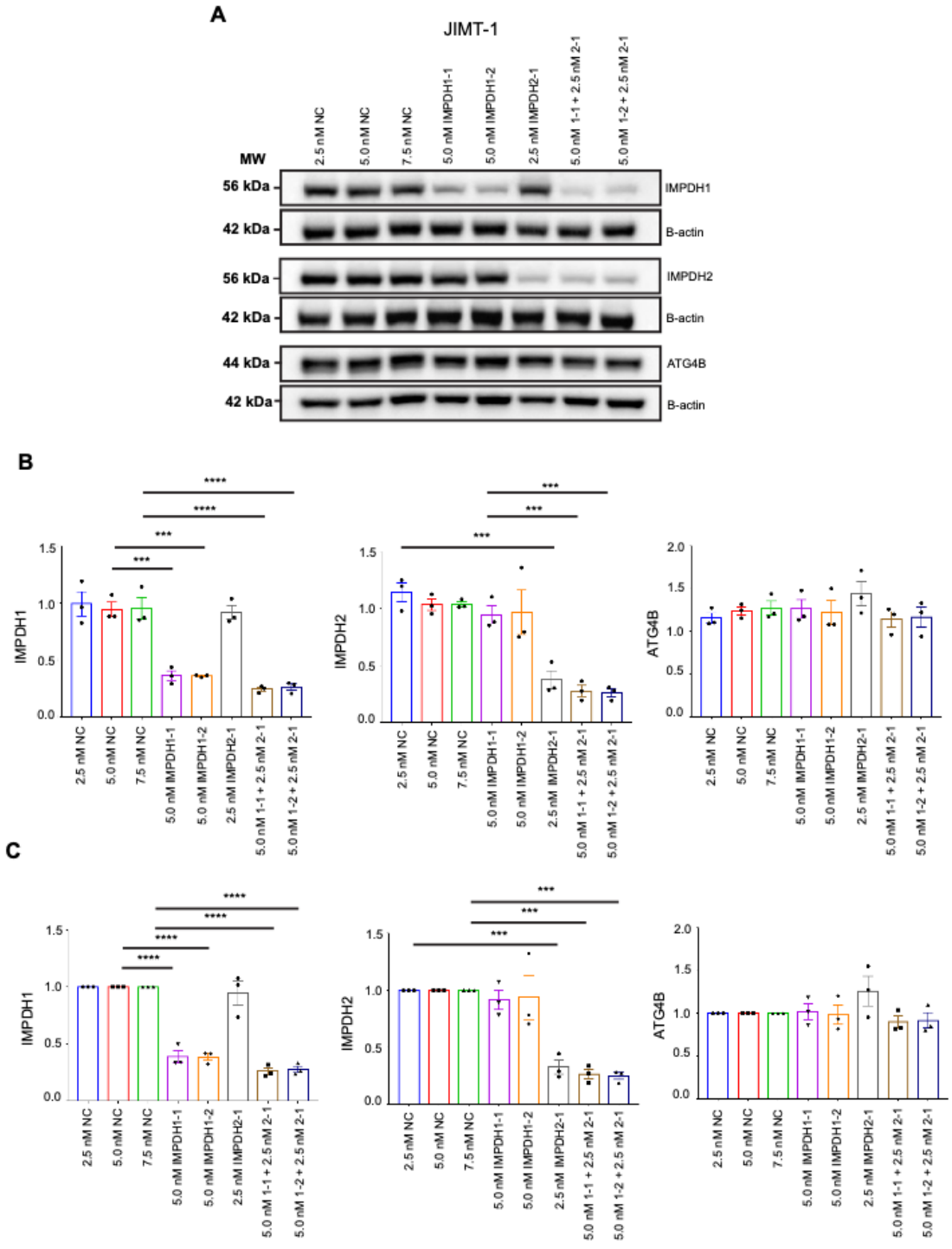

Figure A.1. Genetic knockdown of IMPDH1 and/or IMPDH2 does not lead to significant changes in ATG4B protein levels

(A) Parental JIMT-1 cells were subjected to siRNA-mediated knockdown of IMPDH1 and/or IMPDH2 as described in methods. Cells were harvested for western blot analyses for IMPDH1, IMPDH2, ATG4B and B-actin following siRNA treatments. Representative western blots are shown.

(B) Absolute quantifications of IMPDH1, IMPDH2 and ATG4B protein levels were determined relative to B-actin loading controls and are shown to depict variability between biological replicates. (C) Normalized quantifications of IMPDH1, IMPDH2 and ATG4B levels were determined relative to B-actin loading controls and then normalized to respective NC (negative control) siRNA controls depending on siRNA concentrations to control for variabilities in absolute values between biological replicates. For B and C, one way ANOVA with Tukey's multiple comparisons test was used to evaluate statistical differences, and error bars represent SEM. 3 biological replicates were performed.

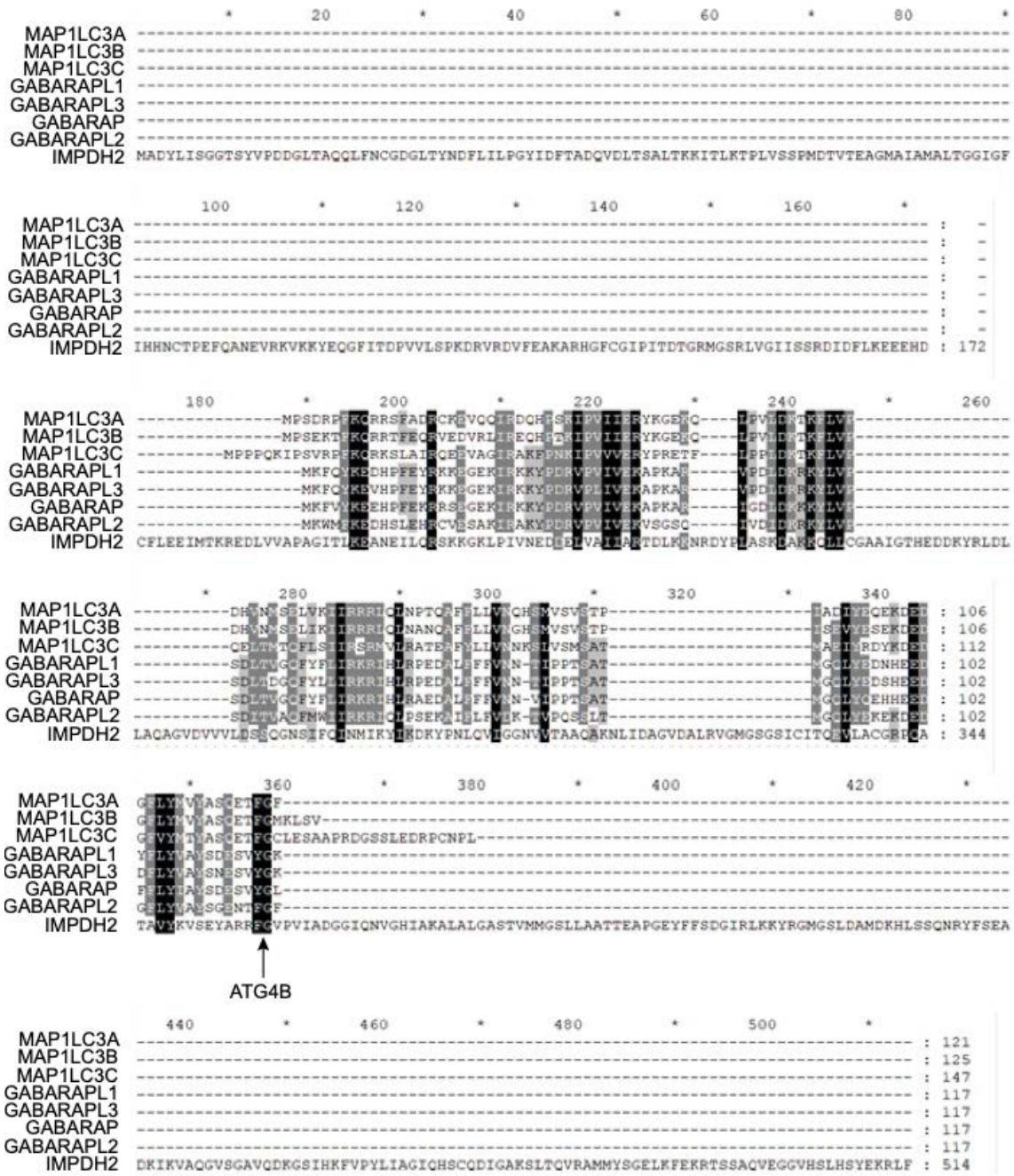

Figure A.2. Multiple sequence alignment of human IMPDH2 and ATG8 proteins reveal several regions of shared homology.

FASTA sequences of human IMPDH2 and ATG8 proteins (LC3 and GABARAP family) were obtained from Uniprot. Multiple sequence alignment was performed using ClustalQ (version 1.2.2). A gap opening penalty of 11 and extension penalty of 0.2 was imposed. Alignments were visualized and annotated using CLC Sequence Viewer (Version 8.0) to highlight conservation of amino acids and amino acid properties. Shades of grey reflect conservation, where darker shades reflect higher conservation and lighter shades reflect lower conservation. The canonical site on pro-ATG8 proteins cleaved by ATG4B is indicated in the figure.

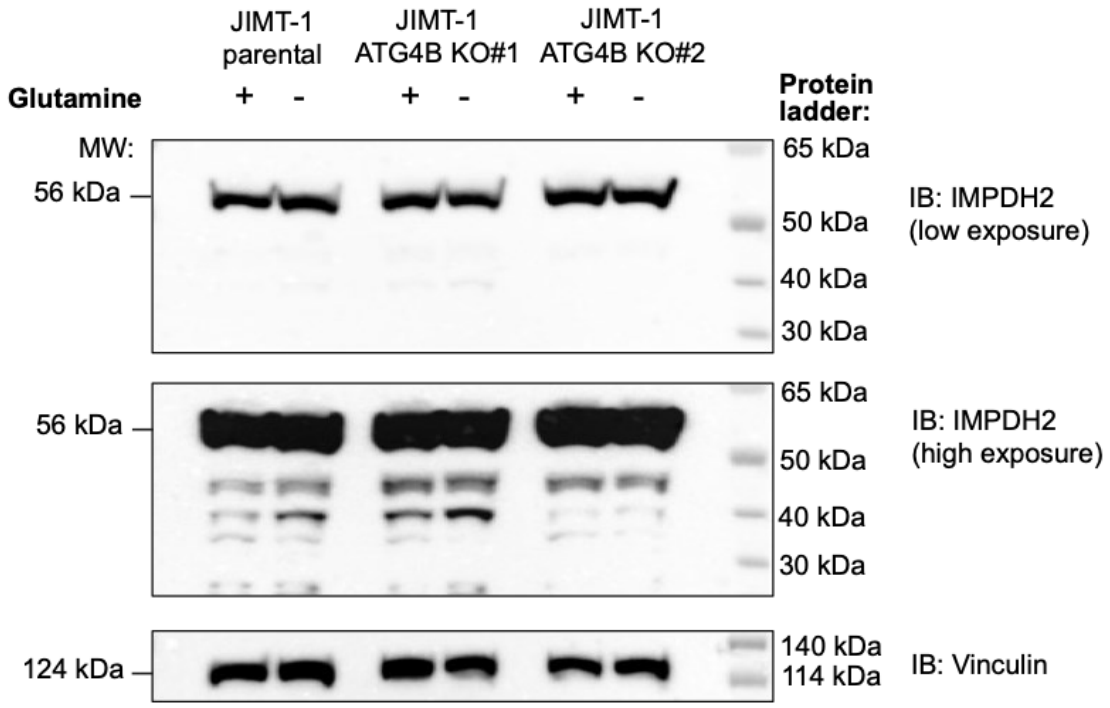

Figure A.3. Genetic loss of ATG4B does not alter IMPDH2 band patterns.
Parental and ATG4B KO JIMT-1 cells were grown in full or glutamine-deprived media for 48 hours and harvested for western blot analysis of IMPDH2 and vinculin (loading control). Cleavage of IMPDH2 between residues 359 and 360 is hypothesized based on the MSA results from Figure A2 and should result in a 359 and 155 amino acid residue. Genetic loss of ATG4B is expected to abolish bands at approximately 39kDa and 17kDa. Western blot images from pilot investigation are shown.